



**The effects of tissue-specific proteinase
activated receptor-2 (PAR-2) ablation on
remodelling events found in bone and
cartilage, using a murine destabilisation of
the medial meniscus (DMM) model**

Angela Kate Habgood BM, BSc (Hons)

Thesis submitted for Doctor of Philosophy

Institute of Cellular Medicine

January 2017

Abstract

Osteoarthritis (OA) is a common musculoskeletal disease, associated with significant cost to the National Health Service (NHS) and physical consequences to the sufferer. It is known that cartilage degradation and subchondral sclerosis are hallmark features of OA. However, it is not known in which tissue pathological changes occur first. By identifying this, future therapeutics could be guided more accurately to maximise their benefit.

This study has highlighted significant problems in generating a reliable and reproducible human-derived model of cartilage catabolism using human mesenchymal stem cells (hMSCs). Generating such a model is important, as it will allow assessment of potential therapies in a physiologically relevant human model, and further work is needed in this area. However, one significant finding from this work was that the addition of matriptase to a cytokine stimulus enhanced proteoglycan and collagen degradation from cartilage discs and macro-pellets. Matriptase is a serine proteinase, and is involved in cartilage catabolism through activation of pro-MMPs and signaling via PAR-2. These findings therefore support the role of matriptase in OA pathogenesis, specifically cartilage catabolism.

Proteinase-activated receptor-2 (PAR-2) is known to be involved in OA pathogenesis, with global ablation of this receptor preventing abnormal remodelling events in the cartilage and subchondral bone. In this study, tissue-specific ablation of PAR-2 revealed that loss of PAR-2 conferred its primary beneficial effect in the bone by preventing subchondral sclerosis. The debate about whether cartilage or bone changes occur first in OA remains controversial, but it was apparent from various time-course studies that bone changes occurred first, followed by cartilage catabolism during OA progression. However, in this study it was also evident that cartilage damage could occur independently of subchondral sclerosis, which is in opposition to the long standing view that subchondral sclerosis is a prerequisite for cartilage damage to occur. Thus, this study highlights that targeting either the cartilage or bone may be beneficial for therapies, although for ease of use, targeting the bone may be more clinically useful. Furthermore the importance of PAR-2 expressed on chondrocytes in the development and maturation of osteophytes was evident in this study.

Acknowledgements

Firstly, I would like to thank my main supervisor Professor Drew Rowan for his guidance, support and continuous help, enabling me to gain confidence, enjoy and complete my PhD. Additionally, many thanks go to my co-supervisors Dr Allie Gartland and Dr Mark Birch.

Sharon Watson provided much help and assistance with histology techniques, making it fun, and providing a source of interesting conversations. Also, Valerie Affleck and Hua Lin carried out the genotyping, for which I am very grateful. I spent several placements with Professor Rob van't Hof (University of Liverpool) and Dr Allie Gartland (University of Sheffield) learning micro-CT techniques, enabling me to perform my analysis. Dr Carmen Huesa (University of the West Scotland) also provided guidance on performing micro-CT analysis, which was very helpful.

I would also like to thank Dr Matt Barter and Professor David Young for their advice on tissue engineering. My progression panel (Professor Nick Europe-Finner and Professor Mike Briggs) also provided guidance on my PhD, which was helpful. Thanks also to MRG for friendship, support and advice throughout my PhD. Finally, I would like to thank CIMA for funding my PhD, and last but not least my family for their encouragement and providing ongoing motivation to complete my PhD.

Table of Contents

Abstract	iii
Acknowledgements	iv
Abbreviations	xix
1. Chapter 1: Introduction	
1.1 Ageing and the musculoskeletal system	1
1.1.1 How ageing impacts on different components of the musculoskeletal system	1
1.1.1.1 Skeletal muscle	1
1.1.1.2 Tendons	2
1.1.1.3 Bone	2
1.1.1.4 Cartilage	3
1.1.2 Physical activity and the musculoskeletal system	4
1.2 Osteoarthritis	4
1.3 Cartilage and subchondral bone	6
1.3.1 Cartilage	6
1.3.1.1 Chondrocytes	8
1.3.1.2 Extracellular Matrix	9
1.3.2 Subchondral bone	11
1.4 Cartilage and subchondral bone changes in OA	12
1.4.1 Alterations in OA cartilage	12
1.4.2 Subchondral bone changes in OA	14
1.5 The interplay between cartilage and subchondral bone in OA	17
1.5.1 Functional interaction	18
1.5.2 Increased vascularization promoting cross talk	18
1.6 Proteinase activated receptor-2	20
1.6.1 Structure and activation	20
1.6.2 PAR-2 signalling	22
1.6.3 PAR-2 in OA	22
1.7 Proteinases involved in matrix turnover in the joint	24
1.7.1 ADAMTS (a disintegrin and metalloproteinase with thrombospondin motif)	24
1.7.2 Matrix metalloproteinases (MMPs)	25

1.7.3 Serine proteinases	26
1.8 Matriptase	28
1.9 Interleukin-1 (IL-1)	31
1.10 Oncostatin-M (OSM)	31
1.11 Aims of study	32
2. Chapter 2: Materials and Methods	
2.1 Materials	33
2.1.1 Biochemical reagents	33
2.1.2 Molecular Biology reagents	33
2.1.3 Cytokines	34
2.1.4 Cell and tissue culture reagents	34
2.1.5 Commercially available kits	35
2.1.6 Histology reagents	35
2.1.7 Micro-computed tomography	35
2.1.8 Animal work	36
2.1.9 Other reagents	36
2.2 Methods	36
2.2.1 Genetic manipulation of mice	36
2.2.2 Destabilization of the medial meniscus (DMM) surgery in C57BL/6 mice	39
2.2.3 Collection of mouse limbs and processing for histology/IHC	43
2.2.4 Xiphisternum micro-dissection and RNA extraction	44
2.2.5 Reverse transcription polymerase chain reaction (RT-PCR)	45
2.2.6 Semi-quantitative polymerase chain reaction	46
2.2.7 Quantitative Real-time polymerase chain reaction (qPCR)	49
2.2.8 Histology staining	50
2.2.9 Immunohistochemistry	52
2.2.10 Micro-Computed tomography	54
2.2.10.1 Scanning and reconstruction	55
2.2.10.2 Analysis subchondral bone medial and lateral epicondyles tibia	57
2.2.10.3 Osteophyte analysis	61
2.2.10.4 Subchondral tibial bone measurements	62

2.2.11 Cartilage discs and pellets produced from differentiated human mesenchymal stem cells (hMSCs)	64
2.2.12 Cartilage digestion	66
2.2.13 Glycosaminoglycan assay	67
2.2.14 Hydroxyproline (OHP) assay	68
2.2.15 MMP activity assay	70
2.2.16 Quantitative assessment of cartilage damage	71
2.2.17 Statistical analysis	72

3. Chapter 3: The use of tissue engineering to generate a reliable and reproducible model of cartilage catabolism

3.1 Introduction	73
3.2 Results	75
3.2.1 A model of tissue engineered cartilage disc catabolism	75
3.2.1.1 Pilot study to assess the effects of IL-1 + OSM on cartilage catabolism	75
3.2.1.2 The effects of IL-1 + OSM +/- matriptase or IL-1 alone on cartilage catabolism	77
3.2.1.3 The effects of IL-1 + OSM +/- matriptase or IL-1 alone on MMP activity	81
3.2.1.4 Histology of cartilage discs	83
3.2.2 A model of cartilage catabolism in a tissue-engineered micro-pellet model	85
3.2.2.1 Experimental donor and cytokine concentration details	85
3.2.2.2 The effects of IL-1 + OSM on cartilage catabolism	85
3.2.2.3 The effects of IL-1 + OSM on MMP activity	88
3.2.2.4 Histology of micro-pellets	91
3.2.3 A model of cartilage catabolism using tissue-engineered cartilage macro-pellets	93
3.2.3.1 Experimental donor and cytokine concentration details	93
3.2.3.2 The effects of IL-1 + OSM +/- matriptase on cartilage catabolism	93
3.2.3.3 The effects of IL-1 + OSM +/- matriptase on MMP activity	96
3.2.3.4 Histology of tissue-engineered cartilage macro-pellets	99

3.3 Discussion	101
3.3.1 Tissue-engineered cartilage discs have uniform and abundant ‘cartilage-like’ features as evidenced by histology	101
3.3.2 Reliable and reproducible early proteoglycan catabolism in response to a catabolic stimulus in a tissue-engineered cartilage disc and macro-pellet model	102
3.3.3 Variable collagen catabolism in response to a catabolic stimulus in a tissue-engineered-cartilage disc model, but no such effect seen in a micro- or macro-pellet model	104
3.3.4 Significant pro-MMP and active MMP activity observed in cytokine +/- matrilase stimulated tissue-engineered cartilage disc, micro- and macro-pellet models	106
3.3.5 Summary	108
4. Chapter 4: Analysis of subchondral bone and cartilage remodelling in a murine OA model	
4.1 Introduction	109
4.2 Results	111
4.2.1 Mouse weights and subchondral bone measurements	111
4.2.1.1 Mouse weights	111
4.2.1.2 Subchondral tibial bone measurements at 4, 8, 12 and 16 weeks post DMM or sham surgery	111
4.2.2 Immunohistochemistry	113
4.2.2.1 PAR-2 up-regulation in a DMM model relative to sham	113
4.2.2.2 Matrilase immunohistochemistry	116
4.2.3 Micro-CT analysis for subchondral sclerosis	119
4.2.4 Micro-CT analysis for alterations in trabeculae within the subchondral bone	121
4.2.5 Micro-CT and histology images for osteophytes in the murine DMM model versus sham	123
4.2.6 Micro-CT analysis of osteophyte morphology	128
4.2.7 Cartilage damage assessed qualitatively and quantitatively	130
4.2.7.1 Qualitative assessment of cartilage damage	130
4.2.7.2 Quantitative OARSI cartilage damage score	133

4.2.8 Correlation analysis	135
4.2.8.1 Correlation between cartilage damage score and subchondral bone remodelling or osteophyte morphology	135
4.2.8.2 Correlation between subchondral bone remodelling and osteophyte morphology	135
4.3 Discussion	138
4.3.1 Mouse weights and tibial measurements	138
4.3.2 Up-regulation of PAR-2 in a DMM model relative to sham, but lack of ST14 staining	138
4.3.3 Subchondral sclerosis in a murine DMM model	139
4.3.4 Alterations in trabecular morphology in the murine DMM model	141
4.3.5 Osteophyte morphology in the murine DMM model	142
4.3.6 Cartilage damage in the murine DMM model	143
4.3.7 Summary	146
5. Chapter 5: Tissue-specific gene ablation of matriptase in a surgically-induced (DMM) murine OA model	
5.1 Introduction	148
5.2 Results	149
5.2.1 Confirmation of matriptase ablation	149
5.2.1.1 Semi-quantitative PCR analysis (genotyping)	149
5.2.1.2 qPCR – matriptase	150
5.2.1.3 Immunohistochemistry – matriptase	151
5.2.2 Mouse weights and subchondral bone measurements	151
5.2.2.1 Mouse weights	152
5.2.2.2 Subchondral tibial bone measurements: wild type compared to cartilage-specific matriptase ablated mice	153
5.2.3 Micro-CT analysis of subchondral sclerosis and trabecular morphology	155
5.2.3.1 Subchondral sclerosis	155
5.2.3.2 Alterations in trabecular morphology	156
5.2.4 Micro-CT and histology images for osteophytes	158
5.2.5 Micro-CT analysis of osteophyte morphology in cartilage-specific matriptase ablated mice relative to wild type	160

5.2.6 Cartilage damage in cartilage-specific matriptase ablated mice relative to wild type	162
5.2.6.1 Qualitative assessment of cartilage damage	162
5.2.6.2 Quantitative assessment of cartilage damage	163
5.2.7 Correlation analysis	163
5.3 Discussion	164
5.3.1 Confirmation of gene ablation	164
5.3.2 Mouse weights and subchondral tibial bone measurements	164
5.3.3 Does cartilage-specific ablation of matriptase confer any protection against cartilage degradation and subchondral bone remodelling?	165
5.3.4 Cartilage-specific matriptase ablation effects osteophyte morphology	166
5.3.5 Summary	167
6. Chapter 6: Tissue-specific gene ablation of PAR-2 in a surgically induced (DMM) OA murine model	
6.1 Introduction	168
6.2 Results	169
6.2.1 Confirmation of PAR-2 ablation in a murine OA model	169
6.2.1.1 Semi-quantitative PCR analysis (genotyping)	169
6.2.1.2 qPCR (PAR-2)	170
6.2.1.3 Immunohistochemistry (PAR-2)	171
6.2.2 Mouse weight and subchondral bone measurements	174
6.2.2.1 Mouse weights	174
6.2.2.2 Subchondral tibial bone measurements: tissue-specific PAR-2 ablated mice compared to wild type	175
6.2.3 Micro-CT analysis of subchondral sclerosis and trabecular morphology	178
6.2.3.1 Cartilage-specific PAR-2 ablated mice	178
6.2.3.1.1 Subchondral sclerosis	178
6.2.3.1.2 Alterations in trabecular morphology	179
6.2.3.2 Bone-specific PAR-2 ablated mice	181
6.2.3.2.1 Subchondral sclerosis	181

6.2.3.2.2 Alterations in trabecular morphology	182
6.2.4 Micro-CT and histology images for osteophytes	184
6.2.5 Micro-CT analysis of osteophyte morphology in tissue-specific PAR-2 ablated mice relative to wild type	187
6.2.5.1 Cartilage-specific PAR-2 knock-out mice	187
6.2.5.2 Bone-specific PAR-2 knock-out mice	187
6.2.6 Cartilage damage in tissue-specific PAR-2 ablated mice relative to wild type	190
6.2.6.1 Qualitative assessment of cartilage damage	190
6.2.6.2 Quantitative assessment of cartilage damage	192
6.2.7 Correlation analysis	192
6.3 Discussion	194
6.3.1 Confirmation of gene ablation	194
6.3.2 Mouse weights and subchondral bone measurements of the transgenic mice compared to wild type	195
6.3.3 Does cartilage-specific gene ablation of PAR-2 confer any protection against cartilage degradation or subchondral bone remodelling?	195
6.3.4 Does bone-specific gene ablation of PAR-2 confer any protection against cartilage degradation of subchondral bone remodelling?	197
6.3.5 Cartilage-specific PAR-2 ablation effects osteophyte morphology	198
6.3.6 Summary	198
7. Chapter 7: General discussion	
7.1 Perspective	200
7.2 Tissue-specific ablation of PAR-2 confers some protection against abnormal subchondral bone remodelling and cartilage degradation, but should cartilage or bone be targeted with therapeutics?	200
7.3 Cross-talk between cartilage and subchondral bone in the progression of OA is not a prerequisite for cartilage damage to occur	203
7.4 The effects of tissue-specific PAR-2 ablation on osteophyte development and maturation	204
7.5 PAR-2 and musculoskeletal ageing	205

7.6 Potential use of biomarkers to detect early stage OA	205
7.7 Human-derived cartilage model of catabolism	206
7.8 Future work	207
7.9 Key findings of this study	208
8. Appendices	
Appendix A Floxed PAR-2 (F2rl1) allele	210
Appendix B Wild type PAR-2 allele	224
Appendix C Measurement of subchondral sclerosis separating the subchondral plate from the underlying trabecular bone	229
Appendix D Genotyping	230
9. References	237

List of figures and tables

Chapter 1

Figure 1.1 Representation of knee OA	5
Figure 1.2 Structure of cartilage	8
Figure 1.3 Structure of aggrecan	10
Figure 1.4 Micro-CT representation of murine subchondral tibial bone	11
Figure 1.5 Osteophyte images on micro-CT and histology	14
Figure 1.6 Micro-CT representation of subchondral sclerotic bone	16
Figure 1.7 Structural features and mechanism of PAR-2 activation	21
Table 1.1 The 5 main groups of matrix-metalloproteinases	25
Figure 1.8 Matriptase role in collagen breakdown	30

Chapter 2

Figure 2.1 F2rl1 vector design	37
Figure 2.2 Diagram of mouse knee joint	39
Table 2.1 Table of primers used for genotyping	47
Figure 2.3 Orthogonal images on dataviewer for analysis	57
Figure 2.4 Volume of interest for analysis of medial aspect of tibial subchondral bone	58
Figure 2.5 Coronal cross-sectional images of tibial medial epicondyle to define ROI to analyse subchondral sclerosis	59
Table 2.2 Parameters for analysis for subchondral thickening at the medial and lateral epicondyles	59
Figure 2.6 Coronal cross-sectional images of tibial medial epicondyle to define ROI to analyse subchondral trabecular bone	60
Figure 2.7 Coronal cross-sectional images of tibial medial epicondyle to define ROI as one region	61
Figure 2.8 Volume of interest for analysis of tibial subchondral bone for osteophyte analysis	61
Figure 2.9 ROI for tibial osteophyte analysis	62
Table 2.3 Parameters for tibial osteophyte analysis	62
Figure 2.10 Micro-CT representation of murine tibia for bone measurements	63
Figure 2.11 Micro-CT representation of murine tibia for bone measurements	63
Table 2.4 Donor characteristics	64

Chapter 3

Figure 3.1-3.2 Assessment of proteoglycan and collagen release in response to a cytokine stimulus	76-78
Figure 3.3 Assessment of proteoglycan and collagen release in response to a cytokine stimulus +/- matriptase	79
Figure 3.4 Assessment of proteoglycan and collagen release in response to a cytokine stimulus	80
Figure 3.5 Assessment of MMP activity in response to a cytokine stimulus +/- matriptase	82
Figure 3.6 Histology representation of cartilage discs	84
Figure 3.7-3.8 Assessment of proteoglycan release in response to a cytokine stimulus	86-87
Figure 3.9-3.10 Assessment of MMP activity in response to a cytokine stimulus	89-90
Figure 3.11 Histology representation of cartilage micro-pellets	92
Figure 3.12 Assessment of proteoglycan release in response to a cytokine stimulus	94
Figure 3.13 Assessment of proteoglycan release in response to a cytokine stimulus +/- matriptase	95
Figure 3.14 Assessment of MMP activity in response to a cytokine stimulus	97
Figure 3.15 Assessment of MMP activity in response to a cytokine stimulus +/- matriptase	98
Figure 3.16 Histology of cartilage macro-pellets	100

Chapter 4

Figure 4.1-4.2 Tibial bone measurements	112-113
Figure 4.3 Immunohistochemistry PAR-2 in wild type DMM or sham mice	114
Figure 4.4 Immunohistochemistry PAR-2 in wild type naïve mice	115
Figure 4.5 Immunohistochemistry ST14 in wild type DMM or sham mice	117
Figure 4.6 Immunohistochemistry ST14 in wild type naïve mice	118
Figure 4.7 Measurement of subchondral sclerosis in the wild type murine OA model	120
Figure 4.8 Measurement of trabecular morphology in the wild type murine OA model	122

Figures 4.9-4.12 Micro-CT and histology representation of osteophytes in the murine DMM model (4, 8, 12 and 16 weeks post-surgery)	124-127
Figure 4.13 Micro-CT analysis of osteophyte morphology	129
Figures 4.14-4.15 Histology representation of cartilage damage on the medial aspect of the tibia (4, 8, 12 and 16 weeks post-surgery)	131-132
Figure 4.16 Quantitative assessment of cartilage damage	134
Figure 4.17-4.18 Correlation analysis	136-137
Chapter 5	
Figure 5.1 Quantitative PCR (ST14)	150
Figure 5.2 Weights of wild type and cartilage-specific matriptase ablated mice	152
Figure 5.3 Subchondral tibial bone measurements	154
Figure 5.4 Measurement of subchondral sclerosis in wild type and cartilage-specific ST14 ablated mice	155
Figure 5.5 Measurement of trabecular morphology in wild type and cartilage-specific ST14 ablated mice	157
Figure 5.6 Osteophyte representation of cartilage-specific ST14 knock-out mice	159
Figure 5.7 Analysis of osteophyte morphology, comparing cartilage-specific ST14 ablated mice to wild type mice	161
Figure 5.8 Qualitative assessment of cartilage damage	162
Figure 5.9 Quantitative assessment of cartilage damage	163
Chapter 6	
Figure 6.1 Quantitative PCR analysis of PAR-2	170
Figure 6.2 Immunohistochemistry (PAR-2) in wild type, cartilage-specific and bone-specific PAR-2 ablated DMM mice	172
Figure 6.3 Immunohistochemistry (PAR-2) in wild type, cartilage-specific and bone-specific PAR-2 ablated sham mice	173
Figure 6.4 Mouse weights of wild type and tissue-specific PAR-2 ablated mice	174
Figure 6.5 Subchondral tibial bone measurements; cartilage-specific PAR-2 ablated strain	176
Figure 6.6 Subchondral tibia bone measurements; bone-specific PAR-2	177

ablated strain	
Figure 6.7 Measurement of subchondral sclerosis in wild type and cartilage-specific PAR-2 ablated mice	178
Figure 6.8 Measurement of trabecular morphology in wild type and cartilage-specific PAR-2 ablated mice	180
Figure 6.9 Measurement of subchondral sclerosis in wild type and bone-specific PAR-2 ablated mice	181
Figure 6.10 Measurement of trabecular morphology in wild type and bone-specific PAR-2 ablated mice	183
Figure 6.11 Osteophyte representation of cartilage-specific PAR-2 knock-out mice	185
Figure 6.12 Osteophyte representation of bone-specific PAR-2 knock-out mice	186
Figure 6.13 Analysis of osteophyte morphology; cartilage-specific PAR-2 ablated mice and wild type mice	188
Figure 6.14 Analysis of osteophyte morphology; bone-specific PAR-2 ablated mice and wild type mice	189
Figure 6.15 Qualitative assessment of cartilage damage	191
Figure 6.16 Quantitative assessment of cartilage damage	193
Chapter 8	
Figure 8.1 Base pair product size of floxed and non-floxed PAR-2 allele	210
Figure 8.2 Floxed PAR-2 allele	223
Figure 8.3 Wild type PAR-2 allele	228
Figure 8.4 Measurement of subchondral sclerosis in a wild type murine OA model	229
Figure 8.5 Semi-quantitative PCR for floxed ST14 allele	230
Figure 8.6 DNA reference ladder	230
Figure 8.7 Semi-quantitative PCR (genotyping) cartilage-specific matriptase exon 2 ablated mice	231
Figure 8.8 Semi-quantitative PCR floxed PAR-2 allele	232
Figure 8.9 Semi-quantitative PCR cartilage-specific PAR-2 exon 2 ablated mice	233
Figure 8.10 Semi-quantitative PCR floxed PAR-2 allele	234

Figure 8.11 Semi-quantitative PCR col2;cre	235
Figure 8.12 DNA reference ladder	235
Figure 8.13 Semi-quantitative PCR oc;cre	236
Figure 8.14 DNA reference ladder	236

Abbreviations

ACLT	Anterior cruciate ligament transection
ADAMTS	A disintegrin and metalloproteinase with thrombospondin motif
ADL	Activities of daily living
AGEs	Advanced glycation end products
AlkP	Alkaline phosphatase
ALN	Alendronate
AMC	GP-7- amino-4-methoxy coumarin
AP-1	Activator protein 1
APMA	4-aminophenylmercuric acetate
BAC	Bacterial artificial chromosome
Bach1	BTB Domain And CNC Homolog 1
BMD	Bone mineral density
BMI	Body mass index
BNC	Bovine nasal cartilage
BSA	Bovine serum albumin
BV/TV	Bone Volume/Tissue Volume
CBC	Comparitive Biology Centre
CCD	Charge coupled device
Col2	Collagen type II
CTX-II	Carboxy-Terminal Telepeptides of Type II collagen
CUB	Complement proteases C1r/C1s-urchin embryonic growth factor-bone morphogenetic protein
DAB	Dimethylaminobenzaldehyde
DMB	Dimethylmethylene Blue
DMM	Destabilisation of the medial meniscus
DNA	Deoxyribonucleic acid
dNTP	Deoxyribonucleotide triphosphate
DPBS	Dulbecco's phosphate buffered saline
DTT	Dithiothreitol
E4BP4	Nuclear factor, interleukin 3 regulated – NFIL3
ECM	Extracellular matrix
EDTA	Ethylenediaminetetraacetic acid

ES cells	Embryonic stem cells
F2RI1	Proteinase activated receptor-2
FGF	Fibroblast growth factor
FRT	Flippase recognition target
GAG	Glycosaminoglycan
GDP	Guanosine diphosphate
GH	Growth hormone
GPCR	G-protein coupled receptor
GTP	Guanosine triphosphate
HAI-1	Hepatocyte growth factor activator inhibitor
H&E	Haematoxylin and Eosin
hMSC	Human mesenchymal stem cell
HRT	Hormone replacement therapy
IL-1	Interleukin-1
IGD	Interglobular domain
IGF-1	Insulin-like growth factor-1
IHC	Immunohistochemistry
IMPC	International Mouse Phenotype Consortium
JNK	c-Jun N-terminal kinase
LCR-F1	Locus control region factor 1
LDL	Low density lipoprotein
MAPK	Mitogen-activated protein kinase
MIA	Mono-iodine-acetate
Micro-CT	Micro-computed tomography
MLI	Meniscal-ligamentous injury
MMP	Matrix metalloproteinase
MMTL	Medial menisco-tibial ligament
MRG	Musculoskeletal Research Group
MRI	Magnetic resonance imaging
MSCGM	Mesenchymal stem cell growth medium
MT-MMP	Membrane bound MMP
MTP	Medial tibial plateau
NACWO	Named Animal Care and Welfare Officer

NF kappa B	Nuclear factor kappa-light-chain-enhancer of activated B cells
NHS	National Health Service
NOF	Neck of femur
OA	Osteoarthritis
OARSI	Osteoarthritis Research Society International
OC	Osteocalcin
ODD	Object detector distance
OHP	Hydroxyproline
OP	Osteoporosis
OPG	Osteoprotegerin
OSM	Oncostatin-M
PAR-2	Proteinase activated receptor-2
PBS	Phosphate buffer solution
PBV	Percentage Bone Volume
PCR	Polymerase chain reaction
Pro-uPA	Pro-urokinase-type plasminogen activator
PTH	Parathyroid hormone
qPCR	Quantitative Polymerase Chain Reaction
RAGE	Receptor for advanced glycation end products
RANKL	Receptor activator of nuclear factor kappa-B ligand
RNA	Ribonucleic Acid
ROI	Region of interest
RT-PCR	Reverse Transcription Polymerase chain reaction
SD	Standard deviation
SE	Standard error
SEA	Sperm protein-enteropeptidase-agrin
SERM	Selective oestrogen-receptor modulator
SOD	Source object distance
SPECT	Single-photon emission computed tomography
ST14	Matriptase
STAT	Signal transducer and activator of transcription
TbN	Trabecular Number
TbSp	Trabecular Separation

TbTh	Trabecular thickness
TGF- β	Transforming growth factor-beta
TIMP	Tissue inhibitor of metalloproteinase
TM	Transmembrane
TNF- α	Tumour necrosis factor alpha
TTSP	Type II transmembrane serine proteinases
UV	Ultraviolet
VEGF	Vascular endothelial growth factor
VOI	Volume of interest
Zip 8	A zinc importer involved in zinc homeostasis and activation of matrix-degrading enzymes

Chapter 1: Introduction

1.1 Ageing and the musculoskeletal system

Due to improved healthcare the population is slanting towards an older demographic with the percentage of people aged over 65 and 85 years of age expected to increase by 107% and 133%, respectively, by 2030 [2]. Naturally, as people age their organ systems become less effective and pathology can arise from ageing. This is apparent in the musculoskeletal system whereby musculoskeletal disorders are the most frequently reported in the elderly population [3]. Among the most common musculoskeletal disorders in the elderly are sarcopenia (muscular atrophy), osteoporosis (OP) and osteoarthritis (OA). These disorders can cause limitations of activities in older people with 5.7% of those aged 65-75 unable to perform 1 or more of 5 basic activities of daily living (ADL) such as dressing and eating, increasing to 10.8% in those aged 75-84 [4, 5]. Due to this, musculoskeletal disorders have public health implications with physical and social impacts from pain and reduced quality of life, expenditure on diagnosis and treatment and indirect costs from inability to work [3-5]. The musculoskeletal system is composed of muscle, tendon, fascia, bone and cartilage, which are interconnected biomechanically, biochemically and micro-structurally [6]. Ageing of the musculoskeletal system is a risk factor for the development of OA [4, 7], and this will be explored further looking specifically at each component of the musculoskeletal system.

1.1.1 How ageing impacts on different components of the musculoskeletal system

1.1.1.1 Skeletal muscle

Normally, skeletal muscle is quiescent but has marked regenerative ability due to the presence of muscle stem cells (satellite cells) [8]. However, as people age this regenerative ability declines and muscles decrease in strength, size, endurance and weight. By the age of 70 the muscles have lost 40% of their mass and reduced 30% in strength, manifesting as sarcopenia [9]. As people age there are morphological alterations in muscle where the muscle tissue is replaced by adipose and fibrotic tissue so

muscle contains more non-contractile tissue, which impacts on muscular strength [10]. Subsequently this loss of muscular strength has a negative effect on the stability of joints, such as the knee, predisposing to OA and falls [3, 6].

1.1.1.2 Tendons

Tendons connect muscle to bone and are fibrous connective tissue bands composed mainly of collagen. Other components include decorin, biglycan and lumican which act together to lubricate and organise collagen fibre bundles in a highly organised structure. With ageing this organised structure is disrupted due to enzymatic and non-enzymatic cross-linking of collagen fibres, causing an aberrant collagen structure, a less stable tendon with progressive degradation. Damaged tendons have little capacity to fully recover and impact on the stability of the joint as people age increasing the risk of joint pathology such as OA [11, 12].

1.1.1.3 Bone

Bone development during the embryonic period is either by intramembranous ossification or endochondral ossification, forming flat bones or long bones, respectively. In total, there are 206 bones in the human skeleton with the majority being long bones. The skeleton shapes the body, allows movement, protects soft organs and provides muscle attachment for movement. Structurally, bone is composed of cortical and trabecular bone with osteoblasts, osteoclasts and osteocytes involved in bone formation, bone resorption and mechano-sensitivity, respectively. In women, the human skeleton grows until the age of 18 (21 in men) with nearly 90% of adult skeletal mass obtained by the end of the teenage years. The peak bone mass obtained by the age of 30 can be maintained but not built [3, 6]. At this stage there is a net loss of bone tissue due to an imbalance between bone absorption and bone formation, accounting for a 1% loss of bone mass per year after the age of 35 in men and 2-3% loss after menopause in women [13]. The main reason for this loss of bone mass is due to a decrease in circulating estradiol, decreasing by 85% in women after the menopause and by 47% during the lifespan of males [13, 14]. Also contributing to this loss of bone mass is a decline in the production of growth hormone (GH) which decreases by 14% per decade in men and

women, causing a decrease in insulin-like growth factor (IGF)-1 and IGF-2 correlating with a reduced bone mineral density (BMD) and increased hip fracture risk [15, 16].

Subsequently, many older people develop OP characterized by low BMD and micro-architectural deterioration of bone tissue resulting in an increased risk of fractures [12]. This reduction in BMD as people age also impacts on joints, where OA is more prevalent in people with a low BMD, prevented with a bisphosphonate such as alendronate [17].

1.1.1.4 Cartilage

Cartilage is essential to deal with compressive loads, lubrication and transmission of the load to the underlying subchondral bone and all this depends on its complex structure [18, 19]. The structure of cartilage and its function are discussed in more detail in section 1.3.1, but here the focus is on how cartilage changes with age and the impact this has on predisposing to diseases such as OA. The main changes occurring in cartilage due to ageing are:

- 1) A catabolic state due to a loss of sensitivity to IGF-1 and transforming growth factor-beta (TGF- β), which are anabolic growth factors [20, 21]. Also with ageing there is an increase in AGEs (advanced glycation end products) and RAGE (receptor for advanced glycation end products) in chondrocytes [22, 23], which upon activation stimulates catabolic signaling pathways, resulting in up-regulation of pro-inflammatory cytokines, a disintegrin and metalloproteinase with thrombospondin motif (ADAMTS) and matrix-metalloproteinases (MMPs) resulting in cartilage degradation [24, 25].
- 2) A change in the structure of the extracellular matrix (ECM), due to chondrocytes having a reduction in synthetic activity, resulting in a net loss of proteoglycans [7]. Also calcification of cartilage occurs, which can have functional effects on the transmission of load to the underlying subchondral bone, discussed further in section 1.5 [26, 27].

So, it is clear from the effects that ageing has on all components of the musculoskeletal system that pathology commonly arises, such as OA. One conservative treatment to prevent OA is undertaking regular physical activity.

1.1.2 Physical activity and the musculoskeletal system

Regular physical activity benefits all components of the musculoskeletal system and has preventative effects on OA. Both skeletal muscle and bone are positively affected by exercise [28]. The reduction in muscle mass caused by ageing is prevented, and the strength and aerobic capacity of muscle is improved in the elderly who take part in regular exercise [29-31]. The improved quadriceps strength stabilises the knee joint and prevents development of OA [3]. The other main benefit of exercise on the musculoskeletal system is that repetitive weight bearing on bones caused by exercise maintains BMD, hence preventing OP and fractures [32], and also perhaps prevents the development of OA [17]. There of course needs to be caution in the elderly undertaking exercise as skeletal muscle is damaged more easily in the elderly increasing the risk of injury. Encouraging the older population to undertake exercise will maintain the integrity of the musculoskeletal system aiding in the performance of daily activities and maintenance of independence in years to come [3, 11, 28].

1.2 Osteoarthritis (OA)

OA is the most common joint disease in the world with two-thirds of the population older than 60 years of age suffering from this disabling disease. Not only does OA cause significant pain and disability to those affected, it also carries a huge health expenditure in Western healthcare systems such as the National Health Service (NHS) which is likely to increase in the future with an ageing population [7, 33]. OA is thought of as a syndrome consisting of joint pain, stiffness and associated functional problems having a significant impact on quality of life [7]. Any joint can be affected, however typically the knee, hands or hip are affected [34]. The pathogenesis of OA is multifactorial involving the articular cartilage, subchondral bone, ligaments, capsule, synovial membrane and periarticular muscles [7]. Typically, an osteoarthritic joint displays progressive damage of articular cartilage and subchondral bone remodelling with osteophyte formation. In addition, synovial inflammation, fibrosis of ligaments, tendons, menisci and capsules can be found (see figure 1.1) [34]. OA can be divided into primary and secondary, the latter developing due to trauma to the joint. In its later stages OA is classically characterized by focal cartilage degradation, involvement of subchondral bone and synovium and the formation of osteophytes. Typical radiological findings in late stage OA include joint-space

narrowing, osteophytes, subchondral bone thickening or sclerosis, subchondral bone cyst formation and calcification of areas of hyaline cartilage (figure 1.1) [7].

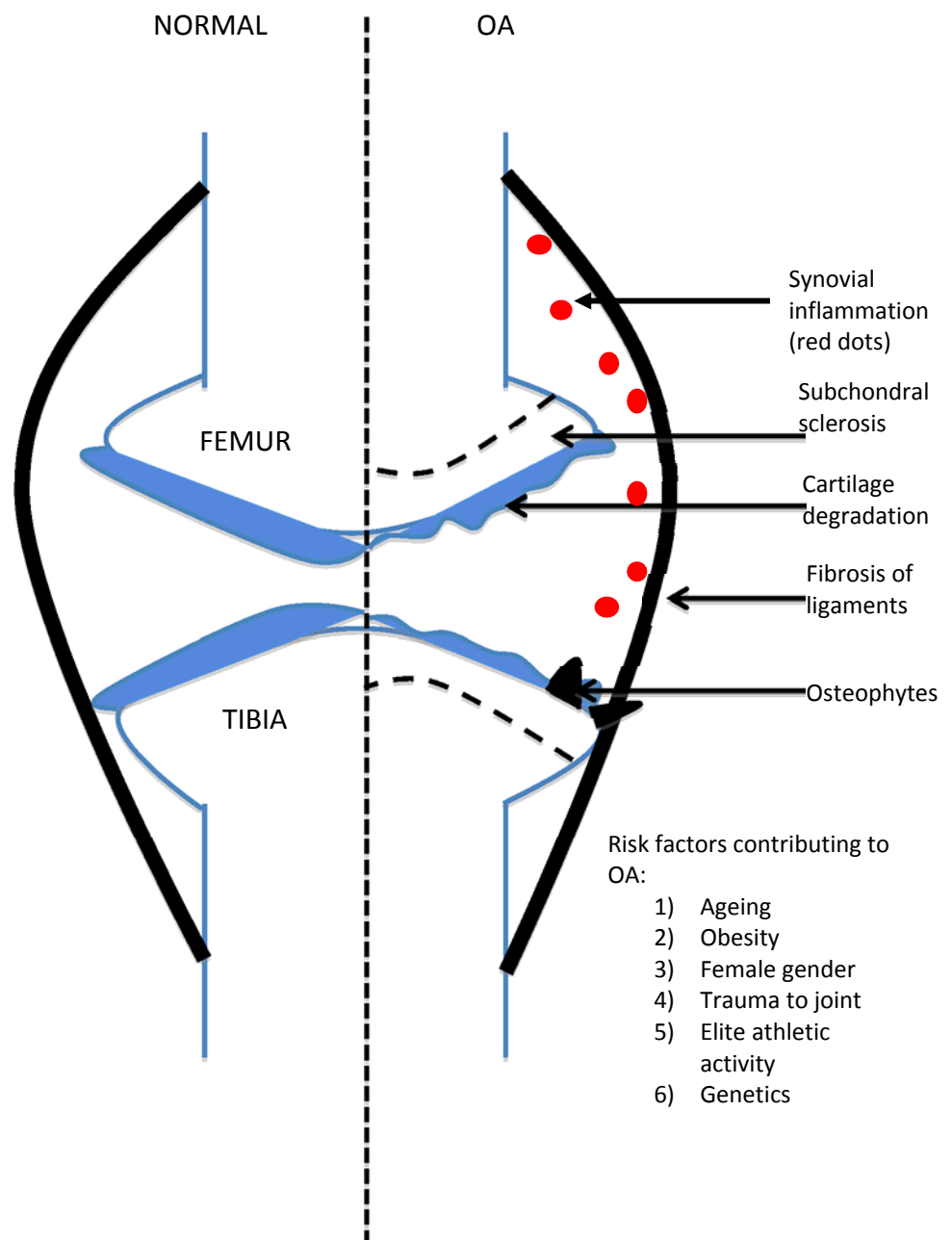


Figure 1.1: Representation of knee OA. The characteristic features of OA in the knee, including subchondral sclerosis, cartilage degeneration, osteophyte formation and fibrosis of ligaments. In addition there is also a degree of synovitis in OA. The main risk factors for the development of OA are also highlighted.

As suggested in figure 1.1, there are a number of risk factors contributing towards OA. Genetic factors are known to contribute towards acquisition of OA [35]. However, the combination of genetics and environmental factors have a complex interplay in the pathogenesis of OA, and in most cases these two factors interact initiating OA. It is well known that obesity contributes towards OA, however it is less well defined whether this is due to the increased weight bearing on joints or fat-derived hormones [36, 37]. Other risk factors include female gender, with an increased risk of OA following menopause [38]. Also joint alignment abnormalities, trauma and elite athletic activity disturb the mechanical loading of the joint causing initiation of OA [39, 40]. Increased age (as discussed in section 1.1) also contributes towards OA development [7, 38]. Due to the disability and economic impact of OA it is important to find treatments and cures. To date, there is no known treatment that prevents OA or cures late stage OA. The main treatments available are pharmacological therapy to help alleviate pain with analgesia and non-pharmacological therapy such as losing weight, aids and equipment such as altered footwear and introducing gentle exercise [33, 41]. Surgery is the last stage in the treatment of OA, and finding a strategy to prevent or at least further delay late stage OA would be extremely beneficial. It is important to find new and innovative therapies to cure or prevent OA, which would not only improve quality of life of sufferers but also reduce the NHS expenditure on OA [42].

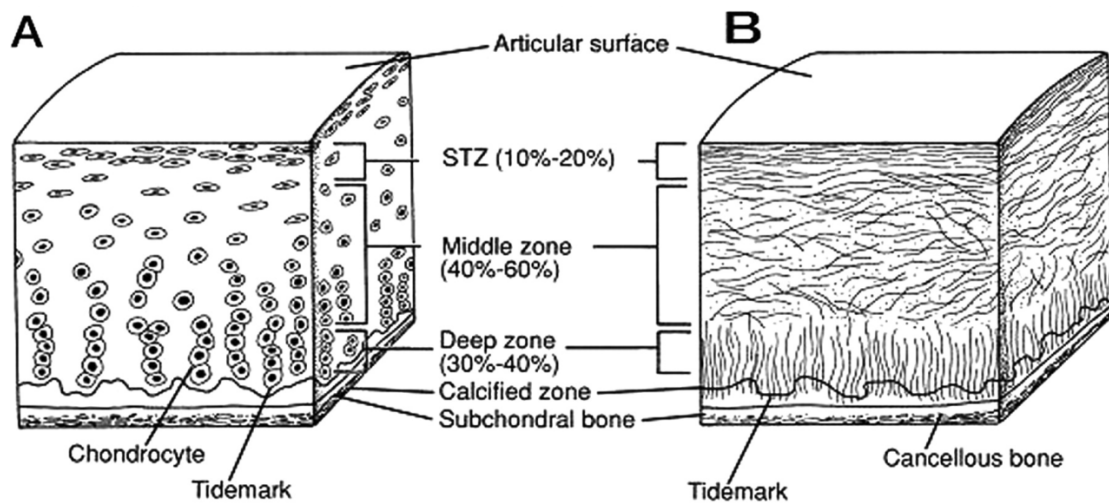
1.3 Cartilage and subchondral bone

1.3.1 Cartilage

Articular cartilage is hyaline cartilage and is a crucial component of the knee, hip and hand joints providing a smooth, lubricated surface for articulation and transmission of loads. These joints are commonly affected by OA, however the main focus of this project involves the knee joint. It is worth recognising that the genes and signalling pathways in knee OA compared to hip OA are very different and so one cannot necessarily correlate findings in knee OA to hip OA. The knee joint is a functional unit consisting of the femur, tibia and fibula, connecting ligaments, muscle, soft tissue and hyaline cartilage [7]. The articular cartilage is at the centre of this functional unit and plays an important role in load transfer across the joint, and is implicated in the pathogenesis of OA, along with the

underlying subchondral bone and synovial joint lining [43]. Hyaline cartilage is present at the ends of the femur, tibia and fibula lying underneath the menisci, and interplays with the subchondral bone in load transfer across the joint. The thickness of the cartilage at the knee joint is roughly 6.0-6.4 mm in humans, but varies in other joints depending on its size [7]. The only cell type present in cartilage is the chondrocyte, which make up 1-10% of the tissue volume. Chondrocytes produce the ECM, which is composed of roughly 70% water, 15-20% type II collagen and 3-10% hydrophilic sulphated proteoglycans. These components of cartilage play a vital role in retaining water in the ECM, which helps maintain its mechanical properties. Preserving this organized architecture of cartilage is important in maintaining the function of cartilage [44-46]. Due to the cartilage having no blood vessels the chondrocytes get their nutrition from the surrounding synovial fluid by diffusion through the ECM. In addition to having no blood vessels, cartilage also has no lymphatic or nerve supply, which contributes towards articular cartilage having limited ability for intrinsic healing and repair [47, 48].

Cartilage is divided into four zones: superficial, middle, deep and calcified layers, each with a different organization of chondrocytes and collagen, as shown in figure 1.2. The superficial zone is the thinnest layer and provides most of the tensile properties of cartilage. This characteristic is due to the superficial zone having the highest content of collagen (type II and IX), which runs parallel to the articular surface [46, 49]. The chondrocytes in this zone are flattened. The middle zone is the thickest and has radial bundles of thick collagen and spherical chondrocytes [49]. This region has the highest content of proteoglycans, compared to the superficial and deep zones [46]. In the deep zone the chondrocytes and collagen fibers are arranged perpendicular to the articular surface. This zone contains the lowest density of chondrocytes [49]. As shown in figure 1.2, the tidemark separates the deep zone from the calcified zone. In the deep zone the chondrocytes are hypertrophic [49].



A) Diagram of chondrocyte arrangement in cartilage B) Diagram of collagen arrangement in cartilage

Figure 1.2: Structure of cartilage. There are 4 zones of cartilage with different arrangements of chondrocytes and collagen as described:

- 1) STZ – superficial zone, where collagen runs parallel to articular surface (B) and chondrocytes are flattened (A)
- 2) Middle zone – containing radial bundles of thick collagen (B) and spherical chondrocytes arranged in radial columns (A)
- 3) Deep zone – collagen fibres perpendicular to articular surface (B) and chondrocytes arranged in columns, parallel to collagen fibres (A)
- 4) Calcified zone separated from deep zone by tidemark (A and B)

This structure of cartilage changes considerably in OA as detailed in text. Taken from Buckwalter et al. [44, 48]

1.3.1.1 Chondrocytes

These specialised cells originating from mesenchymal stem cells are the resident cell in articular cartilage and are involved in the development, maintenance and repair of the ECM [50]. The size, morphology, number and metabolic activity of chondrocytes varies depending on which zone of cartilage they are found in. The greatest density of chondrocytes are found in the superficial zone. This is in contrast to the deep zone where the lowest density of chondrocytes are found [50]. Chondrocytes do not form cell-to-cell contacts for direct signalling, however they do have transmembrane-receptors, which enable ECM synthesis and maintenance, controlled by various stimuli such as growth factors, mechanical loads and hydrostatic pressures. Depending on the stimulus, chondrocytes can have a catabolic or anabolic effect on cartilage [51, 52]. Despite the specialised activity of chondrocytes, they have limited ability to replicate impacting on healing of cartilage in response to injury [48, 53].

1.3.1.2 Extracellular matrix (ECM)

The cartilage ECM is composed mainly of type II collagen and proteoglycans, in particular aggrecan [54]. There is also a significant amount of water in the ECM (interstitial fluid) mainly contained in the superficial zone, which plays a role in the nutrition of the cartilage and its ability to withstand significant loads [46].

Collagens

Type II collagen is the major macromolecule of articular cartilage representing 90-95% of collagen in the ECM. Other types of collagen present include collagen types I, IV, V, VI, IX and XI but in minor proportions. Type II collagen form fibres and fibrils intertwined with proteoglycans and the minor collagens stabilise the type II collagen network. Acting together collagens help with the mechanical properties of the cartilage by providing tensile stiffness and strength [49, 55].

Type II collagen consists of 3 identical polypeptide chains (α -chains) that intertwine forming a triple helix. The α -chains are initially synthesised as pro- α -chains with propeptides at both their N and C termini. These propeptides are later removed by proteolysis after secretion into the ECM forming 2 types of type II procollagen – type IIA procollagen and type IIB procollagen. The predominant form present in cartilage is type IIB procollagen. The resulting amino acid composition of polypeptide chains is mainly glycine and proline, with hydroxyproline forming hydrogen bonds along the molecule providing stability. The collagen fibrils are formed by aldimine-derived crosslinks between collagen molecules. These fibrils can resist tensile forces and thermal or mechanical dissociation. The type II collagen molecule is resistant to most proteases except the matrix metalloproteinases (MMPs) namely MMP-1, MMP-8 and MMP-13 [49, 55].

Type XI collagen represents about 3% of total collagen in articular cartilage. It is synthesised and secreted similar to type II collagen as a procollagen, but only the C-propeptide is proteolytically removed. Type XI collagen molecules form fibrils in association with type II collagen molecules. Type IX collagen forms 1% of the total collagen found in articular cartilage and is composed of 3 different α -chains forming a

heterotrimeric molecule. The type IX collagen molecules crosslink with type II collagen molecules via aldimide-derived crosslinks providing mechanical strength.

The other types of collagen are found in lesser amounts but provide important structural organisation in articular cartilage giving important shear and tensile properties stabilising the matrix [55].

Proteoglycans

A proteoglycan is a protein that has glycosaminoglycan (GAG) chain attached to it, which can be chondroitin sulphate, keratan sulphate, or dermatan sulphate. Aggrecan, the most abundant proteoglycan in cartilage contains two GAG chains – chondroitin sulphate and keratan sulphate, as shown in figure 1.3. The negative charge of the sulphate groups contained in the GAG chains attracts ions such as sodium and potassium contained in the interstitial fluid, and so proteoglycans play an important role in maintaining hydration of cartilage, and its ability to withstand forces during articulation [56].

The structure of aggrecan includes three globular domains – G1, G2 and G3, with a GAG attachment region separating G2 and G3. Aggrecan is found as large aggregates containing many aggrecan monomers bound to hyaluronan (HA) via its G1 domain. A small glycoprotein (link protein) homologous to the N-terminal of aggrecan, helps stabilise the aggrecan aggregates [56] (figure 1.3).

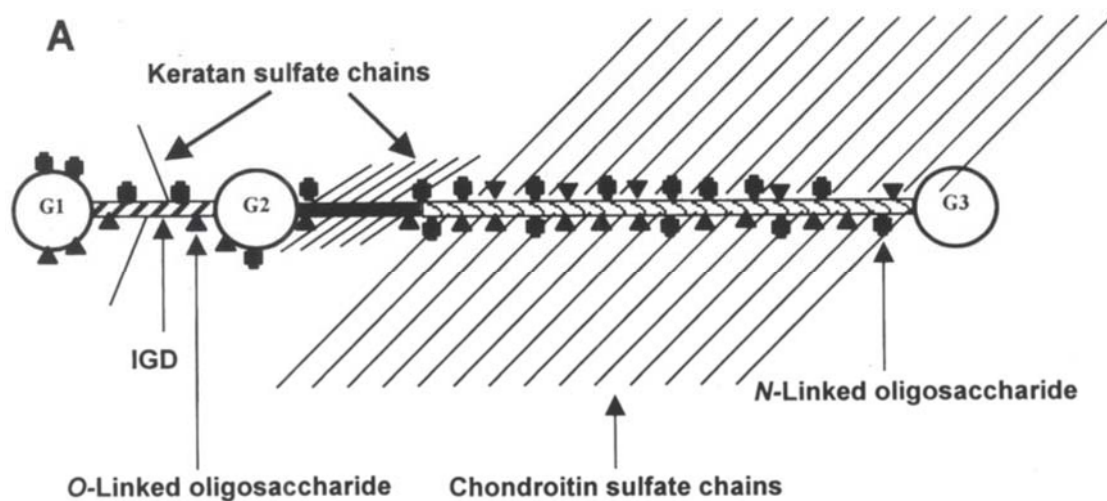


Figure 1.3: Structure of aggrecan. Aggrecan structure showing its three globular domains, intraglobular domain (IGD) separating G1 and G2, and large GAG attachment region between G2 and G3. G1 can bind to HA forming aggregates along with link protein. Taken from Kiani et al. [57]

Other proteoglycans found in cartilage include decorin, biglycan and fibromodulin, which are leucine-rich proteoglycans. They differ in GAG composition compared to aggrecan, with decorin and biglycan containing chondroitin/dermatan sulphate chains and fibromodulin having keratan sulphate chains. Decorin and fibromodulin can bind to collagen types I and II, and so are thought to play roles in organising the ECM. Biglycan does not bind to collagen and its function is not known [56].

1.3.2 Subchondral bone

Initially, OA was thought of primarily as a disease of cartilage however it is now known that subchondral bone plays an important role in the pathogenesis of OA [41, 43].

Subchondral bone (also known as peri-articular bone) is a layer of dense bone and can be divided into three layers: the subchondral bone plate, the subchondral trabecular bone and the bone at the joint margins (where osteophytes develop via endochondral ossification) (figure 1.4).

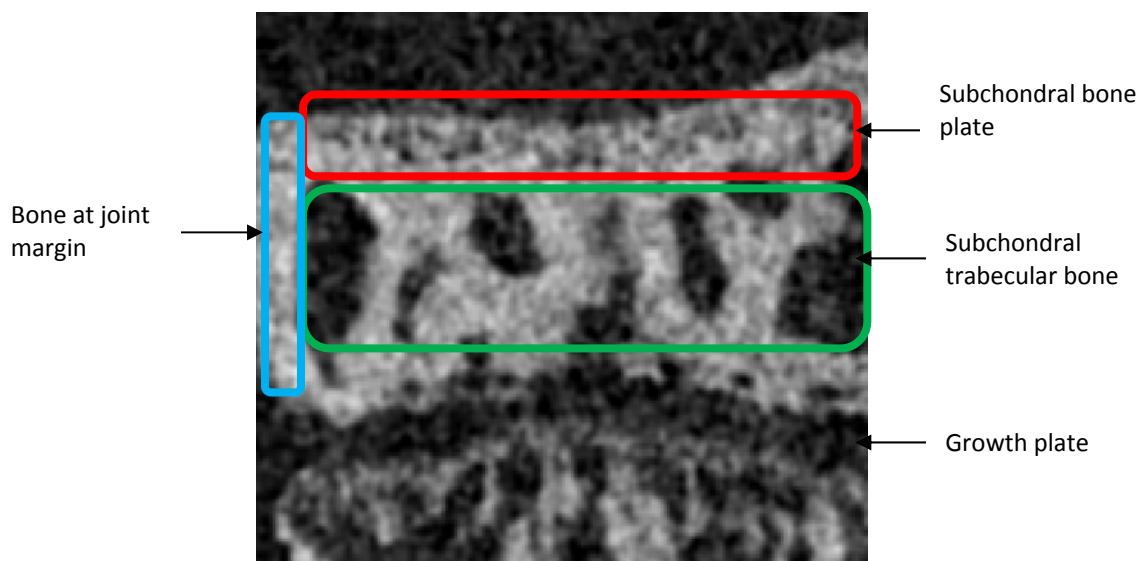


Figure 1.4: Micro-CT representation of murine subchondral tibial bone. The red region represents the subchondral bone plate. Green region represents subchondral trabecular bone, and the blue region represents bone at the joint margin. The growth plate is also highlighted.

The subchondral bone plate is made up of cortical bone, which is poorly vascularized and nonporous. This subchondral bone region is closely related to the overlying cartilage and plays a crucial role in load transmission [41, 58]. Subchondral bone provides most cushioning to the joint as it is more abundant and has a low modulus of elasticity compared to articular cartilage [58, 59]. Due to subchondral bone having an important

shock-absorbing and supportive function in joints, it is known to be a crucial component in normal joint protection. Not only does subchondral bone supply nutrients to cartilage, it can absorb about 30% of the joint load, providing a crucial base for joint cartilage [42]. Depending on the location of the joint and the amount of load bearing, the thickness of the subchondral bone varies. For example, the subchondral bone would be thicker in central weight bearing joints, such as the knee.

In the subchondral trabecular bone the trabeculae are orientated in different directions, which results in different mechanical properties depending on the plane of loading [41, 42]. Another important feature of subchondral bone is providing an incongruent joint surface. This enables the center of the joint to move axially during loading, transmitting stresses to the cortical bone whilst maintaining nourishment to the superficial layer of articular cartilage [59]. Pathological forces (perhaps due to obesity) may affect the incongruous joint shape and cushioning ability of subchondral bone thus altering the physiological balance in the joint [59]. Subchondral bone consists of type I collagen fibrils, which are cross-linked by pyridinoline and are the main organic component of bone. The three cell types present in subchondral bone are osteocytes, osteoblasts and osteoclasts. Osteocytes are normally quiescent but respond to mechanical stimuli by activating osteoblasts and osteoclasts hence effecting bone modelling and remodelling. Osteoblasts produce collagen and bone matrix, and osteoclasts are involved in bone resorption. The bone matrix is composed primarily of inorganic material, with about 25% comprising organic matrix and cells. Also present in the matrix are non-collagenous proteins, including proteoglycans and osteocalcin [41-43].

1.4 Cartilage and subchondral bone changes in OA

1.4.1 Alterations in OA cartilage

Previously discussed is the fact that ageing is a risk factor for OA, and so it is not surprising that many characteristics of aged cartilage mirror those found in OA. The effects of ageing on cartilage have been discussed in section 1.1.1, and contribute towards progression of OA due to disrupting cartilage homeostasis. The following is a brief re-cap of the changes found in cartilage in ageing:

- 1) A catabolic state due to de-sensitivity of chondrocytes to anabolic factors, and accumulation of AGE and RAGE;
- 2) Change in structure of ECM with reduction in proteoglycan content, and calcified cartilage.

These changes in cartilage with ageing (a catabolic state and change in structure) are similar to the changes that occur in OA as detailed below.

During the early stages of OA the metabolism of cartilage changes dramatically. Initially in an attempt to repair cartilage chondrocytes increase the synthesis of proteoglycans, however ultimately there is a net loss of proteoglycan from the matrix as time progresses due to the reduced anabolic and increased catabolic activity of chondrocytes discussed above [7, 60]. The 'repair' phase of OA in the early stage may keep OA clinically silent for a few years. However, as this process continues there is net proteoglycan loss. The net loss of proteoglycan disturbs the interplay between type II collagen and proteoglycans and the cartilage becomes stiffer, which affects the mechanical loading of the joint [11]. Ultimately, this leads to disruption of the collagen network. The collagen in the superficial zone becomes fibrillated, and this is followed by deep fissure formation [60].

At this stage of OA, chondrocytes in the middle and deep zone undergo hypertrophic differentiation. These hypertrophic chondrocytes produce type X collagen, pro-inflammatory cytokines and factors involved in the matrix mineralization process such as alkaline phosphatase, instead of type II collagen and aggrecan produced by healthy chondrocytes [61]. Thus, the cartilage becomes calcified, impacting on the mechanical loading of the underlying subchondral bone. There is also an inflammatory component to OA mediated by synovitis and inflammatory cytokines produced by the hypertrophic chondrocytes. A 'pannus' develops overlying the cartilage, which consists of fibroblasts and inflammatory cells [7]. This results in stimulation of chondrocytes producing increased levels of catabolic proteinases, such as MMPs and ADAMTS, which cleave the collagen fibres and degrade proteoglycans, respectively, in the cartilage matrix. Also some pro-inflammatory cytokines, such as interleukin-1 (IL-1), can induce apoptosis of chondrocytes, and hence lead to further cartilage degradation [7]. These changes ultimately lead to extensive break down of cartilage and exposure of the underlying subchondral bone, which is irreversible, resulting in subchondral bone changes.

1.4.2 Subchondral bone changes in OA

The subchondral bone changes that occur in OA include:

- 1) formation of new bone at the joint margins (osteophytes)
- 2) development of subchondral bone cysts
- 3) vascular invasion of the calcified cartilage from the subchondral bone and duplication of the tidemark
- 4) a biphasic phenomenon in subchondral bone with initial subchondral plate thinning followed by subchondral plate thickening (sclerosis) as the disease progresses
- 5) modification of the architecture and mineralization of subchondral trabecular bone [4-6, 59, 62]

1) Osteophyte formation

In OA, the eventual complete loss of cartilage leads to smooth eburnated bone and osteophytes are thought to form in order to stabilize the eburnated deformed joint in the articular cavity. This theory is supported by the fact that osteophytes are located at sites of joint loading. Osteophytes are formed by proliferation of periosteal cells at the joint margin, which subsequently differentiate into chondrocytes and undergo hypertrophy and create an enlarging skeletal outgrowth at the joint margin through the process of endochondral ossification requiring vascularisation, such as occurs in OA [7, 41]. An image of an osteophyte in a murine OA model is shown in figure 1.5.

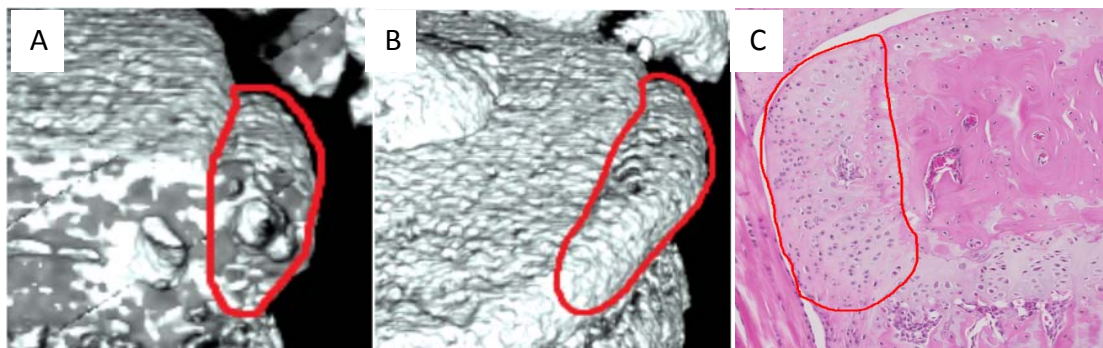


Figure 1.5: Osteophyte images on micro-CT and histology. Images A and B represent murine osteophytes seen on micro-CT at the joint margin of the medial aspect of the tibia (highlighted in red). Image C shows how the osteophytes look on H&E staining, with an area of increased cell proliferation on the medial aspect of the tibia (highlighted in red). All images taken from the same mouse with surgical induction of OA by DMM surgery (aged 14 weeks)

2) Subchondral bone cysts

Subchondral bone cysts have been found to occur most commonly at sites of increased biomechanical loading such as the medial tibia. These bone cysts tend to develop in sites of subchondral bone attrition and are associated with development and worsening of cartilage loss [62].

3) Vascularisation of cartilage from subchondral bone

Vascular invasion of the cartilage from the underlying subchondral bone is a crucial step in the progression of OA enabling crosstalk between cartilage and subchondral bone, discussed in detail in section 1.5. In OA there is an initial increase in osteoclast activity and the osteoclasts migrate towards the articular surface forming channels connecting the cartilage and subchondral bone [63]. In these channels the subchondral marrow is replaced by fibrovascular mesenchymal tissue and vascularisation occurs driven by factors such as vascular endothelial growth factor (VEGF) released from sclerotic OA osteoblasts and hypertrophic chondrocytes [63]. This increased vascularisation not only promotes crosstalk between cartilage and subchondral bone but is also involved in endochondral ossification leading to formation of the osteophytes found in OA, and also promotes transition of the calcified cartilage layer into a new layer of bone [63, 64].

4) Biphasic phenomenon in subchondral bone

Although in OA there is subchondral sclerosis as the disease progresses, initially there is in fact subchondral plate thinning at an early stage of OA followed by sclerosis, evidenced in several animal studies [65-67]. This biphasic phenomenon in subchondral bone found in OA is due to abnormal mechanical stress, inducing osteoblasts to become sclerotic and produce altered factors. Some of these factors include IGF-1, RANKL, VEGF, MMP-3 and -9, TGF- β and α 1 type I collagen [68-72]. The cause of the initial bone resorption is not known, however it is possible that it is due to up-regulation of RANKL from the sclerotic osteoblasts, which promotes osteoclast differentiation and activity [73]. These osteoclasts then secrete cathepsin k, which causes bone resorption [74]. Also increased production of MMP-3 and -9 from sclerotic osteoblasts will contribute to activation of collagenases and

degradation of denatured collagens, respectively, contributing to the early bone resorption [75].

This is followed by subchondral sclerosis later in OA progression (figure 1.6). This is likely due to increased levels of IGF-1 and TGF- β synthesised by sclerotic osteoblasts. Increased IGF-1 results in resistance to parathyroid hormone (PTH), due to down regulation of its receptor, inhibiting RANKL production from osteoblasts and so there is reduced activity of osteoclasts and less bone resorption which may contribute to the sclerosis seen in OA [76]. TGF- β is involved in osteoblast differentiation and matrix synthesis. It also promotes osteoprogenitor proliferation and reduces the ability of osteoblasts to secrete RANKL, and so inhibits osteoclast activity [77]. Therefore, increased levels of TGF- β are likely to play a role in the subchondral sclerosis seen in OA.

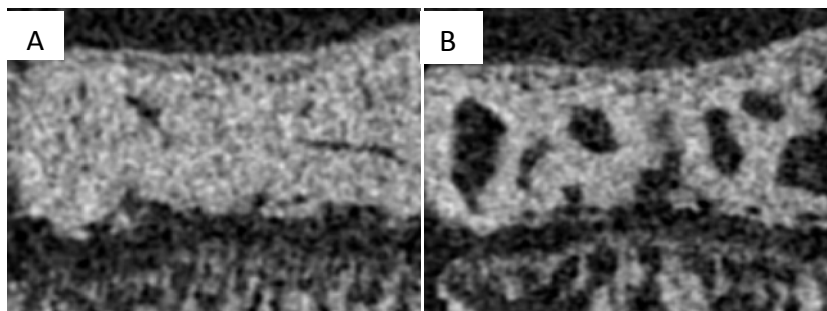


Figure 1.6: Micro-CT representation of subchondral sclerotic bone. Image A shows murine sclerotic subchondral bone characterized by a higher bone density (increased area of opacification), compared to B which is non-sclerotic with visible trabeculae.

5) Modification of architecture and mineralisation of subchondral bone

There are significant architectural alterations in the subchondral bone in OA pathogenesis. These include alterations in BV/TV (percentage bone volume), trabecular thickness (TbTh), trabecular number (TbN) and trabecular separation (TbSp). However, there are conflicting reports as to the specific alterations that occur [65-67, 78-81]. This may be due to different modes of OA induction, species studied and time point analysed. Ultimately, this altered architecture of subchondral bone in OA alters tissue stress and strain distribution [82]. These altered forces, further contribute to abnormal subchondral bone remodelling [83-85]. In depth analysis of subchondral architectural alterations in a murine OA model have been studied in my research, and will be discussed extensively.

There are conflicting reports regarding whether OA is associated with a high or low bone mineral density (BMD) even in the same joint analysed [86]. Supporting the link between a low BMD and OA is a study by Lee et al., who found a reduction in BMD was associated with progression of knee OA [87]. Also a study by Cox et al. found a link between low BMD in the tibia and increased cartilage damage [88]. A correlation in humans has also been found between osteoporosis (characterized by a low BMD) and OA in several studies [89, 90], and also in several animal studies [17, 91-93]. Supporting the argument of a low BMD being associated with OA is the fact that sclerotic osteoblasts secrete increased amounts of $\alpha 1$ type I collagen which has a lower affinity for calcium than $\alpha 2$ type I collagen. This is associated with a lower BMD and a reduced mechanical strength, impacting on the overlying cartilage [94, 95].

Conversely, several studies found an increased BMD is associated with progression of hip and knee OA [96-99]. The mechanism for the link between high or low BMD and OA are unknown, however Li et al. have proposed this might be due to altered mechanical properties of subchondral bone associated with an abnormal BMD (T-score below -1 found on dual-energy x-ray absorptiometry), specifically altered bone stiffness, impacting negatively on the overlying cartilage [100-102].

1.5 The interplay between cartilage and subchondral bone in OA

As discussed, cartilage and bone are both involved in the pathogenesis of OA, and it is known that cartilage and bone interact together in this process [103, 104]. However, it is not known in which tissue changes occur first initiating OA. By having an understanding of how cartilage and bone interact together in OA pathology, one can comprehend how halting pathology in one specific tissue can prevent progression of OA in related tissues.

The two main factors involved in crosstalk between cartilage and subchondral bone in OA are:

- 1) Functional interaction
- 2) Increased vascularization

1.5.1 Functional interaction

There are functional interactions between bone and cartilage due to the transmission of mechanical loads between both tissues. A mechanical load varies depending on the structure of the tissue crossed. Therefore any changes in the structure of cartilage would impact on the mechanical load that arrives at the subchondral bone and hence alter the response of the subchondral bone. This also applies if there were changes to the subchondral bone, as this would impact on the load reaching the cartilage and hence alter its response to this load, causing a pathological response [61]. As discussed there are considerable changes to the structure of cartilage and subchondral bone in OA as it progresses, and so in this respect there is crosstalk between cartilage and subchondral bone in OA due to changes in either tissue effecting the transmission of the mechanical load and abnormal remodelling in the tissue [61].

This functional interaction has been highlighted in studies by Thambyah et al. [64, 105]. As discussed, cartilage has a specific structure allowing controlled compression of the matrix and transmission of load to the underlying subchondral bone. This group found that in degenerative bovine cartilage there was an altered indentation profile compared to healthy cartilage, corresponding with an altered ability to transmit forces through the ECM to the underlying subchondral bone.

Further evidence for altered functional interaction between cartilage and subchondral bone has been highlighted in other studies. Li et al. found the subchondral bone in OA patients was sclerotic corresponding with lower stiffness [101, 106]. Day et al. found that in samples of human OA subchondral bone there was a 60% reduction in stiffness compared to control, and this correlated with significant cartilage damage [107]. Furthermore, Ko et al. discovered cyclic compression of a murine knee joint caused significant subchondral sclerosis, and this corresponded with degeneration of cartilage at the site of loading, suggesting that each tissue responds to the local mechanical environment and to reciprocal changes in other tissues [108].

1.5.2 Increased vascularization promoting crosstalk

In normal joints there is no vascularization of cartilage from the underlying subchondral bone and hence minimal 'communication' between these tissues, however in OA neo-

vascularization occurs whereby calcified cartilage is vascularized from the subchondral bone mainly due to increased synthesis of VEGF from hypertrophic chondrocytes and sclerotic osteoblasts [104]. This increased vascularization in OA cartilage has been shown in a study by Pan et al. [103]. Highlighting the importance of increased vascularization into the cartilage in OA pathology, is a study by Mahjoub et al., who found a correlation between a higher number of vessels penetrating the articular cartilage and a higher modified Mankin score of cartilage damage [61]. This finding is likely due to the ability of factors produced by sclerotic osteoblasts and hypertrophic chondrocytes, found in OA, being able to transfer freely between the cartilage and subchondral bone, causing an alteration in the metabolism of chondrocytes and osteoblasts, and a pathological response [109].

As discussed, some of the factors produced by hypertrophic chondrocytes in OA include alkaline phosphatase (alkP), VEGF, cytokines including interleukin-1 (IL-1 α and β), tumour necrosis factor alpha (TNF- α), type X collagen, and this shifts cartilage towards a catabolic state due to up-regulation of aggrecanases and collagenases, and also increased chondrocyte apoptosis [7, 61, 110]. In addition, alkP promotes matrix mineralization, and over-production of type X collagen promotes endochondral bone ossification in the cartilage, which will lead to abnormal functional interactions between cartilage and subchondral bone as discussed [61, 111, 112].

In OA, the osteoblasts also become sclerotic and secrete altered factors including insulin-like growth factor-1 (IGF-1), receptor activator of nuclear factor kappa-B ligand (RANKL), VEGF, TGF β and MMP-3 and -9 [68]. Increased production of RANKL will alter the balance of the RANKL/osteoprotegerin (OPG) system in bone. RANKL regulates osteoclast activity and differentiation so has a role in bone remodelling, and OPG can inhibit the actions of RANKL, hence the balance of this system is important in skeletal homeostasis. It has been found in human OA that there are two subgroups based on either having a low or high RANKL/OPG ratio with subsequent effects on remodelling of bone seen in OA [113]. A study by Byron et al. found the OPG/RANKL ratio was reduced in subchondral bone of OA rabbits, suggesting abnormal bone remodelling as seen in OA [114]. Furthermore, due to increased vascularization of the cartilage in OA, RANKL produced from the sclerotic osteoblasts can pass freely to the cartilage altering the ratio. A reduction in OPG relative to RANKL will have a negative effect on cartilage, as it has been found that OPG has a

protective effect on cartilage, with a reduction in OPG leading to cartilage catabolism [93].

Increased IGF-1 production results in resistance to parathyroid hormone (PTH), due to down-regulation of its receptor [115], and this will inhibit RANKL production from osteoblasts and alter bone remodelling, such as is seen in OA [76]. The increased production of MMP-3 and -9 by sclerotic osteoblasts can activate collagenases, and degrade denatured collagens, respectively (as described in section 1.7) and this will cause abnormal remodelling of cartilage and bone. Increased VEGF synthesised by both hypertrophic chondrocytes and sclerotic osteoblasts promotes vascularization, and formation of osteophytes via endochondral ossification [63]. TGF β is also synthesised from sclerotic osteoblasts, and is likely to play a role in the development of osteophytes and subchondral sclerosis, as seen in OA [77, 116]. The resultant change in subchondral bone architecture will thus impact negatively on transmission of mechanical forces to the cartilage, and lead to cartilage degradation [116].

Of pertinence to my research are proteinase-activated receptor-2 (PAR-2) and matriptase, discussed further in sections 1.6 and 1.8. PAR-2 is likely also involved in crosstalk between cartilage and subchondral bone in OA, as it is upregulated in OA chondrocytes [117]. Upon PAR-2 activation, there is production of pro-inflammatory cytokines and MMPs, via MAPK signalling [118-121], which can then pass to the subchondral bone due to increased vascularization. The cytokines and MMPs can then adversely affect remodelling of cartilage and subchondral bone, as discussed. Matriptase is also upregulated in OA cartilage and is likely involved in pathological communication between cartilage and subchondral bone in OA. Matriptase is an activator of PAR-2 and can also convert pro-collagenases to active collagenases [122], discussed further in section 1.8. Matriptase will also therefore play a role in the crosstalk and abnormal remodelling events seen in OA cartilage and subchondral bone.

1.6 Proteinase activated receptor-2 (PAR-2)

1.6.1 Structure and activation

PAR-2 is a G-protein coupled receptor (GPCR), displaying common structural characteristics, with a 7 hydrophobic transmembrane (TM) domain, an extracellular amino terminus and an intracellular carboxyl terminus. (Refer figure 1.7) PAR-2 has a

unique activation mechanism, whereby a serine proteinase (such as matriptase) effects proteolytic cleavage within the N-terminus, exposing a tethered ‘cryptic’ receptor-activating N-terminal sequence that can bind to the conserved second extracellular loop. This subsequently changes the conformation of the intracellular loops, enabling interaction with heterotrimeric G proteins ($G\alpha\beta\gamma$) inducing GDP release from $G\alpha$ and binding of GTP. Subsequently $G\alpha$ and $G\beta\gamma$ disassociate and can activate multiple effector signaling pathways (refer figure 1.7) [123-128].

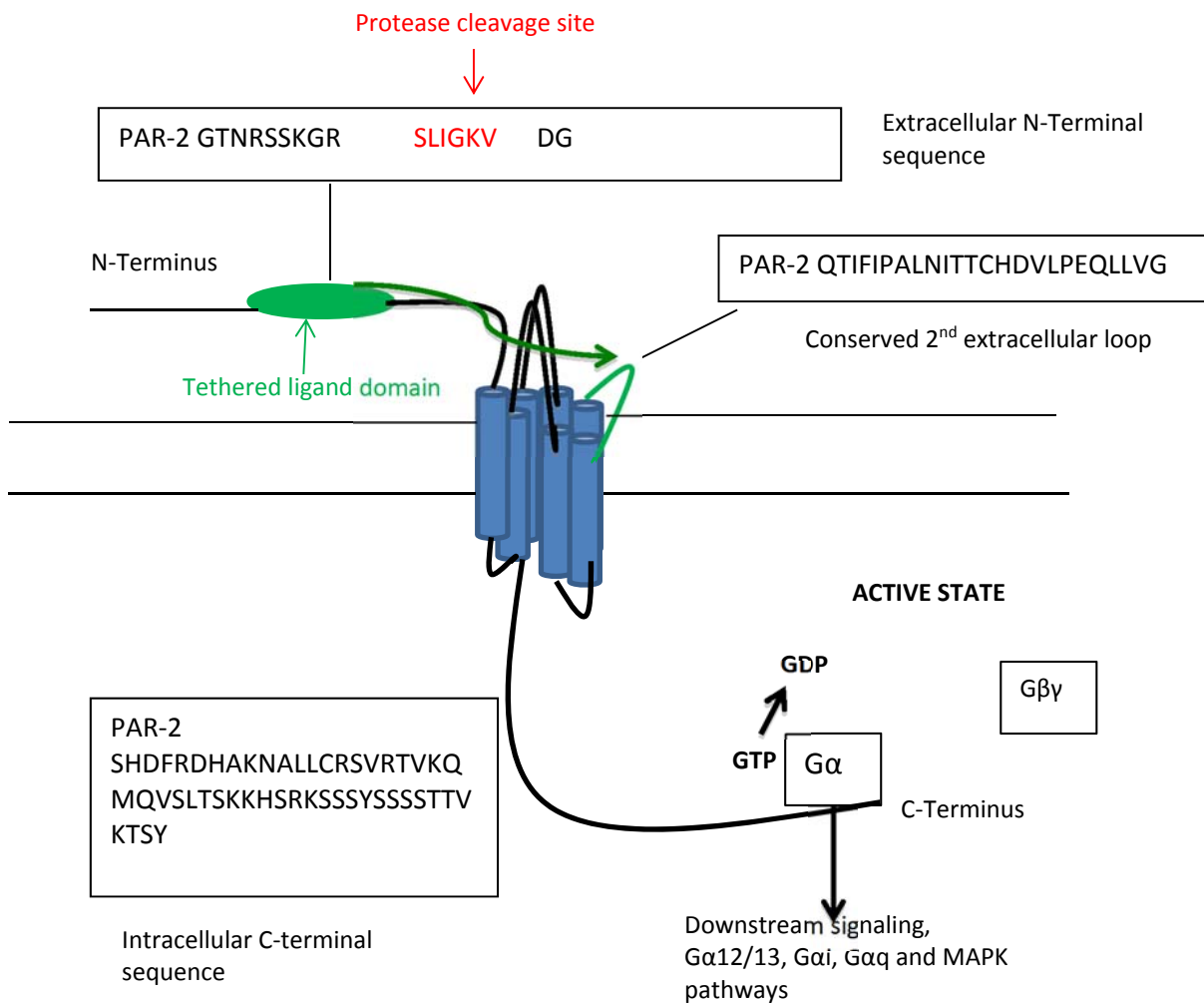


Figure 1.7: Structural features and mechanism of PAR-2 activation. A serine protease (such as matriptase) cleaves the PAR receptor at a specific point in the N-terminal domain (in red), revealing a previously cryptic N-terminal sequence of receptor (in green), which is defined as a ‘tethered ligand’. This tethered ligand can then interact with the conserved second extracellular loop and activates the receptor. Human sequences of the tethered ligand, the second extracellular loop and the intracellular C-terminus are shown in the labelled boxes. Adapted Steinhoff et al. and Macfarlane et al.

There are 21 G α subunits, of which G α_i , G α_q and G $\alpha_{12/13}$ are relevant to PAR-2 signaling events. As suggested in figure 1.7, the specificity of G protein coupling to GPCRs is found in the C-terminal domain and also depends on the specific structural conformational changes of the receptor upon proteolytic activation [127, 128].

The main transcription factor binding site in the gene promoter of human PAR-2 is c-Fos, which regulates its activity (taken from Qiagen website).

1.6.2 PAR-2 signaling

PAR-2 has very complex signaling pathways, many of which are yet to be defined. As suggested in figure 1.7 the mitogen activated protein kinase (MAPK) pathways are involved in PAR-2 signaling [128]. An important endpoint of MAPK signaling is the activation of AP-1, a transcriptional regulatory protein, which induces the expression of pro-inflammatory cytokines and MMPs, which are involved in OA pathology [118-121, 128].

1.6.3 PAR-2 in OA

PAR-2 is widely expressed in various tissues including the brain, heart and skin, and out of all the PARs it is the most strongly implicated in disease states [129]. A wealth of evidence has highlighted PAR-2 as an important component in the pathophysiology of OA [117, 130, 131]. A study by Kelso et al., found PAR-2 protein was significantly upregulated in acute joint inflammation in the articular tissue [130, 132]. This up-regulation of PAR-2 in inflammatory states, such as in OA, has also been found in studies by Boileau et al. and Ferrell et al. who elicited higher levels of PAR-2 in OA chondrocytes compared to control [117, 131]. Additionally, in personal communication with Dr Emma Blain (Cardiff University) PAR-2 was up-regulated almost 5-fold at 1- and 7-days post mechanical load of 3.5MPa, suggesting a role of altered mechanical loading and up-regulation of PAR-2.

Importantly, PAR-2 agonists are also upregulated in the joint in inflammatory conditions such as rheumatoid arthritis (RA) and OA, including tryptase with its likely source coming from mast cells [133, 134]. A functional link between mast cells, PAR-2 and inflammatory

joint disease such as OA has been discovered by Palmer et al. This group found that by giving a mast cell degranulator (compound 40/80) to mice it resulted in synovial vasodilatation, which was absent in PAR-2 'knock-out' mice [135]. The likely candidate released from these mast cells, subsequently activating PAR-2 and causing inflammation is β -tryptase. Palmer et al. found that by giving β -tryptase to PAR-2 'knock-out' mice the joint swelling and hyperemia was significantly reduced compared to the wild-type response [135]. Although tryptase released from mast cells is predominantly activating PAR-2 causing joint inflammation in conditions such as OA, other serine proteinases are likely to be involved too, such as matriptase [122, 136].

These studies provide evidence that PAR-2 is involved in the inflammatory component in OA, with Ferrell et al. also finding that by injecting a PAR-2 agonist (SLIGRL-NH₂ and ASKH95) to wild type mice there was significant joint swelling and hyperemia which lasted for up to 72 hours, in contrast with PAR-2 'knock-out' mice who had a significantly lower grade response [117]. Interestingly, this inflammatory component involving PAR-2, in OA correlates with cartilage degradation. In the study by Ferrell et al. they found that histological examination of the cartilage in wild type mice after PAR-2 activation revealed severe arthritic changes including cellular infiltration, synovial hyperplasia and articular cartilage damage. This is in contrast to PAR-2 'knock-out' mice, which had significantly less damage to the cartilage, indicating the loss of a key inflammatory component mediated by PAR-2 [117]. A further study by Ferrell et al. also found that in mice at 8 weeks post surgically induced OA, cartilage damage was significantly increased in wild-type compared to PAR-2 'knock-out' mice. This cartilage damage also correlated with osteosclerosis of the subchondral bone in wild type compared to 'knock-out', which had significantly less subchondral sclerosis [137].

A study carried out by Boileau et al. discovered that the cartilage degradation initiated by PAR-2 is due to a significant up-regulation of MMP-1 and MMP-13, and also IL-1 β which adds to the catabolic effect [131]. This mechanism is mediated by the complex signaling pathways upon PAR-2 activation, as discussed, including MAPK signaling causing up-regulation of pro-inflammatory cytokines and MMPs.

PAR-2 is also up regulated in OA subchondral bone osteoblasts, and upon its activation various MMPs such as MMP-1 and MMP-9 are up regulated along with pro-inflammatory cytokines and RANKL, resulting in abnormal metabolism of these cells [138]. The elevated levels of MMP-1 and MMP-9 in the bone are linked to the bone resorptive mechanism in OA, and act in synergy with the catabolic effects of IL-6 and RANKL. The mechanisms for up-regulation of these factors include the MAPK signaling pathways mediated by PAR-2 [139]. These findings suggest that PAR-2 is involved not only in cartilage destruction, but also in the complex abnormal bone remodeling that occurs in OA.

These studies provide evidence for the crucial role of PAR-2 in cartilage and bone pathology in OA. Although it is known PAR-2 is involved in inflammation, catabolism of cartilage and subchondral bone remodeling found in OA, it is still unknown in which tissue PAR-2 ablation confers its primary protective effect. This project aims to identify this using a postulated chondroprotective (collagen II inducible PAR-2 'knock-out') murine model and also a postulated bone-protective (osteocalcin inducible PAR-2 'knock-out') murine model. In addition an activator of PAR-2, matriptase, has also been ablated specifically in cartilage, in a murine OA model to elicit any protection against the bone and cartilage changes observed in OA.

1.7 Proteinases involved in matrix turnover in the joint

Proteinases belong to the family of proteases. In general terms proteases hydrolyse a peptide bond in a polypeptide chain. Proteases can be subdivided into exopeptidases or endopeptidases depending on the position of the peptide bond they hydrolyse [75]. Of relevance to OA are the endopeptidases, which include the matrix-metalloproteinases (MMPs), adamalysins and serine proteinases, all known to play a role in OA [136, 140, 141].

1.7.1 ADAMTS (a disintegrin and metalloproteinase with thrombospondin motif)

ADAMTS are the main proteinases responsible for aggrecan cleavage, mainly the aggrecanases – ADAMTS-1, -4, -5, -8 and -15. They are activated by pro-protein convertases, including furin. The ADAMTS class of proteinases are involved in cartilage

catabolism by cleavage of aggrecan in the interglobular domain (IGD), specifically at Glu373-Ala374, separating the G1 and G2 regions [142]. These specific aggrecan fragments have been found in arthritic synovial fluids [140]. To date five aggrecanases have been identified (ADAMTS-1, -4, -5, -8 and -15) which have all been found to cleave aggrecan at the Glu373-Ala374 bond [143]. There are also other cleavage sites in the chondroitin sulphate-rich region of aggrecan mediated by ADAMTS-4 and -5 [144, 145].

1.7.2 Matrix-metalloproteinases (MMPs)

MMPs can be classified into 5 main groups according to substrate specificity, outlined in table 1.1.

Group	MMPs	Substrate
Collagenases	MMP-1 (collagenase-1), MMP-8 (collagenase-2), MMP-13 (collagenase-3), MMP-18 (collagenase-4)	Collagen types I, II and III
Gelatinases	MMP-2 (gelatinase A), MMP-9 (gelatinase B)	Denatured collagens – gelatins; MMP-2 types I, II and III collagen
Stromeolysins	MMP-3 (stromelysin-1), MMP-10 (stromelysin-2), MMP-11 (stromelysin-3)	ECM components and activation of pro-MMPs
Matrilysins	MMP-7, MMP-26	ECM components and activation of cell surface molecules
MT MMPs	MMP-14 (MT1 MMP), MMP-15 (MT2 MMP), MMP-16 (MT3 MMP), MMP-17 (MT4 MMP), MMP-24 (MT5 MMP), MMP-25 (MT6 MMP)	ECM components and activation of pro-MMPs. MT1-MMP types I, II and III collagen

Table 1.1 – The 5 main groups of matrix metalloproteinases [75]

Most MMPs are secreted as inactive zymogens and are activated by proteinases in a stepwise manner involving a cysteine switch mechanism. The regulation of MMP activity is important for normal tissue homeostasis including transcriptional regulation, regulation of activation of pro-MMPs, control of the localization and clearance of MMPs and inhibition of MMP activity [75, 146, 147]. This regulation prevents any unwanted effects and pathology arising such as arthritis. MMPs are known to be involved in OA pathology and this will be discussed.

Initial work suggesting MMPs are involved in cartilage catabolism have been shown in studies by Fosang et al. and Struglics et al., who discovered MMP-derived aggrecan fragments in the synovial fluid of human OA joints [148-150]. Therefore it was thought

that MMPs are involved in aggrecan degradation by cleaving aggrecan within the interglobular domain at Asn341-Phe342 bond. However, more recent work by Sandy et al. showed that the majority of aggrecan fragments were cleaved at the aggrecansae site (Glu373-Ala374) mediated by ADAMTS enzymes, rather than MMPs [140, 151, 152]. There is still some debate that MMPs may be involved in late stage aggrecan degradation independent of ADAMTS activity [153], however from the depth of knowledge it appears that ADAMTS enzymes play the most pivotal role in aggrecan degradation [140, 152, 154], whereas MMPs are mainly involved in C-terminal trimming of aggrecan producing the aggrecan fragments specific for MMP activity in OA synovial fluid, and so have no catabolic effect on aggrecan [151, 152, 155].

However, the collagenase subfamily of MMPs (MMP-1, -8 and -13) are thought to play a major role in the collagen degradation seen in OA. Tetlow et al. found increased expression of these collagenases in human OA cartilage specimens [141]. MMP-13 has the most potent specificity for collagen type II [156], and is thought to be the main collagenase involved in collagen breakdown in OA, with its expression increased in OA cartilage [157, 158]. This activity mediated by MMP-13 in OA is detrimental in cartilage degradation, as collagen breakdown is irreversible and cannot be repaired.

Some other minor roles involved in collagen breakdown in OA are thought to be carried out by MMP-3 which was also found to be up-regulated in human OA cartilage [141], and can activate the collagenases [159], suggesting a crucial role of this stromelysin in OA mediated cartilage breakdown. Of the other MMPs it is thought that MMP-8 (collagenase), MMP-2 (gelatinase) and MMP-14 (MT1-MMP) may also play roles in collagen breakdown due to their ability to cleave type II collagen, and the additional role of MMP-2 activating pro-MMP-13 [146, 156, 160]. It is important to identify the key enzymes involved in collagen break-down as this is the final irreversible step in OA pathology resulting in significant pain and mobility problems in a patient.

1.7.3 Serine proteinases

Milner et al. has written a comprehensive review of serine proteinases involved in arthritis. This includes serine proteinases involved in the coagulation and complement

cascade, immune cell-derived serine proteinases and high temperature requirement proteinases. These serine proteinases likely contribute towards OA pathogenesis by degrading ECM components, activating cytokines, growth factors and chemokines [136]. With particular relevance to my research is the fact that serine proteinases can also activate PARs causing subsequent G-protein signalling events [136]. As discussed PAR-2 signalling is involved in inflammation and MMP production (for more detail refer section 1.6), which contribute towards OA pathology such as cartilage degradation and synovial inflammation.

Cartilage collagen degradation is a detrimental step in OA pathology, and this step is mediated by collagenases, specifically MMP-1 and -13. Activation of these pro-collagenases via removal of its pro-domain is a key step in collagen resorption. It has been found that both furin- and trypsin-like serine proteinases are involved in this pro-MMP activation step [136]. Plasmin can also activate pro-MMPs and so the plasminogen activator (PA)/plasmin cascade is also of relevance in OA. These processes involving furin-like serine proteinases, and the PA/plasmin cascade activating pro-MMPs with subsequent collagen breakdown will now be examined in more detail.

In OA there is increased plasmin activity and more PAs present in OA cartilage [161]. Milner et al. went on to elicit the effects of addition of plasminogen to bovine nasal cartilage (BNC) treated with or without IL-1 + OSM. As expected the addition of plasminogen to stimulated cartilage there was a significant increase in collagen release by day 7, corroborating the idea that plasmin activates pro-collagenases. Addition of an inhibitor of MMPs (BB94) completely blocked IL-1 + OSM + plasminogen mediated collagen release in BNC. This highlights that plasminogen activates MMPs, and the final pathway in collagen degradation is MMP mediated [161]. This finding of significant collagen release in stimulated BNC was repeated using human articular cartilage with similar results. This work by Milner et al. provides evidence that serine proteinases are involved in the activation of pro-collagenases and breakdown of cartilage [161].

Another serine proteinase involved in OA pathology, namely cartilage breakdown are the furin-activated enzymes. All MT-MMPs and MMP-11 contain a conserved recognition motif for the pro-protein convertase furin. Also the aggrecanases, ADAMTS-4 and

ADAMTS-5 contain this furin cleavage site. Furin levels are increased in osteoarthritic cartilage, and are postulated to play an important role in cartilage degradation [162]. Milner et al. found that the addition of a furin inhibitor (Dec-RVKR-CH₂CL) to BNC explant cultures stimulated to resorb with IL-1 + OSM reduced release of collagen fragments in a dose dependent manner. Furthermore this inhibitor reduced active collagenases present in the media of stimulated BNC explants. The addition of this furin inhibitor to BNC explants also partially blocked proteoglycan release too, due to inability to activate ADAMTS-4 and -5 [162]. These findings suggest that the serine proteinase furin likely plays a role in the mechanisms leading to cartilage breakdown in the arthritic joint.

From these findings, it is highly likely that cartilage resorption found in OA involves both serine proteinases, MMPs and ADAMTS interacting together in a cascade of events. Also related to the serine proteinase family, are the type II transmembrane serine proteases (TTSPs), which includes matriptase, and this TTSP has been extensively studied in this project with regards to its role in cartilage catabolism, and will be discussed further.

1.8 Matriptase

As discussed serine proteinases play important roles in OA, and a member of this class, matriptase has been investigated in my research in a model of cartilage breakdown. Matriptase is a serine proteinase, specifically a type II transmembrane serine proteinase (TTSP) [163, 164]. It has the common features of other TTSPs including a catalytic domain, a transmembrane domain, a short cytoplasmic domain and a variable length stem region [163, 164].

Matriptase has the broadest pattern of expression of all the TTSPs being detected in a wide range of both human and murine tissues. Its highest expression was identified in the colon, stomach, prostate, skin and kidney, and restricted mainly to the epithelial compartments of embryonic and adult tissues, where it plays a crucial role in the epidermal barrier function. Interestingly, Milner et al. identified that in OA cartilage, matriptase was only detected in locations where PAR-2 was also present, suggesting that PAR-2 acts as a sentinel for proteinase-mediated injury signals, such as matriptase

expression due to joint destabilization, leading to PAR-2 activation and signaling [122, 163, 164] .

Lin et al. characterized matriptase and found close association of matriptase with a Kunitz-type serine protease inhibitor, named hepatocyte growth factor activator inhibitor (HAI-1) [165]. Matriptase is predominantly expressed in epithelial lined tissues and is absent from most tissues of mesenchymal origin. Its expression is also closely correlated with HAI-1 [166].

The activation of matriptase is complex, involving its catalytic domain, non-catalytic domains and its inhibitor HAI-1. Matriptase can be activated by other active proteases or by itself. This occurs through proteolytic cleavage at a specific activation motif preceding the catalytic domain [166]. The non-catalytic domains involved in matriptase activation include its LDL receptor class A domain, SEA and CUB domains. HAI-1 plays a role in its activation by forming a matriptase-HAI-1 activation complex, in which the LDL receptor class A domain of HAI-1 helps facilitate transactivation of matriptase [166].

Active matriptase has been implicated in OA. Work by Milner et al. assessed serine proteinase gene expression in femoral head cartilage obtained from patients with either hip OA or fractured neck of femur (NOF) by carrying out a low-density array. It was found that there was a statistically significant increase in matriptase gene expression in OA cartilage. In addition HAI-1 gene expression was also significantly elevated in OA cartilage [122]. This shows that in addition to the furin and plasminogen activator members of the serine proteinases, matriptase (a TTSP) also likely plays a role in the mechanisms of OA induced cartilage breakdown.

Milner et al. went on to show that matriptase is an activator of pro-MMP-1 and also pro-MMP-3 (as found by Jin et al. [167]), and can also activate PAR-2. This is addition to its ability to also activate uPA to convert plasminogen to plasmin and subsequent up-regulation of collagenases. Therefore matriptase has direct and indirect roles inducing cartilage breakdown [122].

As mentioned matrix metalloproteinase (MMP) expression is upregulated in OA cartilage. This group went on to elicit that MMPs activate pro-MMP-1 and pro-MMP-3 producing active collagenolytic enzymes. Corroborating this effect it was found that when MMP-1 was added to BNC explant cultures treated with IL-1 + OSM there was enhanced collagen release [122]. This is due to several signaling pathways converging to cause increased expression of collagenases and hence cartilage breakdown. The signaling pathways in chondrocytes causing up-regulation of ADAMTS and MMPs in response to IL-1 + OSM have been discussed in sections 1.9 and 1.10. MMP signaling pathways include activation of pro-MMP-1 and pro-MMP-3 via cleavage within the bait region (Arg-Arg bond), and this intermediate species generates a fully active MMP with an N-terminal Phe capable of collagenolysis. Additionally, MMP converts pro-uPA to uPA generating active plasmin from plasminogen and activation of pro-MMP-1 [122].

Interestingly MMP stimulated BNC explants by itself elicited no significant collagen release, but there was collagen release in human OA cartilage explants treated with MMP. This suggests that an additional signaling pathway is required for cartilage breakdown in non-OA cartilage, which is likely to be PAR-2 signalling. As discussed PAR-2 is up-regulated in OA, and this may explain the effects seen in MMP stimulated BNC explants which, have lower levels of PAR-2 expression compared to OA cartilage with higher levels of PAR-2 expression. Indeed Milner et al. only found PAR-2 and MMP expression in chondrocytes from an OA mouse model compared to minimal expression in the control group using immunohistochemical analysis [122].

Corroborating the importance of PAR-2 mediated signaling induced by MMP in cartilage breakdown, Milner et al. found that by using a PAR-2 inhibitor (SAM-11) in human OA cartilage explants, there was a significant reduction in collagen release [122]. As discussed, MMP can also activate pro-uPA into active uPA converting plasminogen to plasmin with subsequent pro-MMP-1 and -3 activation with consequent cartilage breakdown. This myriad of effects on cartilage breakdown induced by MMP is highlighted in figure 1.8.

There are a number of transcription factor binding sites in the promoter of matriptase, which controls its activity in humans. These include NF-Kappa B (and B1), E4BP4, Bach1, and LCR-F1 (taken from Qiagen website).

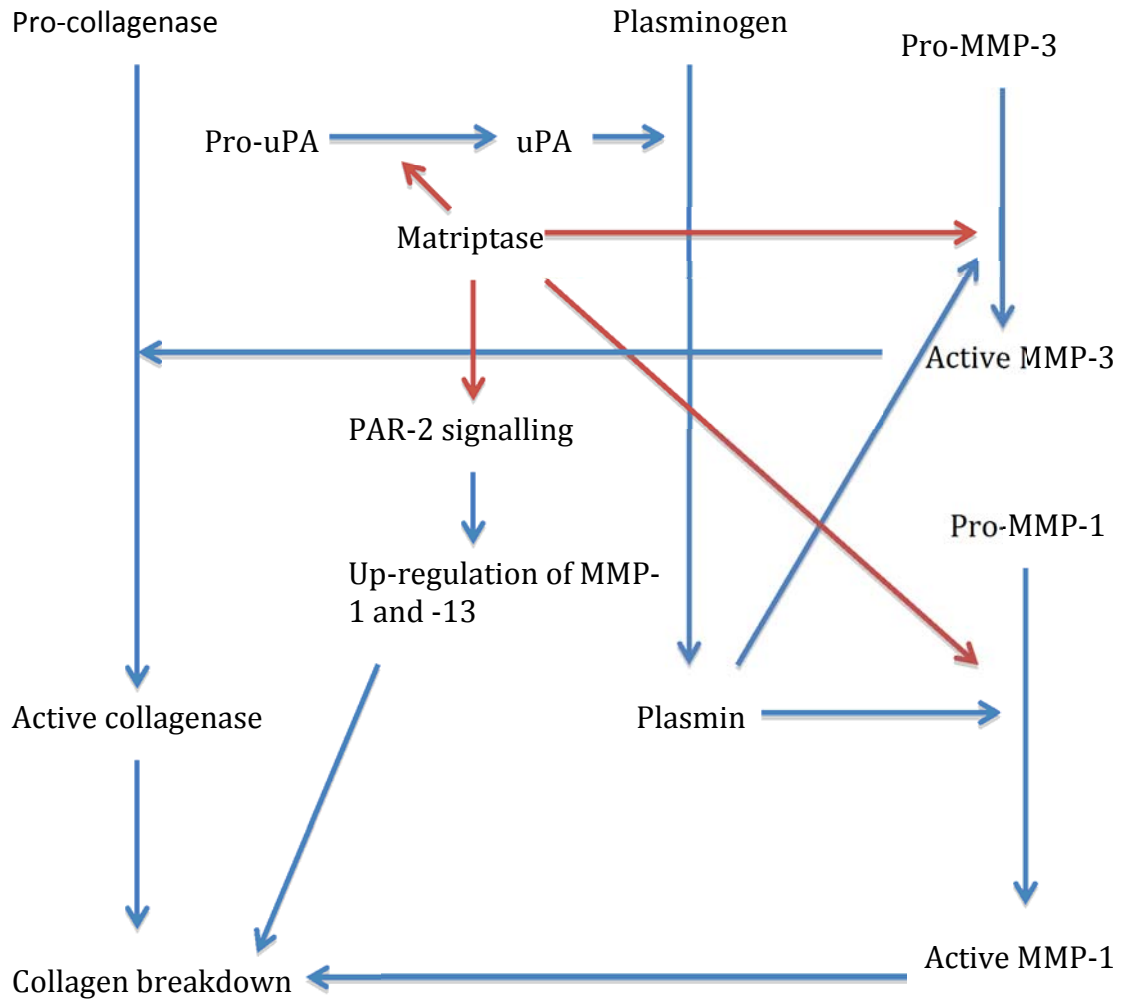


Figure 1.8: Matriptase role in collagen breakdown. Matriptase has multiple actions including activation of pro-MMP-1 and -3, which thus activate the collagenases causing collagen breakdown. Matriptase can also activate urinary plasminogen activator (uPA) converting plasminogen to plasmin, subsequently causing activation of pro-MMP-1 and -3 and resultant activation of collagenases and collagen breakdown. Importantly matriptase can also activate PAR-2 with resultant up-regulation of MMP-1 and MMP-13 and collagen breakdown.

1.9 Interleukin-1 (IL-1)

Cartilage catabolism is a common feature of OA and RA, and it is known that cytokines play a role in this process, including IL-1 and oncostatin-M (OSM) [168]. I have used these cytokines in an in vitro study of cartilage breakdown using tissue-engineering techniques in my research.

IL-1 was identified several decades ago as a catabolic factor in cartilage via activation of chondrocytes and subsequent production of cartilage degrading proteinases, such as matrix-metalloproteinases (MMPs) and ADAMTS (a disintegrin and metalloproteinase with thrombospondin motif) [169, 170]. These proteinases play roles in collagen and proteoglycan breakdown respectively [140-142, 157, 158, 171]. IL-1 also has a negative anabolic effect on proteoglycan synthesis [172, 173]. These effects of IL-1 will therefore cause significant cartilage breakdown in an in vivo model, highlighted in several studies [174-176]. The catabolic effect of IL-1 on aggrecan is due to cleavage of aggrecan within the interglobular domain (IGD), specifically at Glu373-Ala374 via ADAMTS proteinases [140, 143, 171, 177].

IL-1 signalling pathways in chondrocytes causing up-regulation of ADAMTS and MMPs, include the mitogen-activated protein kinase (MAPK) family, specifically c-Jun N-terminal kinase (JNK) and p38, subsequently resulting in production of phosphorylated activator protein (AP-1) transcription factor which regulates many MMP genes [120, 121].

1.10 Oncostatin-M (OSM)

As mentioned another cytokine involved in cartilage catabolism is OSM [168, 178], and this has also been utilized in a tissue-engineered model of cartilage catabolism.

OSM has been identified very early on as having a pro-catabolic and negative anabolic effect on cartilage, similar to IL-1 as evidenced in various studies [179] [180-182]. However, only when OSM was used in combination with IL-1 was there significant collagen release [183, 184], suggesting that both of these cytokines are required for significant induction of MMP-1, -3 and -13 activity and subsequent collagen breakdown.

The reason why OSM by itself cannot induce collagen release is likely due to the fact that OSM induces TIMP-1 (tissue inhibitor of metalloproteinases) production, which blocks the effects of MMPs [183, 184]. OSM also has complex signaling pathways in chondrocytes involving JAK (janus kinase)/STAT (signal transducer and activator of transcription) and MAPK pathways [185, 186], which induce ADAMTS-4 and MMP-13 expression and subsequent cartilage catabolism.

1.11 Aims of study

1. To generate a reliable and reproducible model of cartilage catabolism derived from a human source. I aimed to use this to analyze the effects of matriptase and PAR-2 over-expression on cartilage catabolism.
2. Utilize tissue-specific PAR-2 and matriptase ablated mice, and compare remodelling events in cartilage and bone to wild type mice, using a surgical model of OA. This would provide more information on the role of PAR-2 and matriptase in OA progression.

Chapter 2: Materials and methods

2.1 Materials

2.1.1 Biochemical reagents

Papain (from *Carica papaya*), cysteine-HCl, 2-amino-2-hydroxymethyl-propane-1,3-diol hydrochloride (Tris-HCl), calcium chloride, chloroform, β -mercaptoethanol, sodium chloride, L-cysteine hydrochloride, *p*-dimethylaminobenzaldehyde (DAB), Ethidium Bromide (3,8-Diamino-5-ethyl-6-phenylphenanthridinium bromide), L-hydroxy-proline, bovine serum albumin (BSA), Poly(ethylene glycol) (PEG 6000), Brij 35 (Polyethylene glycol dodecyl ether), MMP substrate (MCA-Lys-Pro-Leu-Gly-Leu-DNP-Dpa-Ala-Arg-NH₂), glycine, chondroitin sulfate sodium shark cartilage, sodium acetate, citric acid tri-sodium salt, citric acid, sodium dihydrogen phosphate and disodium hydrogen phosphate were obtained from Sigma-Aldrich. (Poole, UK) Trizol reagent was purchased from Life Technologies (Invitrogen). Ethylenediaminetetraacetic acid (EDTA) (1mM) and Chloramine T was purchased from BDH (Poole, UK). O-ring screw-cap tubes (2ml) were obtained from Sarstedt (Leicester, UK) and eppendorfs (1.5ml) were obtained from Starlabs (Milton Keynes, UK). Flat-bottomed and V-bottomed 96-well plates were obtained from Greiner Bio-One (Gloucestershire, UK). GP-7- amino-4-methoxy coumarin (AMC) was purchased from Bachem (Essex, UK). 4-aminophenylmercuric acetate (APMA) was purchased from Sigma-Aldrich. Matriptase was produced in-house by Prof. Alistair Hawkins (Newcastle University), essentially as described by Desilets et al. [187], at a stock concentration of 10.3 μ M in Tris buffer pH 9 (50mM Tris, 1mM β -mercaptoethanol), stored at -80°C until use.

2.1.2 Molecular Biology Reagents

Primers for PAR-2 and ST14 genotyping were designed and sequences provided by Dr Neil Dear and Dr Thomas Bugge, respectively [188]. The specific primers were subsequently purchased from Sigma-Aldrich. Agarose (electrophoretic grade) was purchased from Invitrogen. SuperScript III Reverse Transcriptase, 5x first strand buffer, dithiothreitol (DTT) (0.1M) and RNase OUT were purchased from Life Technologies. Random hexamers (20 μ g)

and deoxynucleotide mix (10mM) (dNTP containing dATP, dCTP, dGTP and dTTP) were purchased from Sigma-Aldrich. GeneRuler Express DNA ladder and Gene Ruler 1kb plus DNA ladder were purchased from Life Technologies. TaqMan Universal MasterMix II was purchased from Applied Biosystems (CA, USA). RNase- and DNase-free water was purchased from Sigma-Aldrich. RNase zap was purchased from Life Technologies. A MixerMill MM 400 tissue homogeniser was used from the OAG Group MRG, purchased from Retsch (Hope Valley, UK).

2.1.3 Cytokines

IL-1 α was a gift from Dr Keith Ray (GlaxoSmithKline, Stevenage, UK) at a concentration of 670ng/ml in Dulbecco's modified Eagle's medium (DMEM) (0.1% bovine serum albumin (BSA)), and was stored at -20 °C until use. Recombinant OSM was made in-house (method described in Staunton et al. [189]) at a concentration of 50 μ g/ml, in Dulbecco's phosphate buffered saline (DPBS) (with 0.1% BSA) and stored at -80 °C. IL-1 α and OSM were diluted to appropriate concentrations and filtered through a 0.22 μ m filter in culture medium prior to experimental work.

2.1.4 Cell and tissue culture reagents

DMEM was obtained from Gibco BRL (Paisely, UK). L-Glutamine, penicillin-streptomycin, Trypsin-EDTA solution 1x (0.5g trypsin from porcine pancreas and 0.2g EDTA) and Dulbecco's Phosphate Buffer solution (DPBS) were obtained from Sigma-Aldrich. Mesenchymal stem cell growth medium (MSCGM) and DMEM with glucose (DMEM 4.5g/L Glucose) were obtained from Lonza (Slough, UK). Dexamethasone, L-Ascorbic acid 2-phosphate sesquimagnesium salt hydrate, L-proline and ITS+1 (insulin, transferrin, selenium, linoleic acid) liquid medium supplement (100x) were obtained from Sigma-Aldrich. Recombinant human TGF-beta 3 (E.coli derived) was obtained from Peprotech (London, UK). Human bone marrow mononuclear cells (cryoamp 25 million cells 2M-125C) were obtained from Lonza. All donor cells were obtained from patients aged less than 25 years old. Human fibroblast growth factor-2 (FGF-2) was obtained from R&D systems (Abingdon, UK). Centrifuge tubes, 50ml and 15ml were obtained from Corning (High Wycombe, UK). Syringes (10ml) were obtained from Scientific Laboratory Supplies

Ltd. (Nottingham, UK) and syringe driven 0.22µm filters were obtained from Merck Millipore (Hertfordshire, UK). Transwell inserts and 24 well culture plates were obtained from Merck Millipore and 96-well v-bottomed plates were obtained from Greiner Bio-One, and were ultra-violet (UV) light irradiated prior to use. Sterile 30g needles were obtained from BD MicroLance (Dorset, UK) and T75 (75cm²) cell culture flasks were obtained from Corning.

2.1.5 Commercially available kits

RNeasy mini-kit and RNase-free DNase set were obtained from Qiagen (Crawley, UK). Mouse on Mouse elite peroxidase kit, Vectastain elite ABC Kit (rabbit IgG), DAB substrate, Avidin/Biotin Blocking Kit were obtained from Vector Lab (Peterborough, UK). Taqman gene expression assays were purchased from Applied Biosystems. Phire green Hot Start II PCR master mix and Phire Animal Tissue Direct PCR kit were purchased from Life Technologies. SAM-11 (PAR-2) mouse monoclonal antibody was purchased from Santa-Cruz (Texas, USA). ST14 (matriptase) rabbit polyclonal antibody was obtained from Sigma-Aldrich.

2.1.6 Histology Reagents

Mayer's haematoxylin, Scott's tap water, Eosin, Weigert's iron haematoxylin, Fast Green, Safranin-O, Alcian Blue, Nuclear Fast Red solution, Biebrich scarlet-acid fuchsin, alinine blue and DPX mountant were all purchased from Sigma Aldrich. Slides (superfrost), cover slips and histology cassettes were purchased from CellPath (Newtown, UK). 10% buffered paraformaldehyde was purchased from Sigma-Aldrich. Formical-2000 was purchased from Quartett (Berlin, Germany). Hydrogen peroxide blocking reagent was obtained from Abcam (Cambridge, UK).

2.1.7 Micro-computed tomography

A SkyScan 1172 desktop high resolution in vitro micro-computed tomography (micro-CT) scanner was used under the supervision of Prof. Rob van't Hof at the University of Liverpool. The software used included SkyScan NRecon to reconstruct cross sectional

images, CTAn version 1.5.0 for measuring quantitative parameters, CTVox providing a virtual 3D viewing environment by surface and volume rendering and Data Viewer, which displays reconstructed images. Again the software was provided by Prof. Rob van't Hof, University of Liverpool.

2.1.8 Animal work

Conditional floxed PAR-2 (F2r11) mice were generated by Dr Neil Dear at the University of Leeds, using embryonic stem (ES) cells purchased from The Wellcome Trust Sanger Institute (Cambridge, UK). Conditional floxed matriptase (ST14) mice were a gift from Dr Thomas Bugge in USA [188]. Col2;Cre mice were a gift from Prof. Mike Briggs, Newcastle University, and Oc;Cre mice were a gift from Prof. Tim Skerry University of Sheffield. All animal husbandry was carried out at the Comparative Biology Centre (CBC), Newcastle University. All surgical equipment (sterilised) was provided by the CBC, Newcastle University with use of surgical and anaesthetic facilities. All animal work was carried out under the Home Office Animals (Scientific Procedures) Act 1986.

2.1.9 Other reagents

All other chemicals and biochemical used were commercially available analytical grade reagents obtained from Sigma-Aldrich Company Ltd., Fisher Scientific, Life Technologies or BDH, unless otherwise stated.

2.2 Methods

2.2.1 Genetic manipulation of mice

Principle

There is considerable interest in annotating the human genome with functional information allowing an understanding of the molecular mechanisms and pathways underlying normal and pathological development. The mouse is a good experimental model to fulfill these requirements by genetically manipulating its genome [190, 191].

With the use of the BAC map (which stores DNA covering the vast majority of the mouse genome) and gene targeting techniques the mouse genome has been successfully modified allowing functional analysis to take place. Briefly, the first step is to design a targeting vector and then electroporate the vector into ES cells, where homologous recombination occurs. By the process of positive selection and PCR analysis, the required ES cells are then injected into the mouse blastocyst and offspring analyzed for the degree of chimerism [191].

In my research, I had two strains of genetically modified mice, which were conditional knockout mice generated by gene targeting. Specifically the conditional knockout mice were matriptase (ST14) and PAR-2 (F2r1) strains.

Materials

- ST14 conditional knockout mice C57BL/6N (Dr Thomas Bugge, USA)
- F2r1 conditional knockout mice C57BL/6N (Dr Neil Dear, University of Leeds)
- Col2-Cre C57BL/6N mice (Prof. Michael Briggs, The Centre for Life, Newcastle University)
- Oc-Cre mice C57BL/6N (Prof. Tim Skerry, University of Sheffield)
- Comparative Biology Centre (CBC) Newcastle University

Methods

F2r1 Vector design

The targeting vector design shown in figure 2.1 was generated from the International Mouse Phenotype Consortium (IMPC) database, and had been electroporated into ES cells and transferred to a mouse blastocyst to produce a first conditional knockout mouse, specifically C57BL/6N mice colony Jax EPD0592_3_B04-2.

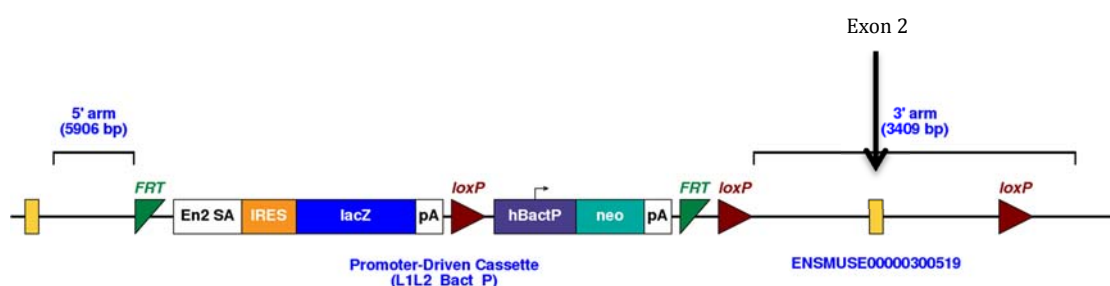


Figure 2.1: F2r1 vector design. A conditional F2r1 allele with a neomycin cassette flanked by FRT sites, allowing removal of the neomycin cassette upon addition of FLP recombinase. Exon 2 flanked by loxP sites can be ablated upon addition of Cre recombinase. Adapted from IKMC website.

Of importance, in correspondence with Prof. Skarnes at the Wellcome Trust Sanger Institute, when the BAC targeting vector was produced for F2r11, small deletions were made at the recombineered junctions, specifically near the loxP sites. Due to this when carrying out semi-quantitative PCR for genotyping the floxed allele (149bp) was indeed smaller than the non-floxed allele. (173bp) To provide evidence for this I have attached an annotated genomic sequence in the appendices for both the genetically modified (Appendix A) and wild-type alleles (Appendix B) for F2r11, showing the small deletions upon its engineering and the positions of the primers used in PCR analysis. Details of the primers are provided in section 2.2.6. The primers used to detect the floxed PAR-2 allele were p2/p3 and primers used to detect successful ablation of exon 2 were p1/p3. The genomic sequence shown in Appendix A for the floxed allele was present in the mouse and can be manipulated with the use of FLP and Cre recombinases to produce the required genetic ablation by the use of dual recombinase strategies.

FLP recombinase

The first step performed with the F2r11 conditional mice was to introduce FLP recombinase by crossbreeding with FLP mice. This allowed removal of the neomycin cassette between the two FRT sites shown in figure 2.1. This prevents any problems with interference of the knockout.

Cre recombinase

After FLP recombinase was performed the genomic sequence in the mouse contains a floxed exon 2 shown in figure 2.1. Exon 2 can now be removed specifically in the cartilage or bone by crossbreeding the mice with a col2-Cre mouse or Oc-Cre mouse, respectively giving a product of 116 bp on semi-quantitative PCR. This ablation of exon 2 produces a frame-shift mutation and a null allele, confirmed on the IMPC website.

ST14 vector design

The design of the targeting vector introduced into ES cells and transferred to a mouse blastocyst to produce a first conditional knockout mouse was taken from a paper by List et al. Details about the targeting vector, floxed allele and ST14 allele after recombination are provided in the paper by List et al. [188]. The primer details are detailed in the paper by List et al. [188], essentially the primers used to detect floxed or non-floxed alleles were

p5/p4, resulting in 450bp for the floxed allele and 425bp for non-floxed. After excision of exon 2 the product is 450bp and 900bp before excision with the neomycin cassette, using primers p5/p3. Details of the primers and PCR reaction are given in section 2.2.6.

Cre recombinase

The mouse containing the ST14 floxed allele was crossed with a col2-Cre mouse in order to produce a cartilage specific ST14 knockout mouse. The ablation of exon 2 produces a frame-shift mutation, and a null allele. List et al. showed that this ablation of exon 2 resulted in ablation of ST14 mRNA and protein in the intestine, detected on quantitative PCR and immunohistochemistry, respectively [188].

2.2.2 Destabilization of the medial meniscus (DMM) surgery in C57BL/6 mice

Principle

The medial meniscotibial ligament (MMTL) anchors the medial meniscus to the tibial plateau, shown in figure 2.2. After sectioning the MMTL, the medial meniscus is displaced medially resulting in altered mechanical stress, especially at the medial aspect of the tibia [192].

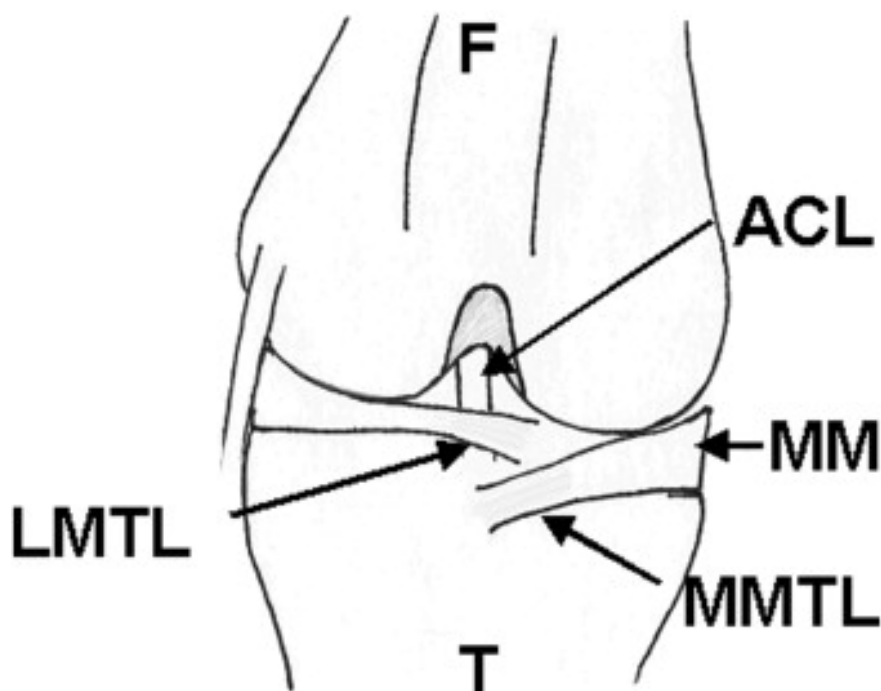


Figure 2.2: Diagram of mouse knee joint. F=femur. T=tibia. MM=medial meniscus. MMTL=medial meniscotibial ligament. LMTL=lateral meniscotibial ligament. In DMM the MMTL is sectioned destabilizing the MM. Taken from Glassson et al. 2007 [192]

Glasson et al. found DMM surgery more closely reflects the more slowly progressive human OA, compared to other methods such as the ACLT (anterior cruciate ligament transection) model, which has more severe OA and erosion of subchondral bone [192]. Therefore the DMM model was used in my study.

Materials

- Surgical kit: Tissue cauteriser (plus spare AA batteries), foil, 2 x scissors for skin incision, swabs and cotton buds, 2 x fine curved forceps, 2 x other small forceps, round handle blade holder plus 5.0mm blade, (Medical Sterile Products, MSP, 59M) for MMTL incision, wound clips, clip applier and remover. The kit was autoclaved prior to use. All kit was provided by the CBC.
- Buprenorphine (0.15ml per mouse of 3µg/ml solution), 25g needle, 1ml syringe, sterile saline. All this was provided by the CBC.
- CBC surgical room containing microscope, hydrex pink, eye gel, anaesthetic chamber, oxygen, isoflurane, heating pad and post-operative recovery incubator.

Method

DMM surgery was carried out by either Dr Craig Bullock or Dr Wang Hui. Pre-operative preparation was carried out by either myself or Valerie Affleck.

1. Before surgery the surgeon prepared the surgical kit and autoclave. Gloves, gowns, drapes and buprenorphine were ordered from theatre. The surgeon checked the mice were in adequate health and printed off monitoring and record forms. The surgeon ensured an experimental protocol was in place for the procedure/experiment to be conducted, and ensured the relevant COSHH (Control of Substances Hazardous to Health)/risk assessments were in place for any chemicals.
2. On the day of surgery the surgeon collected the autoclaved surgical kit, Hydrex Pink, syringes (1ml) and needles (25g). The assistant prepared the analgesia (buprenorphine).
3. The assistant then prepared for surgery – oxygen levels and spare cylinders, top-up vaporiser with isoflurane were checked. The assistant then checked clippers were charged and spare batteries were available for the tissue cauteriser. The recovery incubator and hot bead sterilizer were switched on.

4. The assistant collected mice from the holding room, checking the general condition of each mouse prior to starting the procedure.
5. The surgeon prepared the surgical area, and wore a sterile gown, sterile gloves, hairnet and facemask. The surgical field was covered with a sterile drape and sterile drapes were used to cover the mouse (with a small window cut out for the knee joint). Autoclaved tin foil was available to wrap around the microscope and other equipment to maintain sterility. The surgeon was vigilant that once they were sterile, they did not touch any non-sterile items. This is implemented in Glasgow (and other establishments, for example Nottingham).
6. The assistant weighed the mouse, recording the weight on the monitoring and record forms.
7. The assistant placed the mouse in an anaesthetic induction box and anaesthetized the mouse. Initial anaesthesia was at 3-3.5% isoflurane in 1L/minute oxygen and then maintained at 2-3.5% isoflurane in 1L/minute oxygen during surgery. Once the righting reflex was lost the mouse was removed from the induction box and placed in a nose cone. The left knee joint was shaved and sprayed with Hydrex pink.
8. Pre-operative analgesia was given subcutaneously into the flank of the mouse (buprenorphine, 0.15ml per mouse of a 3µg/ml solution) by the assistant.
9. The mouse was placed in the surgical area with a heating pad underneath and covered with a sterile drape, ensuring the left knee joint was accessible. The left foot was secured in place using tape, so that the knee was at a roughly 90° angle.
10. The assistant ensured that appropriate anaesthetic levels were provided, adjusted accordingly to the mouse's response.
11. The surgeon then carried out the procedure. A longitudinal medial incision was made on the left knee joint, just adjacent to the patellar ligament and extended caudal and rostral to expose the knee joint. This incision was made with scissors or a scalpel blade and was kept to the minimum size possible to reduce trauma, but large enough to successfully dissect and section the MMTL.
12. Large blood vessels were identified surrounding the area to be dissected and gently cauterised.

13. Using a scalpel blade, a full-length mediolateral incision was made to expose the patellar ligament. This incision was then extended medially at the caudal end to open the joint capsule and expose the intra-articular fat pad.
14. Using a pair of curved forceps the patella ligament was gently gripped and the surgeon began to dissect the fat pad exposing the medial meniscus, using another pair of curved forceps. The meniscus was located towards the bottom of the fat pad.
15. Once the medial meniscus was visualized, its path was followed medially to identify the MMTL. Using smooth cutting motions, without applying too much pressure, the MMTL was cut using the special needle blade. (Extra attention was paid to avoid any damage to the tibial and femoral surface). This normally took a few cuts (3-5), but once free the meniscus was able to move freely and easily. The meniscus was displaced laterally once the ligament was cut to prevent re-stabilisation of the joint.
16. The surgeon ensured there was no heavy bleeding in the joint at the end of the surgery. If bleeding developed pressure was applied for a few seconds with a sterile cotton swab. If the bleeding did not stop, the vessel was cauterised.
17. The skin overlying the knee joint was clipped using sterile clips. Two to three clips were adequate, ensuring the clips were secured. The clips were tightened using tissue forceps.
18. The mouse was placed in a recovery incubator and monitored.
19. The surgical instruments were cleaned using the autoclaved kidney dish and sterile water. The surgical instruments were placed in the hot bead steriliser for a few seconds and allowed to cool.
20. The surgery was then repeated on the next mouse.
21. A few hours after the surgery, the general condition of the mice was checked to ensure successful recovery. Clips were also checked. According to the Home Office regulations, clips can only be replaced once the wound site was clean. These checks were carried out by the surgeon, unless responsibility was formally transferred to another competent person.
22. The following day post-surgery mice received analgesia.
23. Throughout the duration of the study animal health (including weights) were monitored and recorded. Any issue should be raised with the PiL holder in the first

instance, followed by animal technicians or NACWO (Named Animal Care and Welfare Officer).

24. Seven days post-surgery wound clips were removed.

2.2.3 Collection of mouse limbs and processing for histology/IHC

Principle

DMM surgery took place in the left mouse knee joint therefore this limb was dissected for histological analysis. The fixative (paraformaldehyde) fixed the tissue by cross-linking of proteins, terminating any on-going biochemical reactions, which preserved cells and tissues in preparation for sectioning and staining. Decalcification removed the calcium ions from the bone making the bone softer and more flexible allowing sections to be taken on the microtome. Next the decalcified joints underwent processing – dehydration, clearing and infiltration. The joints were passed through baths of progressively more concentrated ethanol to remove the water, followed by xylene (a hydrophobic clearing agent, which removed the ethanol) and finally molten paraffin wax, which infiltrated the joint and removed the xylene. Next the joints were externally embedded in molds using molten paraffin wax. The embedded joints then underwent longitudinal sectioning using a microtome, and staining.

Materials

- Dissecting kit – 2x scissors, scalpel blade holder, scalpel blades, 2x tweezers

Method

Mice were sacrificed under schedule 1 of the Animals (Scientific Research) Act 1986. The ipsilateral and contralateral limbs were dissected. The skin was cut around the ankle and a longitudinal incision was made up the limb to the hip. The limb could then be cut off at the level of the hip. The muscle and soft tissue were dissected off, and the limb placed in 10% buffered paraformaldehyde for fixation. After 48 hours the limb was transferred either to 70% ethanol for later use in micro-CT, or was decalcified for histology. For decalcification the limb was washed in distilled water for 5 minutes, and then placed in 8ml of Formical 2000 for 16 hours to allow decalcification. The limb was then washed in distilled water, and placed in a labeled histology cassette. The joints were then stored in

phosphate buffer at 4°C and transferred to the BioBank for processing. After processing and embedding the joints were sectioned using a microtome, carried out by Research Histologist – Sharon Watson. Serial sections (4µm) were cut and transferred to slides using a water bath at 32°C. The sections were then used for histology staining and IHC.

2.2.4 Xiphisternum micro-dissection and RNA extraction

Principle

The xiphisternum of the mouse is made up of hyaline cartilage composed of chondrocytes, proteoglycans and collagen type II. [193] Therefore this tissue provides a good source of cartilage to detect cartilage specific gene ablation. The xiphisternum was homogenized in the presence of Trizol, which solubilizes cells, proteins and nucleic acids from the tissue. Trizol contains guanidine isothiocyanate and phenol, which isolated RNA, DNA and protein fractions from cell and tissue samples, upon addition of chloroform. After addition of chloroform and centrifugation, three layers form including an aqueous layer (containing the RNA) an intermediate layer (containing the DNA) and a bottom layer (containing protein) [194]. The RNA was then isolated using mini columns in the Qiagen RNeasy kit by binding of RNA to the silica membrane, whilst washing away any contaminants. The addition of a DNase I step removed any contaminating genomic DNA. The final RNA was eluted in RNase free water.

Materials

- Dissection kit: scissors, scalpel blades and holder, forceps and tweezers
- Qiagen RNeasy Kit (Qiagen catalogue number 74104)
- Qiagen DNase I (Qiagen catalogue number 79254)
- MixerMill 400 tissue homogenizer (Retsch)

Method

Mice were sacrificed under schedule 1 of the Animals (Scientific Procedures) Act 1986. The mouse was sprayed with 100% ethanol. All dissecting equipment was sprayed with 100% ethanol and RNase zap. The skin overlying the rib cage was cut making a longitudinal vertical excision to expose the xiphisternum (appears white). The soft tissue

overlying the xiphisternum was carefully excised allowing the xiphisternum to be dissected. All soft tissue and any remaining bone were trimmed from the xiphisternum, leaving only the cartilaginous xiphisternum. The xiphisternum was then placed in an RNase free eppendorf, and snap frozen in liquid nitrogen.

The tissue was then homogenized using the MixerMill MM 400 tissue homogeniser (Retsch). All equipment was autoclaved and cleaned with RNase zap prior to use. The vials were cooled in liquid nitrogen and 1ml of Trizol was added. Once the Trizol was frozen the tissue sample was carefully added to the vial. The vials were secured shut and placed in the homogenizer to undergo 2 minutes of homogenization at 100Hz. The sample was thus ground up in the Trizol, and was carefully transferred to an RNase free eppendorf using a spatula. Chloroform (500 μ l) was then added and the sample shook vigorously for 2 minutes and left at room temperature on a rocker for 10 minutes. The sample was then centrifuged at 4°C for 30 minutes at 12000g to separate the RNA phase from DNA and proteins. The RNA aqueous phase was then carefully pipetted into an RNase free eppendorf and 100% ethanol (0.5 volume of RNA phase) was added. This sample was then added to a Qiagen mini column, and steps followed as per manufacturer's instructions. Briefly, the sample was applied to the mini column and centrifuged at 8000g for 15 seconds and the flow through discarded. Next the column was washed to remove contaminants, and flow through discarded. Then 40 μ l of DNase I was applied to the column and incubated at room temperature for 15 minutes. The column was then washed three times, according to the manufacturer's instructions. Finally the RNA was eluted in 30 μ l of RNase free water contained in the Qiagen RNeasy kit. To quantify the RNA a Nanodrop ND 1000 spectrophotometer was used, measuring the absorbance at 260nm, along with ratios for contamination 260/280 and 260/230. The ratio of absorbance at 260nm and 280nm was used to assess the purity of the RNA. A ratio of \sim 2 was generally accepted as 'pure'. If the ratio was appreciably lower, then it may indicate the presence of protein, phenol or other contaminants which absorb strongly at or near 280nm. As a secondary measure of nucleic acid purity, the 260nm and 230nm ratio was used. Expected values were in the range 2.0-2.2. If the ratio was appreciably lower it may indicate the presence of contaminants which absorb at 230nm. The RNA was then stored at -80°C for later use in qPCR.

2.2.5 Reverse Transcription polymerase chain reaction (RT-PCR)

Principle

RT-PCR produces cDNA from an RNA template, and provides a useful strategy for analyzing gene expression. Reverse transcription requires random hexamers (Pd(N)₆) which bind to random complementary sites in the RNA, to act as primers for dNTPs to synthesise cDNA which is initiated by the polymerase – Superscript III Reverse Transcriptase. The addition of RNase OUT and DTT prevent RNA degradation and prevent dimerization, respectively.

Method

A master mix was made first, by adding 1µl of random hexamers (1µg/ml) and 1µl of dNTPs (10mM) into a DNase and RNase free PCR tube, and then up to 1µg of RNA was added, making the final volume up to 13µl with DNase free water. The mixture was placed in the PCR thermocycler for 5 minutes at 65°C, and immediately afterwards placed on ice. Another master mix was then made containing 0.5µl Superscript III, 2µl DTT (0.1M), 4µl 5x first strand buffer and 0.5µl of RNase OUT. From this mixture, 7µl was added to the sample on ice (final volume 20µl) and placed in the thermocycler. Specifically the settings were 25°C for 5 minutes, 50°C for 60 minutes and 75°C for 15 minutes, to allow synthesis of cDNA. The cDNA was then stored at -20°C until use. Prior for use in qPCR, specific dilutions were made as detailed in section 2.2.7.

2.2.6 Semi-quantitative polymerase chain reaction (PCR)

Principle

Genomic DNA was extracted from a mouse allowing a specific gene of interest to be amplified using PCR. PCR is a well-known technique enabling amplification of a specific DNA fragment from only trace amounts of DNA, cDNA or RNA [195]. The specificity of the primers allows amplification of a specific gene. It is a chain reaction whereby one DNA molecule is used to produce two copies, four, then eight etc. in an exponential manner. In order to do this, a polymerase is able to add nucleotides (the four bases adenine, thymine, cytosine and guanine) to the denatured DNA strand to form double stranded DNA. The primer is specific to the region of DNA and also acts as a template allowing

addition of nucleotides [196]. The resultant DNA strand can then act as a template for the synthesis of further DNA. The three major steps in PCR are denaturation, annealing and extension henceforth amplifying the specific region of DNA, in a thermal cycler machine. The product can be visualized in two ways. This can be by staining of the DNA product with ethidium bromide, which intercalates between the two strands of DNA, or a more modern technique which utilizes specific probes, which can be degraded releasing the reporter from the quenching region and emit fluorescence (section 2.2.7). The method used here was semi-quantitative and utilized agarose gel electrophoresis to visualize the PCR product [195]. The basic principle of agarose gel electrophoresis is separation of DNA molecules using an electric field where negatively charged molecules migrate towards a positive anode. The DNA molecule can then be visualized using ultraviolet (UV) illumination, which visualizes the DNA molecule due to the intercalation of ethidium bromide between the DNA strands.

Materials

- Primers for ST14 (matriptase) and PAR-2 (F2r11), designed by Dr Thomas Bugge and Dr Neil Dear, respectively. All purchased from Sigma-Aldrich. (Table 2.1)

Primer	Sequence
ST14 common reverse P5	5'-GTGGAGGTGGAGTTCTCATACG-3'
ST14 floxed forward P4	5'-CAGTGCTGTTGAGCTTCCTCTT-3'
ST14 targeted deletion forward P3	5'-GCATGCTCCAGACTGCCTTG-3'
PAR-2 targeted exon 2 deletion forward P1	5'-CTAGAAAGTATAGGAACTTCGTGCG-3'
PAR-2 floxed forward P2	5'-AAACAGTGTGATGCTCACTC-3'
PAR-2 common reverse P3	5'-GGAATCTACACCTGGCCTTGT-3'
Col2-Cre forward	5'-TCCAATTTACTGACCGTACA-3'
Col2-Cre reverse	5'-AAACAGCATTGCTGTCACTT-3'
Oc-Cre forward	5'-TGATGGACATGTTGAGGGATC-3'
Oc-Cre reverse	5'-CAGCCACCAGCTTGCATGA-3'

Table 2.1: Table of primers used for genotyping

- Phire green Hot Start II PCR master mix (Life technologies)
- Electrophoresis buffer – Tris-acetate-ethylenediamine tetraacetic acid (TAE) buffer: 0.04 M Tris (pH 8), 5.7 % (v/v) glacial acetic acid and 0.001 M EDTA
- GeneRuler Express DNA ladder (Life Technologies)
- Gene Ruler 1kb plus DNA ladder (Life Technologies)
- Phire Animal Tissue Direct PCR kit (Life Technologies)

Method

Genomic DNA extraction was carried out from a mouse ear notch sample, using Phire Animal Tissue Direct PCR Kit. The dilution method was used, which briefly involved placing the tissue sample in 20 μ l of dilution buffer, and adding 0.5 μ l of DNA Release Additive. The sample was then vortexed, and left at room temperature for 5 minutes and then incubated at 98 $^{\circ}$ C for 2 minutes. Finally the sample was vortexed and pulse spun in a bench-top micro-centrifuge. The DNA was thus present in the solution.

After genomic DNA extraction the specific region of DNA was amplified by PCR, for visualization via gel electrophoresis. The Phire green Hot start II PCR master mix contained Phire Hot Start II DNA polymerase, nucleotides and optimized reaction buffer including MgCl₂. The Phire polymerase was enhanced and faster and provided greater yields compared to Taq polymerase. This was due to the enhanced polymerase having a unique double stranded binding domain allowing short extension times and high yields. The first step was to make up a master mix for the number of samples one has. The master mix includes 10 μ l of Phire green Hot Start II PCR master mix, 0.5 μ l of specific primers (10 μ M) needed (final concentration 0.25 μ M per 20 μ l reaction volume), 1 μ l of DNA sample and addition of DNase free water to make the master mix up to 20 μ l. Next, 20 μ l of the sample (with specific DNA sample and primers) was added to each well in a PCR-plate. These samples were then cycled through PCR with specific settings detailed below.

PCR settings adequate for ST14, PAR-2, OC-cre and Col2-cre:

- 1: 98 $^{\circ}$ C 5 minutes
- 2: 98 $^{\circ}$ C 5 seconds
- 3: 61 $^{\circ}$ C 5 seconds (Annealing temperature)
- 4: 72 $^{\circ}$ C 20 seconds
- 5: Go to step 2 repeat 40 times
- 6: 72 $^{\circ}$ C 1 minute
- 7: 4 $^{\circ}$ C infinite

The only alteration to these settings was for detecting the targeted deletion of PAR-2 exon 2, where the annealing temperature was 55 $^{\circ}$ C. Whilst the DNA was amplified an agarose gel was prepared. A 3% gel was adequate for PAR-2 and ST14 and a 2% gel was adequate for OC;cre and Col2;cre. To make an agarose gel, the agarose was diluted in TAE buffer. To make one gel 120ml is sufficient, so to make a 1% gel 1.2g of agarose was

added and so forth. 1µl of ethidium bromide was added to 50ml of dissolved agarose. The solution was poured into a plastic cast and a comb was placed into the gel depending on the number of samples one has. Once the gel has set it was transferred to the gel electrophoresis machine in its cast covered in TAE buffer. To the first well 5µl of ladder was added, and then 10µl of each PCR reaction to the remaining wells. A current of 120mV was then passed through the gel to allow migration of DNA products. These DNA fragments were then visualized with UV light using the GelDoc machine, due to intercalation of ethidium bromide. The DNA fragments were compared to the ladder to detect the variously sized products.

2.2.7 Quantitative Real-time Polymerase Chain reaction (qPCR) – TaqMan probe based

Principle

This method of PCR allows for both detection and quantification of the PCR product in real time, whilst it is being synthesized by measurement of a fluorescent reporter molecule [197]. TaqMan probes are labeled with a fluorescent reporter (fluorescein FAM) at the 5' end, and a quencher (rhodamine TAMRA) at the 3' end of the probe sequence. Fluorescence-resonance energy transfer (FRET) from the reporter to the quencher enables suppression of reporter molecule fluorescence. After annealing of the forward and reverse primers to the target sequence, the TaqMan probe is designed to anneal between these primer sites, and is hydrolyzed by the 5'-3' exonuclease activity of the Taq polymerase. Probe hydrolysis results in release of the reporter from the quencher, and hence a cumulative increase in fluorescence which is proportional to the amount of transcript present. If no product is present the TaqMan probe does not bind, and the reporter remains quenched, with no fluorescence seen [197].

Materials

- TaqMan Gene Expression Assay F2r11 Mouse (Applied Biosystems)
- TaqMan Gene Expression Assay ST14 Mouse (Applied Biosystems)
- TaqMan Gene Expression Assay col2a1 (Applied Biosystems)
- TaqMan Gene Expression Assay GAPDH (Applied Biosystems)
- TaqMan Gene Expression Master Mix (Life Technologies)

Method

The cDNA was diluted to 1ng/μl using DNase free-water. Separate master mixes were made for F2r11, ST14, col2a1 and GAPDH by adding 5ul of TaqMan Gene Expression Master Mix and 0.5μl of each specific gene assay. 5μl of cDNA was added to each well for a total amount of 5ng. Next, 5μl of each specific gene master mix was added to the relevant wells. The plate was pulse spinned and then placed in the Real-Time PCR thermocycler. Thermal cycling conditions comprised an activation stage at 95°C for 10 min. This was followed by a two-step program consisting of 95°C for 15 seconds and 60°C for 60 seconds, repeated for 40 cycles. The presence of GAPDH as a housekeeper gene enabled analysis of Ct (threshold cycle) values on Microsoft Excel, to give a quantification of gene expression.

2.2.8 *Histology staining*

Principle

The four stains used in my research were:

- Haematoxylin and Eosin staining (H&E)
- Safranin-O staining
- Alcian Blue staining
- Masson's Trichrome

The basic histological staining for the assessment of cell and tissue morphology and distribution is H&E stain. Haematoxylin is a dark blue/violet stain that is basic/positive and binds to basophilic substances (such as DNA or RNA in the nucleus which are acidic and negatively charged). Eosin is a pink/red stain, which is acidic/negative, and binds to acidophilic substances (such as protein, which are basic and positively charged). Therefore H&E stains cell nuclei blue/purple and the cartilage/bone matrix pink. Safranin-O is a cationic (positively charged) dye that stains proteoglycans including glycoaminoglycans (which are negatively charged), and hence detects cartilage. The cartilage will be stained red and the nuclei black. The background will be stained bluish/green due to the presence of Fast Green as a counter-stain. This contrast in color enables one to assess cartilage damage easily under a microscope. Safranin-O is proportional to proteoglycan content in normal cartilage, however it is not a sensitive

indicator of proteoglycan content in cartilage in which glycosaminoglycans have been depleted, or are in low abundance [198].

Alcian Blue is also a cationic dye used to stain acidic mucopolysaccharides and proteoglycans, such as glycosaminoglycans in cartilage producing a blue stain. Both Alcian Blue and Safranin-O can be used to assess chondrogenesis, by detecting cartilage matrix proteoglycans. Alcian Blue provides more intense staining than Safranin-O, due to the fact that it has a higher affinity for the sulfur in cartilage compared to Safranin-O [198].

Masson's Trichrome staining, as the name implies, produces a three-color staining pattern by using several different dyes. A haematoxylin stain is used first to stain the nuclei black. Acid dyes were used to stain the acidophilic cytoplasm pink. Collagen fibers are also acidophilic, however colour differently from the cytoplasm due to the action of phosphomolybdic-phosphotungstic acids, which are taken up by the connective tissues, and then replaced by aniline blue in a type of substitution reaction of one acid for another, producing a blue color.

Method

All histological staining was carried out by Sharon Watson (Research Histologist MRG). Briefly for H&E staining slides were de-waxed in xylene and rehydrated through graded ethanol (100-70%). Slides were incubated in Mayer's Haematoxylin for 1.5 minutes, washed in running tap water and then incubated in Scott's tap water for 30 seconds. Slides were then washed in running tap water, and then stained with Eosin for 2 minutes. After a further wash slides were dehydrated in graded ethanols (70-100%) cleared in xylene and mounted with a cover slip using DPX.

For Safranin-O slides were de-waxed and hydrated as before, followed by incubation in Weigert's haematoxylin for 10 minutes. Slides were then washed in distilled water and dipped in acid ethanol and washed in distilled water again. Next slides were washed in running tap water for 10 minutes, stained in Fast Green for 5 minutes and dipped in 1% acetic acid for 10 seconds. Then slides were stained in Safranin-O for 5 minutes. Finally slides were dehydrated in graded ethanols, cleared in xylene and mounted as before.

For Alcian Blue staining similar de-wax and hydration steps were performed. Next slides were incubated in Alcian Blue dye for 30 minutes and washed in running tap water for 2 minutes. Slides were then rinsed in distilled water and counterstained in nuclear fast red

solution for 5 minutes, with a further wash in running tap water. Slides were then dehydrated and cleared in xylene and mounted as before.

Masson's Trichrome staining followed the same initial steps of de-wax and hydration, and then stained in Weigert's haematoxylin solution for ten minutes. After washing in running tap water for 10 minutes and washing in distilled water, slides were stained in Biebrich scarlet-acid fuchsin for 10 minutes. Slides were then washed in distilled water and incubated in phosphomolybdic-phosphotungstic acid solution for 10 minutes, and then transferred to aniline blue solution for 10 minutes. Slides were rinsed in distilled water and incubated in 1% acetic acid solution for 5 minutes. Slides were then washed in distilled water and then dehydrated, cleared in xylene and mounted using DPX (a mixture of distyrene (a polystyrene), a plasticizer (tricresyl phosphate), and xylene) and a cover slip.

2.2.9 Immunohistochemistry (IHC)

Principle

IHC is the process of detecting antigens in tissue sections, using specific antibodies, which detect the antigen of interest. The sample undergoes antigen retrieval to make the epitopes available for antibody binding, which is due to the formation of methylene bridges during fixation, which cross-link proteins and mask antigenic sites. Heat induced epitope retrieval (HIER) was used, which breaks the methylene bridges, exposing the antigenic sites. The staining method used in my research depends on biotin and peroxidases for amplification and detection of target antigens, respectively. In order to prevent false positive and high background detection, the endogenous forms of these proteins need to be quenched or masked. Incubation in 3% H₂O₂ blocks endogenous peroxidase, and an Avidin/Biotin blocking kit blocks all endogenous biotin, biotin receptors and avidin binding sites present in tissues. Also, a blocking reagent was used to bind to non-specific sites (reactive sites), which prevents non-specific binding of primary and secondary antibodies. Importantly this blocking reagent needs to be prepared from the species in which the secondary antibody was made.

The primary antibody used was either a monoclonal or a polyclonal antibody. Each has their own advantages and disadvantages. Essentially, polyclonal antibodies have higher

affinity and wide reactivity, but lower specificity compared to monoclonal antibodies. The main advantage of monoclonal antibodies is their higher specificity compared to polyclonal antibodies. The secondary antibody binds to the primary antibody, specific to the antigen of interest. A preformed complex between avidin and a biotinylated peroxidase enzyme (ABC) was added, which binds to the secondary antibody. Upon addition of 3,3'-Diaminobenzidine (DAB) substrate a brown precipitate is formed, due to the action of peroxidase. A counterstain (Mayer's Haematoxylin) was then used to provide contrast allowing the primary stain to stand out. The brown staining (specific to the antigen of interest) is then analyzed using a microscope.

Materials

- Vector Mouse on Mouse Elite Peroxidase kit (Vector Lab PK-2200)
- Avidin/Biotin blocking kit (Vector Lab SP-2001)
- DAB substrate (Vector Lab SK-4100)
- Vectastain elite ABC kit (rabbit IgG) (Vector Lab PK 6101)
- 10mM sodium citrate buffer pH6 (2.4g sodium citrate dehydrate added to 1 liter distilled water)
- Primary antibodies (SAM-11 mouse monoclonal antibody and ST14 rabbit polyclonal antibody)

Method

IHC was carried out by myself or Sharon Watson (Research Histologist, MRG).

The specific dilutions of primary antibody optimized for use were 1:150 SAM-11 and 1:50 ST14.

SAM-11

1. Place slides in 60°C oven for 30 minutes prior to IHC
2. All incubations were carried out at room temperature
3. De-paraffinize and hydrate slides in xylene (2 x 5 minutes) followed by 2 minutes each in 100, 95 and 75% alcohol
4. Rinse for 5 minutes in tap water
5. Warm citrate buffer in microwave (~7 minutes)
6. Place slides in boiling citrate buffer for 6 minutes

7. Place slides in PBS and draw wax rings around tissue sections
8. Incubate sections in 3% H₂O₂ for 5 minutes
9. Wash sections in PBS (2 x 2 minutes)
10. Perform Avidin/Biotin block by incubating in Avidin for 15 minutes, briefly washing in PBS and then incubating in Biotin for 15 minutes
11. Incubate sections in MOM mouse Ig blocking reagent for 1 hour
12. Wash sections in PBS (2 x 2 minutes)
13. Incubate sections in MOM diluents for 5 minutes
14. Tip off excess diluent and incubate sections in optimized diluted primary antibody (1/150) – SAM-11 (use MOM diluents) for 30 minutes
15. Wash sections in PBS (2 x 2 minutes)
16. Apply MOM biotinylated anti-mouse IgG reagent and incubate for 10 mins
17. Wash sections in PBS (2 x 2 minutes)
18. Apply vectastain ABC reagent and incubate for 5 minutes
19. Wash sections in PBS (2 x 5 minutes)
20. Apply DAB reagent and incubate for 5 minutes
21. Rinse for 5 minutes in running tap water
22. Incubate sections in Mayer's Haematoxylin for 30 seconds
23. Wash in water
24. Incubate sections in Scott's tap water for 40 seconds
25. Rinse for 2 minutes in running tap water
26. Dehydrate slides in 50, 70, 80 and 100% alcohol for 1 min each followed by xylene (2 x 2 minutes)
27. Mount and coverslip using DPX mountant

ST14

The same method was utilized as described for SAM-11, with a few alterations. In step 11 a different blocking reagent was used from the Vectastain elite ABC kit, (rabbit IgG) which was prepared from the species in which the secondary antibody was made, to bind to non-specific sites. Step 13 was omitted. In step 14 the primary antibody used was anti-ST14. The secondary antibody used in step 16 was also different. An anti-rabbit biotinylated, affinity purified anti-immunoglobulin secondary antibody was used contained in the Vectastain elite ABC kit. (Rabbit IgG) The same process was then

followed by adding a preformed ABC complex (with peroxidase activity) producing a brown precipitate upon addition of DAB.

2.2.10 Micro-computed tomography (micro-CT)

Principle

In general terms CT involves acquisition of sequential radiographic projections taken at different angles around the object of interest giving a three-dimensional radiographic image. These projections can then be reconstructed using a cone-beam volumetric (Feldkamp) algorithm. There are several different types of CT including micro-CT, multidetector CT (MDCT) mainly used clinically and high-resolution peripheral quantitative CT (HR-pQCT) for extreme detail [199, 200]. Micro-CT is widely used for imaging of bones in animal models and has been used in this project. There are 2 types of micro-CT scanners for in vitro or in vivo imaging, the main difference being that in the former the specimen rotates and in the latter the x-ray system rotates [200, 201]. However both of these scanners have features in common. Both types of micro-CT scanners consist of a tungsten anode x-ray tube with a small focal spot, coupled to a high-resolution x-ray detector. An in vitro micro-CT scanner (SkyScan 1172) was used in this project. The design of in vitro micro-CT scanners allows adjustment of source-object distance (SOD) and object-detector distance (ODD) allowing source-detector distance (SDD) adjustment and this has the advantage of optimizing geometric magnification level [200, 201]. All micro-CT systems use x-ray tubes and the SkyScanner 1172 used in this project uses a micro-focus x-ray tube where an electron beam is produced on the tip of a tungsten filament and focused by several magnetic lenses onto a focal spot of <math><5\ \mu\text{m}</math> on a transmission target. The x-ray source is 20-100kV (10W). The transmission target has a thin layer of tungsten electroplated on a carrying material. This allows a cone-shaped beam of radiation to irradiate a digital x-ray detector and produce an x-ray projection with a detail detectability ranging from

Materials

Equipment used as detailed in section 2.1.7.

Method

2.2.10.1 Scanning and reconstruction

The dissected tibia and femur were fixed in 10% buffered paraformaldehyde for 48 hours, and then stored in 70% ethanol. For preparation three knee joints were placed in a drinking straw (filled with 70% ethanol) with a base, which can be secured in the scanner. To activate the SkyScan 1172 insert key and turn clockwise. Open the shortcut to SkyScan 1172 on the computer. Activate the x-ray source to start the scanner. Open the door of the SkyScan 1172 and secure the straw into the rotating device. Close the door and press the 'TV' icon to visualise the 3 joints. Select 'set oversize scan' and press 'start' which will give an image of the three joints contained in the straw. Enter a prefix name for the joint to be scanned and select the region to be scanned and press 'single scan'. Repeat this for all 3 joints. Once all 3 joints have been selected press 'start scan'. Next adjust the settings for the scan. For all scans a 0.5 aluminium filter should be used, 0.5 rotations should be selected and the camera should be on the medium setting (2000x1024 pixels). For a high resolution scan 4.5µm resolution should be selected and for a low resolution scan 9µm should be selected. Press start and scanning will begin.

The scanned images are reconstructed using NRecon software. Open shortcut to NRecon on reconstruction computer and open 'GPU reconstruction server local version 1.6.9.3'. Open one of the scanned JPEG images and select standard.mouse bone.rcp as the protocol for measuring the parameters. Select 'start' and 'preview' giving a cross sectional image of a scanned bone. Adjust the box on the screen ensuring that there is minimal 'dead-space'. Press 'start' and 'add to batch'. Once all three joints have been added to the NRecon system select 'start batch' and all the tomography projection images will be reconstructed for each joint. Analysis can now take place on the reconstructed images using CTan, CTvox and DataViewer software.

2.2.10.2 Analysis subchondral bone medial and lateral epicondyles (EC) tibia

The same methodology was carried out for both medial and lateral epicondyles, therefore only analysis of medial epicondyle has been described. Open DataViewer and a high resolution scan, which should give 3 orthogonal sections shown in figure 2.3 below.

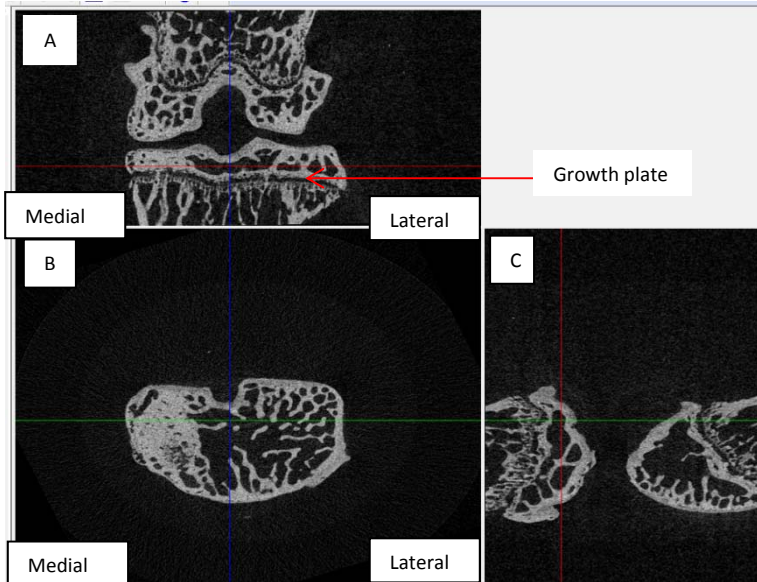


Figure 2.3: Orthogonal images on dataviewer for analysis. Cross-sectional images on dataviewer of a high resolution scan. Image A coronal view; image B transverse view; image C sagittal view. Images A and B should be straightened as shown in the image with the same orientation for all analysis.

Firstly orientate the bone in the same direction for all samples ensuring the medial aspect of the tibia is on the left side and lateral aspect on the right side, as shown in figure 2.3.

Next straighten the bone so the growth plate is aligned correctly by rotating images A and B, shown in figure 2.3 above. The next step is to save a volume of interest (VOI), which only includes the medial aspect of subchondral bone of the tibia, as this was analyzed.

Select 'Actions' and 'save as VOI' and a new box will appear as shown in figure 2.4. Ensure the file is saved as 'coronal' and adjust the box so only the area to be analyzed is included (refer figure 2.4). Save the dataset in a new folder.

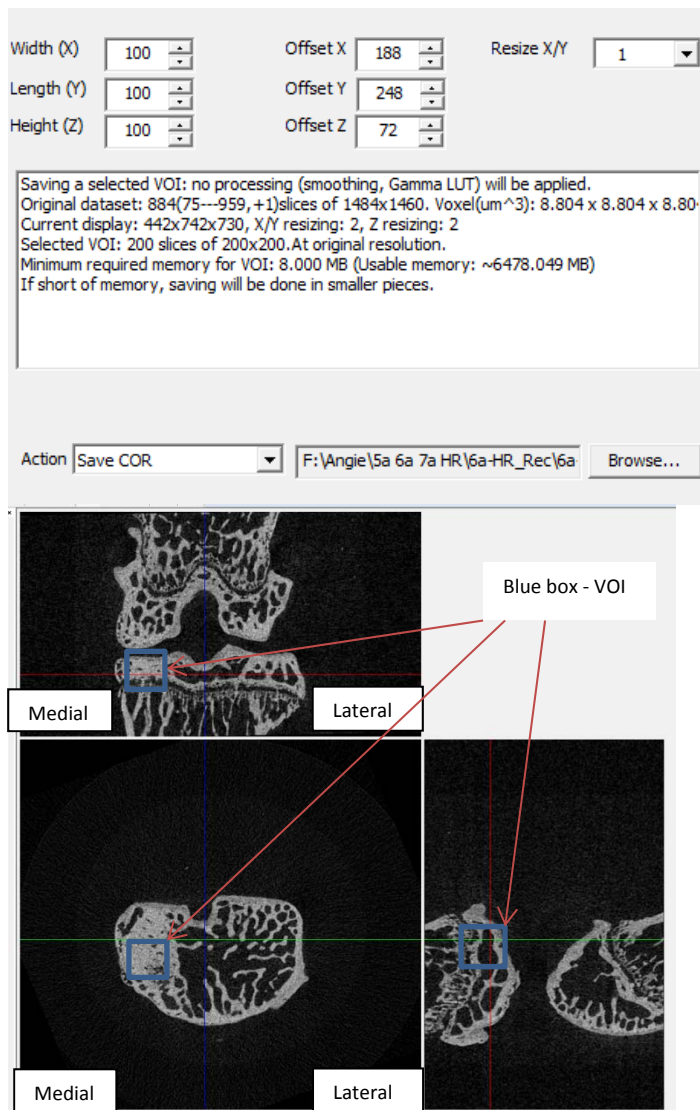


Figure 2.4: Volume of interest for analysis of medial aspect of tibial subchondral bone. Having selected 'save as VOI' a box (shown in blue) will appear. The width (X), length (Y) and height (Z) need to be adjusted to only include the medial aspect of subchondral bone of tibia. The dimensions need to be the same for all analyses which are X – 100, Y – 100 and Z – 100, giving a box enclosing the volume of interest. Once the VOI has been selected save the VOI as a coronal dataset and in the relevant folder, and a coronal dataset will be saved of the VOI which can be analysed on CTan described in text.

Now a VOI has been saved including only the area of interest, this was analyzed on CTan. Initially, I attempted to separate the subchondral plate from subchondral trabecular bone as two separate 'regions of interest' (ROI) to analyze both subchondral sclerosis and the subchondral trabecular bone. However, as shown in figure 1.6, when the subchondral bone becomes sclerotic it becomes impossible to separate these two regions. Therefore after discussion with Dr Carmen Huesa (University of Glasgow) I decided to select both the subchondral plate and trabecular bone as one region, which provided a more accurate analysis. I will describe both methods I attempted below.

To start ROI analysis, open CTan and the coronal subchondral dataset saved. In order to analyze subchondral sclerosis of the tibia medial epicondyle a ‘region of interest’ (ROI) needs to be selected including only the subchondral plate thickening. Select ROI and draw the area of subchondral plate thickening. Scroll through all the coronal images and draw around the ROI for all sections (100 in total). This ROI should be accurately defined throughout all of the 100 slices, refer figure 2.5.

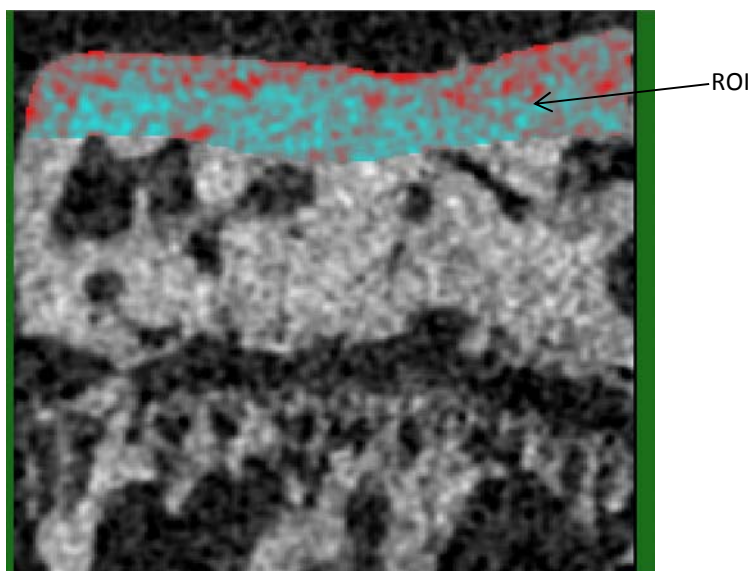


Figure 2.5 – Coronal cross sectional images of tibial medial epicondyle to define ROI to analyse subchondral sclerosis. The coronal dataset saved on dataviewer of the medial epicondyle of the tibia is opened on CTan giving 100 coronal images of the VOI. The red area is the ROI, which is the area of subchondral sclerosis. This red area needs to be accurately drawn through all 100 cross sectional images in order to analyze subchondral sclerosis. Subchondral sclerosis was analyzed by measuring TbTh (trabeculae thickness) in μm .

Once the ROI has been defined save the ROI. Open the ROI in CTan and click on ‘binary image’ on the toolbar and ensure the threshold is 80 and 255. Next click on ‘custom processing’ and select the ‘batman’ icon. Add the parameters for analysis and define these, detailed in table 2.2 below.

Parameter	Settings
Filtering	Median. 2D space. Radius 1
Threshold	80 low. 255 high. Global
Bitwise operations	Image=image AND ROI
Despeckle	Remove black speckles. 2D space. Less than 500 pixels. Apply to image
Morphological operations	Closing 3D space. Round radius 2. Apply to image
Despeckle	Sweep 2D space. All except largest object. Apply to image
3D analysis	Select basic values, trabecular thickness, 3D model and anisotropy

Table 2.2 – Parameters for analysis of subchondral plate thickening at the medial and lateral epicondyles

Select 'run' and the data will be analysed which can be viewed on an excel spreadsheet by saving as .csv file. This process for analysis of subchondral thickening at the medial epicondyle of the tibiae was the same as for analysis of the femora medial and lateral epicondyle subchondral thickening. For subchondral trabecular analysis, similar to above, a coronal dataset needs to be saved of the medial epicondyle of the tibia on dataviewer as described. This dataset was opened on CTan giving 100 coronal cross-sectional images of the medial epicondyle of the tibia. The ROI needs to be defined as shown in figure 2.6.

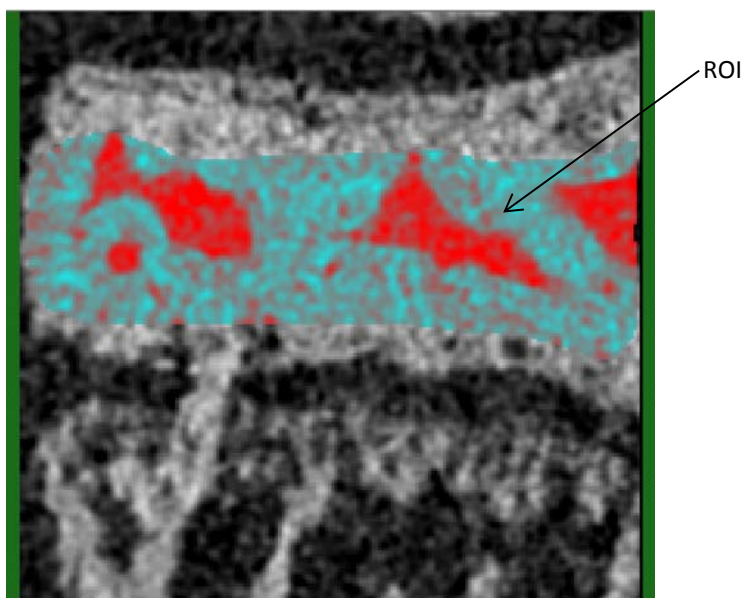


Figure 2.6 – Coronal cross sectional images of tibial medial epicondyle to define ROI to analyse subchondral trabecular bone. The coronal dataset saved on dataviewer of the medial epicondyle of the tibia is opened on CTan giving 100 coronal images of the VOI. The red area is the ROI which is the area of subchondral trabecular bone. This red area needs to be accurately drawn through all 100 cross-sectional images to analyse subchondral trabecular bone.

Save the ROI and follow the same steps as above for analysis using the same parameter values shown in table 2.2. The excel spreadsheet with all relevant data was transferred to SPSS for analysis to take place. Of note all analysis on CTan was carried out in 'pixel' units. Exactly the same process described above was carried out when analyzing the subchondral plate and subchondral trabecular bone as one ROI. The only difference was the ROI selected and the measurement analyzed for subchondral sclerosis (BV/TV) shown in figure 2.7.

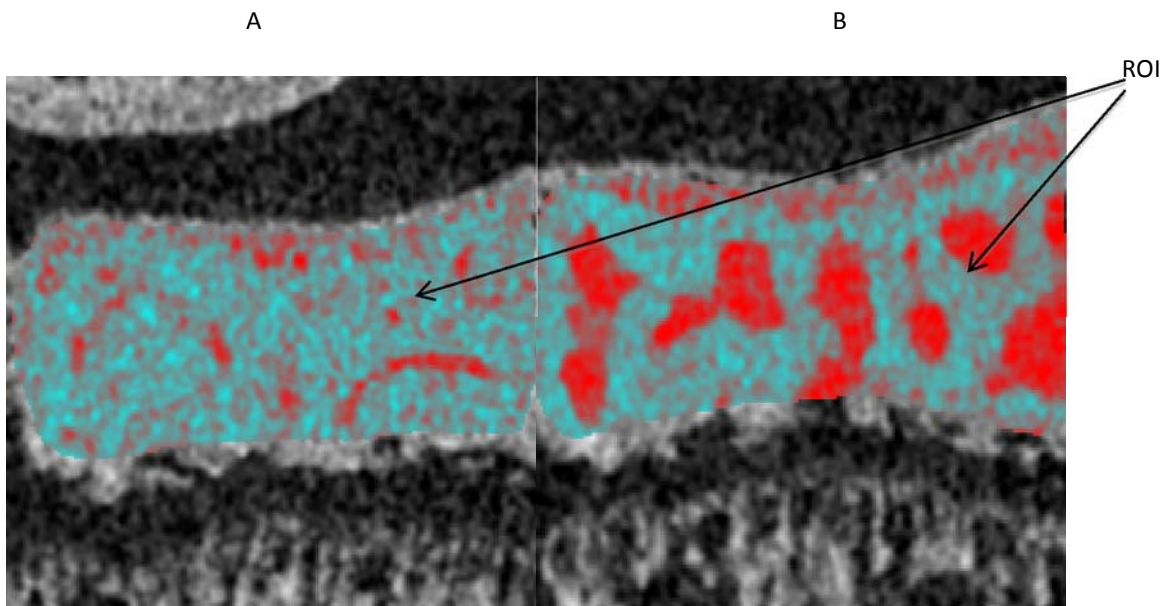


Figure 2.7: Coronal cross sectional images of tibial medial epicondyle to define ROI as one region. Image A shows sclerotic subchondral bone and the difficulty separating subchondral plate and subchondral trabecular bone as two separate ROIs. Image B shows non-sclerotic bone. The ROI in red is the same for both sclerotic and non-sclerotic bone to allow comparison between samples. Subchondral sclerosis was analyzed by measuring BV/TV (%).

2.2.10.3 Osteophyte analysis

Open dataviewer and select a VOI as described, including all subchondral bone of the tibia, as shown in figure 2.8.

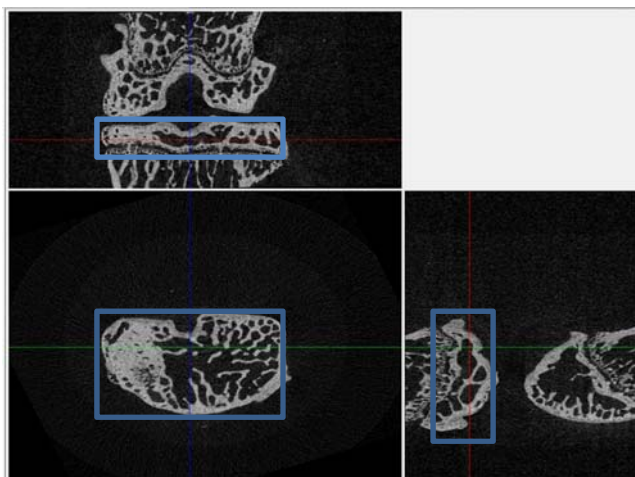


Figure 2.8: Volume of interest for analysis of tibial subchondral bone for osteophyte analyses. Having selected 'save as VOI' a box (shown in blue) will appear. The width (X), length (Y) and height (Z) need to be adjusted to include all subchondral bone of tibia. The dimensions need to be adjusted for all analyses by changing the X, Y and Z values as described, but do not need to be the same, giving a box enclosing the volume of interest. Once the VOI has been selected save the VOI as a coronal dataset and in the relevant folder, and a coronal dataset will be saved of the VOI which can be analysed on CTan described in text.

This coronal dataset can now be opened on CTan and osteophytes analysed. Select ROI and draw around the largest osteophyte and do this through all cross sections until the osteophyte disappears, refer figure 2.9.



ROI for osteophyte analysis

Figure 2.9 – ROI for tibial osteophyte analysis. A ROI (in red) is drawn around an osteophyte and accurately defined through all coronal cross sectional images. Next select ‘bottom of section’ and ‘top of section’ to define where the osteophyte begins and ends.

Once the ROI has been defined save the ROI and process as described above. Table 2.3 shows the parameter values used for analysis.

Parameter	Settings
Filtering	Median. 2D space. Radius 1
Threshold	80 low. 255 high. Global
Despeckle	Remove black speckles. 2D space. Less than 50 pixels. Apply to image
3D analysis	Select basic values, trabecular thickness

Table 2.3 – Parameters for tibial osteophyte analysis

The data output on excel was used for analyses on SPSS. Of specific interest was Tissue volume (TV), indicating the size of the osteophyte, Bone volume (BV) indicating the amount of bone in the osteophyte and BV/TV representing percentage bone volume in the osteophyte.

The osteophytes were also counted on CTvox, which gives a 3-dimensional (3D) picture of the knee joint allowing detection of osteophytes. The number of osteophytes were counted for each knee joint and documented.

2.2.10.4 Subchondral tibial bone measurements

Measurements of the tibia including the shaft and subchondral region were taken, as the tibia was the focus of my micro-CT analysis. The measurements were taken using CTan SkyScan software, shown in figure 2.10. Measurements were taken in the shaft just below the subchondral region and in the subchondral region itself, as this is where there is

significant weight bearing. (Figure 2.10) This will allow wild type tibial morphology comparison to the mice with specific gene ablation. I was unable to measure the shaft of the femur due to preparation of the sample for micro-CT where the shaft of the femur was excised to facilitate scanning.

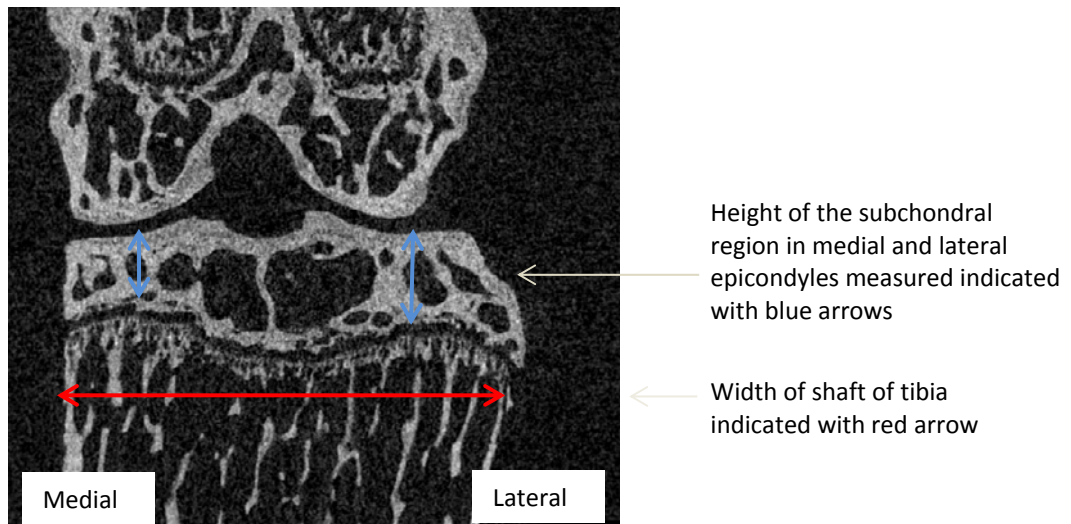


Figure 2.10: Micro-CT representation of murine tibia for bone measurements. The width of the shaft of the tibia (indicated with red arrow) was measured on CTan software in mm. Also the height of the subchondral region in both the medial and lateral epicondyles (indicated with blue arrows) was measured in mm.

The width of the subchondral region of the tibia was also measured using CTan SkyScanner software, shown in figure 2.11.



Figure 2.11: Micro-CT representation of murine tibia for bone measurements. The width of the tibia subchondral region (red arrow) was measured in mm for each mouse using CTan software.

2.2.11 Cartilage discs and pellets produced from differentiated human mesenchymal stem cells (hMSCs)

Principle

Human mesenchymal stem cells (hMSCs) have been shown to develop into a variety of anchorage-dependent mesenchymal cell types, such as bone and cartilage [202]. Using and adapting the methods described by Murdoch et al. and Johnstone et al. cartilage discs and pellets have been formed from hMSCs, respectively [203, 204]. I used these tissue-engineering techniques to produce a reliable and reproducible model of cartilage degradation, by stimulating these cartilage discs and pellets with cytokines and matrix metalloproteinase. Importantly the stimulation was carried out in serum free medium, as serum contains chondroprotective factors such as IGF-1, with no effect on tissue viability [205, 206].

Methods

Donor details

Human bone marrow mononuclear cells from 7 different donors aged less than 25 years old were purchased from Lonza, cryopreserved. The donor details are listed in table 2.4 below.

Donor	Donor characteristics	Lot Number
Donor 1	20 year old male, black	080750B
Donor 2	21 year old female, black	080754A
Donor 3	22 year old male, Hispanic	080781B
Donor 4	21 year old female, black	080825B
Donor 5	19 year old male, black	081276B
Donor 6	22 year old female, black	071508A
Donor 7	24 year old female, black	071671B

Table 2.4: Donor characteristics

Isolation and culture of bone marrow mesenchymal stem cells from bone marrow mononuclear cells

Human bone marrow stem cells were isolated from human bone marrow mononuclear cells by culturing in MSCGM (supplemented with FGF 5ng/ml) for 2-4 days. The adherent stem cells were then expanded in monolayer in MSCGM until colony-forming units (CFUs)

were observed. Cultures were maintained in a humid atmosphere of 5% CO₂/95% air at 37°C. Once cells had reached confluence they were passaged using trypsin/EDTA at a split ratio of 1:3.

Chondrogenic differentiation of human mesenchymal stem cells into cartilage discs and pellets

Chondrocyte differentiation media

- 47.5ml DMEM 4.5g/L Glucose (Lonza)
- 50 µl of 10µg/ml TGFβ3 stock (10ng/ml final concentration) (Peprotech)
- 50µl of 100µM dexamethasone stock (100nM final concentration) (Sigma-Aldrich)
- 500µl of 5mg/ml Ascorbic acid-2-phosphate stock (50µg final concentration) (Sigma-Aldrich)
- 500µl of the 4mg/ml Proline stock (40µg/ml final concentration) (Sigma-Aldrich)
- 500µl of 100x ITS+L premix (insulin, transferrin, selenium, linoleic acid) (1x final concentration) (Sigma-Aldrich)
- 500µl L-Glutamine (Sigma-Aldrich)
- 500µl Penicillin/Streptomycin (Sigma-Aldrich)

Chondrogenesis into discs and pellets

Isolated hMSCs were re-suspended in chondrogenic culture medium, detailed above. Both cartilage micro- and macro-pellets were produced, by using aliquots of 50,000 and 200,000 hMSCs in 1 ml of medium, respectively, which were spun down in a 96-well v-bottomed plate or 15ml polypropylene tubes, respectively, at 240g for 5 minutes in a bench-top centrifuge. These pellets were cultured in the same manner, as for hMSC culture using an incubator. Media was changed every 4-5 days up until 14 days when chondrogenesis was stopped.

For chondrogenesis into cartilage discs, transwells were used. Aliquots of 500,000 cells in 100µl of media were pipetted onto 6.5-mm diameter, 0.4µm pore size polycarbonate transwell filters. These were then spun in a 24 well plate at 200g for 5 minutes, and then 500µl of chondrogenic medium was added to the lower well, which submerged the

membrane and cells. These were incubated as described, for 14 days, changing the media every 4-5 days.

Stimulation of cartilage discs and pellets with IL-1, OSM and matriptase

Cartilage discs were carefully cut out from the membrane and placed in a 24 well plate, and were washed with warmed PBS. Pellets remained in the 15ml polypropylene tubes, or 96-well v-bottomed plate, with all traces of media removed and washed in warmed PBS.

These cartilage discs and pellets were stimulated with IL-1/OSM/matriptase or combinations of these diluted in DMEM. Control discs were used by addition of DMEM with no cytokine or matriptase addition. Final concentrations of IL-1/OSM/matriptase used in each experiment, has been detailed in each individual graph in chapter 3, with stock concentrations provided in section 2.1.

Each experiment had different numbers and variations of each stimulation group, detailed further in the results section. Medium was removed and stored at -80°C every 4-5 days and re-stimulated at these time points. Stimulation was carried out over a 3-week period and at the end of the experiment the disc was either papain digested and used for GAG and hydroxyproline assays, or fixed for 30 minutes in 10% buffered paraformaldehyde, place in a cassette wrapped in tissue paper and used for histology (refer section 2.2.8 for staining methods). The stored medium was used for GAG and hydroxyproline assays to elicit proteoglycan and collagen release, respectively.

2.2.12 Cartilage digestion

Principle

Papain is a cysteine protease consisting of a single polypeptide chain with three disulphide bridges and a sulfhydryl group, giving papain its enzyme activity. Papain can digest most protein substrates by cleaving peptide bonds of basic amino acids, including the ones contained in collagen type II (glycine, proline and hydroxyproline) and can also solubilise sulphated glycosaminoglycans from the core protein in proteoglycans such as aggrecan. Before use, papain is typically dissolved in phosphate buffer containing cysteine-HCL and EDTA, which act as stabilising/activating agents [207]. Due to its activity

it can be used in cartilage digestion releasing its components such as sulphated GAGs and hydroxyproline, which can subsequently be used for GAG and hydroxyproline assays.

Materials

- Phosphate buffer 0.1M, pH6.5: 137ml solution A and 63ml solution B. Solution A=0.1M NaH₂PO₄ (9.36g in 600ml distilled water). Solution B=0.1M Na₂HPO₄ (7.1g in 500ml distilled water).
- Papain (0.25g in 10ml phosphate buffer) store at 4°C.
- Cysteine-HCl 0.078g in 10ml phosphate buffer.
- EDTA 0.19g disodium salt in 10ml phosphate buffer.

Methods

Place the cartilage sample in an O-ring screw-cap tube and add 350µl phosphate buffer per sample. Make up a master mix of 100µl papain, 50µl cysteine-HCL and 50µl EDTA per sample (multiply depending on the number of samples). Add 200µl of the master mix to each sample. Ensure all cartilage samples are in the solution and the lids are secured tight. Incubate at 65°C for at least 6 hours. After incubation add 450µl phosphate buffer to the sample. The digested cartilage samples can now be used for GAG and OHP assays.

2.2.13 Glycosaminoglycan (GAG) assay

Principle

Proteoglycans, mainly aggrecan, make up the cartilage matrix. As described in section 1.3.1, aggrecan has GAG chains attached to it, mainly chondroitin sulphate chains [57]. These sulphated GAGs are broken down and released from the cartilage matrix in OA, and there have been different techniques introduced to measure this release of sulphated GAG. Taylor and Jeffree et al. were the first to introduce dimethylmethylene (DMB) blue as a strongly metachromatic dye to measure sulphated glycosaminoglycans by changing colour, as it provides a label for the free sulphated glycosaminoglycan chains [208]. This technique has since been adapted as there was interference by polyanions other than sulphated glycosaminoglycans, such as hyaluronic acid [209]. These adaptations include lowering the pH and increasing the salt concentration of the DMB to prevent interaction with hyaluronic acid, and hence improving the selectivity of the assay for sulphated GAGs.

Similarly papain digestion of the cartilage sample eliminated interference by other proteins and glycoproteins [209]. Chondroitin sulphate especially chondroitin-6-sulphate is found in sharks fin, and this source of chondroitin sulphate has been used to produce standards for a straight line calibration curve in order to determine release of sulphated GAG from the tissue engineered cartilage discs and pellets [210].

Materials

- Dimethyl-methylene blue (DMB) solution pH3 : 3.04g glycine, 2.37g sodium chloride, 791.67ul 12M concentrated hydrochloric acid; make up to litre with distilled water and add 16mg DMB. Absorbance should be ~0.3 read at 530nm on Tecan plate reader.

Methods

Make up the chondroitin sulphate standards. A stock solution of the chondroitin sulphate should be made at 1mg/ml concentration diluted in phosphate buffer. From the chondroitin stock solution standards should be made ranging from 0-40µg/ml in order to produce a straight line calibration curve. Add 40µl standard per well in duplicates, and also 40µl sample per well in duplicates (making appropriate dilutions). Once all standards and samples have been pipetted into a 96 well plate add 250ul DMB solution to each well using a multi-channel pipette, and read the absorbance immediately on the Tecan plate reader at 530nm. From the standards a straight line calibration curve was produced using Microsoft Excel, allowing calculation of the amount of GAG in the sample (µg), by using the equation $y=mx+c$.

2.2.14 Hydroxyproline (OHP) assay

Principle

Type II collagen predominantly type IIb procollagen formed of 3 polypeptide α -chains is found in articular cartilage. The amino acid composition of these polypeptide chains is mainly glycine and proline, with hydroxyproline residues forming hydrogen bonds along the molecule. In OA, matrix metalloproteinases such as MMP-1, 8 and 13 breakdown this collagen structure releasing hydroxyproline residues. These hydroxyproline residues can

be measured by spectrophotometric determination detailed below, allowing quantification of collagen release, and hence cartilage breakdown [211]. A similar method to that of Bergman et al. has been utilised here [211]. The colour yield produced in the assay (detailed below), is accurately proportional to hydroxyproline concentration, and hence collagen breakdown seen in OA. A calibration curve, produced by using various concentrations of hydroxyproline (OHP), was used to determine the concentration of hydroxyproline in each sample by using the equation $y=mx+c$.

Materials

- Acetate-citrate buffer pH6 (57g sodium acetate+37.5g tri-sodium citrate+5.5g citric acid+385ml isopropanol and make up to litre with distilled water).
- DAB 4.5 M stock in 70% (v/v) perchloric acid, stored 4°C.
- Chloramine T 250 mM in dH₂O, made fresh.

Methods

Add 130µl sample into an O-ring screw-cap tube and an equal amount of HCl. Incubate samples for 4 hours at 105°C in an oven. This process allowed break-down of the molecular bonds between individual collagen strands into small peptides such as hydroxyproline. Pipette all of a sample (acid hydrolysed) into a 96 deep well plate and spin for 7 hours in Genevac EZ-2 speedvac (Genevac Ltd, Ipswich, UK) at 55°C on aqueous phase to allow the acid to evaporate, leaving hydroxyproline residues which were re-suspended in 130µl distilled water. For the assay, two solutions were prepared – solution A and solution B. For solution A, 250 mM chloramine T was diluted 1:4 in acetate-citrate buffer, and for solution B, 4.5 mM DAB was diluted 1:3 in propan-2-ol. Make up the OHP standards (0-30µg/ml) from stock (1mg/ml), to produce a straight line calibration curve. Similar to the GAG assay 40µl of standard and sample was added to each well in duplicates. Add 25µl solution A per well using a multi-channel pipette and start timer. Once 4 minutes have elapsed add 150µl solution B per well. Seal the plate tight with a plate sealer on and incubate for 35 minutes at 65°C for colour development so the absorbance can be assessed. Once the incubation period is over, measure the absorbance using a Tecan plate reader at 560nm. The amount of hydroxyproline in µg was then calculated using the straight line calibration curve.

Percentage release GAG/hydroxyproline

To work out percentage release the total amount of GAG/hydroxyproline in each disc/pellet and also the amount released into the media at each time point were added together. From the total amount of GAG/hydroxyproline in each pellet/disc, percentage release can be calculated at each time point using the following equation:

$$\frac{[(\text{GAG/hydroxyproline } (\mu\text{g}) \text{ in medium}) / (\text{GAG/hydroxyproline in medium} + \text{GAG/hydroxyproline disc})] \times 100}{}$$
The percentage release of GAG and hydroxyproline was considered to be representative of the release of proteoglycan and collagen, respectively.

2.2.15 MMP activity assay

Principle

A fluorescence quenched MMP substrate – FS-6 (MCA-Lys-Pro-Leu-Gly-Leu-Dpa-Ala-Arg-NH₂) was used for the quantification of MMP activity in media of cultured tissue engineered cartilage discs and pellets, especially collagenase-1 and -2 [212]. Dpa quenches the fluorescence of the MCA, but MMP cleavage of the Gly-Leu bond separates the Dpa and MCA, with resultant excitation of AMC (7-amino-4-methylcoumarin) and increasing fluorescence (excitation 360nm, emission 400nm). 4-aminophenylmercuric acetate (APMA) can activate MMPs via disassociation of the cysteine residue from the active zinc site, and was used to elicit any pro-MMPs present in the media of cartilage discs and pellets. AMC was used as a fluorescence reference standard.

Materials

- Assay buffer - 100 mM Tris HCl, pH 7.5, 100 mM NaCl, 10 mM CaCl₂, 0.1% (w/v) PEG-6000, 0.05% (w/v) Brij-35. This was filtered through a 0.2 μm filter and pre-warmed to 37°C before use.
- FS-6 (MCA-Lys-Pro-Leu-Gly-Leu-Dpa-Ala-Arg-NH₂) - 5 mM dissolved in DMSO. Stored -20°C in the dark.
- 10 mM APMA stock solution - 35.2 mg APMA was dissolved in 200 μl DMSO and made up to 10 ml with 100 mM Tris-HCl, pH 8.5. Stored in the dark at 4°C for up to 3 months.
- AMC standard 5mM dissolved in methanol. Stored at -20°C in the dark.

Method

Two separate reactions were analyzed:

1. Assessment of MMP activity, by pipetting 5 μ l of media from control or cytokine stimulated cartilage discs/pellets and 75 μ l assay buffer into each well, and then addition of 20 μ l FS-6 substrate to detect any fluorescence indicating MMP-activity.
2. Assessment of pro-MMP activity, by pipetting 5 μ l of media (as above), 5.33 μ l APMA and 69.66 μ l of assay buffer into each well. Similar to above 20 μ l of FS-6 substrate was then added. The fluorescence emitted gives an indication of pro-MMPs, which have been activated upon addition of APMA.

The working concentration of APMA was 0.67mM by doing a 1 in 15 dilution (5.33 μ l in 80 μ l). FS-6 was initially diluted to 250 μ M by carrying out a 1 in 20 dilution in assay buffer. The FS-6 substrate was warmed for 10 minutes at 37°C before making a further 1 in 5 dilution by adding 20 μ l of FS-6 substrate to 80 μ l of sample in each well, giving a final working concentration of 50 μ M. The AMC standard was added at a concentration of 5 μ M, which is equivalent to 10% substrate hydrolysis (FS-6 substrate 50 μ M). AMC was diluted in assay buffer. Blank wells were included containing 80 μ l assay buffer (analysis 1) and 74.67 μ l assay buffer and 5.33 μ l APMA (analysis 2).

Prior to addition of FS-6 substrate, the plate was incubated at 37°C for one hour. Then pre-warmed FS-6 substrate was added – 20 μ l in each well. The plate was pulse spun and then fluorescence measured in a fluoremeter, at 10-minute intervals. The reaction was stopped when approximately 10% of substrate had been hydrolyzed. The data was analyzed by subtraction of the blank measurement (buffer alone) from the sample well. This allowed measurement of MMP and pro-MMP activity.

2.2.16 Quantitative assessment of cartilage damage

After staining the mouse joints with Safranin-O the OARSI scoring system was used to assess cartilage damage in DMM or sham operated mice. This was carried out blinded by two independent assessors. (Professor Drew Rowan and Professor David Young) There were four mice in each group and six sections analysed per mouse (24 sections total per

group) giving a global representation of cartilage damage in each group. Two analyses were carried out including best overall maximum score of cartilage damage and best combined summed score of cartilage damage. For the best overall maximum score the highest score of cartilage damage across all 24 sections in each group was taken giving one score. The best combined summed score involved taking the highest score of cartilage damage for each mouse within each group (4 scores per group) and adding the four scores together to get the best combined summed score of cartilage damage [1].

2.2.17 Statistical Analysis

A normality test using the Shapiro-Wilk statistic was carried out to detect whether data were normally distributed. For normally distributed data a parametric test was carried out using SPSS. Either an independent samples T-test or a one-way ANOVA test with a post hoc Tukey test were performed on all normally distributed data using SPSS with levels of statistical significance shown as * $p \leq 0.05$, ** $p \leq 0.01$ and *** $p \leq 0.001$. I have used a one-way ANOVA test when I had an independent variable with two or more conditions to compare the means, and I utilized a post hoc Tukey test to determine where the significant differences were. I did not want to investigate the interaction between the different independent variables on the dependent variable therefore, I did not use a two-way ANOVA. Additionally, I did not have subgroups within my independent groups, so a nested ANOVA was not indicated. The SPSS 15.0 software package (SPSS UK Ltd, UK) was used. Using Microsoft Excel, a Student's t-Test was performed on normally distributed data, with the same levels of significance indicated above. The statistical test used for analysis was indicated within the figure or text throughout my thesis. Only relevant comparisons and significant differences have been highlighted in the text. For correlation analysis the Spearman's correlation coefficient (r) was used to test the strength of linear association between two variables using SPSS.

Chapter 3: The use of tissue engineering to generate a reliable and reproducible model of cartilage catabolism

3.1 Introduction

Cartilage catabolism is a common feature of OA due to raised levels of cytokines and other factors, such as matrix metalloproteinases [136, 141, 213], which induce the production of proteolytic enzymes such as MMPs and aggrecanases causing cartilage degradation. There have been many studies of in vitro cartilage catabolism in response to cytokines. Different sources of cartilage have been utilised, investigating their responsiveness to IL-1 + OSM, some of which include human nasal cartilage [178], bovine nasal cartilage [183], human [178], porcine [173], and bovine articular cartilages [214]. Despite being a highly potent stimulus and reproducibly eliciting proteoglycan degradation in response to IL-1 + OSM, there has been difficulty producing a reliable and reproducible model of collagen breakdown, particularly using human cartilage. This is most probably since most human cartilage samples tend to be end-stage OA. Therefore, there is a need to generate a model of normal human cartilage that will reproducibly respond to cytokine treatment by releasing significant collagen from the matrix. This will allow the analysis of over-expression of specific genes and their role in cartilage catabolism as well as assessment of therapies.

In this chapter the combination of IL-1 + OSM has been extensively utilised in a tissue-engineered model of cartilage catabolism derived from a human source. This was because IL-1 + OSM are the most potent initiators of this effect, and so have been used to try and generate a reliable and reproducible model of proteoglycan and collagen catabolism [178, 183, 215].

Both IL-1 α and IL-1 β are thought to play a role in the pathogenesis of OA, with IL-1 α proposed to be early acting and IL-1 β more dominant in advanced disease. Their actions in OA include up-regulation of MMPs and enhanced production of the pro-inflammatory mediator nitric oxide (NO) [216]. The concentrations of IL-1 α and IL-1 β in OA synovial fluid were 15 ± 22 and 8 ± 16 pg/ml, respectively. In OA cartilage the concentrations were 183 ± 391 (IL-1 α) and 0 ± 1 (IL-1 β) pg/g [217]. OSM is also thought to play a role in the pathogenesis of OA however its exact mechanism of action is yet to be defined. Some of its actions in OA include joint inflammation and depletion of proteoglycans in the

cartilage [218]. The concentration of OSM in OA synovial fluid and OA cartilage were 38 ± 121 pg/ml and 220 ± 424 pg/g, respectively [217].

OSM (0.1-100ng/ml) by itself can cause proteoglycan degradation and inhibit proteoglycan synthesis [181], however it does not cause collagen breakdown (50ng/ml) [178, 183]; this cytokine, therefore was not used by itself. IL-1 has similar effects to OSM, although studies by Morgan et al. and Cawston et al. show IL-1 alone (5ng/ml) is more effective at causing collagen breakdown than OSM [178, 183]. In contrast, IL-1 (5ng/ml) + OSM (50ng/ml) in combination act synergistically to enhance proteoglycan release, and also cause significant collagen release in some experiments, but this was variable [178, 183, 184, 214].

Matriptase has been implicated in OA and cartilage catabolism as discussed in section 1.8. Milner et al. showed that the addition of matriptase (30-100nM) to bovine cartilage explants stimulated with IL-1 (1ng/ml) + OSM (10ng/ml) significantly enhanced collagen release. Matriptase (30-100nM) by itself had no such effect on collagen release, however when matriptase (100nM) was incubated with human OA cartilage with no cytokines there was significant collagen release. This effect was due to up-regulation of PAR-2 in human OA cartilage, as a PAR-2 inhibitor (SAM-11) blocked this effect. No such release was observed for normal human articular cartilage due to lack of PAR-2 expression [122]. Over-expression of PAR-2 in a reliable and reproducible human derived tissue-engineered cartilage model would allow more detailed investigation of the effects of PAR-2 in 'healthy' human cartilage. The aims of this chapter were:

1. To produce tissue engineered cartilage discs, micro- and macro-pellets from hMSCs with cartilaginous properties (presence of proteoglycans and collagen) evidenced by histological staining.
2. Generate a reliable and reproducible model of cartilage breakdown (in terms of proteoglycan and collagen breakdown) by stimulating tissue-engineered human cartilage discs and pellets with IL-1 + OSM.
3. To elicit the effects of matriptase on tissue-engineered cartilage discs and pellets, both by itself and in combination with IL-1 + OSM.

4. If aims one, two and three were achieved, I aimed to over-express PAR-2 in a cartilage disc/pellet model using a lenti-viral approach, and assess its effects on cartilage catabolism upon the addition of matriptase.

3.2 Results

3.2.1 A model of tissue-engineered cartilage disc catabolism

For the cartilage disc model, four separate stimulation experiments from two different hMSC donors were used. (Donor 071508A and 071671B, section 2.2.11) The number of repeats in each group and stimulation conditions used were dependent on the number of cartilage discs successfully produced, as this was unreliable. The methodology carried out was following a published protocol [203], and due to this and time constraints all experiments were carried out consecutively and batch histology completed at the end.

3.2.1.1 Pilot study to assess the effects of IL-1 + OSM on cartilage catabolism

An initial pilot study was performed using an initial concentration of cytokines specifically IL-1 (1ng/ml) + OSM (10ng/ml) to analyse the catabolic effect on tissue-engineered cartilage discs. Work carried out by Morgan et al. elicited significant proteoglycan release from human nasal cartilage when using this stimulus [178]. As shown in figure 3.1, similar to Morgan et al., I also observed GAG release at day 3 in the cytokine- stimulated group, relative to control in the disc model. However, also shown in figure 3.1 in contrast to the work carried out by Morgan et al., I did not detect any collagen release using these cytokine conditions at any time point. Therefore, in subsequent experiments I used a higher concentration of cytokines. I also altered the methodology, whereby at each time point the culture medium was harvested from every disc in a specific group, and each disc was re-stimulated and remained in culture at each time point until the end of the experiment when it was stored at -80°C. This allowed statistical analysis, error bars and percentage GAG release to be performed on all future similar experiments.

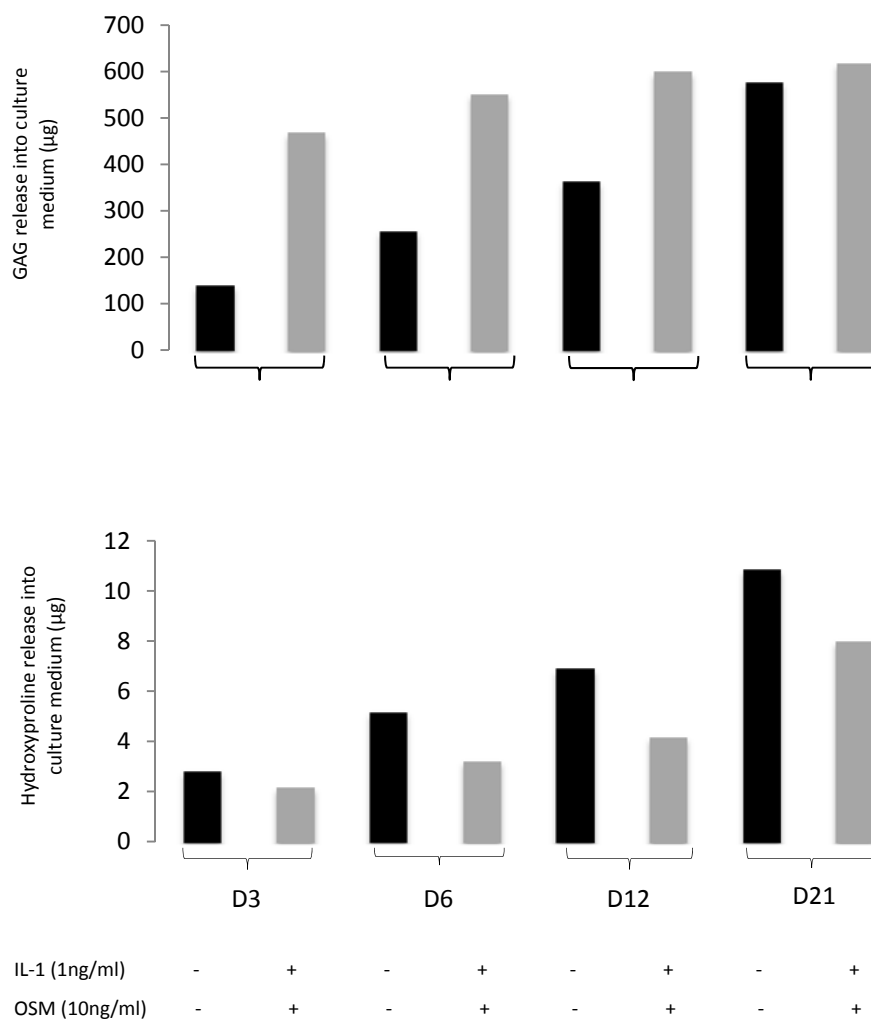


Figure 3.1: Assessment of proteoglycan and collagen release in response to a cytokine stimulus. Eight cartilage discs were generated from hMSCs with four discs in the control group and four discs in the cytokine stimulated group, as described in section 2.2.11. In this initial pilot study at each time point both medium and disc were harvested and so no error bars or statistical test could be carried out as only one sample of culture medium from one disc was analysed at each time point. The remaining discs were re-stimulated at each time point and the old medium discarded. Represented in these bar charts are cumulative proteoglycan (GAG) and collagen (hydroxyproline) release, whereby GAG/hydroxyproline release at day 3 has been added to day 6 in each group, and so forth. GAG and hydroxyproline assays were performed on the medium from the tissue-engineered cartilage discs (section 2.2.13 and 2.2.14) and GAG and hydroxyproline released into the medium was measured in µg. D3 represents day 3 and so forth. Donor 071508A.

3.2.1.2 The effects of IL-1 + OSM +/- matriptase or IL-1 alone on cartilage catabolism

For each of the three separate cartilage disc experiments (figures 3.2, 3.3 and 3.4) I analysed GAG and hydroxyproline release.

In figure 3.2, there was a statistically significant difference between groups in terms of proteoglycan degradation, as determined by a one-way ANOVA ($F(11,24) = 535.764$, $p < 0.001$). A Tukey post hoc test revealed that the IL-1 (5ng/ml) group and IL-1 (2ng/ml) + OSM (20ng/ml) group caused significant proteoglycan degradation at days 5 ($p < 0.001$), 10 ($p < 0.01$) and 15 ($p < 0.01$) relative to control, with a roughly 4-fold, 3-fold and 2-fold increase relative to control at days 5, 10 and 15, respectively, in both groups. Similarly, a one-way ANOVA test revealed significant differences between groups in terms of hydroxyproline release in figure 3.2, ($F(11,24) = 26.837$, $p < 0.001$), with a Tukey post hoc test revealing an almost 2-fold increase in hydroxyproline release in the IL-1 + OSM group, relative to control at day 21 ($p < 0.01$).

Shown in figure 3.3, a one-way ANOVA test revealed significant differences between groups in terms of proteoglycan degradation ($F(15,40) = 1164.385$, $p < 0.001$). Using a Tukey post hoc test there was a significant increase in proteoglycan degradation in the IL-1 (2ng/ml) + OSM (20ng/ml) group and IL-1 (2ng/ml) + OSM (20ng/ml) + matriptase (103nM) group at all time points, relative to control. There was an almost 4-fold and 3-fold increase in proteoglycan degradation in both groups at days 5 and 10 compared to control ($p < 0.001$) respectively, and roughly 2-fold increase in proteoglycan degradation at days 15 ($p < 0.01$) and 21 ($p < 0.05$) in both groups, relative to control. The addition of matriptase to IL-1 + OSM enhanced GAG release at all time points with a significant enhancement of GAG release compared to the IL-1 + OSM alone at day 5 ($p < 0.05$). Conversely, matriptase stimulation by itself had no such effect on GAG release compared to control, only reaching slight significance in terms of GAG release compared to control at day 21 ($p < 0.05$).

Referring to figure 3.3 there were significant differences between groups in terms of hydroxyproline degradation using a one-way ANOVA test ($F(15,40) = 1328.948$, $p < 0.001$). The Tukey post hoc test detected an almost 3-fold increase in hydroxyproline degradation at all time points in the IL-1 (2ng/ml) + OSM (20ng/ml) + matriptase (103nM) group relative to control ($p < 0.001$).

Referring to figure 3.4, there was significant proteoglycan degradation at all time points in the IL-1 (2ng/ml) + OSM (20ng/ml) group relative to control, with a roughly 2-fold increase in proteoglycan degradation at days 5 and 10 ($p < 0.001$). In terms of hydroxyproline degradation there was a roughly 3-fold increase in hydroxyproline degradation at days 15, 20 and 25 in the IL-1 (2ng/ml) + OSM (20ng/ml) group relative to control ($p < 0.01$).

It was clear to see a reproducible and reliable response in terms of proteoglycan degradation, when using IL-1 (2ng/ml) + OSM (20ng/ml) as a catabolic stimulus, across three separate experiments. Additionally, the addition of matriptase to the cytokine stimulus enhanced GAG release in one experiment (figure 3.3). However, there was a variable response to this stimulus on hydroxyproline degradation across three independent experiments. IL-1 (5ng/ml) alone had no effect on collagen release at any time point, (figure 3.2) similar to observations by Morgan et al. using human nasal cartilage [178]. I therefore decided not to use IL-1 (5ng/ml) in future experiments. In figure 3.3, the addition of matriptase to the IL-1 + OSM stimulus promoted significant collagen release at all time points relative to control. However, matriptase by itself had no such effect on collagen release.

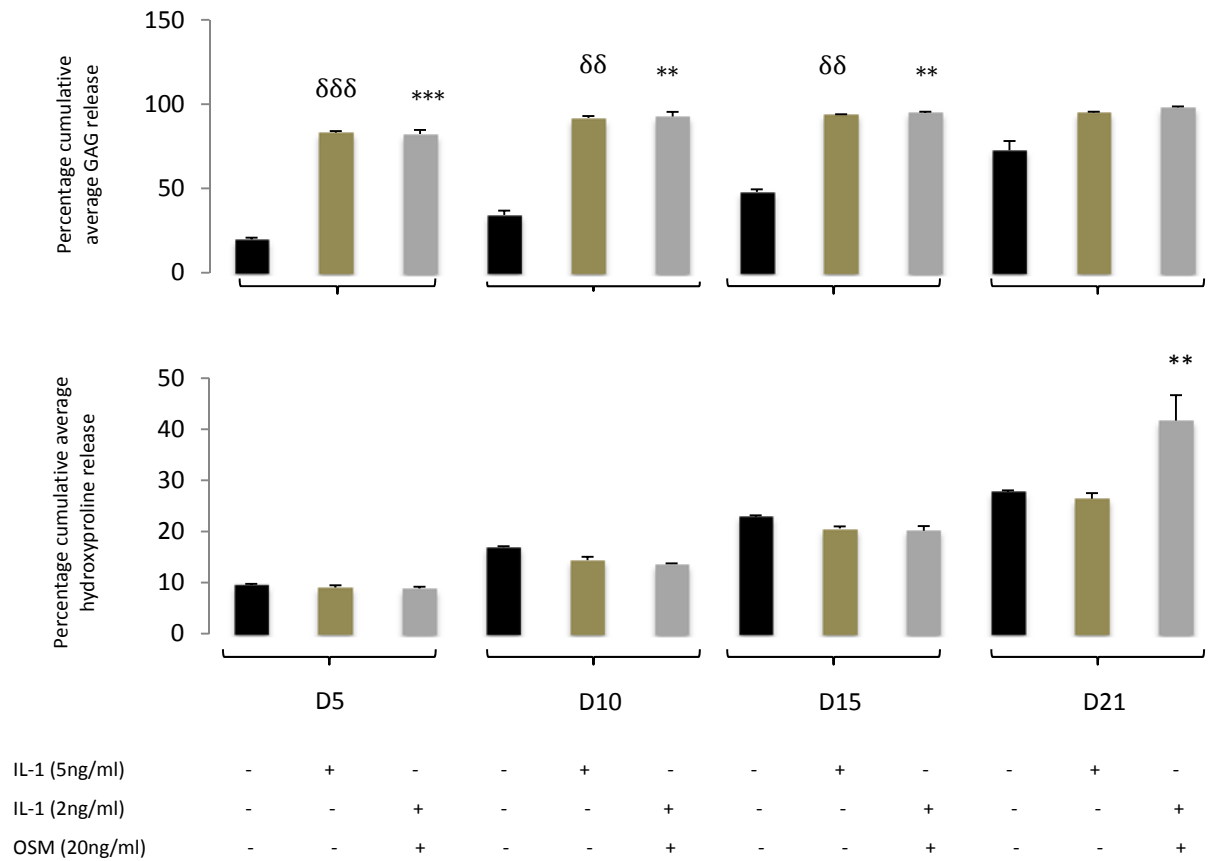


Figure 3.2: Assessment of proteoglycan and collagen release in response to a cytokine stimulus. Cartilage discs were generated from hMSCs and stimulated with cytokines as described in section 2.2.11. There were three discs in each group. At each time point medium was harvested from each disc and stored at -80°C . All the discs remained in culture and were re-stimulated at each time point until the end of the experiment (day 21) when the discs were harvested, rinsed in PBS and stored at -80°C . GAG and hydroxyproline assays (section 2.2.13 and 2.2.14) were performed on the medium of each disc at each time point. The discs were papain digested (section 2.2.12) and GAG and hydroxyproline assays performed on the resultant medium. The total amount of GAG or hydroxyproline was then calculated for each disc. Percentage release was calculated by dividing GAG or hydroxyproline release at each time point by the total content of GAG and hydroxyproline for each disc. The average release of GAG and hydroxyproline at each time point was then calculated from the three discs in each group at each time point. Cumulative average percentage GAG or hydroxyproline release was then calculated by adding average percentage release at each time point for each group. * control compared to IL-1 (2ng/ml) + OSM (20ng/ml). δ control compared to IL-1 (5ng/ml). ** $p < 0.01$ *** $p < 0.001$. D5 represents day 5 and so forth. Error bars \pm 1 SD of mean. Donor 071508A. A one-way ANOVA test with post hoc Tukey test were performed.

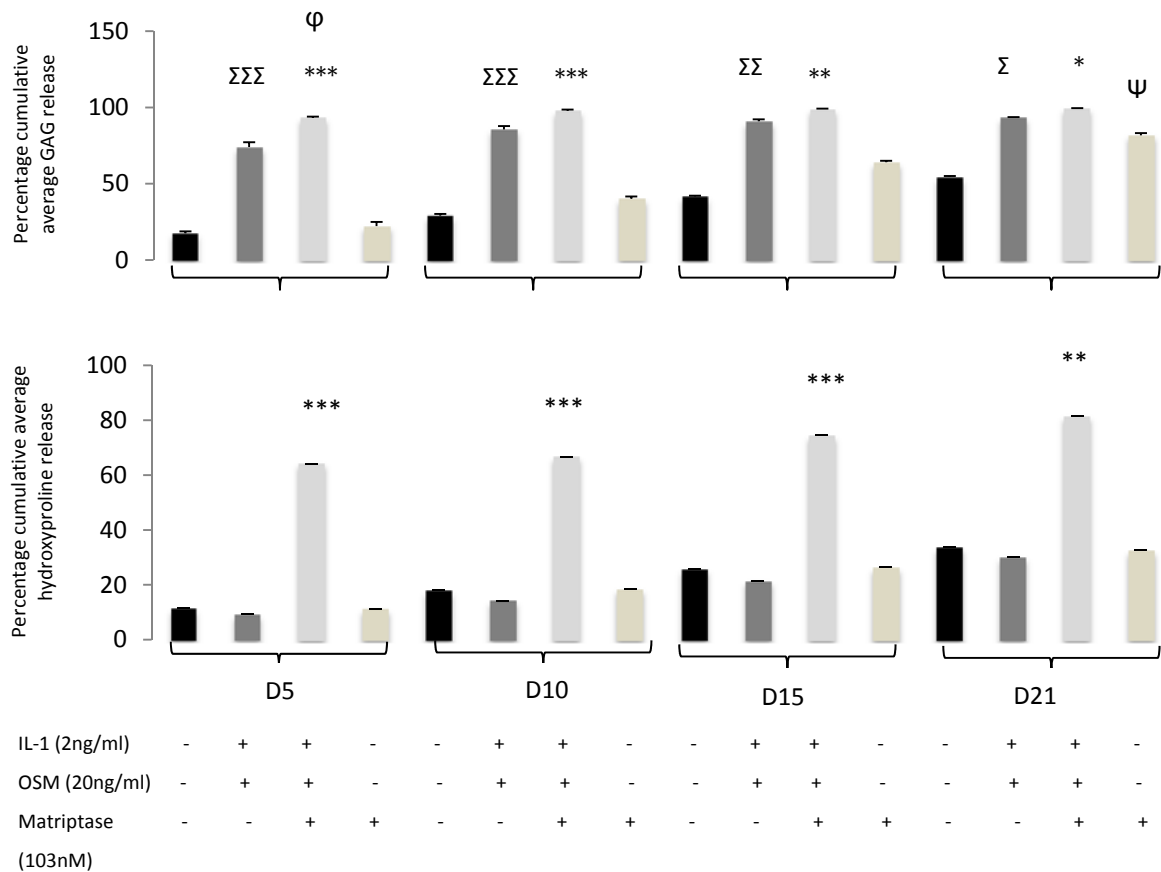


Figure 3.3: Assessment of proteoglycan and collagen release in response to a cytokine stimulus +/- matriptase. Cartilage discs were generated from hMSCs and stimulated with cytokines +/- matriptase as described in section 2.2.11. There were three discs in each group, except four discs in the IL-1 (2ng/ml) + OSM (20ng/ml) + matriptase (103nM) and matriptase (103nM) groups. Discs were processed and analysed as described in figure 3.2. * control compared to IL-1 (2ng/ml) + OSM (20ng/ml) + matriptase (103nM). Σ control compared to IL-1 (2ng/ml) + OSM (20ng/ml). Ψ control compared to matriptase (103nM). Φ IL-1 (2ng/ml) + OSM (20ng/ml) compared to IL-1 (2ng/ml) + OSM (20ng/ml) + matriptase (103nM). * $p < 0.05$ ** $p < 0.01$ *** $p < 0.001$. D5 represents day 5 and so forth. Error bars +/- 1 SD of mean. Donor 071508A. A one-way ANOVA test with post hoc Tukey test were performed.

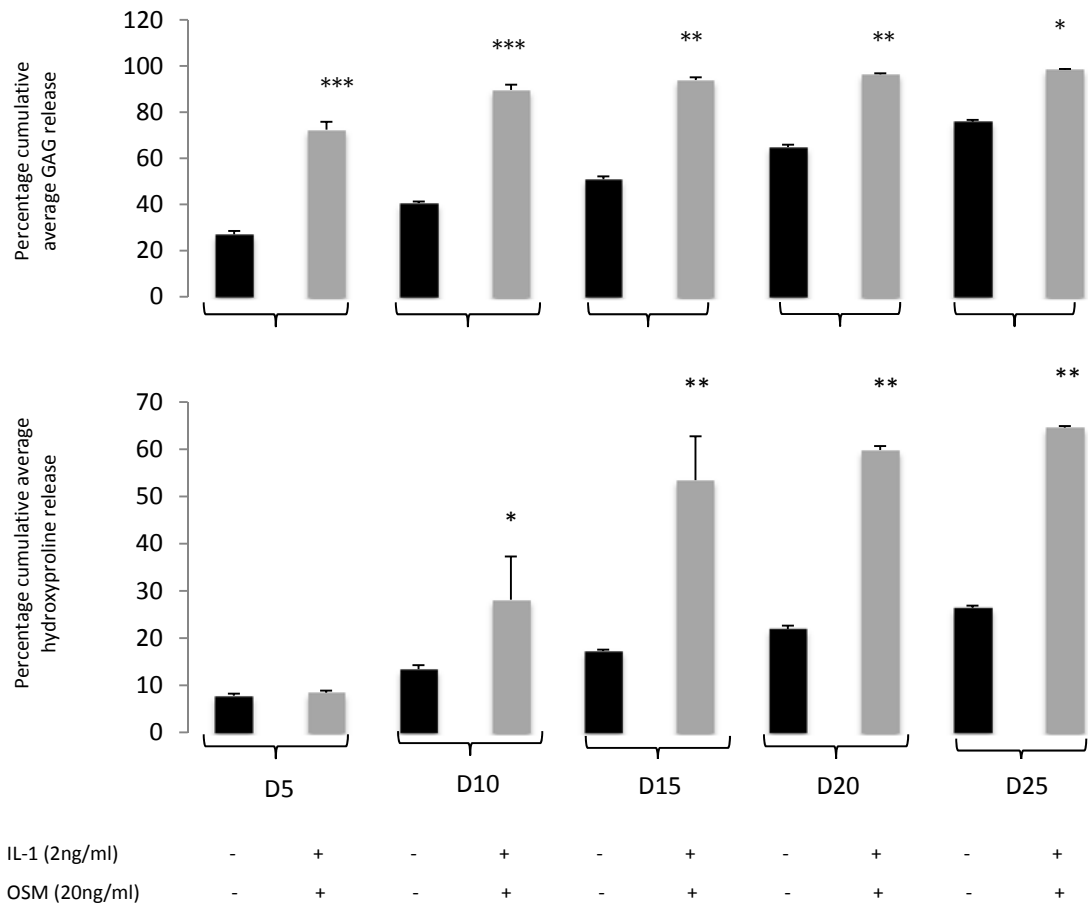


Figure 3.4: Assessment of proteoglycan and collagen release in response to a cytokine stimulus. Cartilage discs were generated from hMSCs and stimulated with cytokines as described in section 2.2.11. There were four discs in each group. Discs were processed and analysed as described in figure 3.2. * control compared to IL-1 (2ng/ml) + OSM (20ng/ml). * p<0.05 ** p<0.01 *** p<0.001. D5 represents day 5 and so forth. Error bars +/- 1 SD of mean. Donor 071671B. An independent samples T-test was performed.

3.2.1.3 The effects of IL-1 + OSM +/- matriptase or IL-1 alone on MMP activity

In the experiments carried out in section 3.2.1.2, I also wanted to identify if there was any MMP or pro-MMP activity in the culture medium of these stimulated cartilage discs. In order to do this I carried out a MMP activity assay. (Detailed in section 2.2.15) Shown in figure 3.5A one can observe that there was slight MMP activity in the IL-1 (2ng/ml) + OSM (20ng/ml) stimulated group at day 21 (no addition of APMA) and this may account for the collagen release observed in this group. There was also significant pro-MMP activity (with the addition of APMA) in the IL-1 + OSM stimulated group relative to control. A similar observation was seen in figure 3.5B, in the IL-1 + OSM stimulated group, with slight MMP activity and significant pro-MMP activity relative to control. There was no MMP activity in the IL-1 (5ng/ml) stimulated group relative to control, (figure 3.5A) however there was significant pro-MMP activity compared to control. In figure 3.5B, there was significant MMP activity in the IL-1 + OSM + matriptase stimulated group relative to control, and this would explain the collagen release observed in this experiment. There was also significant pro-MMP observed in this group relative to control. As expected, matriptase stimulation by itself had no such effect on either MMP or pro-MMP activity relative to control.

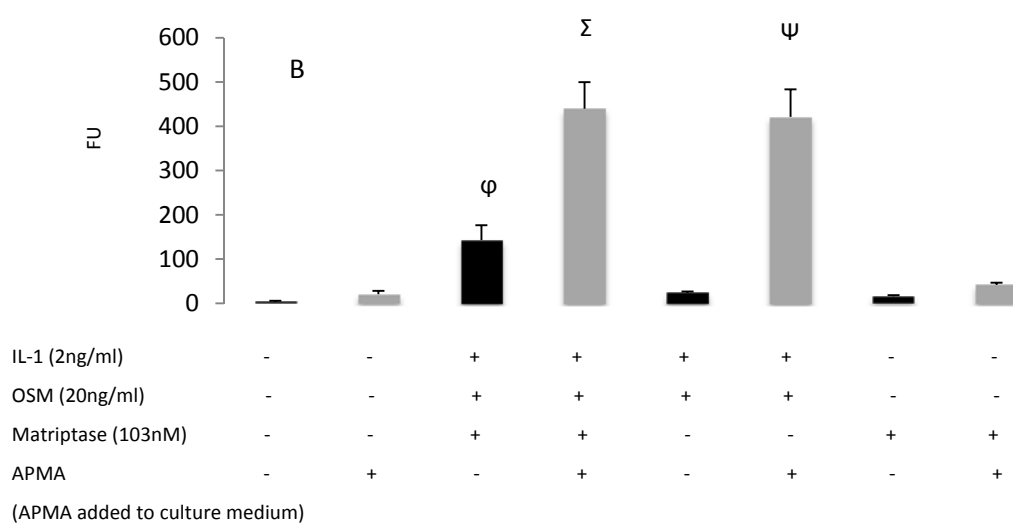
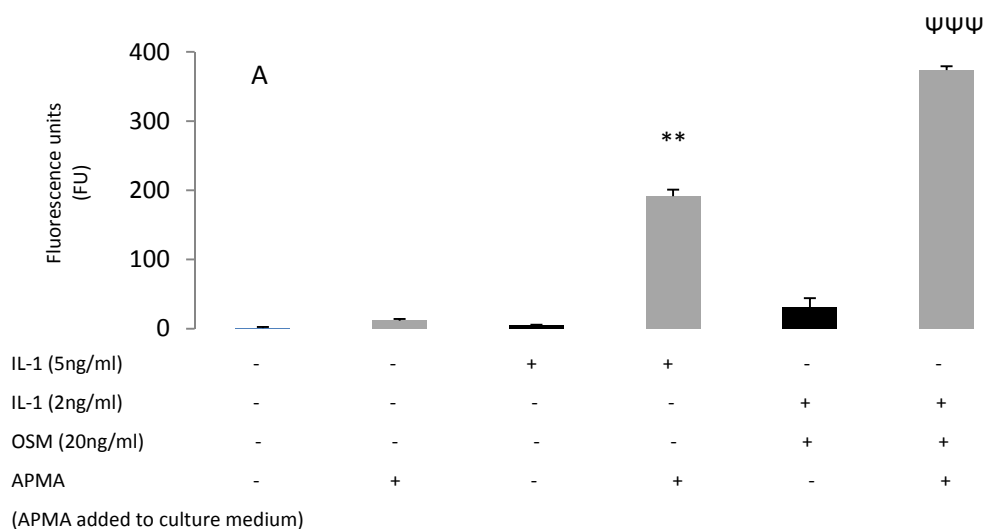


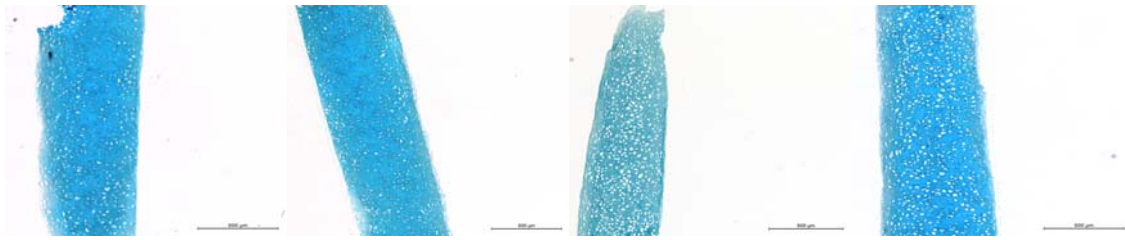
Figure 3.5: Assessment of MMP activity in response to a cytokine stimulus +/- matriptase. Cartilage discs were generated from hMSCs and stimulated with cytokines. At each time point medium was harvested from each disc and stored at -80°C. All the discs remained in culture and were re-stimulated at each time point until day 21 when the discs were harvested; rinsed in PBS and stored at -80°C. A MMP activity assay was performed on the medium of three discs from each group to detect pro-MMP or MMP activity. (Section 2.2.15) Bar chart A relates to figure 3.2 and bar chart B relates to figure 3.3. The assay was performed on medium at day 21. * represents control + APMA pro-MMP activity compared to IL-1 (5ng/ml) + APMA pro-MMP activity. Ψ represents control + APMA pro-MMP activity compared to IL-1 (2ng/ml) + OSM (20ng/ml) + APMA pro-MMP activity. ϕ represents control MMP activity compared to IL-1 (2ng/ml) + OSM (20ng/ml) + matriptase (103nM) MMP activity. Σ represents control + APMA pro-MMP activity compared to IL-1 (2ng/ml) + OSM (20ng/ml) + matriptase (103nM) + APMA pro-MMP activity. Ψ $p < 0.05$ ** $p < 0.01$ $\Psi\Psi\Psi$ $p < 0.001$. Black bars represent no APMA addition to medium (MMP activity) and grey bars represent APMA addition to control or stimulus medium (pro-MMP activity). Error bars +/- 1 SD of mean. Donor 071508A. An independent samples T-test was performed.

3.2.1.4 Histology of cartilage discs

For each of the four cartilage disc experiments, a cartilage disc was harvested at day 14 (prior to any stimulation) and was later used for histological analysis of cartilaginous properties. In figure 3.6, three histological stains were used – Alcian Blue (A) and Safranin-O (B) (proteoglycan content) and Masson's Trichrome (C) (collagen content). This analysis provides evidence that 'cartilage-like' tissue had been successfully engineered [219]. All of these stains are not specific to a particular type of proteoglycan or collagen. Figure 3.6 shows that although the proteoglycan content is abundant, the collagen content is sparse. Additionally, the histology images represented in figure 3.6 despite showing 'cartilage-like' features, do not show that the cartilage generated represents the features of hyaline cartilage found in human articular joints.

Alcian Blue

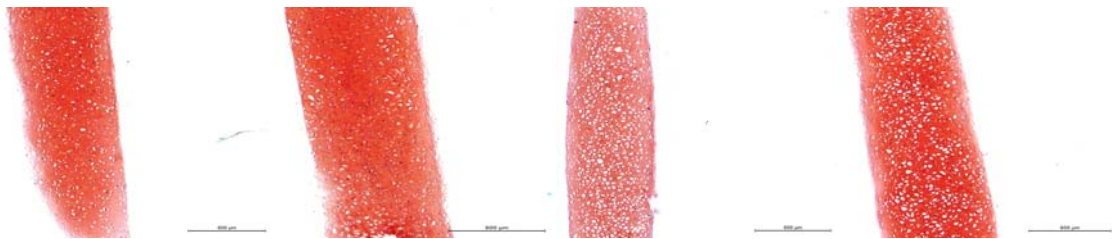
A



Alcian blue staining throughout the cartilage discs

Safranin-O

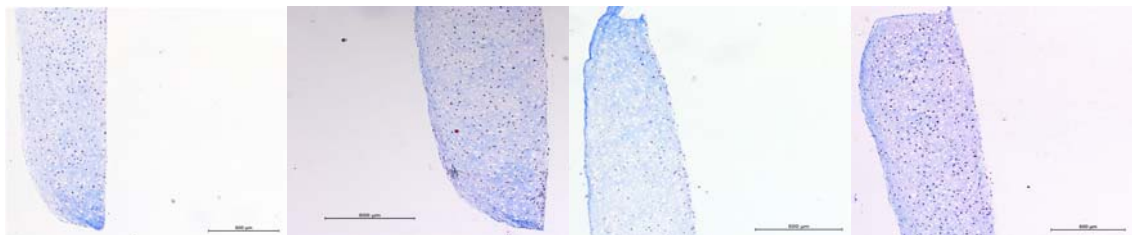
B



Safranin-O red staining throughout the cartilage discs

Masson's Trichrome

C



Blue collagen fibrils inter-weaving throughout the cartilage discs

Figure 3.6: Histology representation of cartilage discs. One tissue engineered cartilage disc from each separate experiment was harvested at day 14 and stored at -80°C . These discs were then washed in PBS, fixed in 10% buffered paraformaldehyde for twenty minutes further rinsed in PBS and then wrapped in tissue paper and paced in a labelled cassette. These fixed discs then underwent processing in graded ethanol and were embedded in molten paraffin wax. The discs were subsequently sectioned using a microtome at $4\mu\text{m}$ longitudinally and stained as described in section 2.2.8. A – Alcian Blue. B – Safranin-O. C – Masson's Trichrome.

3.2.2 A model of cartilage catabolism in a tissue-engineered micro-pellet model

Due to difficulty producing cartilage discs, in terms of multiple donor hMSCs failing to form discs and low numbers of discs formed in each experiment, I explored other more reliable models I could use. After discussion with Dr Matt Barter (Post-Doctoral Researcher, MRG) it became apparent that he had similar problems with many donors failing to make any discs at all, and so it would be difficult to produce a reliable and reproducible model of cartilage catabolism from different hMSC donors using this model. Therefore, I switched to a cartilage pellet model (as described by Johnstone et al. [204]) firstly using a micro-pellet model.

3.2.2.1 Experimental donor and cytokine concentration details

The cartilage micro-pellet model I used included six separate experiments from three different hMSC donors. (080750B, 080754A and 080781B, section 2.2.11) All these experiments were simulated only with IL-1 (2ng/ml) + OSM (20ng/ml) alone, as I wanted to produce reliable and reproducible results with this stimulus in terms of proteoglycan and collagen release before progressing. All micro-pellets formed, which allowed for more repeats in each experiment. Similar to the cartilage disc experiments, all micro-pellet experiments were completed consecutively and batch histology performed at the end, for the same reasons described previously.

3.2.2.2 The effects of IL-1 + OSM on cartilage catabolism

I firstly carried out a preliminary experiment using an initial concentration of cytokines of IL-1 (1ng/ml) + OSM (10ng/ml), similar to the cartilage disc model. However, again I detected no proteoglycan or collagen release. (Data not presented) Therefore all subsequent experiments used a higher concentration of cytokines. As described, work carried out by Morgan et al, Cawston et al. and Durigova et al. detected significant proteoglycan release using IL-1 + OSM as a catabolic stimulus as early as day 7 [178, 183, 214]. From 5 separate experiments using three different hMSC donors I detected significant proteoglycan release at day 3 in all experiments. (Refer figures 3.7 and 3.8) In figure 3.7, there was also significant proteoglycan release at day 6. However, the general trend as the time course progressed was that the control group 'caught-up' in terms of proteoglycan release evidenced in figures 3.7 and 3.8. This effect will be discussed further

in section 3.3. Unlike the cartilage disc model, I did not detect any collagen release from the cytokine-stimulated group relative to control at any time point using this cartilage micro-pellet model, and so no data were presented. An independent samples T-test was performed in all data in sections 3.2.2.2 and 3.2.2.3.

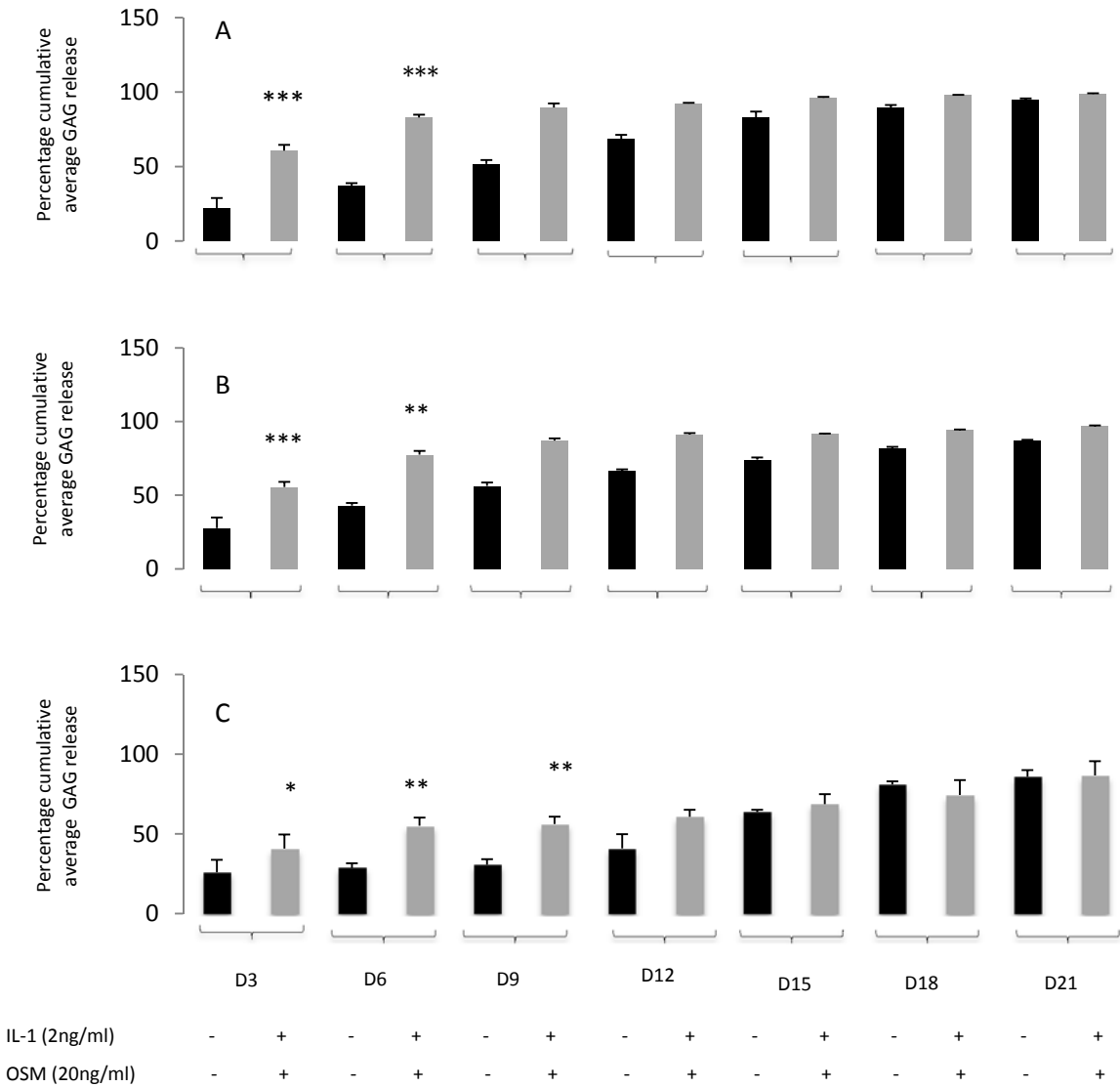


Figure 3.7: Assessment of proteoglycan release in response to a cytokine stimulus. Cartilage micro-pellets were generated from hMSCs and stimulated with cytokines as described in section 2.2.11. At each time point medium was harvested from each micro-pellet and stored at -80°C. All the micro-pellets remained in culture and were re-stimulated at each time point until the end of the experiment (day 21) when the micro-pellets were harvested; rinsed in PBS and stored at -80°C. GAG and hydroxyproline assays (section 2.2.13 and 2.2.14) were performed on the medium of each micro-pellet at each time point. The micro-pellets were papain digested (section 2.2.12) and GAG and hydroxyproline assays performed on the medium. The total amount of GAG or hydroxyproline was then calculated for each micro-pellet. Percentage cumulative average GAG release was calculated as described in figure 3.2. Bar chart A – 15 control and 20 cytokine-stimulated pellets. Bar chart B – 6 control and 15 cytokine-stimulated pellets. Bar chart C – 10 control and 20 cytokine-stimulated pellets. * control GAG release compared to IL-1 (2ng/ml) + OSM (20ng/ml) GAG release. * p<0.05 ** p<0.01 *** p<0.001. D3 represents day 3 and so forth. Error bars +/- 1 SD of mean. Donor 080750B.

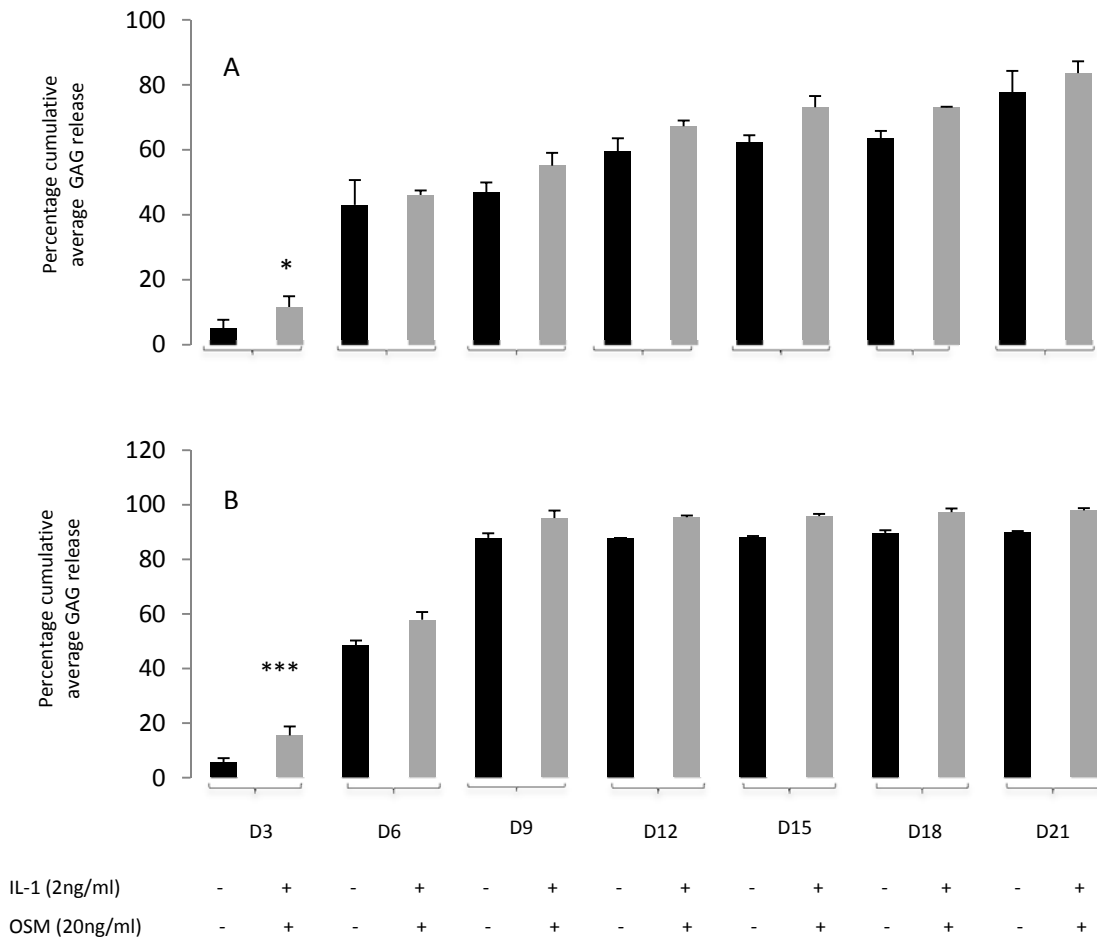


Figure 3.8: Assessment of proteoglycan release in response to a cytokine stimulus. Cartilage micro-pellets were generated, processed and analysed as described in figure 3.7. Bar chart A – 5 control and 10 cytokine-stimulated pellets. Bar chart B – 7 control and 8 cytokine-stimulated pellets. * control GAG release compared to IL-1 (2ng/ml) + OSM (20ng/ml) GAG release. * $p < 0.05$ *** $p < 0.001$. D3 represent day 3 and so forth. Error bars +/- 1 SD of mean. Donor 080754A bar chart A and donor 080781B bar chart B.

3.2.2.3 The effects of IL-1 + OSM on MMP activity

In the experiments detailed in figures 3.7 and 3.8 I next wanted to identify whether there was any MMP or pro-MMP activity in the culture medium of these cytokine-stimulated cartilage micro-pellets, by performing a MMP activity assay described in section 2.2.15. Similar to work carried out by Morgan et al. [178], and Cawston et al. [184] I detected significant MMP activity in the IL-1 + OSM stimulated micro-pellets, (figures 3.9 and 3.10A) albeit at very low levels compared to the cartilage discs. In keeping with work carried out by Cawston et al. [183], and similar to my results with the cartilage discs, the most significant result is significant pro-MMP activity in the culture medium of the IL-1 + OSM stimulated cartilage micro-pellets compared to control, shown in figures 3.9 and 3.10. These results suggest that although there are published protocols for these cartilage micro-pellets, it appears that these tissue-engineered micro-pellets contain little collagen and hence no substrate for the MMPs to act on and so no collagen release was observed. I subsequently went on to determine the micro-pellet collagen content by carrying out histological analysis in section 3.2.2.4.

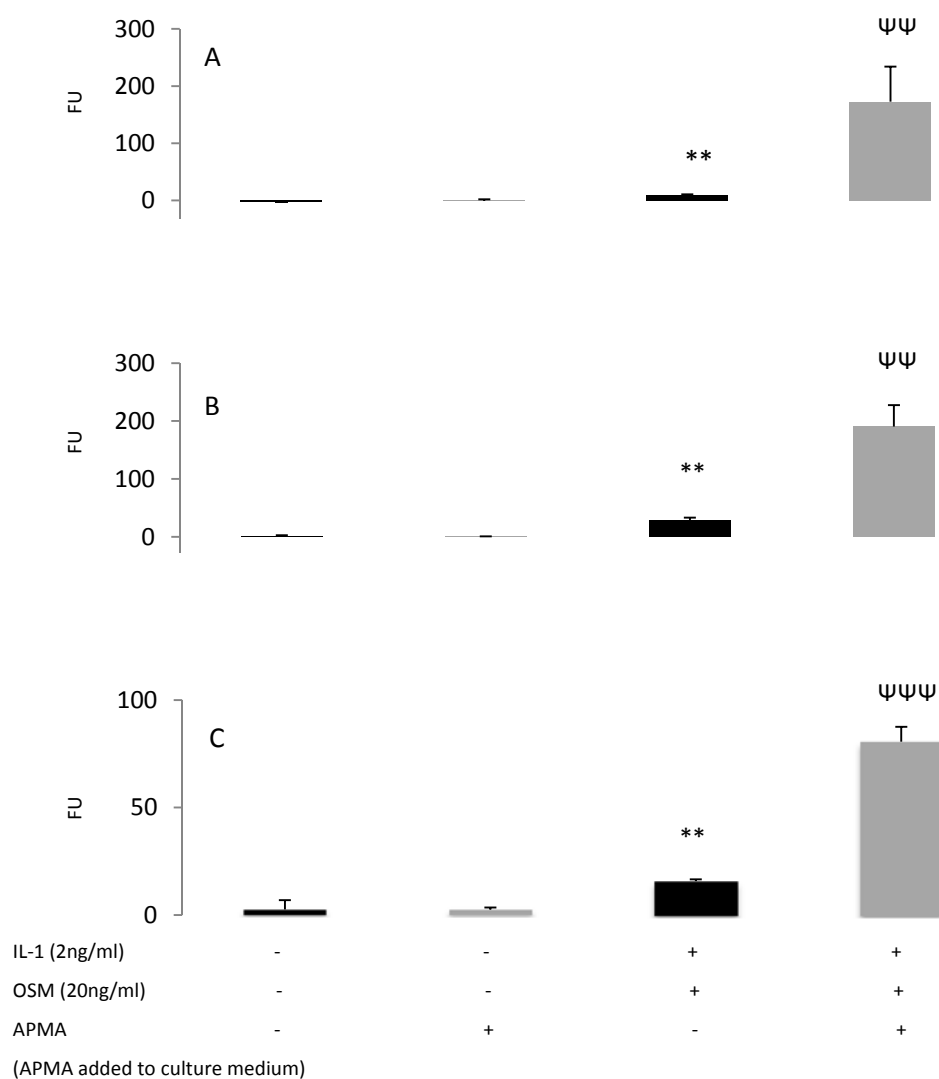


Figure 3.9: Assessment of MMP activity in response to a cytokine stimulus. Cartilage micro-pellets were generated from hMSCs and stimulated with cytokines as described in section 2.2.11. At each time point medium was harvested from each micro-pellet and stored at -80°C. All the micro-pellets remained in culture and were re-stimulated at each time point until the end of the experiment (day 21) when the micro-pellets were harvested; rinsed in PBS and stored at -80°C. A MMP activity assay was performed on the medium of three pellets from each group to detect pro-MMP or MMP activity, as described in section 2.2.15. Bar charts A, B and C correspond to bar charts A, B and C in figure 3.7. The assay was performed on medium at day 21. * control MMP activity compared to IL-1 (2ng/ml) + OSM (20ng/ml) MMP activity. Ψ control +APMA pro-MMP activity compared to IL-1 (2ng/ml) + OSM (20ng/ml) +APMA pro-MMP activity. ** p<0.01 ΨΨΨ p<0.001. Black bars represent no APMA addition to medium (MMP activity) and grey bars represent APMA addition to control or stimulus medium. (Pro-MMP activity) Error bars +/- 1 SD of mean. Donor 080750B.

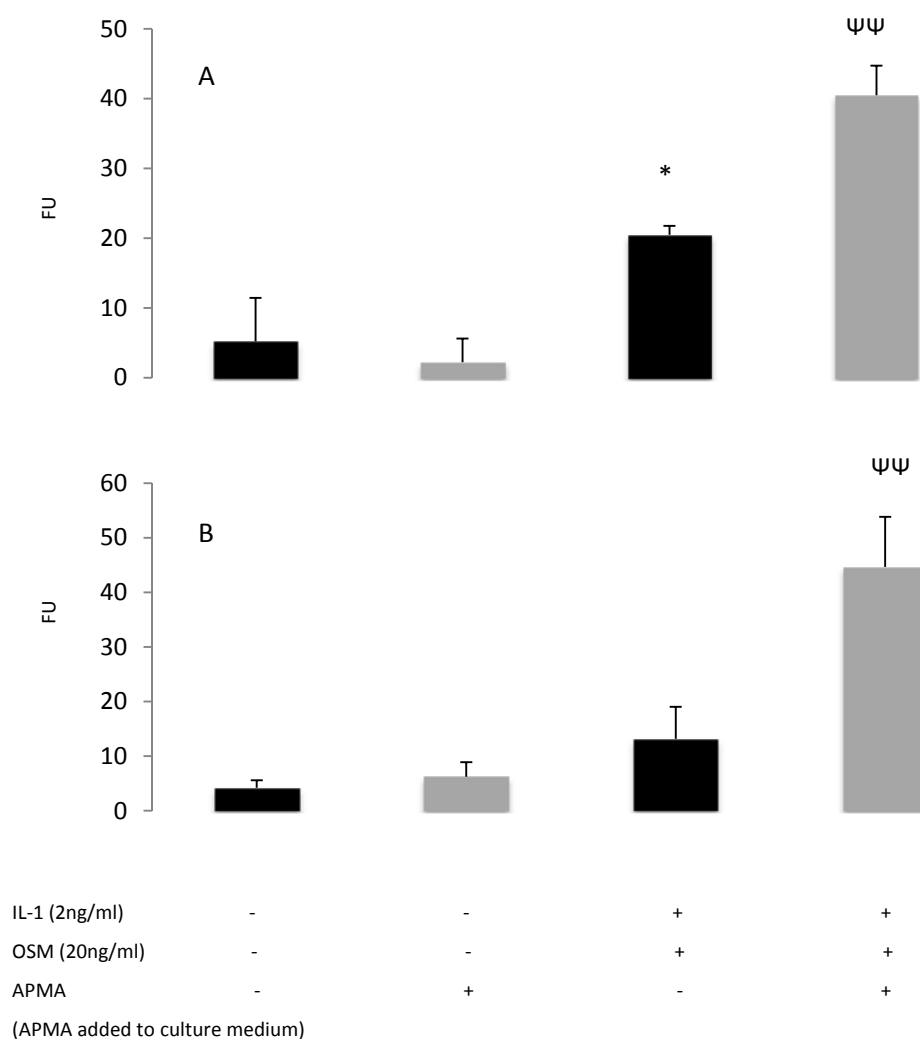


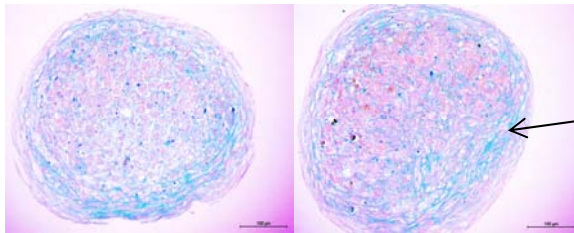
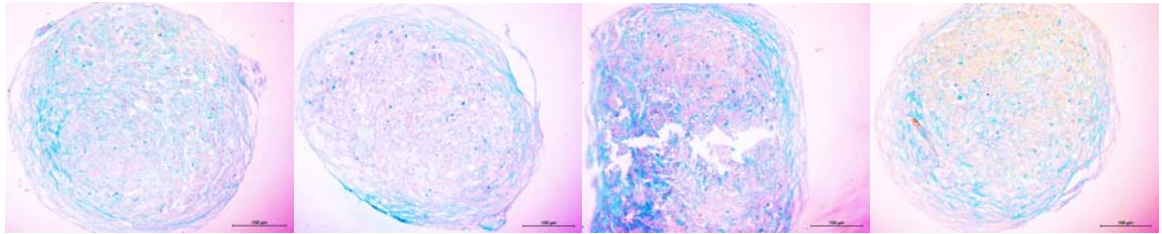
Figure 3.10: Assessment of MMP activity in response to a cytokine stimulus. Cartilage micro-pellets were generated, processed and analysed as described in figure 3.9. Bar charts A and B correspond to bar charts A and B in figure 3.8. The assay was performed on medium at day 21. * control MMP activity compared to IL-1 (2ng/ml) + OSM (20ng/ml) MMP activity. Ψ control +APMA pro-MMP activity compared to IL-1 (2ng/ml) + OSM (20ng/ml) +APMA pro-MMP activity. * p<0.05 ΨΨ p<0.01. Black bars represent no APMA addition to medium (MMP activity) and grey bars represent APMA addition to control or stimulus medium. (Pro-MMP activity) Error bars +/- 1 SD of mean. Donor 080754A bar chart A and donor 080781B bar chart B.

3.2.2.4 Histology of micro-pellets

Six separate cartilage micro-pellet experiments were performed with cytokine stimulation. Similar to the cartilage discs, histological staining was performed on the tissue-engineered cartilage micro-pellets, specifically Alcian Blue (figure 3.11A), safranin-O and Masson's Trichrome. (Figure 3.11B) As discussed in section 2.2.8, safranin-O is not as sensitive an indicator of proteoglycans as Alcian Blue, especially if proteoglycans are in low abundance. I detected no safranin-O staining in any of my micro-pellets, (images not shown) suggesting that there is a low content of proteoglycans. This was confirmed in Alcian Blue staining, where there was found to be very little proteoglycan content compared to the cartilage discs, arranged mainly around the periphery of the micro-pellet. (Figure 3.11A) Similarly Masson's Trichrome showed few collagen fibrils arranged only around the periphery of the micro-pellet. (Figure 3.11B) These findings suggest that these tissue-engineered cartilage micro-pellets are not a very good model to study cartilage catabolism.

Alcian Blue staining

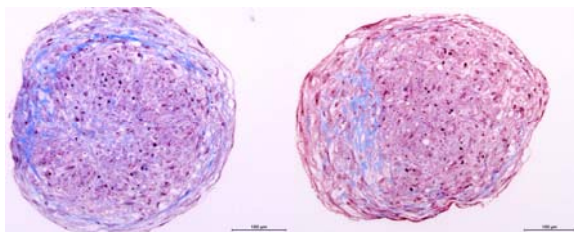
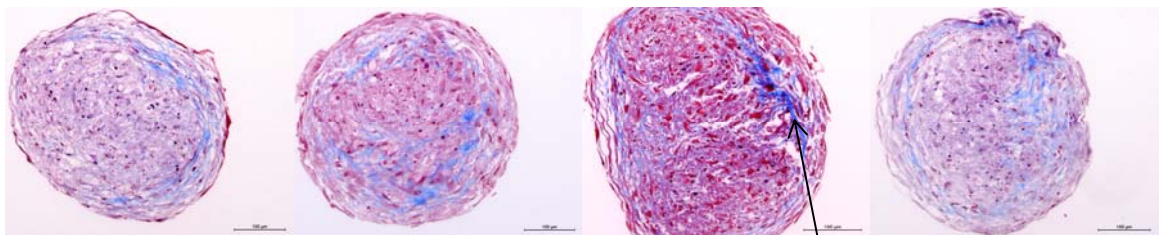
A



Proteoglycan blue fibrils arranged around periphery of the pellets

Masson's Trichrome staining

B



Collagen blue fibrils arranged around the periphery of the pellet

Figure 3.11: Histology representation of cartilage micro-pellets. One tissue engineered cartilage micro-pellet from each separate experiment was harvested at day 14 and stored at -80°C. These discs were then washed in PBS, fixed in 10% buffered paraformaldehyde for twenty minutes further rinsed in PBS and then wrapped in tissue paper and paced in a labelled cassette. These fixed discs then underwent processing in graded ethanol and were embedded in molten paraffin wax. The discs were subsequently sectioned using a microtome at 4µm longitudinally and stained as described in section 2.2.8. A – Alcian blue. B – Masson's Trichrome.

3.2.3 A model of cartilage catabolism using tissue engineered macro-pellets

Due to the disappointing results observed in these micro-pellets in terms of proteoglycan and collagen release and difficulty in trying to obtain a reproducible and reliable model of cartilage catabolism using this model, I had a discussion with Prof David Young and Dr Matt Barter. It was apparent that more promising results had been obtained in the MRG laboratory using a macro-pellet model in terms of histological analysis. Therefore my next step was to perform a similar analysis using a macro-pellet model in order to fulfil my aims.

3.2.3.1 Experimental donor and cytokine concentration details

The macro-pellet model I used included five separate experiments from two different hMSC donors. (Donor 080825B and donor 081276B, section 2.2.11) A similar concentration of cytokines were used as before, and I also investigated the effects of matriptase in this model too. Similarly, all experiments were performed consecutively and batch histology completed at the end for the aforementioned reasons.

3.2.3.2 The effects of IL-1 + OSM +/- matriptase on cartilage catabolism

Similar to previous work [178, 183, 214], I detected significant proteoglycan release at all time points in the IL-1 + OSM stimulated group relative to control, as shown in figure 3.12. There was an almost 5-fold, 4-fold, 3-fold and 2-fold increase in proteoglycan degradation at days 4, 8, 12 and 16 respectively, in the IL-1 + OSM group relative to control ($p < 0.001$). This effect was also observed in figure 3.13A, and occurred later in figure 3.13B, with significant proteoglycan release detected at day 12, 16 and 20.

In figure 3.13A, a one-way ANOVA revealed significant differences between groups ($F(19,25) = 221.638, p < 0.001$). The Tukey post hoc test revealed that the IL-1 + OSM group significantly increased GAG release compared to control ($p < 0.001$) at all time points, with a similar effect observed in the IL-1 + OSM + matriptase group ($p < 0.001$).

There was also significant differences between groups in figure 3.13B, ($F(19,40) = 17.086, p < 0.001$), with the Tukey test showing that at days 12, 16 and 20 IL-1 + OSM significantly increased GAG release, relative to control with an almost 2-fold increase at day 20. The IL-

1 + OSM + matriptase group had a similar effect, with an almost 3-fold increase in GAG release at days 8 and 12, relative to control ($p < 0.001$).

Similar to the analysis performed on cartilage discs, matriptase in combination with cytokine stimulation had an enhancing effect on proteoglycan release shown in figure 3.13B, with significant release at days 8, 12 and 16 compared to stimulation with IL-1 + OSM ($p < 0.05$). However, in figure 3.13A the addition of matriptase had no enhancing effect on proteoglycan release compared to IL-1 + OSM stimulation alone, suggesting donor variability in terms of responsiveness of the cartilage matrix to catabolic stimuli, discussed further in section 3.3. Similar to the cartilage discs, I also found in figures 3.13A and 3.13B there was significant proteoglycan release in the matriptase stimulated group with no cytokine addition at a late time point. (Day 20) I also detected no collagen release in any of the experiments at any time point (similar to the micro-pellet model) therefore no data were presented for this.

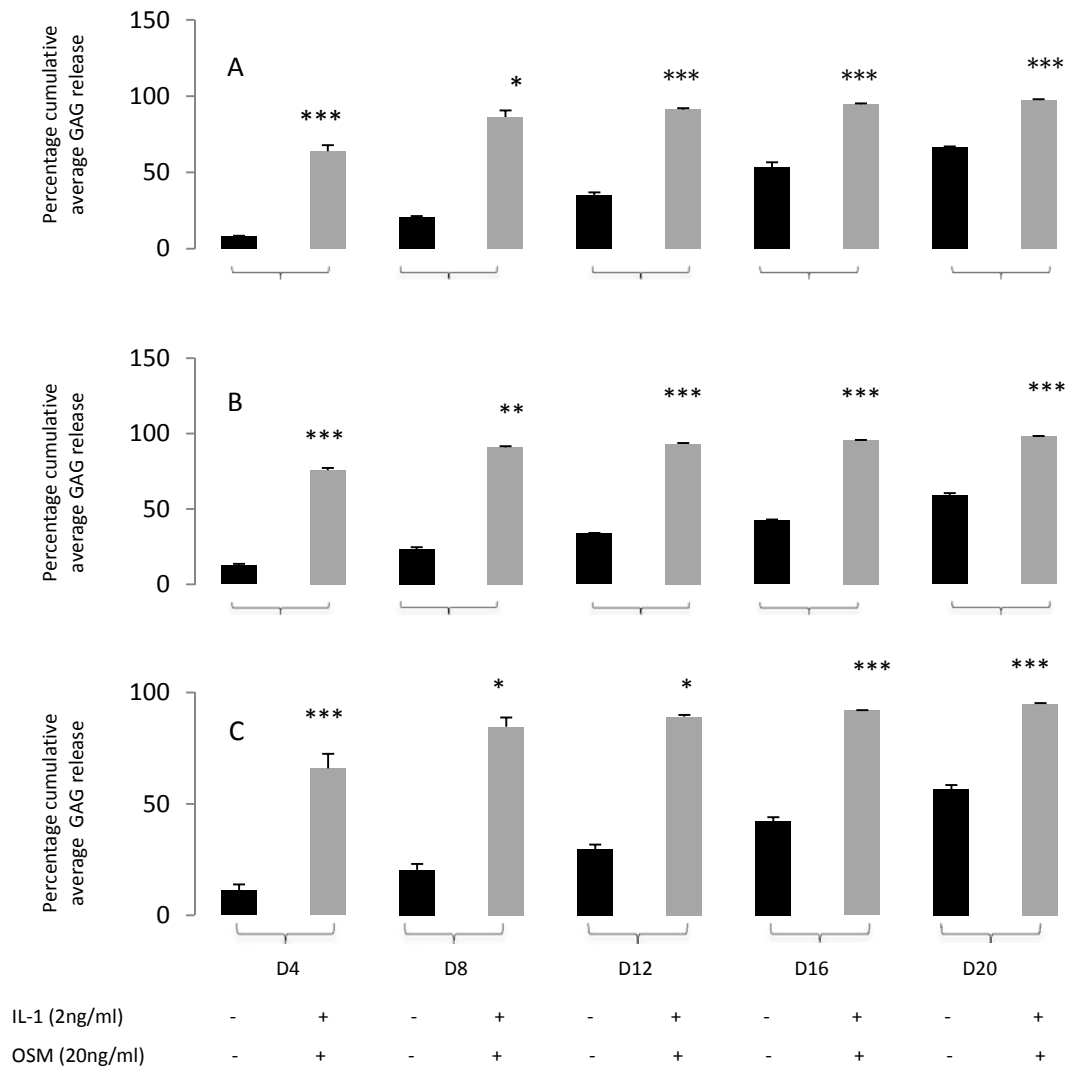


Figure 3.12: Assessment of proteoglycan release in response to a cytokine stimulus. Cartilage macro-pellets were generated from hMSCs and stimulated with cytokines as described in section 2.2.11. At each time point medium was harvested from each micro-pellet and stored at -80°C . All the macro-pellets remained in culture and were re-stimulated at each time point until the end of the experiment (day 21) when the macro-pellets were harvested; rinsed in PBS and stored at -80°C . GAG and hydroxyproline assays (section 2.2.13 and 2.2.14) were performed on the medium of each micro-pellet at each time point. The macro-pellets were papain digested (section 2.2.12) and GAG and hydroxyproline assays performed on the resultant medium. The total amount of GAG or hydroxyproline was then calculated for each micro-pellet. Percentage cumulative average GAG release was calculated as described in figure 3.2. Bar charts A and B – 3 control and 4 cytokine-stimulated pellets in each experiment. Bar chart C – 3 control and 3 cytokine-stimulated pellets. * control GAG release compared to IL-1 (2ng/ml) + OSM (20ng/ml) GAG release. * $p < 0.05$ ** $p < 0.01$ *** $p < 0.001$. D4 represents day 4 and so forth. Error bars +/- 1 SD of the mean. Donors 080825B. (Bar charts B and C) Donor 081276B. (Bar chart A). An independent samples T-test was performed.

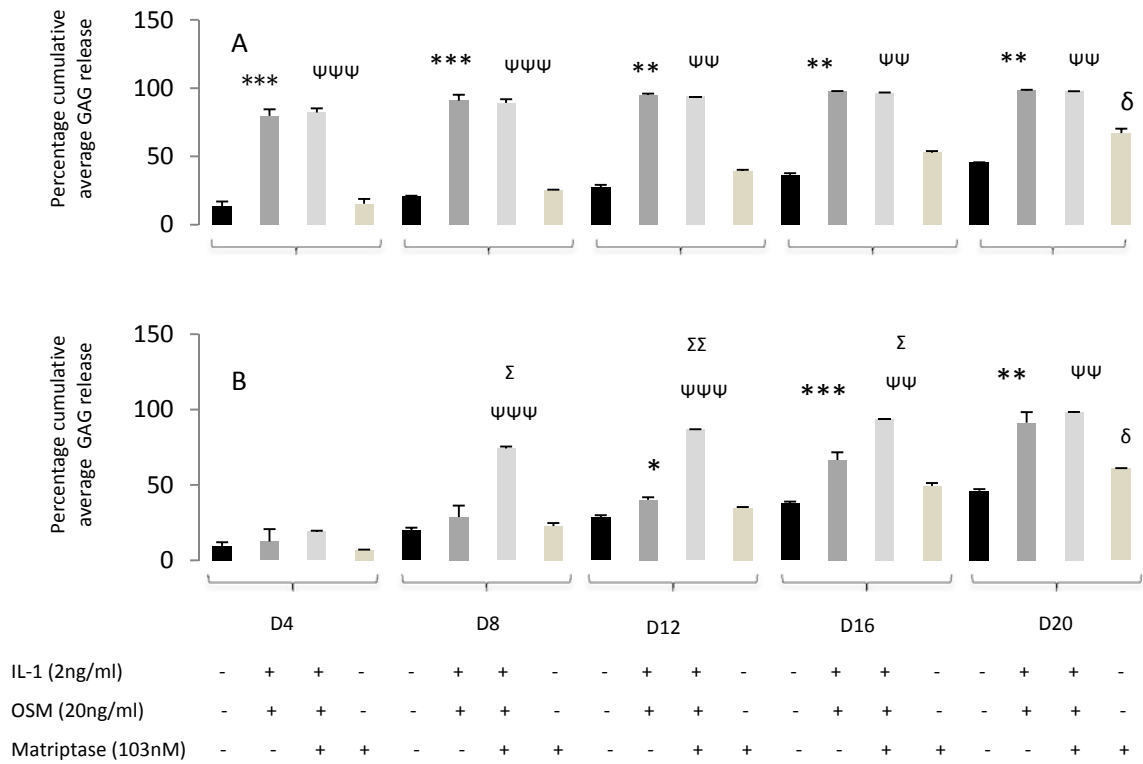


Figure 3.13: Assessment of proteoglycan release in response to a cytokine stimulus +/- matriptase.

Cartilage macro-pellets were generated, processed and analysed as described in figure 3.12. Bar chart A – 2 control, 2 IL-1 + OSM + matriptase, 2 matriptase and 3 IL-1 + OSM pellets. Bar chart B - 4 control, 4 IL-1 + OSM, 2 IL-1 + OSM + matriptase and 2 matriptase pellets. * control GAG release compared to IL-1 (2ng/ml) + OSM (20ng/ml) GAG release. Ψ control GAG release compared to IL-1 (2ng/ml) + OSM (20ng/ml) + matriptase (103nM) GAG release. Δ control GAG release compared to matriptase (103nM) GAG release. Σ IL-1 (2ng/ml) + OSM (20ng/ml) + matriptase (103nM) GAG release compared to IL-1 (2ng/ml) + OSM (20ng/ml) GAG release. Δ p<0.05 ** p<0.01 *** p<0.00. D4 represents day 4 and so forth. Error bars +/- 1 SD of mean. Donor 081276B. (Bar chart A) Donor 080825B. (Bar chart B). A one-way ANOVA test and post hoc Tukey test were performed.

3.2.3.3 The effects of IL-1 + OSM +/- matriptase on MMP activity

Similar to the micro-pellet model, and work carried out by Morgan et al. [178] and Cawston et al. [184], I detected significant MMP activity in the culture medium of the IL-1 + OSM stimulated macro-pellets shown in figures 3.14A and 3.14B. (Albeit at very low levels compared to the disc model) However, this effect was not seen in figures 3.14C or 3.15A and 3.15B, using IL-1 + OSM stimulus alone. Similar to work carried out by Milner et al. [122], and similar to findings in the cartilage disc model, I detected significant MMP activity when matriptase was used in combination with IL-1 and OSM. (Figures 3.15A and 3.15B). Similar to the cartilage disc model, matriptase alone had no effect on MMP activity. However, there was significant pro-MMP activity in the matriptase stimulated group. (Figures 3.15A and 3.15B) In addition, as found in the cartilage disc and micro-pellet model there was significant pro-MMP activity in the IL-1 + OSM stimulated group relative to control in figures 3.14A, 3.14C and 3.15A, (corresponding with work by Cawston et al. [183]) however this pattern did not reach significance in figures 3.14B and 3.15B.

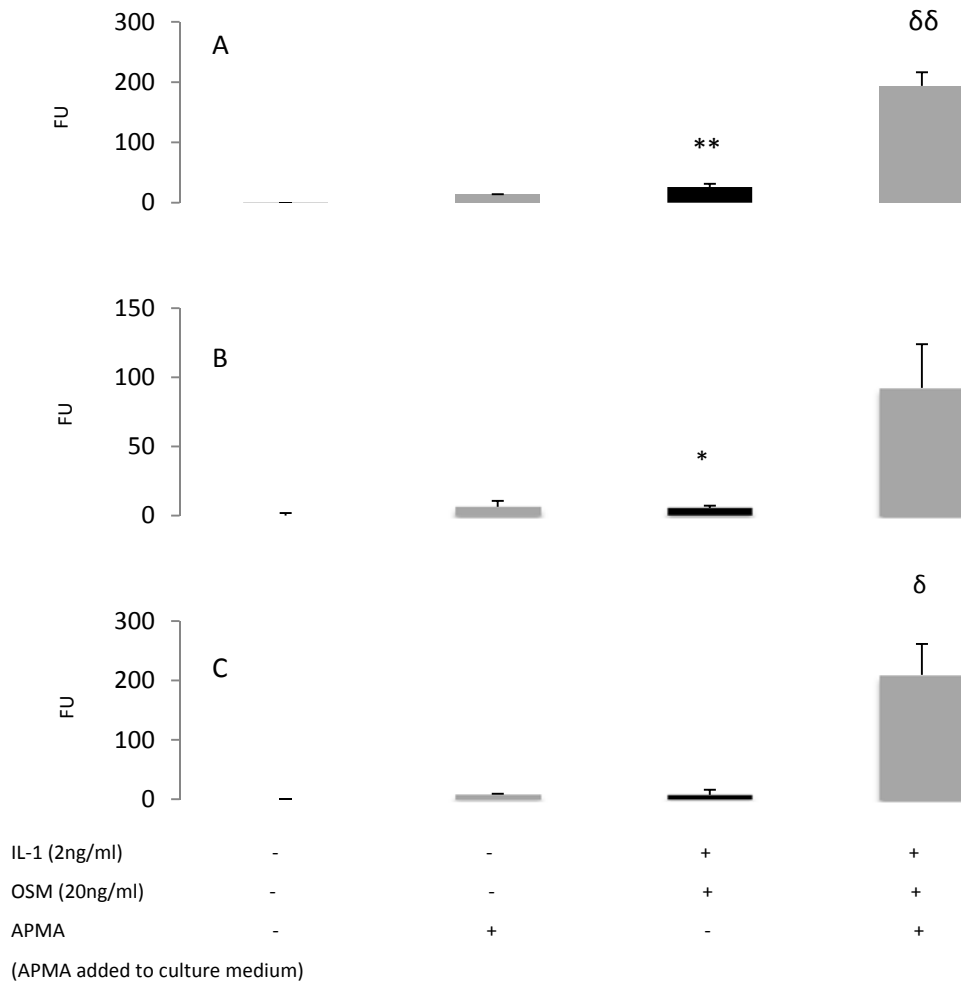


Figure 3.14: Assessment of MMP activity in response to a cytokine stimulus. Cartilage macro-pellets were generated from hMSCs and stimulated with cytokines as described in section 2.2.11. At each time point medium was harvested from each micro-pellet and stored at -80°C. All the macro-pellets remained in culture and were re-stimulated at each time point until the end of the experiment (day 21) when the macro-pellets were harvested; rinsed in PBS and stored at -80°C. A MMP activity assay was performed on the medium of three pellets from each group to detect pro-MMP or MMP activity, as described in section 2.2.15. Bar charts A, B and C correspond to bar charts A, B and C in figure 3.12. The assay was performed on medium at day 20. * control MMP activity compared to IL-1 (2ng/ml) + OSM (20ng/ml) MMP activity. δ control + APMA pro-MMP activity compared to IL-1 (2ng/ml) + OSM (20ng/ml) + APMA pro-MMP activity. * $p < 0.05$ ** $p < 0.01$. Black bars represent no APMA addition to medium (MMP activity) and grey bars represent APMA addition to control or stimulus medium. (Pro-MMP activity) Error bars +/- 1 SD of mean. Donors 080825B. (Bar charts B and C) Donor 081276B. (Bar chart A). An independent samples T-test was performed.

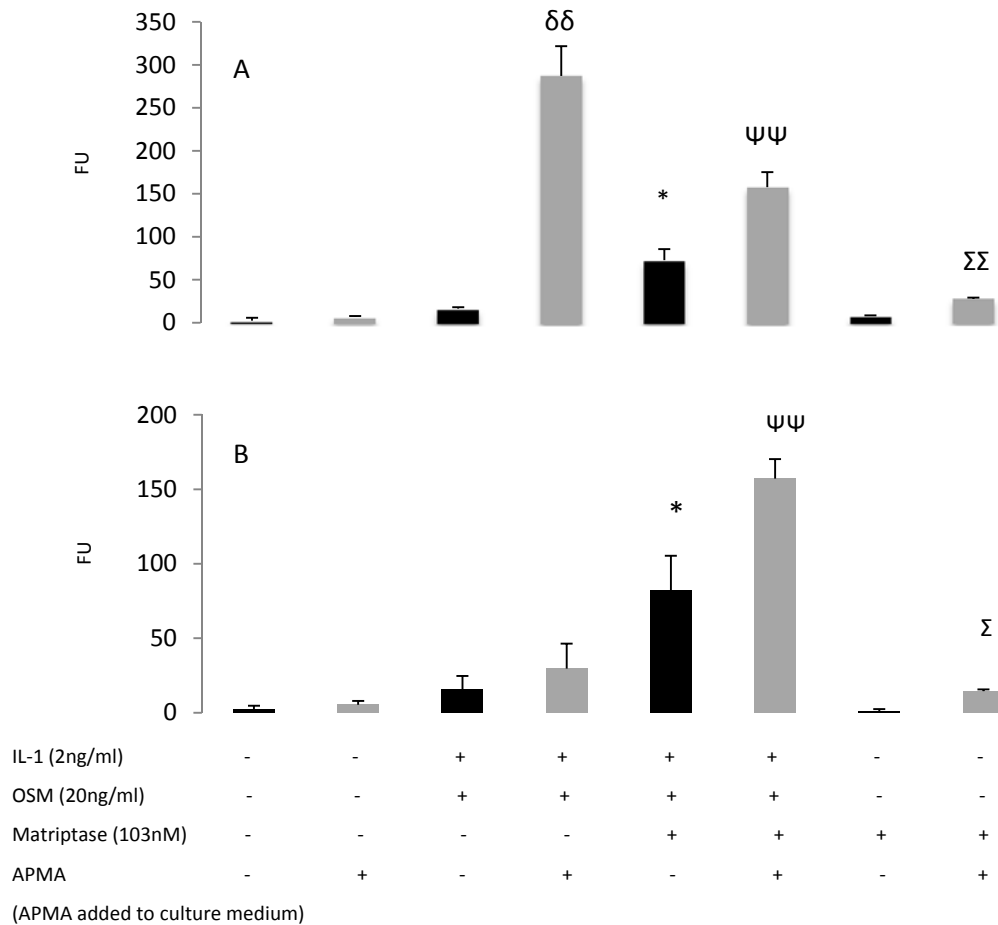


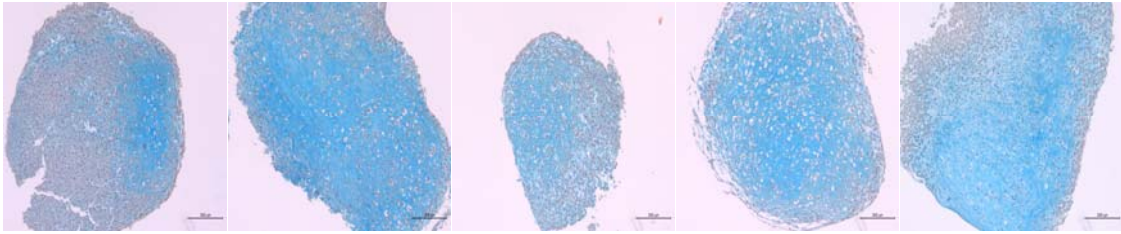
Figure 3.15: Assessment of MMP activity in response to a cytokine stimulus +/- matrilptase. Cartilage macro-pellets were generated, processed and analysed as described in figure 3.14. Bar charts A and B correspond to bar charts A and B in figure 3.13. The assay was performed on medium at day 20. Ψ control + APMA pro-MMP activity compared to IL-1 (2ng/ml) + OSM (20ng/ml) + matrilptase (103nM) + APMA pro-MMP activity. $\delta\delta$ control + APMA pro-MMP activity compared to IL-1 (2ng/ml) + OSM (20ng/ml) + APMA pro-MMP activity. Σ control + APMA pro-MMP activity compared to matrilptase + APMA pro-MMP activity. * control MMP activity compared to IL-1 (2ng/ml) + OSM (20ng/ml) + matrilptase (103nM) MMP activity. * $P < 0.05$ $\Sigma\Sigma$ $p < 0.01$. Black bars represent no APMA addition to medium (MMP activity) and grey bars represent APMA addition to control or stimulus medium. (Pro-MMP activity) Error bars +/- 1 SD of mean. Donor 081276B. (Bar chart A) Donor 080825B. (Bar chart B). An independent samples t-test was performed.

3.2.3.4 Histology of tissue-engineered cartilage macro-pellets

The macro-pellets had a qualitatively higher amount of proteoglycan compared to the micro-pellets with more widespread staining, shown by Alcian Blue (figure 3.16A) and Safranin-O (figure 3.16B) staining. However, similar to the micro-pellets there was very little collagen content (Masson's Trichrome) and it was arranged around the periphery. (Figure 3.16C) The macro-pellet model was a useful model in terms of reliability and reproducibility of proteoglycan breakdown, however despite significant MMP activity seen in some experiments there was no collagen release detected in any experiment, similar to the micro-pellet model, due to too little collagen content. (Figure 3.16C)

Alcian Blue staining

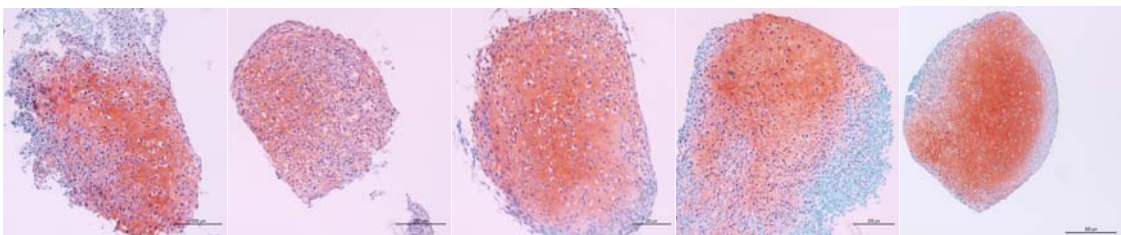
A



Alcian blue staining shown throughout the macro-pellets

Safranin-O staining

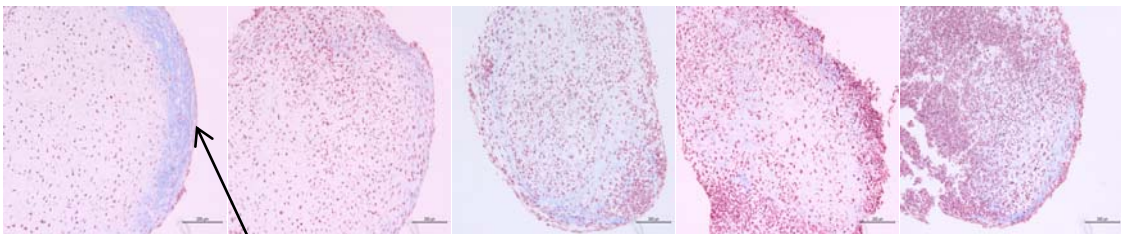
B



Safranin-O red staining throughout the macro-pellets

Masson's Trichrome staining

C



Blue collagen fibrils arranged around the periphery of the macro-pellets

Figure 3.16: Histology representation of cartilage macro-pellets. One tissue engineered cartilage macro-pellet from each separate experiment was harvested at day 14 and stored at -80°C . These discs were then washed in PBS, fixed in 10% buffered paraformaldehyde for twenty minutes further rinsed in PBS and then wrapped in tissue paper and paced in a labelled cassette. These fixed discs then underwent processing in graded ethanol and were embedded in molten paraffin wax. The discs were subsequently sectioned using a microtome at $4\mu\text{m}$ longitudinally and stained as described in section 2.2.8. A – Alcian Blue. B – Safranin-O. C – Masson's Trichrome.

3.3 Discussion

The overall general observation from my work showed that the tissue-engineered cartilage discs have cartilaginous properties and reproducibility and reliably respond to a cytokine stimulus in terms of proteoglycan degradation, but with variable collagen degradation. This is in contrast to the tissue-engineered cartilage micro-pellet model, which had a lower content of proteoglycan and collagen observed by histological analysis resulting in no collagen release in response to a catabolic stimulus. Also shown in section 3.2.2.2, there was much diffusion of proteoglycan into the culture medium with no catabolic stimulus, which will be discussed below. The macro-pellet model was improved in terms of proteoglycan content, however again there was very little or no collagen content. This model, similar to the cartilage disc model, also had reproducible and reliable proteoglycan release in response to a catabolic stimulus but no collagen degradation was detected. Despite the positive features of the cartilage discs mentioned above, I experienced significant difficulty generating these discs with many failed attempts and significant time lost trying to produce these. This problem had also been encountered with other colleagues within MRG. Due to these problems future work was hampered, and these observations will now be explored in further detail.

3.3.1 Tissue-engineered cartilage discs have uniform and abundant ‘cartilage-like’ features as evidenced by histology

Similar to work carried out by Murdoch et al. I found that the cartilage discs had a more uniform distribution of proteoglycan and collagen content, compared to the micro-pellets where the distribution was less homogenous, with most proteoglycan and collagen molecules distributed around the periphery and sparsely in the central region [203]. The macro-pellets had a more uniform distribution of proteoglycan, however again the collagen content was sparse, being arranged around the periphery. From the histological analysis it would also appear that the cartilage discs had a higher content of proteoglycans and collagen fibrils compared to the micro- and macro-pellet models. This has been confirmed in work by Murdoch et al., who found the cartilage discs accumulated 50% more proteoglycan per cell with a higher wet mass compared to the pellet model. Also this group found the cartilage discs had a higher content of type II collagen than the pellets [203]. Although Masson’s Trichrome staining is not specific for a particular type of

collagen, in keeping with work by Johnstone et al. [204] and Murdoch et al. [203], it is likely that a significant proportion of the collagen content is type X collagen (a marker of hypertrophy), despite the addition of dexamethasone and TGF- β . The terminal differentiation into hypertrophic chondrocytes occurs rapidly soon after the appearance of type II collagen [203, 204]. However, Murdoch et al. did find that the cartilage discs had a lower content of type X collagen compared to the pellet model [203]. Therefore, ideally I would have used the cartilage disc model for all experiments, however this was hampered due to significant difficulty generating these discs and time constraints.

3.3.2 Reliable and reproducible early proteoglycan catabolism in response to a catabolic stimulus in a tissue-engineered cartilage disc and macro-pellet model

My results showing significant proteoglycan release in a cartilage disc model upon addition of IL-1 + OSM at an early time point using three separate hMSC donors, is similar to work carried out by Morgan et al. [178], Cawston et al. [183], and Durigova et al. [214] using human nasal cartilage, bovine nasal cartilage and bovine articular cartilage, respectively. In addition a similar effect using IL-1 alone as a catabolic stimulus, has also been observed in studies by Morgan et al. and Cawston et al. using this specific concentration of IL-1 [178, 183]. The significant finding showing enhancement of proteoglycan release upon addition of matrilysin to IL-1 + OSM, is similar to the effect on collagen release found in work by Milner et al. [122].

The effect on proteoglycan catabolism seen upon addition of IL-1 + OSM is likely due to the up-regulation of aggrecanases. Indeed work by Koshy et al. found increased mRNA expression of ADAM-10, ADAMTS-1, and ADAMTS-4 in human chondrocytes (T/C28a4) stimulated with IL-1 and OSM. IL-1 stimulation by itself enhanced ADAMTS-5 mRNA expression, explaining the results I obtained using IL-1 alone [220]. This finding is also confirmed in a study by Milner et al. using bovine nasal cartilage explants, who observed 80% proteoglycan release in response to IL-1 + OSM correlating with induction of ADAMTS-4 and ADAMTS-5 [221].

The enhancing effect on proteoglycan release upon addition of matrilysin to a cytokine stimulus has been examined in a study by Wilkinson et al. who determined that the action of matrilysin induced proteoglycan resorption is due mainly to metalloproteinase activity and a slight enhancement of ADAMTS-4 [222]. As discussed in section 1.8, matrilysin

stimulation of cartilage promotes activation of MMP-1 and -3, and it is likely that the activation of these MMPs played a role in the enhancement of proteoglycan release I observed when matriptase was added to the cytokine stimulus. Matriptase alone had no significant effect on proteoglycan release at an early time point, however by day 21 there was a significant result. (Albeit it very slight) This suggests that matriptase by itself is not a potent initiator of proteoglycan catabolism.

A similar pattern of proteoglycan release was found using a macro-pellet model with similar cytokine and matriptase stimulation conditions. However, there were some donor differences in terms of proteoglycan release in response to cytokines +/- matriptase. This suggests donor variability in terms of chondrogenesis and differing response to catabolic stimuli. Donor variability (both inter- and intra-variability) is a common problem when using hMSCs. There is significant variation in the growth kinetics and gene expression of hMSCs between different donors, as found by Phinney et al. and Siegel et al. [223, 224]. It was found that younger female donors tended towards more colony forming cells, which multiplied more rapidly compared to young and old male donors [224]. The age and gender of the donor may also cause differences in adipogenic, chondrogenic or osteogenic in vitro differentiation of hMSCs due to alterations in the phenotype of the cells. Siegel et al. found that the phenotype of hMSCs differed significantly depending on age and gender of the donor, with younger female donors having a higher percentage of CD146+ cells compared to young and old males. CD146+ cells are mainly tri-potent cells and so have the potential to differentiate into three lineages. Thus the age and gender of the hMSC donor will significantly affect the mesodermal differentiation capacity [224]. Other factors that may account for significant in vitro hMSC variation between donors include the clinical history and physiological status of the donor, which in most cases is unknown [225]. Even within the same donor there is significant heterogeneity (intra-variability) with colony-forming units comprised of cells at different stages of differentiation with varying numbers of mesenchymal progenitors, which varies with passage number too [223, 226]. This inter- and intra-donor hMSC variability will therefore have an impact on the cartilage matrix formed, cell surface receptor expression and response to catabolic stimuli, as observed.

The micro-pellet model did not produce such a pattern of proteoglycan release as seen in the disc and macro-pellet model. The general pattern was significant proteoglycan release

at day 3 in the cytokine stimulated group, however at or beyond day 6 the control group 'catches-up' in terms of proteoglycan release. Therefore, it was likely that the cartilage matrix was not being laid down properly, and the proteoglycans were not being incorporated into the cartilage matrix and were simply diffusing out into the culture medium. This process was enhanced in the cytokine-stimulated group due to the potent catabolic effect, explaining the significant release at an early time point. Indeed, Murdoch et al. found in the cartilage pellet model there was less efficient retention of proteoglycans within the matrix compared to the cartilage discs model, and this would explain the results I observed [203]. The reason for this is that the cartilage discs grow as shallow discs increasing in thickness with a very small change in surface area generating no tensile forces and so no fibrogenic stimuli to compromise chondrogenic differentiation. Conversely, the pellets grow as a sphere with a large continuous increase in surface area, generating more tensile forces and a fibrogenic response in the pellet compromising chondrogenesis and the cartilage matrix formed. Therefore, the discs generate a more robust and homogenous cartilage matrix compared to the micro-pellets [203]. This effect is also compounded by the fact that very little nutrition can reach the centre of the pellet compromising chondrogenesis and the formation of a cartilage matrix, whereas the disc model allows nutrition to reach all the cells enhancing chondrogenesis and formation of a more robust matrix [203]. So, in the micro-pellet model, the matrix is poorly formed and proteoglycans can simply diffuse into the culture medium. This effect observed in the micro-pellet model, is not evident in the macro-pellet model, perhaps because a more robust matrix is formed compared to the micro-pellet model. The tissue-engineered cartilage discs and macro-pellets therefore represent a more reliable and reproducible model of proteoglycan catabolism than the micro-pellet model.

3.3.3 Variable collagen catabolism in response to a catabolic stimulus in a tissue-engineered cartilage disc model, but no such effect seen in a micro- or macro-pellet model

Only in the tissue-engineered cartilage disc model did I detect any collagen release in response to a catabolic stimulus, which was likely due to the micro- and macro-pellets not expressing many collagen fibrils as shown by histology. There was some MMP activity in the culture medium of these cytokine-stimulated micro- and macro- pellets, however

negligible substrate for them to act on so no effect observed, discussed further in section 3.3.4. In three separate cartilage disc experiments from two different donors I obtained three different results in terms of collagen release, highlighting significant intra- and inter-donor variability as discussed in section 3.3.2. This variability in terms of collagen degradation in response to a cytokine stimulus has also been found in a study by Cawston et al. using human articular cartilage with only 20-30% of samples responding [184]. The significant collagen release that I observed in two experiments at a later time point is similar to work carried out by Morgan et al. [178] and Cawston et al. [183].

In line with work carried out by Milner et al. I found significant collagen release upon the addition of matriptase to the cytokine stimulus. This was likely due to the action of matriptase causing activation of collagenases (as discussed in section 1.8) [122], in addition to the up-regulation of MMP-1 and -13 induced by IL-1 + OSM, as observed by Koshy et al. [220], hence creating a large pool of collagenases causing collagen degradation. Therefore the observed collagen release was due to up-regulation and activation of collagenases causing the effect seen. (Discussed further in section 3.3.4)

IL-1 + OSM (with no matriptase addition) also induced collagen release in two independent experiments due to collagenase activity. This corresponds with work carried out by Morgan et al. [178], Cawston et al. [183], Koshy et al. [220], and Barksby et al. [227], who found significant collagenase activity/expression in response to a cytokine stimulus. Adding to this body of evidence showing MMP activity in cartilage in response to a cytokine stimulus is work by Milner et al. who found induction of MMP-1, -3 and -13 in bovine nasal cartilage in response to IL-1 + OSM [221]. Interestingly in response to this cytokine stimulus, Milner et al. also found a general reduction in TIMP-2 and -3 in the cartilage, which would also enhance collagen degradation, as observed [221]. The combination of IL-1 + OSM has also been over expressed intra-articularly into an in vivo murine model using an adenoviral approach, and subsequently detected significant loss of type II collagen staining and enhanced MMP-13 staining using immunohistochemistry [168].

Also corresponding to work by Milner et al. I detected no collagen release with matriptase stimulation by itself. Milner et al. only elicited collagen release in OA cartilage explants with matriptase stimulation. This suggests that matriptase requires either a cell

surface receptor specifically expressed in OA cartilage for its effects, such as PAR-2 or the addition of a cytokine stimulus creating a large pool of MMPs, causing collagen degradation [122].

Due to significant donor variability in generating cartilage discs I could not reproduce further cartilage discs to replicate these experiments and attain some reliability and reproducibility in terms of collagen catabolism, which has hampered future work. As mentioned, the micro- and macro-pellet models contained very little collagen content in their matrix so I could not use these as a model of collagen catabolism.

3.3.4 Significant pro-MMP and active MMP activity observed in cytokine +/- matriptase stimulated tissue-engineered cartilage disc, micro- and macro-pellet models

As described there was significant collagen release in a cartilage disc model. I carried out a MMP activity assay to determine that the collagen degradation was due to MMP activity. Work carried out by Morgan et al. found that the cytokine-induced collagen release seen in human nasal cartilage corresponded with increased MMP-1 and -13 levels [178]. Similarly, Cawston et al. found a marked increase in collagenase activity in bovine nasal cartilage cytokine stimulated samples, correlating with collagen release [184]. Interestingly, other work by Cawston et al. also detected pro-collagenase activity in IL-1 + OSM stimulated bovine nasal cartilage at day 7 and day 14, and also active collagenase activity at day 14 correlating with the collagen release seen [183]. This increased collagenase activity seen in IL-1 + OSM-treated cartilage has also been observed in work by Koshy et al., who found increased gene expression of MMP-1 and -13 in cytokine stimulated human chondrocytes [228]. In addition, MMP-3 gene expression was also increased in these cytokine-stimulated chondrocytes, which is an activator of pro-collagenases [228]. Also, Barksby et al. carried out microarray analysis of RNA from IL-1 + OSM-treated SW1353 chondrocytes and found up-regulation of the genes for MMP-1, -3 and -13 which are involved in collagen degradation [227].

Therefore, it was likely that there was pro-MMP and MMP activity in the tissue-engineered cartilage discs stimulated with IL-1 + OSM that I generated. Indeed, I found in one cartilage disc experiment there was increased MMP activity in the IL-1 + OSM group. Although this was not significant, this increased MMP activity contributed towards the collagen degradation seen in this group. There was also a significant pool of latent MMPs

both in the IL-1 and IL-1 + OSM groups, which could not be activated by this stimulus. In a similar cartilage disc experiment there was no collagen release detected in the IL-1 + OSM group, and this correlated with minimal MMP-activity, but significant pro-MMP activity. However, when matriptase was added to the cytokine stimulus there was significant collagen release and this correlated with significant MMP activity in this group compared to control. Indeed, in addition to the ability of matriptase to activate pro-MMP-3 (with subsequent activation of pro-collagenases), Milner et al. found that matriptase can also activate pro-MMP-1 [122], and these actions in combination with IL-1 + OSM-induced up-regulation and activation of MMPs would explain the resultant increase in MMP activity observed.

Matriptase by itself had no such effect on MMP activity. Interestingly, Milner et al. only found increased MMP-1, -3 and -13 gene expression in OA cartilage explants (expressing PAR-2) treated with matriptase, (corresponding with collagen release) but not bovine nasal cartilage treated samples [122]. It is therefore likely that the tissue-engineered cartilage discs I generated do not express PAR-2, and therefore matriptase by itself had no effect on collagen catabolism.

I also performed a similar MMP activity assay to show that although I detected no collagen release from the micro- and macro-pellets in response to a catabolic stimulus, there was MMP activity present in the culture medium and the negative result was due to too little collagen content in these pellets. Again, the most significant observation was the large pool of latent MMPs generated from the chondrocytes in response to a catabolic stimulus. There was some inter- and intra-donor variability in response of the chondrocytes to produce pro- and active MMPs found between experiments. My results showing significant pro-MMP and active MMP activity in a cartilage model in response to a catabolic stimulus have also been found in studies by Cawston et al. [183, 215], and Morgan et al. [178], using bovine nasal cartilage and human nasal cartilage, respectively. It is clear from my results, and also in work by Milner et al. [221], that activation of pro-collagenases is a key control point dictating whether cartilage collagen catabolism will occur.

3.3.5 Summary

- Compared to the tissue-engineered cartilage micro- and macro-pellets, the cartilage disc model represented a useful model of cartilage catabolism in terms of reliable and reproducible proteoglycan release in response to a catabolic stimulus and detection of collagen release, albeit variable. However, future work was hampered by difficulty generating these cartilage discs, with many donors failing to produce discs at all.
- Tissue-engineered cartilage micro-pellets did not incorporate proteoglycan molecules into their matrix, resulting in subsequent diffusion of proteoglycans into the culture medium with no catabolic stimulus, and so was not a useful model.
- In terms of proteoglycan catabolism analysis the macro-pellet model responded to a cytokine stimulus by degrading proteoglycan using two different donors, however not many (or none at all) collagen fibrils were incorporated into its matrix so collagen catabolism could not be analysed.
- Matriptase had an enhancing effect on proteoglycan and collagen release when used in combination with IL-1 + OSM using a cartilage disc model. A similar effect was seen on proteoglycan catabolism using a cartilage macro-pellet model. Matriptase stimulation by itself had no such effect on proteoglycan and collagen catabolism.
- The cartilage disc model displayed cartilaginous features seen using histology techniques. The macro-pellet and micro-pellet cartilage models had very little, or absent collagen content evidenced by histology and so were not a useful model to use to generate a reliable and reproducible model of cartilage catabolism.
- Despite perseverance I did not fulfil my aims outlined in section 3.1 to generate a reliable and reproducible model of cartilage catabolism in terms of both proteoglycan and collagen release. A significant amount of time was spent trying to generate further cartilage discs, however many donors failed to form discs and the failure to generate reliable cartilage-like material from hMSCs meant that further studies were not possible. Therefore I did not progress to aim four and over-expression of PAR-2.

Chapter 4: Analysis of subchondral bone and cartilage remodelling in a murine OA model

4.1 Introduction

The mouse represents a good experimental model for defining human gene function due to its anatomic, physiologic and genetic similarity to humans. Furthermore, the mouse has a relatively short life span and its genome can be manipulated by molecular means. Scientists are, for example, able to ablate or overexpress genes in the whole animal, or in specific tissues [191]. This will therefore allow the human genome to be annotated with functional information providing an understanding of the molecular mechanisms and pathways underlying normal development and those involved in pathological conditions [191]. Of relevance to my research is assessing the importance of two genes (matriptase and PAR-2) and their role in the pathogenesis of OA when ablated specifically in bone or cartilage.

In order to assess their role in OA, firstly important baseline data on the remodelling events that occur in subchondral bone and cartilage in normal (wild type) murine OA pathology is required. To do this I have used the DMM model (surgical induction of OA) in 10 week-old wild type mice (C57BL/6N) and performed relevant analysis on cartilage and subchondral bone at 4, 8, 12 and 16 weeks post-surgery using micro-CT and histological techniques. Advantages of using a surgical model of OA (such as DMM) rather than a spontaneous model include a faster onset of disease, decreased variability and decreased dependence on genetic background [192]. Similarly, the DMM model is preferred to a collagenase-induced model due to better reliability and reproducibility in terms of cartilage degradation and subchondral sclerosis [229]. All mice used were male as there are significant gender differences in the progression of OA. This has been confirmed in a study by Ma et al. who found more extensive cartilage damage in male mice with surgical induction of OA, compared to female mice due to the protective effects of ovary-derived hormones [230].

Discussed in section 1.2 are the typical findings in cartilage and subchondral bone OA pathology including subchondral sclerosis, cartilage degeneration and osteophyte formation [7]. More detailed information on the subchondral bone and cartilage changes

that occur in OA have been provided utilising animal models. Although there is similarity in observations between animal models (subchondral sclerosis and cartilage degeneration) there is also significant variability in some parameters measured due to different modes of OA induction and different animals used [65, 80, 81, 231]. I have used a C57BL/6N mouse model for both wild type and gene ablation analysis of subchondral bone and cartilage remodelling in a DMM and sham OA model, therefore comparison between different groups of animals can be made. However, extrapolation of observations to human OA should be done with caution. I have used the sham limb (surgical opening of the joint capsule and then closure) as a control in my study instead of the contra-lateral DMM limb, similar to the study by Huesa et al. [232]. This is because there would be altered mechanical weight bearing in the DMM contra-lateral limb affecting the gait pattern with resultant remodelling events in cartilage and subchondral bone, hence skewing the results. The sham limb may also have altered weight bearing and gait pattern, however to a lesser degree so represents a better control model.

The aims of this chapter were:

1. Obtain baseline wild type mouse weights and tibial measurements to compare with the mice with gene ablation for developmental deviances.
2. To analyse subchondral bone changes in a mouse model of OA (surgical induction via DMM at 10 weeks of age) at 4, 8, 12 and 16 weeks post-surgery, by using micro-CT techniques to examine subchondral sclerosis and trabecular morphology.
3. Analyse osteophyte morphology using micro-CT techniques.
4. Analyse cartilage remodelling by histological techniques, and cartilage degradation via the OARSI scoring system at 4, 8, 12 and 16 weeks post-DMM surgery.

4.2 Results

4.2.1 Mouse weights and subchondral bone measurements

Important baseline data were collected including the weights of the mice and measurements of subchondral bone in the tibia enabling comparison to the mice with gene ablation to detect any gross abnormalities.

4.2.1.1 Mouse weights

The weights of the mice were recorded at 10 weeks of age at the time of surgical intervention. The mean weight of the mice was 25.77 grams. (± 1.138)

4.2.1.2 Subchondral tibial bone measurements at 4, 8, 12 and 16 weeks post DMM or sham surgery

Measurements were taken as described in section 2.2.10.4. Figure 4.1A shows that the shaft of the tibia was increased in width in the DMM group compared to sham at each time point, reaching significance at 16 weeks. There was also a stepwise increase in the width of the shaft of the tibia as the time course progressed in both the DMM and sham groups, but this did not reach significance at any time point due to much variation.

Figure 4.1B shows at 4 and 16 weeks post-surgery the height of the subchondral region in the medial epicondyle was less in the DMM group compared to sham, but not reaching significance. At 8 weeks post-surgery the opposite was observed whereby the height of the subchondral region in the medial epicondyle was significantly greater in the DMM compared to sham. There was no difference observed at 12 weeks post-surgery in the DMM group compared to sham.

Figure 4.1C shows that the height of the subchondral region in the lateral epicondyle of the tibia was greater than the medial epicondyle shown in figure 4.1B in both the DMM and sham groups at all time points. The general observation in figure 4.1C was a greater height of the subchondral region in the lateral epicondyle of the tibia in the DMM group compared to sham. This was more evident at 4 and 8 weeks post surgery (although not significant) and minimal at 12 weeks post-surgery and not apparent at 16 weeks post surgery. Also observed in figure 4.1C was that there were no significant differences in the height of the subchondral region in the lateral epicondyle throughout the time course in both the DMM and sham groups.

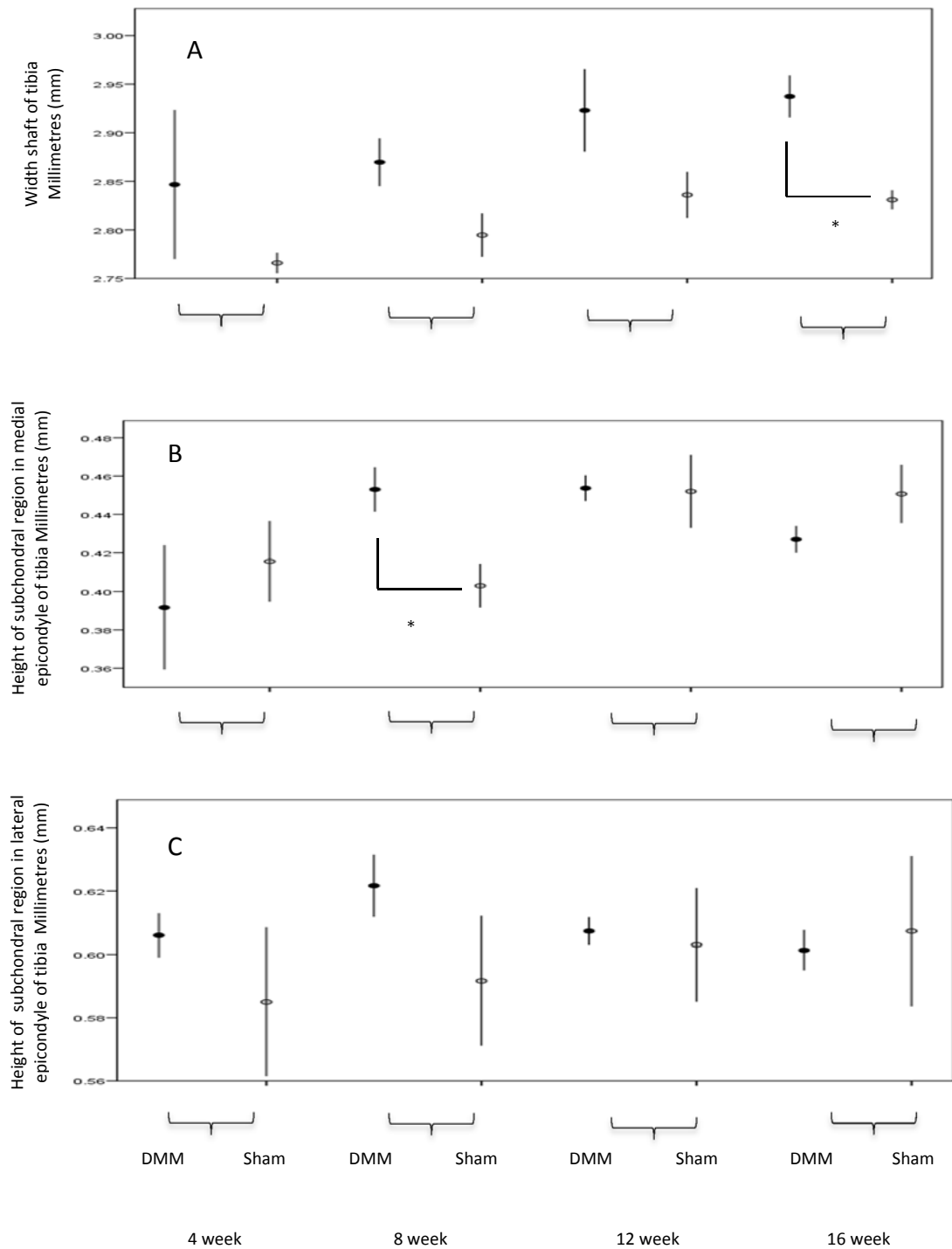


Figure 4.1: Tibial bone measurements. Wild type mice were sacrificed at 4, 8, 12 and 16 weeks post-surgery and had their left limb dissected and fixed in 10% paraformaldehyde. These limbs were subsequently scanned in a micro-CT SkyScanner. From these reconstructed scans, measurements of the subchondral bone and shaft of tibiae were taken using CTan software as described in section 2.2.10.4. 3 DMM and 3 sham mice were used for measurement in each group. The mean width/height is given in mm and error bars +/- 1 SE of the mean. * p<0.05. Independent samples T-test.

Figure 4.2 shows that the width of the subchondral tibial region increased in width from 4 to 16 weeks in the DMM group, however this difference was not significant due to much variation within each group. There were no significant differences observed in the width

of the subchondral tibial region in the sham group throughout the time course. The general trend was an increased width of the subchondral region in the DMM compared to sham group at all time points, reaching significance at 8 and 16 weeks post-surgery.

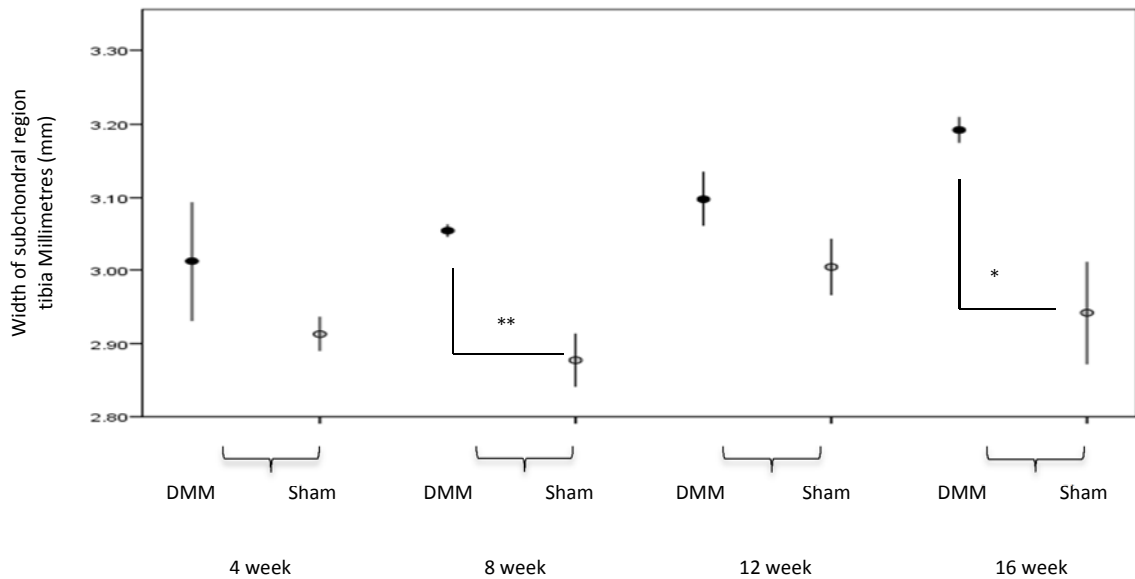


Figure 4.2: Tibial bone measurements. Wild type mice were sacrificed at 4, 8, 12 and 16 weeks post-surgery and were processed and analysed as described in figure 4.1. 3 DMM and 3 sham mice were used for measurement in each group. The mean width/height is given in mm and error bars +/- 1 SE of the mean. * $p < 0.05$ ** $p < 0.01$. Independent samples T-test.

4.2.2 Immunohistochemistry

4.2.2.1 PAR-2 up-regulation in a DMM model relative to sham

Shown in figure 4.3 there was up-regulation of PAR-2 in the cartilage in a DMM model relative to sham, at 8 weeks post-surgery. This is shown by more chondrocytes staining positive (brown) for PAR-2 in the DMM model (figure 4.3 images B and D; higher magnification images of A and C), relative to sham (figure 4.3 images F and H; higher magnification images of E and G). There was very little PAR-2 staining seen in the subchondral bone, even in the DMM model, with only a few osteoblasts staining positive for PAR-2.

Figure 4.4, images A and B represents a wild type naïve mouse staining for PAR-2. It is apparent that there are no cells staining positive for PAR-2, either in the cartilage or subchondral bone of the wild type naïve mouse. All of these images represent mice at 8 weeks post-surgery, as this is the age at which analysis took place for the gene ablated mice (chapters 5 and 6). Figure 4.4, image C represents a positive control for PAR-2 staining. (Murine heart)

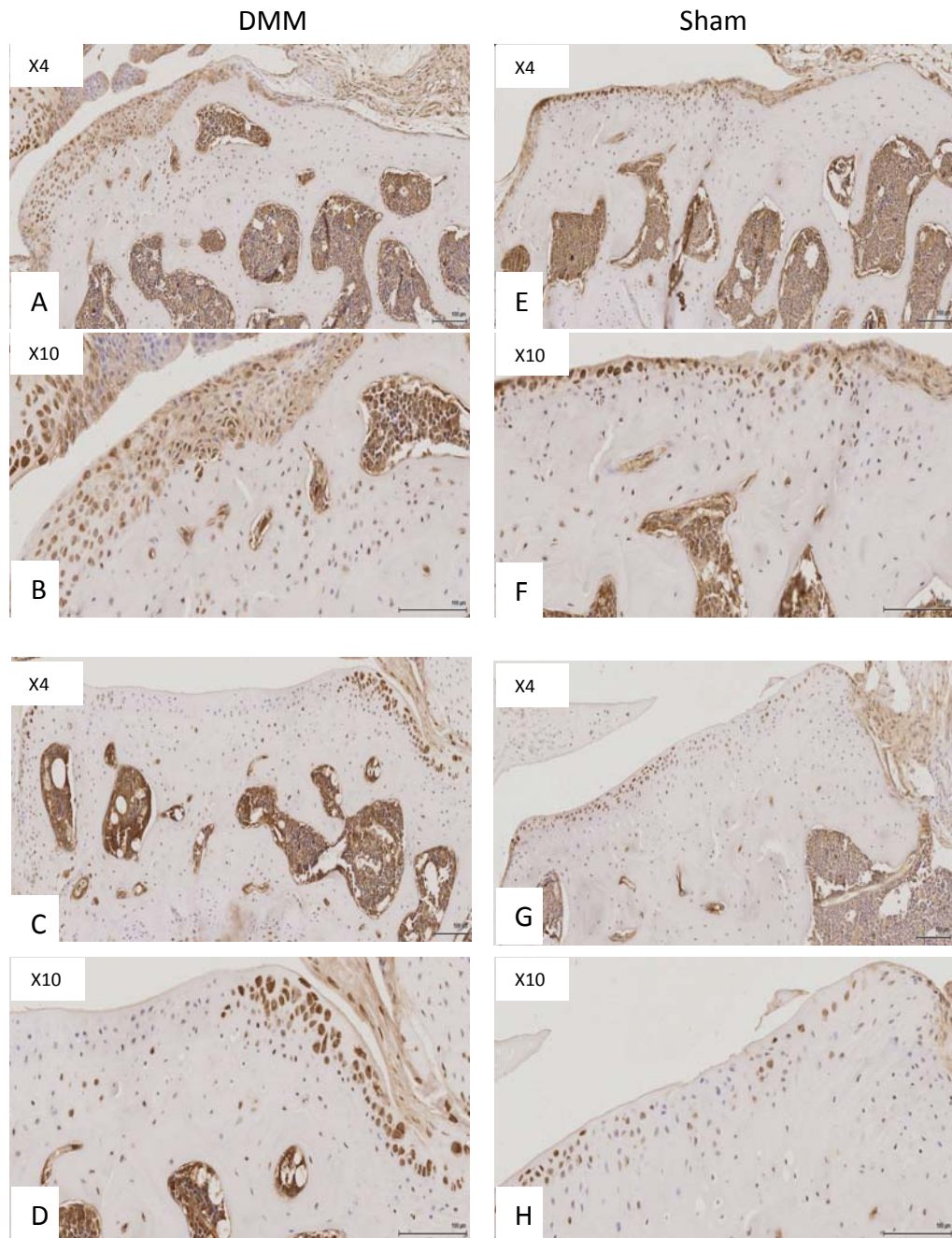


Figure 4.3: Immunohistochemistry PAR-2 in wild type DMM or sham mice. Wild type mice underwent DMM or sham surgery at 10 weeks of age. The mice were sacrificed at 8 weeks post-surgery and the tibia and femur dissected. The joints were fixed in 10% paraformaldehyde for up to 72 hours and then transferred into 70% ethanol. The joints were then decalcified, processed and embedded and sectioned. Sections were cut longitudinally throughout the entire joint. PAR-2 (SAM-11) IHC was then performed as described in section 2.2.9. The stained sections were then analysed using a microscope to detect the presence of PAR-2. (Brown staining) The top two panels are representative of sections taken earlier on in sectioning the joint. The bottom two panels are representative of sections taken later on in sectioning the joint. Two separate magnifications were used, as detailed on image.

Naïve

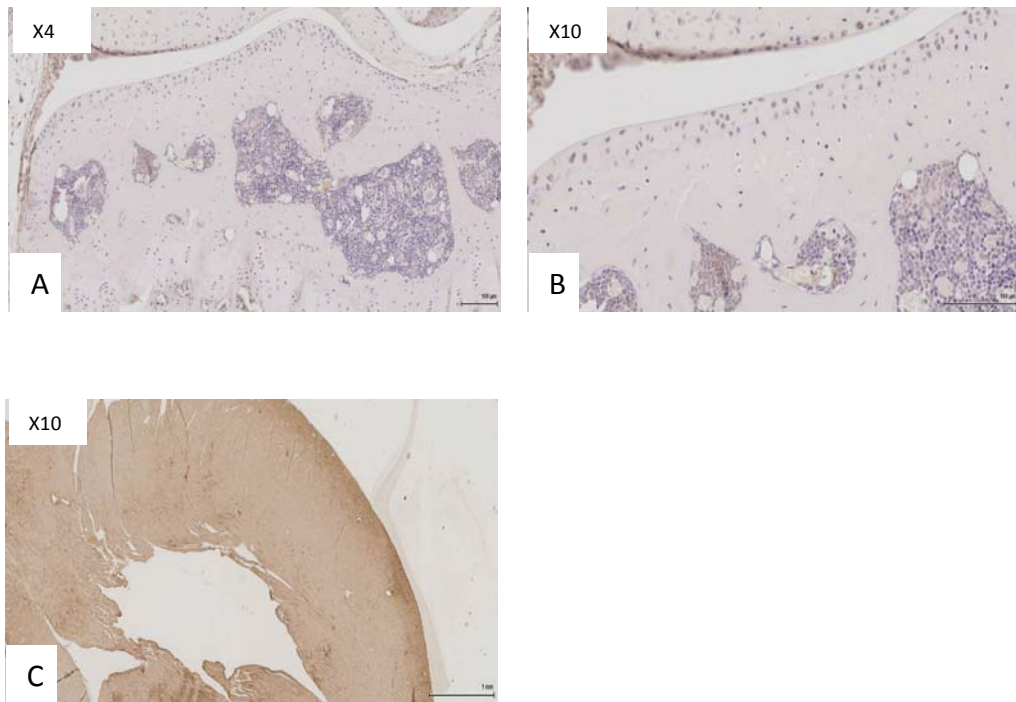


Figure 4.4: Immunohistochemistry PAR-2 in wild type naïve mice. Wild type mice remained naïve and were sacrificed at 18 weeks old and the tibia and femur dissected. Similar preparation was carried out as described in figure 4.3. Images A and B represent a section cut later on in sectioning the joint, using 2 separate magnifications as detailed on image. Image C is a positive control – PAR-2 stained murine heart (also used in figure 4.3).

4.2.2.2 Matriptase immunohistochemistry

Referring to figure 4.5 it is evident that the antibody used in this study (ST14 rabbit polyclonal antibody; Sigma-Aldrich) failed to stain matriptase (brown staining) expressed in chondrocytes or osteoblasts, in a murine DMM (figure 4.5 images B and D; higher magnification images of A and C) or sham model (figure 4.5 images F and H; higher magnification images of E and G).

Also, apparent in figure 4.6 (images A and B) there was lack of matriptase staining in the cartilage or subchondral bone of the naïve wild type mouse. The positive control (murine skin, figure 4.6, images C and D) was positive for matriptase staining and the bone marrow in figures 4.5 and 4.6 showed brown staining, representing matriptase expression. These results will be discussed further in section 4.3.

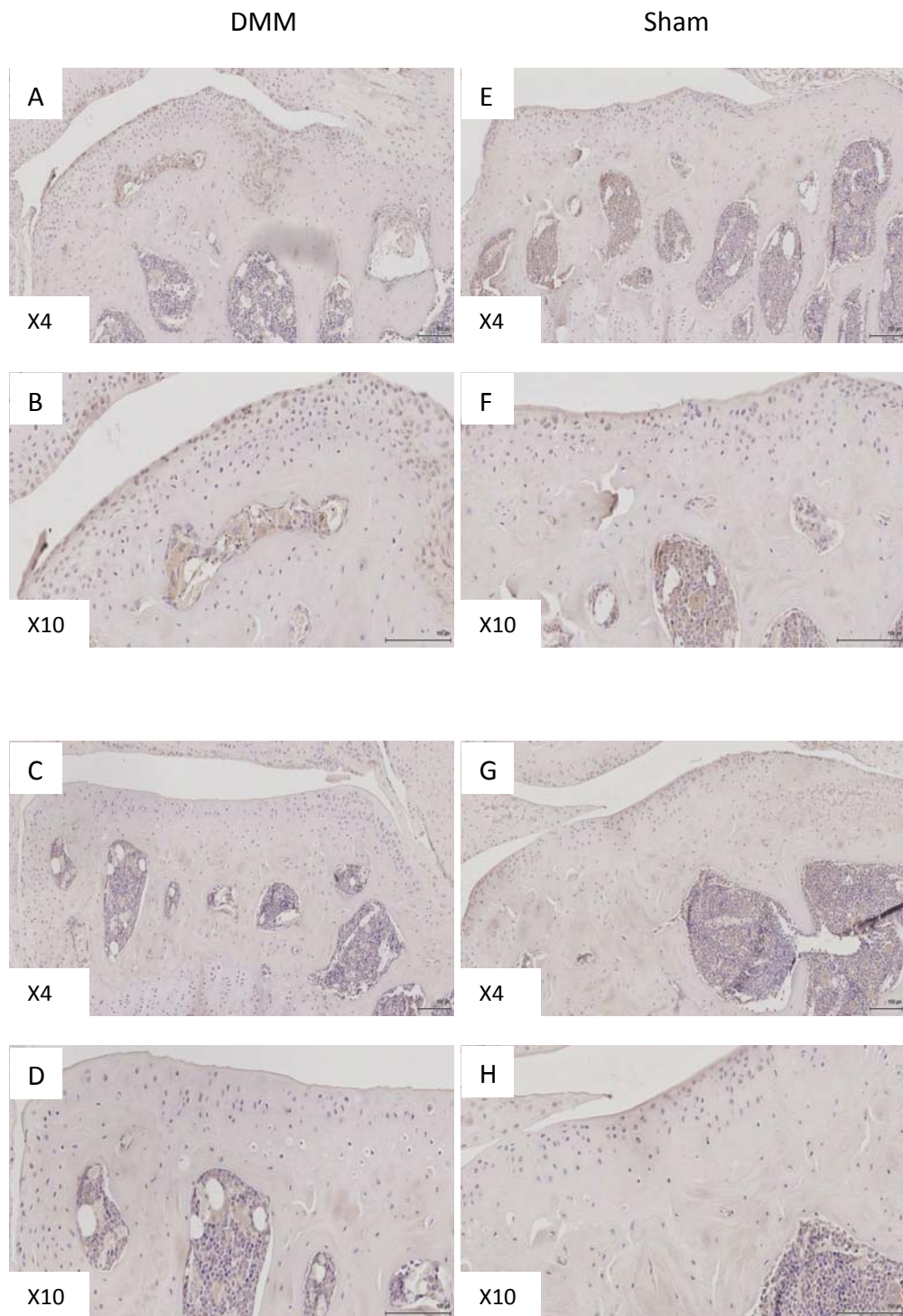


Figure 4.5: Immunohistochemistry ST14 in wild type DMM or sham mice. Wild type mice underwent DMM or sham surgery at 10 weeks of age. The mice were sacrificed at 8 weeks post-surgery and the tibia and femur dissected. The joints were fixed in 10% paraformaldehyde for up to 72 hours and then transferred into 70% ethanol. The joints were then decalcified, processed and embedded and sectioned. Sections were cut longitudinally throughout the entire joint. Matriptase (ST14) IHC was then performed as described in section 2.2.9. The stained sections were then analysed using a microscope to detect the presence of ST14. (Brown staining) The top two panels are representative of sections taken earlier on in sectioning the joint. The bottom two panels are representative of sections taken later on in sectioning the joint. Two separate magnifications were used, as detailed on image.

Naive

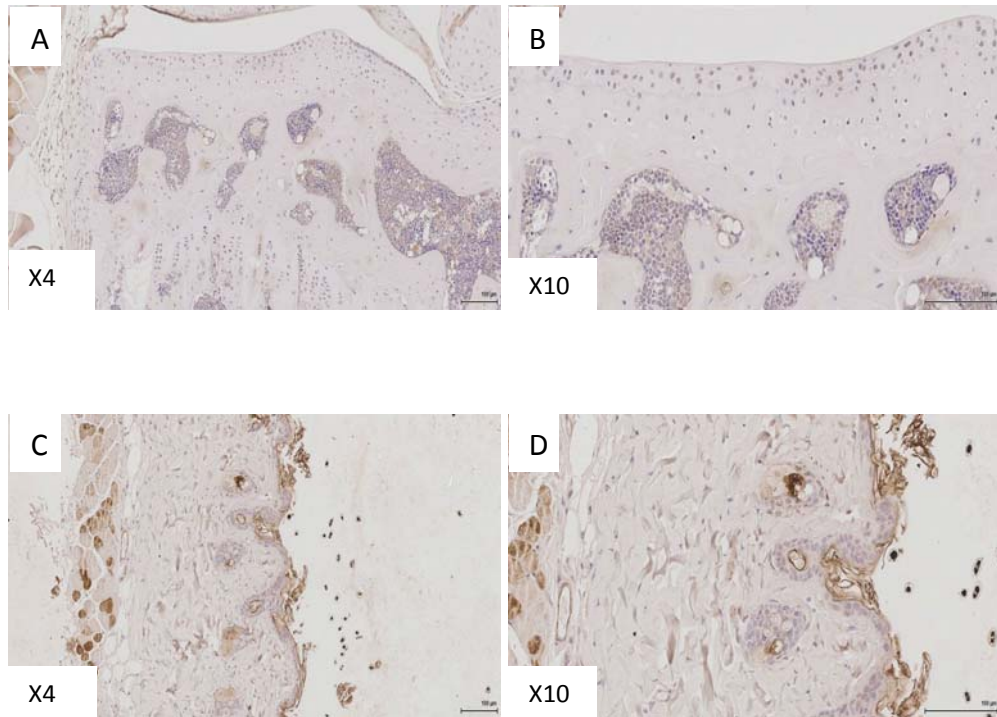


Figure 4.6: Immunohistochemistry ST14 in wild type naïve mice. Wild type mice remained naïve and were sacrificed at 18 weeks old and the tibia and femur dissected. Similar sample preparation was carried out as described in figure 4.5. Images A and B represent a section cut later on in sectioning the joint, using 2 separate magnifications as detailed on image. Images C and D are a positive control – ST14 stained murine skin (also used in figure 4.5), with the magnification as detailed.

4.2.3 Micro-CT analysis for subchondral sclerosis

Subchondral sclerosis is an increased bone density or thickening and is a hallmark feature of OA, and so should be detected in a murine OA model. I attempted two methods for subchondral sclerosis micro-CT analysis as described in section 2.2.10.2. I firstly tried to separate the subchondral plate region from the underlying trabecular bone as two separate ROIs, however as the bone became more severely sclerotic and extended to the epiphyseal bone this became impossible. (Figure 1.6, section 1.4.2) Therefore after discussion with Dr Carmen Huesa (University of Glasgow) and Prof Rob van't Hof (University of Liverpool) I decided to select one ROI including the subchondral plate and underlying trabecular bone as one region as shown in section 2.2.10.2. Both of these methods detected significant subchondral sclerosis in the murine DMM mouse model relative to sham. (Control) The old method is represented in Appendix C, whilst figure 4.7 shows the new method of analysis for subchondral sclerosis.

The difficulty I experienced separating the two regions (subchondral plate region and underlying trabecular bone) to measure trabecular thickness in the plate region has also been observed in a similar murine DMM model and this group similarly used one ROI including the subchondral plate and underlying trabecular bone as one region and measured bone BV/TV (bone volume/tissue volume, expressed as a percentage) as an indicator of subchondral sclerosis [229]. Therefore, due to this and after discussion with Prof Rob van't Hof and Dr Carmen Huesa I analysed BV/TV, also known as percentage bone volume (PBV), in this ROI as an indicator of sclerosis. BV/TV measures the proportion of the ROI occupied by binarised solid objects within a given region of interest, and would be increased in sclerosis due to a higher density and volume of bone (increased area of opacification), as shown in figure 1.6, section 1.4.2.

BV/TV has also been used in other micro-CT studies when analysing subchondral bone sclerosis in animal OA models [65, 233], and thus supports why I utilised this measurement. In addition, Pastoureau et al. found a positive correlation between subchondral plate thickness and BV/TV, indicating BV/TV is a good measure of sclerosis [234]. In this altered method I analysed PBV in both the medial and lateral epicondyles and calculated a ratio of PBV medial:lateral, giving more of a relative indication of sclerosis in the medial epicondyle compared to the lateral epicondyle. Shown in figure 4.7 was significantly increased subchondral sclerosis at every time point in the DMM model

relative to sham, consistent with the observations I detected using the old method in Appendix C. This observation of increased BV/TV (subchondral sclerosis) has also been observed in various animal models of OA [65, 66, 78, 80, 81, 229, 235-237], which is discussed further in section 4.3.

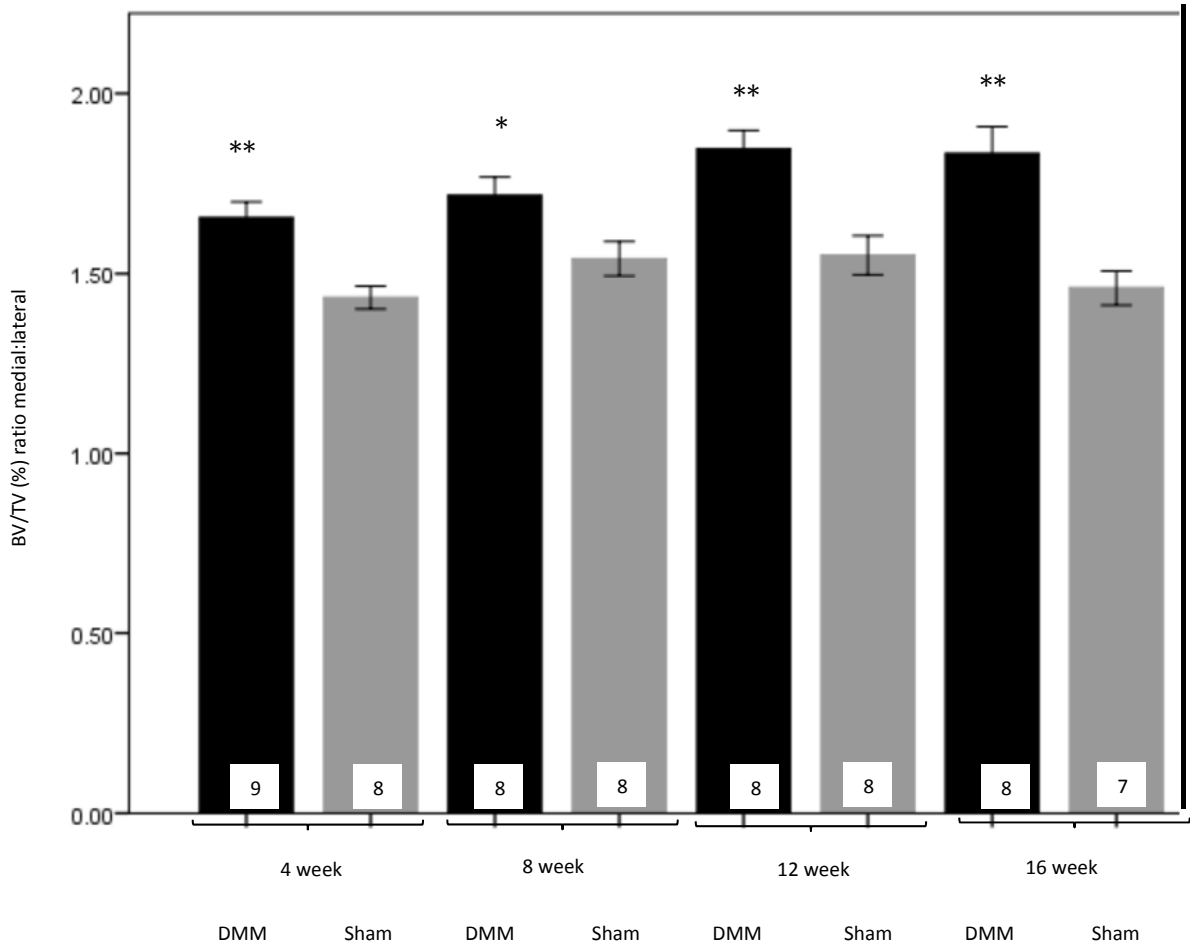


Figure 4.7: Measurement of subchondral sclerosis in the wild type murine OA model. Wild type mice underwent DMM or sham surgery at 10 weeks of age. These mice were then sacrificed at 4, 8, 12 or 16 weeks post-surgery. The affected limb was then dissected and fixed in 10% buffered paraformaldehyde for up to 72 hours and then transferred into 70% ethanol. The limb was then scanned using a micro-CT SkyScanner and the images reconstructed as described in section 2.2.10. Analysis then took place using CTan software as described in section 2.2.10 to measure subchondral sclerosis (BV/TV). The number in the white box represents the number of mice in each group. * compared to sham at 4, 8, 12 and 16 weeks post-surgery. * $p < 0.05$ ** $p < 0.01$. Error bars +/- SEM. An independent samples T-test was performed.

Due to the method of analysis involving separation of the trabecular plate from the underlying subchondral bone as two ROIs becoming impossible when the whole subchondral region (plate and trabecular bone) becomes sclerotic, for all future analysis (including the gene ablation mice) I utilised the altered method analysing one ROI (including the subchondral plate and trabecular region as one ROI).

4.2.4 Micro-CT analysis for alterations in trabeculae within the subchondral bone

The general trend in figure 4.8A was increased trabeculae thickness (in the subchondral trabecular region) in the DMM model relative to sham, which reached significance at 4, 12 and 16 weeks. The same pattern of increased trabecular thickness in the DMM model relative to sham was also seen at 8 weeks however was not significant. My observation of increased trabecular thickness in the murine OA model is a common feature seen in animal OA models and in human OA [65, 66, 78, 80, 81, 229, 235-237], discussed further in section 4.3.

The observation of thicker trabeculae in the tibial subchondral bone with union of trabeculae in the DMM model would result in less separation between the trabeculae in a given ROI. This is shown in figure 4.8B where there was less trabecular separation in the DMM model relative to sham, reaching significance at 4, 8 and 16 weeks. The outlier to these results was at 12 weeks where there was no observed difference in trabecular separation between DMM and sham. This pattern of reduced trabeculae separation in OA has also been observed in human studies [78, 236, 237], and a spontaneous OA guinea pig model [81].

Represented in figure 4.8C were a reduced number of trabeculae in the murine DMM model relative to sham. This pattern was observed at every time point and reached significance at 4 weeks. This observation would fit in with the findings in figures 4.8A and 4.8B where there were thicker trabeculae with reduced separation in the DMM model relative to sham, and so there would be a reduced number of trabeculae due to union of thickened trabecular bones, which I have detected. The observation of reduced number of trabeculae in an OA model has also been found in a human study of OA femoral subchondral bone [236], and in several OA animal studies [65, 80], and so is a common feature of OA. These observations of subchondral sclerosis and altered trabecular morphology in the murine DMM model relative to sham provide crucial baseline data on OA subchondral remodelling events, which I can compare the tissue-specific gene ablation murine OA models to. Several studies have analysed structural model index (SMI) in an animal OA model [81], and a human study [236], both finding a reduced SMI in the OA group relative to control, suggesting the subchondral bone is more plate like in

OA. However my analysis of SMI showed no pattern between DMM and sham throughout the time course, so no data have been plotted for this.

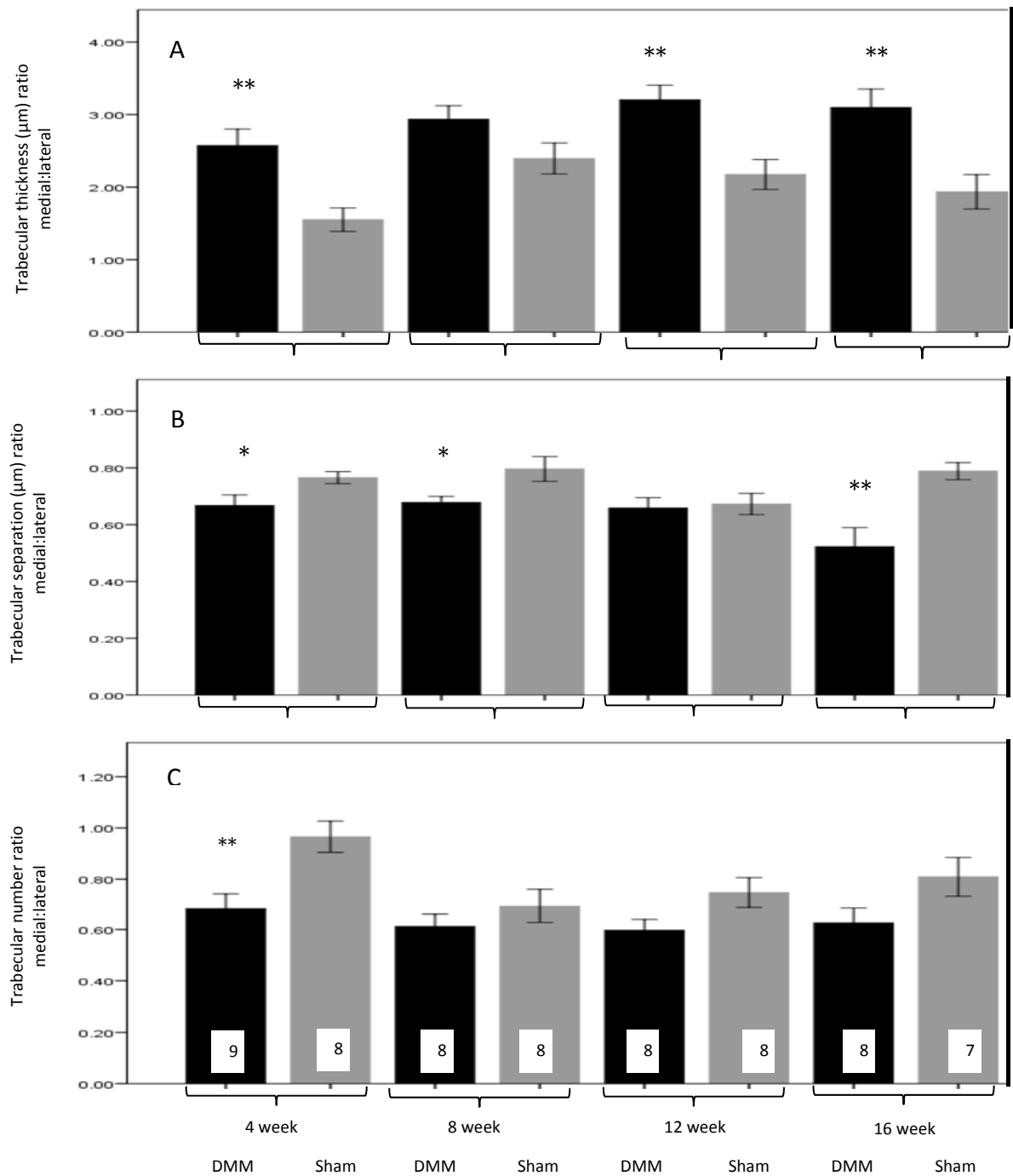


Figure 4.8: Measurement of trabecular morphology in the wild type murine OA model. Images from murine joints as detailed in figure 4.7 were assessed for trabecular thickness (A), trabecular separation (B) and trabecular number (C). The number in the white box represents the number of mice in each group. * compared to sham at 4, 8, 12 and 16 weeks post-surgery. * $p < 0.05$ ** $P < 0.01$. Error bars \pm SEM. An independent samples T-test was performed.

4.2.5 Micro-CT and histology images for osteophytes in the murine DMM model versus sham

Another significant observation in the murine DMM model was osteophyte formation on the medial aspect of the tibia as early as four weeks post-surgery, which were absent in the sham model. The osteophytes I detected in the murine DMM model throughout the time course have been represented on micro-CT and histology in figures 4.9-4.12. The osteophytes I observed were marginal osteophytes located on the medial contour of the tibia following the existing contour providing a broadening of the articular surface, rather than osteophytes located at the ligament insertion sites, which would be more bulb-like. This observation is similar to osteophyte analysis carried out in a murine collagenase-induced OA model [238]. I did not detect any osteophytes on the lateral aspect of the tibia or on the femur.

Osteophyte formation is a common feature of OA and similar to my work various animal models have observed similar results [65, 66, 231, 233, 239], discussed further in section 4.3. Represented in figures 4.9-4.12 were osteophytes on the medial contour of the tibia following DMM surgery both using micro-CT (images A and B) and histological (images C and D) techniques. Image A (figures 4.9-4.12) is a representation of micro-CT showing an osteophyte on the medial contour of a murine tibia (outlined in red dashed lines) following DMM surgery, and image B represents a cross-sectional image of the osteophyte; (red dashed lines) image C is histological representation (H&E) of the osteophyte where there was an area of increased cell proliferation (outlined in black); image D (Safranin-O) represents an osteophyte with cartilaginous features. (Red staining, outlined in black) The sham joint (control) for each time point (figures 4.9-4.12) showed the absence of osteophyte formation in a control limb, both on micro-CT and histological analysis.

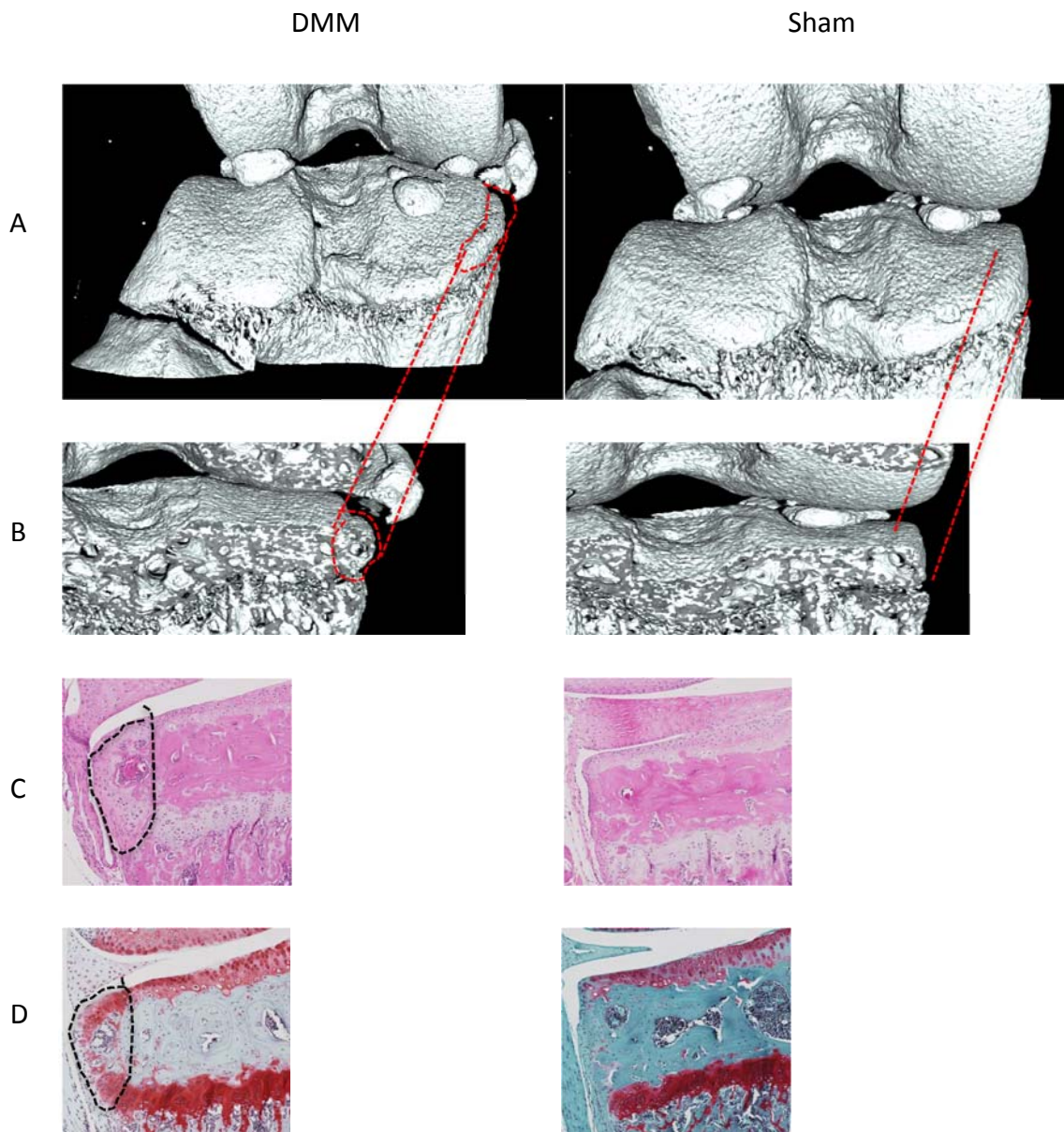


Figure 4.9: Micro-CT and histology representation of osteophytes in the murine DMM model.

Wild type mice underwent DMM or sham surgery at 10 weeks of age. These mice were then sacrificed at 4 weeks post-surgery. The affected limb was then dissected and fixed in 10% buffered paraformaldehyde for up to 72 hours and then transferred into 70% ethanol. The limb was then scanned using a micro-CT SkyScanner and the images reconstructed as described in section 2.2.10. 3D visualisation of the osteophytes then took place, using CTVox software as described in section 2.2.10.3. (Images A and B) Image B is a cross-sectional representation of image A, with the red slashed lines highlighting an osteophyte in the DMM model and smooth contour of the medial aspect of the tibia in the sham model. For images C and D after the bones had been scanned histological analysis then took place as described in sections 2.2.3 and 2.2.8 and visualisation of H&E (C) and Safranin-O (D) stained joints were carried out using a microscope. The black slashed lines in images C and D in the DMM model highlight an osteophyte on the medial aspect of the tibia.

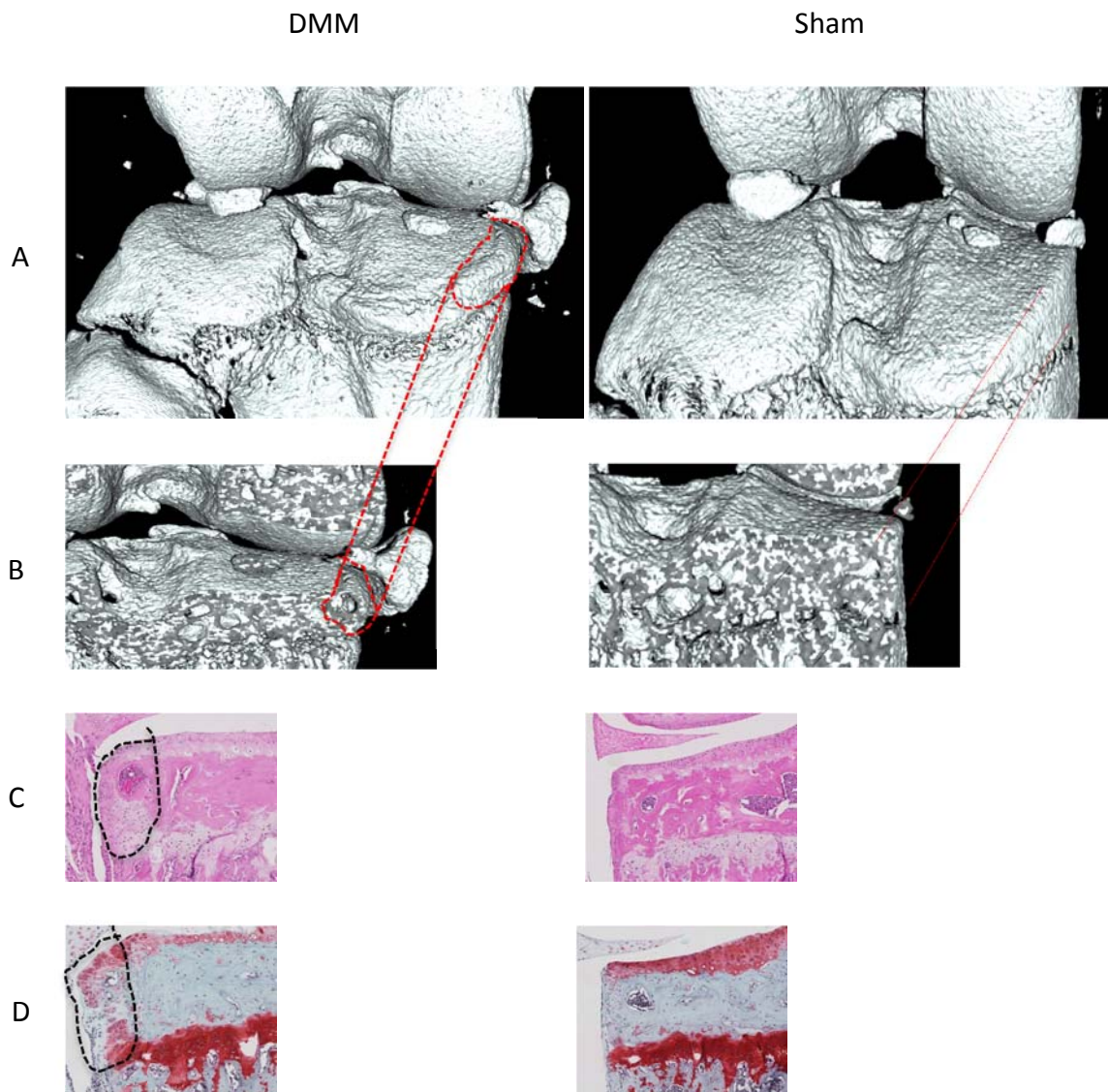


Figure 4.10: Micro-CT and histology representation of osteophytes in the murine DMM model.

Wild type mice underwent DMM or sham surgery at 10 weeks of age. These mice were then sacrificed at 8 weeks post-surgery. The affected limb was then dissected and fixed in 10% buffered paraformaldehyde for up to 72 hours and then transferred into 70% ethanol. The limb was then scanned using a micro-CT SkyScanner and the images reconstructed as described in section 2.2.10. 3D visualisation of the osteophytes then took place, using CTVox software as described in section 2.2.10.3. (Images A and B) Image B is a cross-sectional representation of image A, with the red slashed lines highlighting an osteophyte in the DMM model and smooth contour of the medial aspect of the tibia in the sham model. For images C and D after the bones had been scanned histological analysis then took place as described in sections 2.2.3 and 2.2.8 and visualisation of H&E (C) and Safranin-O (D) stained joints were carried out using a microscope. The black slashed lines in images C and D in the DMM model highlight an osteophyte on the medial aspect of the tibia.

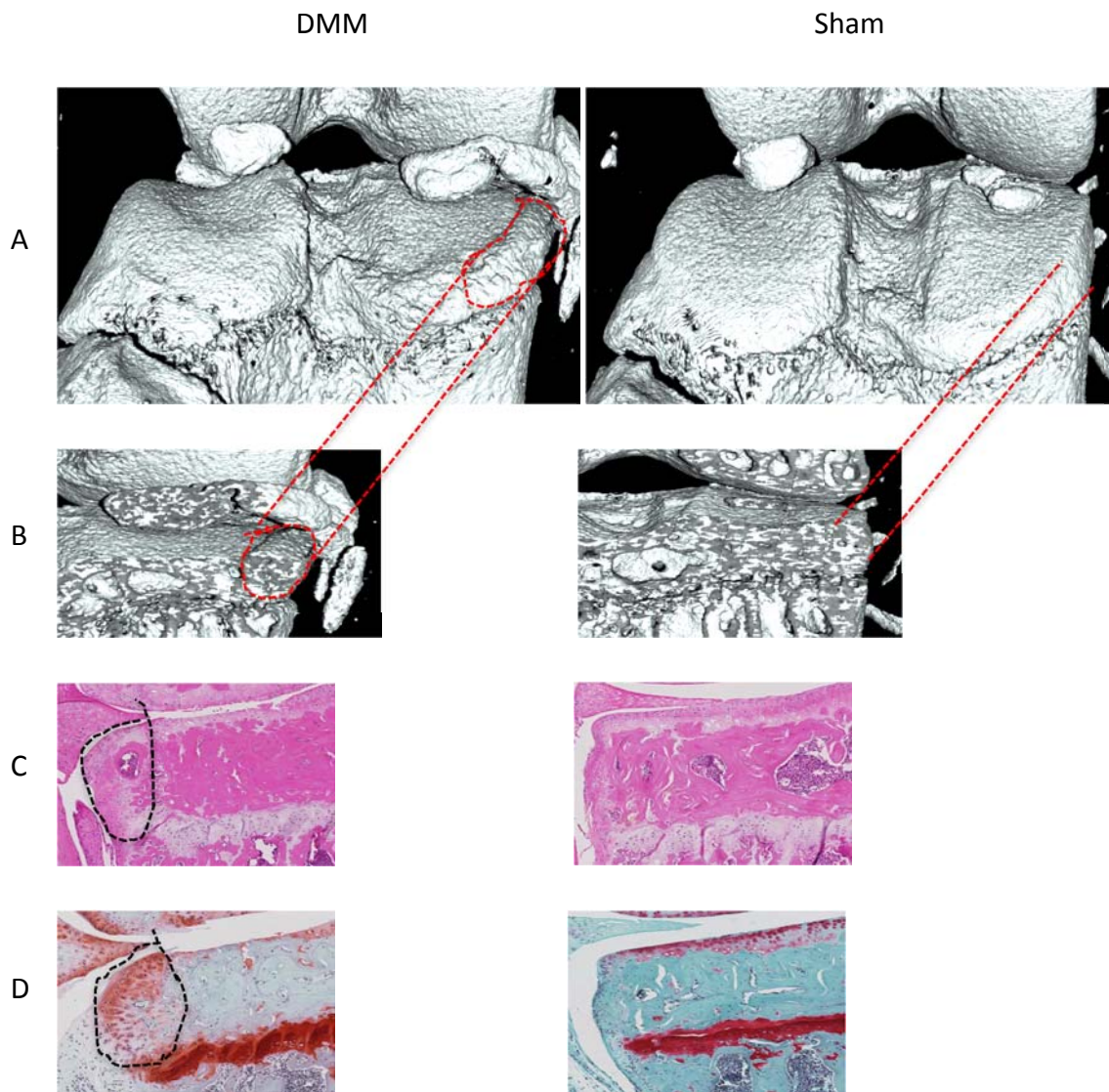


Figure 4.11: Micro-CT and histology representation of osteophytes in the murine DMM model. Wild type mice underwent DMM or sham surgery at 10 weeks of age. These mice were then sacrificed at 12 weeks post-surgery. The affected limb was then dissected and fixed in 10% buffered paraformaldehyde for up to 72 hours and then transferred into 70% ethanol. The limb was then scanned using a micro-CT SkyScanner and the images reconstructed as described in section 2.2.10. 3D visualisation of the osteophytes then took place, using CTVox software as described in section 2.2.10.3. (Images A and B) Image B is a cross-sectional representation of image A, with the red slashed lines highlighting an osteophyte in the DMM model and smooth contour of the medial aspect of the tibia in the sham model. For images C and D after the bones had been scanned histological analysis then took place as described in sections 2.2.3 and 2.2.8 and visualisation of H&E (C) and Safranin-O (D) stained joints were carried out using a microscope. The black slashed lines in images C and D in the DMM model highlight an osteophyte on the medial aspect of the tibia.

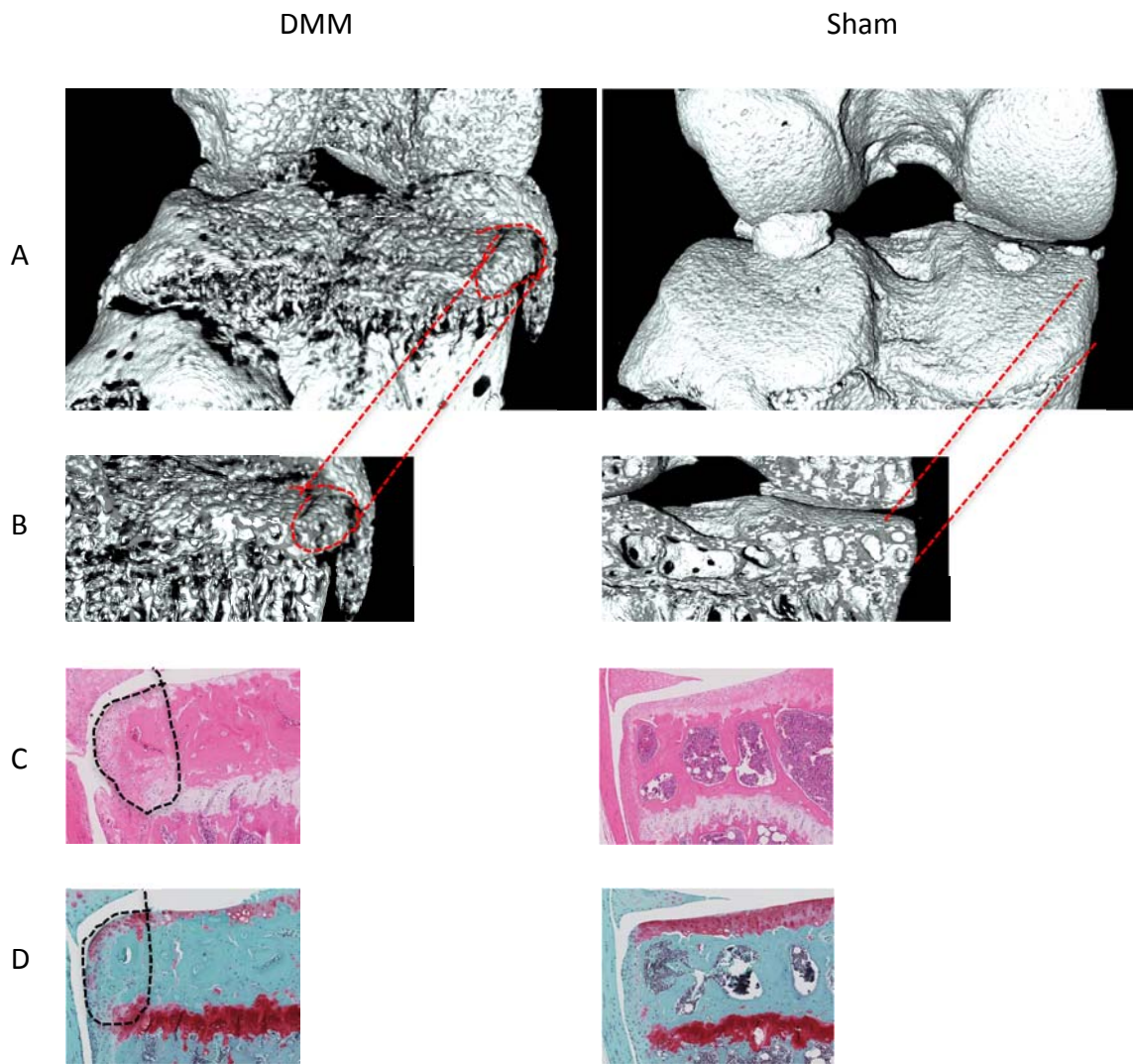


Figure 4.12: Micro-CT and histology representation of osteophytes in the murine DMM model. Wild type mice underwent DMM or sham surgery at 10 weeks of age. These mice were then sacrificed at 16 weeks post-surgery. The affected limb was then dissected and fixed in 10% buffered paraformaldehyde for up to 72 hours and then transferred into 70% ethanol. The limb was then scanned using a micro-CT SkyScanner and the images reconstructed as described in section 2.2.10. 3D visualisation of the osteophytes then took place, using CTvox software as described in section 2.2.10.3. (Images A and B) Image B is a cross-sectional representation of image A, with the red slashed lines highlighting an osteophyte in the DMM model and smooth contour of the medial aspect of the tibia in the sham model. For images C and D after the bones had been scanned histological analysis then took place as described in sections 2.2.3 and 2.2.8 and visualisation of H&E (C) and Safranin-O (D) stained joints were carried out using a microscope. There is significant erosion and pitting of the subchondral bone making osteophyte visualisation difficult. The black slashed lines in images C and D in the DMM model highlight an osteophyte on the medial aspect of the tibia.

4.2.6 Micro-CT analysis of osteophyte morphology

Having established that osteophytes were present in the murine DMM model from 4 weeks through to 16 weeks post-surgery I further went on to analyse osteophyte size (tissue volume), osteophyte bone volume (bone volume) and number of osteophytes in each mouse. The analyses for osteophyte size and bone volume were carried out on the largest osteophyte in each mouse. Shown in figures 4.13A and 4.13B it was apparent that the osteophytes increased in size (tissue volume) from 4 to 16 weeks post-surgery, and correspondingly contained an increased amount of bone (bone volume) from 4 to 16 weeks post-surgery. There are also a fewer number of osteophytes counted at 12 and 16 weeks post-surgery compared to 4 and 8 weeks post-surgery, shown in figure 4.13C. This was due to osteophytes coalescing and forming large osteophytes as the time course progressed post-surgery. Several other animal studies have also observed increasing size of osteophytes in a surgical OA model as the time course progressed [233, 240], discussed further in section 4.3. No osteophytes were detected in the sham joints at any time point. A one-way ANOVA test was performed on graphs A, B and C in figure 4.13, with significant differences between groups identified ($F(7,56) = 27.338, p < 0.001$). The post hoc Tukey test revealed where these differences were found, with the level of significance shown on the graphs.

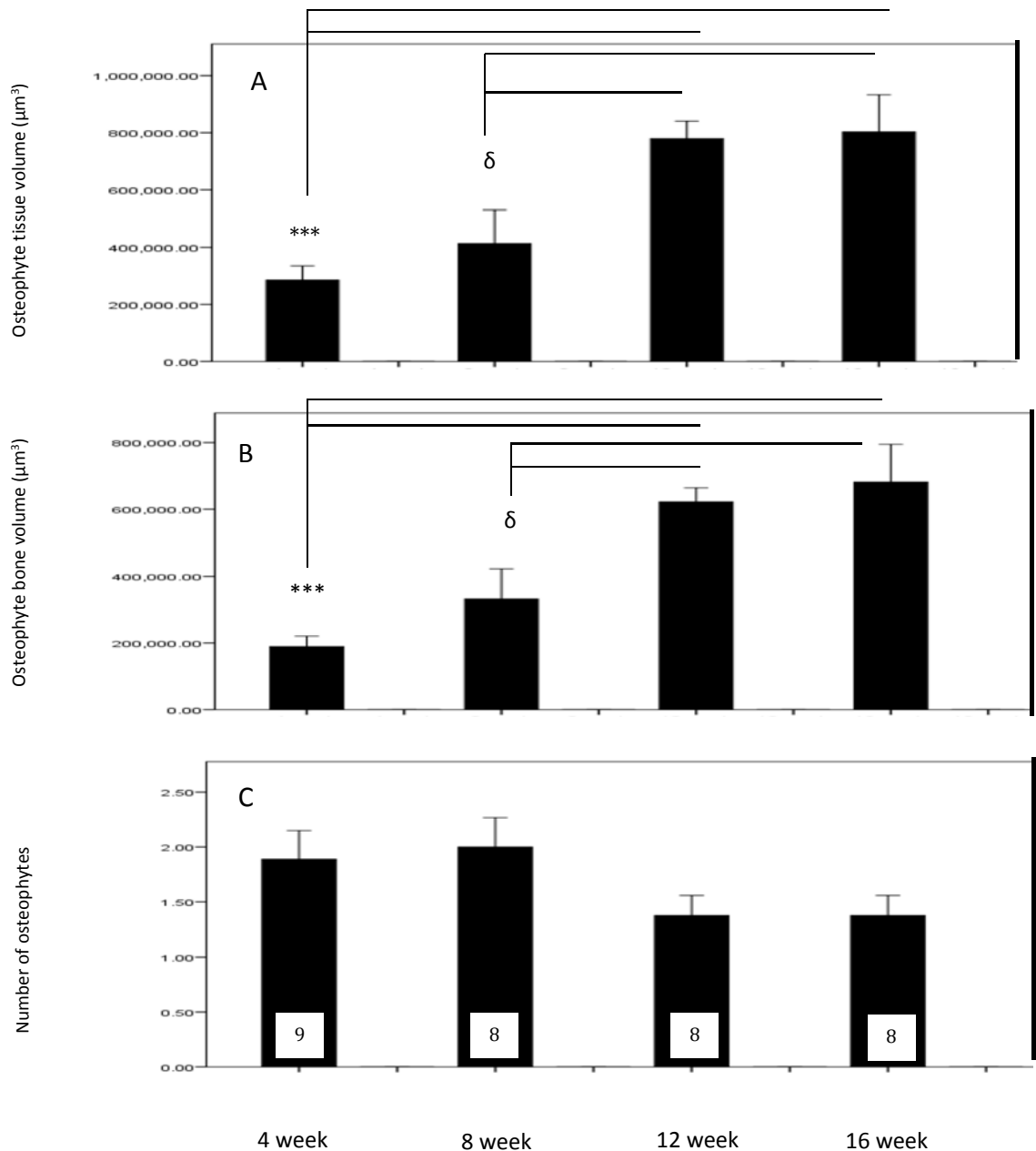


Figure 4.13: Micro-CT analysis of osteophyte morphology. Wild type mice underwent DMM surgery at 10 weeks of age. These mice were then sacrificed at 4, 8, 12 or 16 weeks post-surgery. The affected limb was then dissected and fixed in 10% buffered paraformaldehyde for up to 72 hours and then transferred into 70% ethanol. The limb was then scanned using a micro-CT SkyScanner and the images reconstructed as described in section 2.2.10. The largest osteophyte in each mouse was then analysed for tissue volume (osteophyte size, bar chart A) and bone volume (amount of bone in osteophyte, bar chart B) and osteophytes were also counted using CTvox and CTan software (bar chart C) as described in section 2.2.10.3. The number in the white box represents the number of mice in each group. * compared to 12 week DMM and 16 week DMM mice. δ compared to 12 week DMM and 16 week DMM mice. δ $p < 0.05$ *** $p < 0.001$. Error bars +/- SEM. A one-way ANOVA test with post hoc Tukey test were performed.

4.2.7 Cartilage damage assessed qualitatively and quantitatively

4.2.7.1 Qualitative assessment of cartilage damage

Qualitative assessment of cartilage damage in figures 4.14 and 4.15 showed increased cartilage damage in the DMM model relative to sham at every time point examined. There was also a stepwise increase in cartilage damage observed in the DMM model from 4 to 16 weeks, with very little cartilage remaining in the joint in the DMM model at 16 weeks compared to that at 4 weeks. Represented in figure 4.14 there was proteoglycan loss and fibrillation occurring at 4 weeks post-DMM surgery. At 8 weeks post-DMM the proteoglycan loss and fibrillations were more enhanced with a loss of viable chondrocytes and clustering, leaving exposed subchondral bone. There was very little proteoglycan remaining at 12 weeks in the DMM model leaving exposed subchondral bone and deep fissure formation. (Figure 4.15) The proteoglycan was completely degraded at 16 weeks post-DMM with no viable chondrocytes, leaving exposed subchondral bone and delamination had occurred. (Figure 4.15) Similar to my qualitative findings of cartilage damage as the time course progressed in a DMM model, several other animal studies have found corresponding results [65, 231, 233, 234], discussed further in section 4.3.

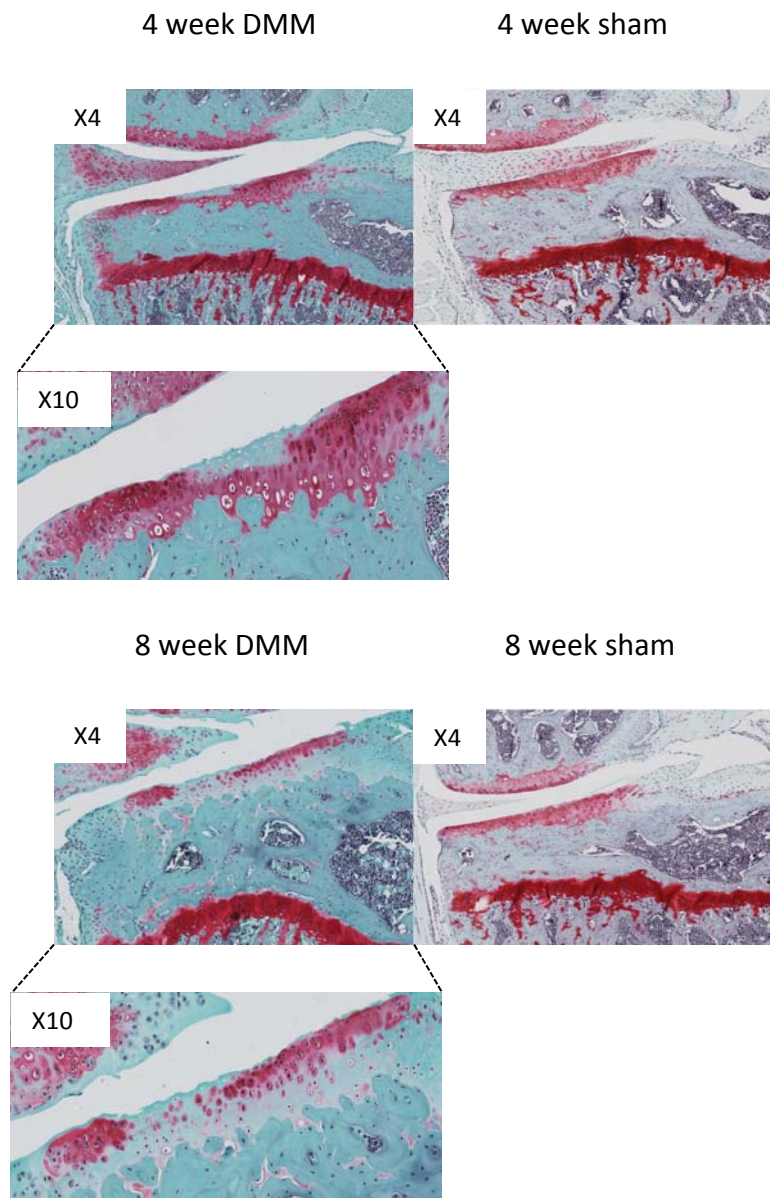


Figure 4.14: Histology representation of cartilage damage on the medial aspect of the tibia. Wild type mice underwent DMM or sham surgery at 10 weeks of age. These mice were then sacrificed at 4 or 8 weeks post-surgery. The affected limb was then dissected and fixed in 10% buffered paraformaldehyde for up to 72 hours and then transferred into 70% ethanol. Histological analyses then took place as described in sections 2.2.3 and 2.2.8. The above images are Safranin-O stained mice tibiae. The red staining is proteoglycan content. The black slashed lines represent a higher magnification image, as detailed. The white box represents the power of magnification.

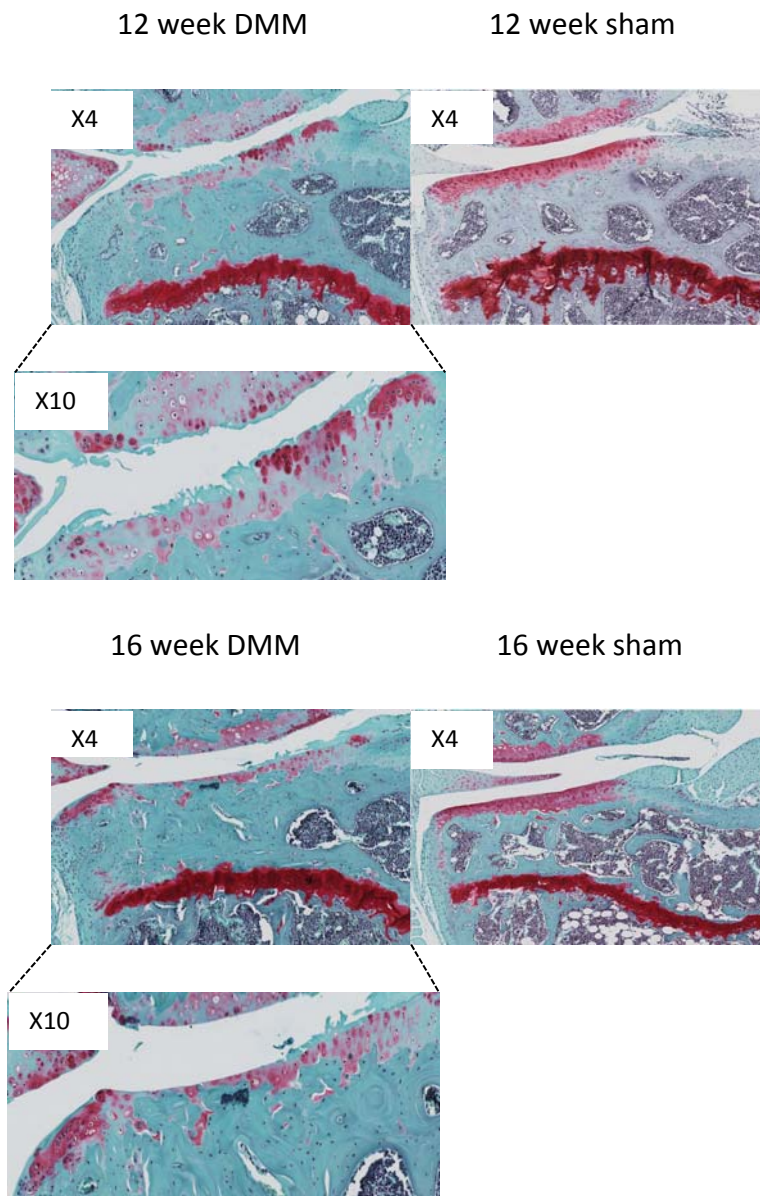


Figure 4.15: Histology representation of cartilage damage on the medial aspect of the tibia. Wild type mice underwent DMM or sham surgery at 10 weeks of age. These mice were then sacrificed at 12 or 16 weeks post-surgery. The affected limb was then processed and analysed as described in figure 4.14. The black slashed lines represent a higher magnification image, as detailed. The white box represents the power of magnification.

4.2.7.2 Quantitative OARSI cartilage damage score

Cartilage damage was assessed using the OARSI histological scoring system for the mouse [1]. I used the OARSI scoring system rather than others (such as the Mankin scoring system) as it is a universal and resilient system for histologic scoring of murine OA allowing comparison of the severity of cartilage degradation across different spontaneous, enzymatic, chemical or surgically-induced murine OA models [1]. The medial tibial plateau (MTP) was assessed, as this is where most cartilage damage occurs in the DMM model [192, 241]. The cartilage damage has been represented as both best overall maximum score (figure 4.16A) and best combined summed score. (Figure 4.16B) (Explained in section 2.2.16) Both these representations showed a stepwise increase in cartilage damage from 4 to 16 weeks in the DMM model. At every time point assessed the cartilage damage was significantly worse in the DMM model relative to sham. This quantitative assessment of cartilage damage (figures 4.16A and 4.16B) links in with the qualitative observations in figures 4.14 and 4.15. Several other animal models of OA have also found worsening cartilage damage as the time course progressed compared to sham, using the OARSI and modified Mankin scoring systems [229, 233], and various other animal studies of OA have found significantly worse cartilage damage in an OA model relative to control [65, 66, 80, 192, 231, 235, 239, 242], discussed further in section 4.3. A one-way ANOVA test was performed, revealing significant differences between groups ($F(7,24) = 71.952, p < 0.001$), with the post hoc Tukey test showing where these differences were found, as detailed on graph B, figure 4.16.

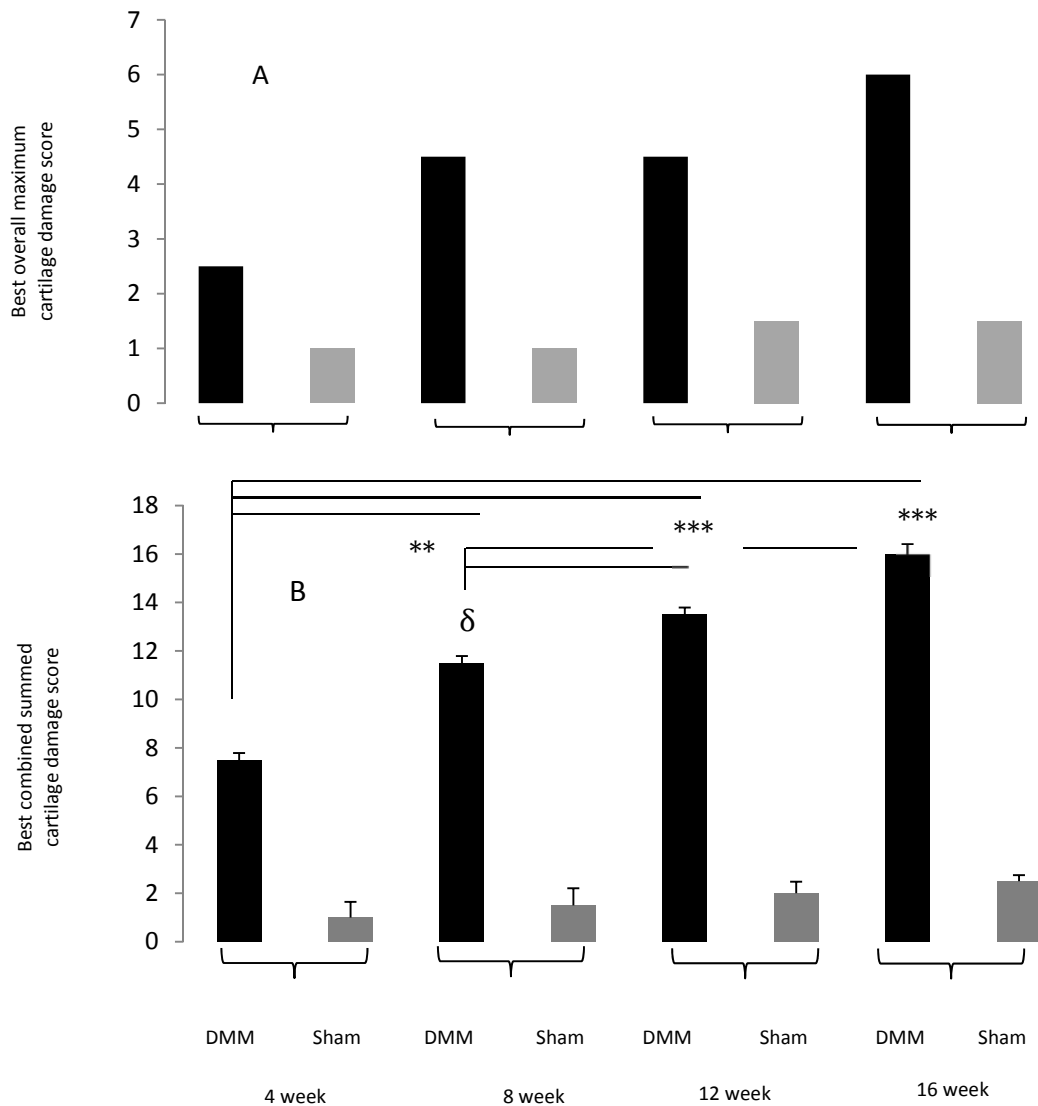


Figure 4.16: Quantitative assessment of cartilage damage. Wild type mice underwent DMM or sham surgery at 10 weeks of age. These mice were then sacrificed at 4, 8, 12 or 16 weeks post-surgery. The affected limb was then dissected and fixed in 10% buffered paraformaldehyde for up to 72 hours and then transferred into 70% ethanol. Histological analyses then took place as described in sections 2.2.3 and 2.2.8. The Safranin-O stained sections were then used to assess cartilage damage using the OARSI histological scoring system for the mouse, as described by Glasson et al. [1] and described in section 2.2.16. There were 4 mice in each group and 6 sections analysed per mouse (24 sections total per group) giving a global representation of cartilage damage in each group. The scoring was carried out blinded by Prof Drew Rowan and Prof David Young. The best overall maximum score of cartilage damage at the medial tibial plateau (MTP) per group is shown in bar chart A. Bar chart B represents the best combined summed score of cartilage damage at the MTP per group. * compared to 8 week DMM, 12 week DMM and 16 week DMM. δ compared to 12 week DMM and 16 week DMM. ** p<0.01 *** p<0.001. Error bars +/- SD. A one-way ANOVA test with post hoc Tukey test were performed.

4.2.8 Correlation analysis

4.2.8.1 Correlation between cartilage damage score and subchondral bone remodelling or osteophyte morphology

Referring to figures 4.17A and 4.17B there was a clear positive correlation between cartilage damage and subchondral sclerosis and trabecular thickness, respectively. This suggests a relationship between cartilage damage and subchondral bone remodelling. Similarly, shown in figures 4.17C and 4.17D there was also a positive correlation between cartilage damage and osteophyte tissue volume (size) and bone volume, respectively. It appears that the more severe the cartilage damage, the larger the osteophytes become with a higher volume of bone contained in them.

4.2.8.2 Correlation between subchondral bone remodelling and osteophyte morphology

There was a clear positive correlation between subchondral sclerosis and trabecular thickness, shown in figure 4.18A. This would be expected as the thicker the trabeculae become the more sclerotic the bone becomes. Interestingly as the subchondral sclerosis becomes more severe there was also a clear positive correlation with osteophyte tissue volume (size) and osteophyte bone volume, figures 4.18B and 4.18C, respectively. A similar positive correlation was also found between trabecular thickness and osteophyte tissue volume and bone volume. (Figures 4.18D and 4.18E) These data suggest that there was a positive correlation between subchondral bone remodelling and osteophyte size and bone volume.

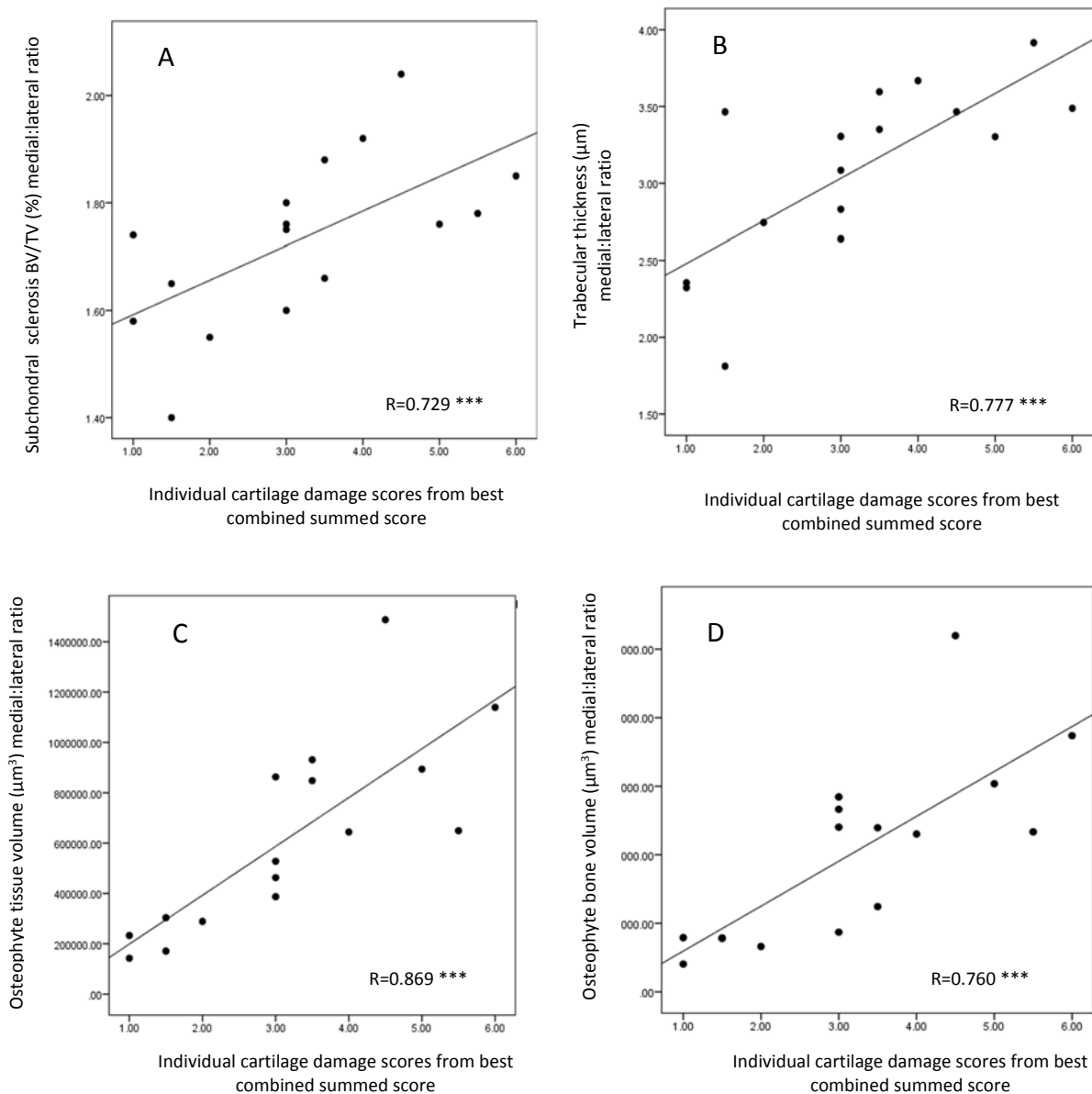


Figure 4.17: Correlation analysis. Wild type mice underwent DMM or sham surgery at 10 weeks of age. These mice were then sacrificed at 4, 8, 12 or 16 weeks post-surgery. The affected limb was then dissected and fixed in 10% buffered paraformaldehyde for up to 72 hours and then transferred into 70% ethanol. The limb was then scanned using a micro-CT SkyScanner and the images reconstructed as described in section 2.2.10. Analysis then took place using CTan software as described in section 2.2.10. Following micro-CT limbs were processed, embedded and stained allowing cartilage damage to be assessed using the OARSI scoring system. Four mice in each group (4 week DMM, 8 week DMM, 12 week DMM and 16 week DMM) were analysed for correlation. The 4 individual cartilage damage scores for each group from the best combined summed score were used in the analysis. Correlation analysis took place using SPSS software. The Spearman's correlation coefficient (r) was used to measure the strength of linear association between two variables with +1 representing a complete positive linear association. * represents the level of significance that the two variables are linearly related. *** $p < 0.001$.

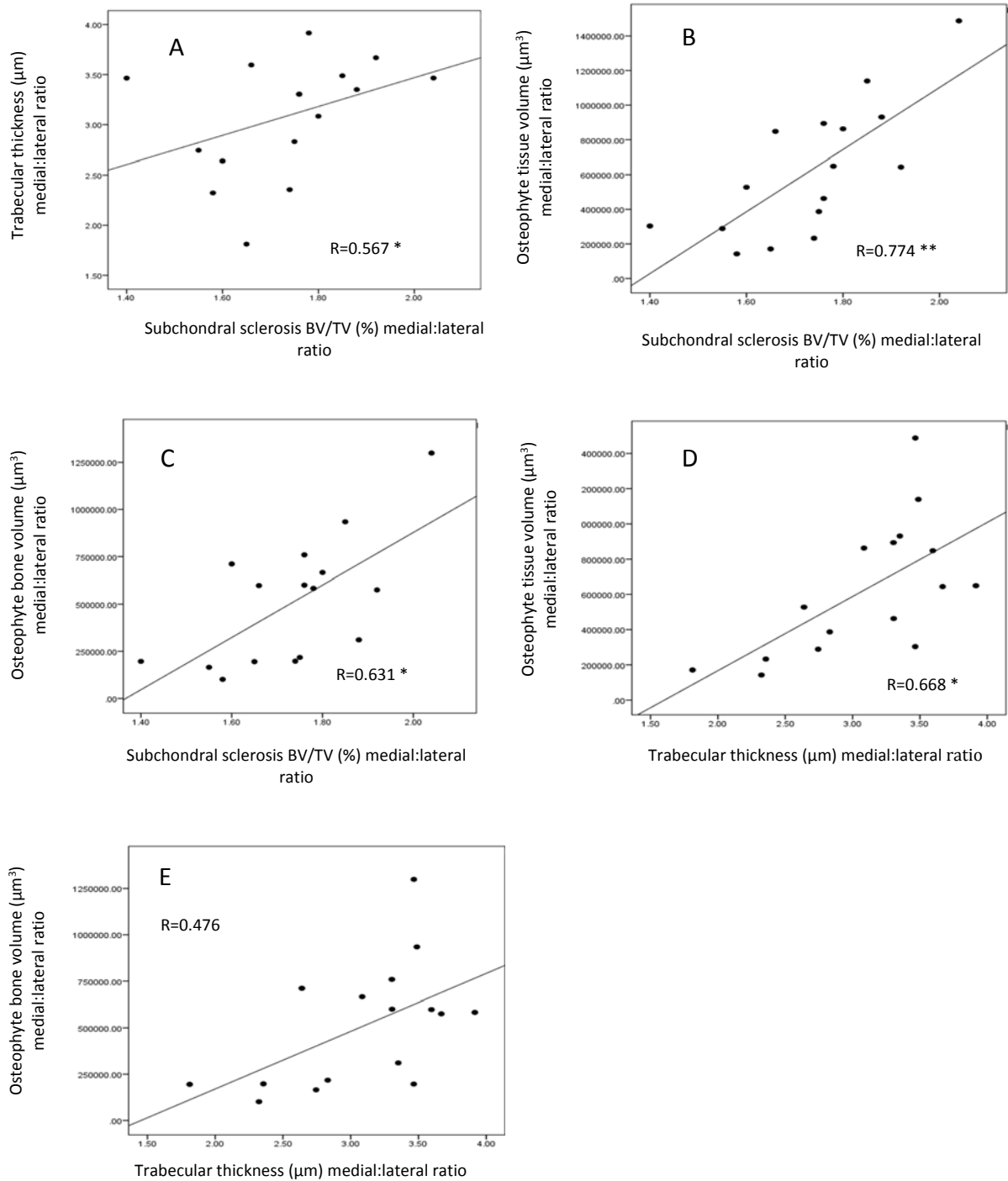


Figure 4.18: Correlation analysis. Sample preparation was carried out as described in figure 4.17. Four mice in each group (4 week DMM, 8 week DMM, 12 week DMM and 16 week DMM) were analysed for correlation. The 4 individual cartilage damage scores for each group from the best combined summed score were used in the analysis. SPSS software was used. The Spearman's correlation coefficient (r) was used to measure the strength of linear association between two variables with +1 representing a complete positive linear association. * represents the level of significance that the two variables are linearly related. * $p < 0.05$ ** $p < 0.01$.

4.3 Discussion

General observations from these results in the murine DMM model show subchondral sclerosis, trabecular thickening, (with reduced trabecular separation and number) osteophyte formation (which increase in size as the time course progressed) and significant cartilage damage compared to sham. These findings are consistent with OA pathology and have also been found in other animal models and provide baseline data on 'normal' OA pathology in a surgically induced OA murine model. However, as mentioned in section 4.1 there are also significant variations in these parameters observed when using different animal models and different modes of induction in OA. My observations and similarities and deviances between different studies will now be discussed.

4.3.1 Mouse weights and tibial measurements

These analyses were performed in order to provide some data on mouse development, which I can compare the mice with gene ablation to in order to detect any developmental deviances. The mouse weights were represented in section 4.2.1.1, and I will use these data to compare to the gene ablated mice in chapters 5 and 6.

It may be expected in the DMM model that there would be altered weight bearing, which may affect the growth and development of the tibial subchondral bone, relative to sham. Indeed, shown in section 4.2.1.2, the width of the shaft of the tibia and the width of the tibial subchondral region was greater in the DMM model relative to sham. Also, there were subtle deviances in the heights of the medial and lateral epicondyles between DMM and sham models, particularly at earlier time points.

4.3.2 Up-regulation of PAR-2 in a DMM model relative to sham, but lack of ST14 staining

Similar to work by Ferrell et al., I observed up-regulation of PAR-2 in cartilage in the DMM model relative to sham. This was represented by more chondrocytes staining positive for PAR-2 in the cartilage in the DMM model relative to sham, at 8 weeks post-surgery [137]. There was very little PAR-2 staining in the osteoblasts contained in the subchondral bone, even in the DMM model. This implicates PAR-2 in OA pathology.

In contrast, using a specific antibody (ST14 rabbit polyclonal; Sigma), there was no expression of matriptase in the cartilage or subchondral bone, even in the DMM model. This was apparent using three separate mice in each group. An explanation for this may be due to lack of sensitivity of the antibody, as Milner et al. detected expression of matriptase in a murine DMM model compared to no matriptase expression in sham operated mice using a different antibody. (Anti-matriptase, catalogue number IM1014) Additionally, this group found increased gene expression of matriptase in OA samples relative to control using qPCR [122]. This work by Milner et al. suggests that matriptase is indeed up-regulated and involved in OA pathology. It can also be postulated that the IHC performed in this study was carried out at a time point which was too late to detect matriptase activity. It may be that matriptase has its actions earlier on in the time course (days, rather than weeks) and so IHC should have been performed on samples earlier on in the time course of OA.

4.3.3 Subchondral sclerosis in a murine DMM model

As discussed in section 4.2.3 I observed an increased subchondral plate thickness (μm) (shown in Appendix C) and increased BV/TV (%) in the subchondral region (indicating subchondral sclerosis) in the murine DMM model relative to sham, which increased as the time course progressed. An increased subchondral plate thickness has been detected in other similar OA animal models with different modes of induction [65, 80, 81, 234, 235, 239]. This effect has been seen in a rat monosodium iodoacetate (MIA) model of OA with significant subchondral plate thickening at two and six weeks-post OA induction [65], and also in a study by Lahm et al. who found significant subchondral plate thickening in a post-traumatic Beagle dog model of OA relative to control [80]. Similarly Wang et al. detected significant subchondral plate thickening in a Dunkin-Hartley guinea pig spontaneous OA model compared to control [81], and Kuroki et al. found a significantly thicker subchondral plate in a canine medial meniscal release model relative to sham [235]. Botter et al. also detected significant subchondral plate thickening in a DMM mouse model (129vEv-Brd) relative to control [239]. An increased subchondral plate thickness in OA has also been confirmed in a meniscectomized guinea pig model at 3 months post-induction relative to sham [234].

Several of these studies also had a corresponding increase in subchondral BV/TV [65, 80, 81, 235]. A murine DMM study by Kim et al. found an increased BV/TV in the medial subchondral bone relative to sham, which increased with time as I have found [229]. An increased BV/TV in the subchondral bone has also been found in a rat model of OA compared to control [65], and in a canine groove model there was also found to be a small increase in BV/TV relative to control [66]. Lahm et al. also found a significant increase in subchondral BV/TV in a post-traumatic Beagle dog OA model relative to control and Wang et al. found a similar significant increase in subchondral BV/TV in a Dunkin-Hartley guinea pig OA model relative to control [80, 81]. Subchondral BV/TV has also been found to be increased in a canine medial meniscal release OA model relative to control [235], and in a human study, where the BV/TV in the subchondral region of the femoral head and acetabulum was significantly higher in advanced OA relative to control [236]. Furthermore, other human studies of hip and knee OA detected significant increases in BV/TV in OA subchondral bone relative to control [78, 237].

In contrast, some studies have found a reduced subchondral plate thickness in animal models of OA. Intema et al. observed a reduced subchondral plate thickness in both a canine ACLT and groove model relative to sham at 20 weeks post-induction and Botter et al. found a reduced subchondral plate thickness in a murine collagenase-induced OA model relative to control at 4 weeks post-induction [67, 231, 242]. Furthermore, Sniekers et al. found a reduced subchondral plate thickness in both a canine ACLT and groove model at 10 and 20 weeks post-induction [66]. The observations of reduced subchondral plate thickness in these studies also corresponded with a reduced BV/TV, which is another indicator of sclerosis that I have utilised [66, 67, 231, 242]. This is confirmed in a study by Boyd et al. who observed a reduced BV/TV in the subchondral bone using a canine ACLT model at 12 weeks post-induction [79].

This suggests that there might be a biphasic phenomenon in osteoarthritis subchondral bone pathology. It has been suggested that there is an early decrease in bone volume and subchondral plate thickness followed by a phase in which the subchondral bone becomes denser and sclerotic. This phenomenon has been observed in a study by Hayami et al. using a rat ACLT and medial meniscus resection model detecting early bone loss in the medial tibial plateau, followed by subchondral sclerosis (measured using BV/TV) as the time course progressed compared to sham [233]. It may be that if I analysed subchondral

sclerosis at an earlier time point (e.g. one week post-induction) I may also observe a similar biphasic response with early bone loss followed by sclerosis. However, a recent similar study using a murine DMM model by Huesa et al. detected no significant changes in BV/TV in the affected limb relative to the contralateral limb as early as day 3 post-surgery, with subchondral sclerosis occurring later on at day 14 post-surgery [232]. These findings suggest that the DMM mode of OA induction does not elicit a biphasic phenomenon, and perhaps is a more aggressive model of OA with features of late stage OA occurring at an early time point, (2 weeks post-induction). This is in contrast to other modes of induction such as those used by Intema et al., Botter et al. Sneikers et al. and Boyd et al. who observed subchondral plate thinning, (even at late time points) eluding that these models are less aggressive in terms of OA subchondral bone remodelling and remain in the early phase of OA [66, 67, 79, 231, 242].

4.3.4 Alterations in trabecular morphology in the murine DMM model

My results show an increased thickness of the trabeculae in the DMM model relative to sham corresponding with reduced trabecular separation and a reduced number of trabeculae. This increased trabecular thickness has also been observed in other OA animal studies [65, 66, 80, 81, 229, 235, 236]. A study by Kim et al. detected increased trabecular thickness with time in both a murine DMM and collagenase-induced model [229]. Increased trabecular thickness has also been observed in a rat OA model (MIA induced) compared to control [65], and in a canine groove model of OA at 10 weeks post-induction relative to sham [66]. Lahm et al. and Wang et al. also found an increased thickness of trabeculae in a canine post-traumatic OA model and Dunkin-Hartley spontaneous OA model relative to sham, respectively [80, 81]. Increased trabecular thickness was also observed in a canine medial meniscus release model relative to sham [235], and Chiba et al. detected a similar effect in human OA subchondral femoral head and acetabulum samples relative to control [236]. Human studies of hip and knee OA also detected increased trabecular thickness in OA subchondral bone relative to control [78, 237]. My observation of increased trabecular thickness in a murine OA model is therefore a common feature seen in animal OA models and in human OA.

I also observed reduced trabecular separation and number, similar to other studies [65, 80, 81, 235, 236]. As mentioned as the trabeculae become thicker they unite together

resulting in reduced separation and number, explaining the results I and others have observed. Interestingly I have found as the trabeculae become thicker (μm) with progression of the time course, there is a positive correlation with subchondral sclerosis. (As assessed BV/TV of the whole subchondral region) This pattern is also apparent in the studies I have highlighted [65, 80, 81, 235, 236]. The results I and others have detected suggest significant anabolic bone remodelling occurring in OA pathology using various animal models and modes of induction. Conversely in the studies where there is subchondral plate thinning, there is reduced bone volume (BV/TV) and trabecular thickness observed [66, 67, 231, 242]. This fits in with the biphasic phenomenon theory where there is early catabolic bone remodelling, followed by anabolic remodelling, apparent in the study by Hayami et al. [233].

4.3.5 Osteophyte morphology in the murine DMM model

Osteophytes were observed in all mice with surgical induction of OA via DMM at every time point, compared to sham joints and the lateral aspect of the tibia where no osteophytes were detected. My observation of osteophyte formation in an animal OA model is similar to work carried out by Hayami et al. using a rat anterior cruciate ligament transection (ACLT) or ACLT combined with resection of the medial menisci. This group found no osteophyte formation in the sham joints of any treatment group but found osteophyte formation as early as two weeks post-surgery in the ACLT and ACLT + medial menisci joints [233]. Also, similar to my observations, Hayami et al. found the osteophytes were mainly located on the contour of the medial tibial plateau. Osteophyte formation in an OA animal model has also been confirmed in a study by Botter et al. using a murine C57BL/6 and C3H/HeJ collagenase model. This group found osteophyte formation in both strains of mice treated with collagenase specifically at the medial side of the tibia where the incidence was 100%. Similar to my observations no osteophytes were detected on the lateral side of the tibia [231]. Another study by Botter et al. using a murine DMM model also detected osteophyte formation on the medial aspect of the tibia [239]. Mohan et al. also observed osteophyte formation in a MIA-induced OA model in all the rats at six and ten weeks post-induction [65]. Similarly Sniekers et al. found osteophytes in both a canine groove and ACLT model located predominantly on the medial site of the tibial plateau. Similar to my observations no osteophytes were seen in any of the control joints [66]. So it is apparent that osteophyte formation is a common feature of OA using animal models,

independent of the animal used or mode of induction, and my results confirm these observations in the murine DMM model.

Similar to the work carried out by Hayami et al. I found that the osteophytes became progressively larger with a higher content of bone as the time course progressed [233]. Hayami et al. detected a significant increase in osteophyte area from 1 week post-surgery to 10 weeks post-surgery in both a rat ACLT and ACLT + resection of medial menisci models, with the ACLT + resection of medial menisci model having the largest osteophytes. [233] Additionally, Hashimoto et al. observed an increasing size of osteophytes in the tibial plateau of a rabbit ACLT model from four to twelve weeks post-induction [240], similar to the pattern I have observed in the murine DMM model. I also found there were fewer osteophytes at 12 and 16 weeks compared to 4 and 8 weeks, which was because the osteophytes began to coalesce producing one large osteophyte instead of several smaller osteophytes.

An interesting observation by van Valburg et al. and van Osch et al. was a correlation between cartilage damage and osteophyte size. Van Osch et al. found the more severe the cartilage damage was on the medial tibial plateau the larger the osteophytes were in a murine collagenase-induced OA model [238]. Similarly, van Valburg found the same relationship between severity of cartilage damage and osteophyte size using a collagenase-induced OA model [243]. Indeed, I have found a similar correlation with increasing size of osteophytes from four to sixteen weeks in the murine DMM model correlating with more severe cartilage damage using the OARSI scoring system from four to sixteen weeks. I have also found a positive correlation between cartilage damage and osteophyte bone volume. Another unique observation I have found is a positive correlation between osteophyte size and subchondral sclerosis/trabecular thickness. A similar positive correlation is also found between osteophyte bone volume and subchondral sclerosis/trabecular thickness. Osteophytes are a common feature of OA, and it will be interesting to observe any difference in osteophyte size and number when ablating genes thought to be involved in OA pathology.

4.3.6 Cartilage damage in the murine DMM model

Qualitative analysis of cartilage damage described in section 4.2.7.1 corresponds with observations in other animal studies of OA using different modes of induction [65, 231,

234]. Similar to my observations, Hayami et al. found articular cartilage fibrillation at 4 weeks-post surgery in an ACLT + resection of medial menisci. This group also found that at more advanced stages (6-10 weeks post-surgery) there were more severe cartilage defects with bone eburnation observed on histology in the ACLT + resection medial menisci model relative to sham, which I have also observed at 8, 12 and 16 weeks post-surgery in the DMM model compared to sham [233]. Botter et al. also observed severe cartilage degeneration resulting in exposed subchondral bone (as seen at 12 weeks and 16 weeks post-surgery in my DMM model) in a murine collagenase induced OA model at 4 weeks post-induction [231]. In a MIA-induced OA rat model by Mohan et al. at 10 weeks post-induction there was proteoglycan loss, loss of viable chondrocytes, vertical fissure formation cartilage fibrillation and delamination in the cartilage in the medial tibial plateau. (MTP) I have similarly observed these changes at 12 and 16 weeks post DMM in the murine model [65]. Furthermore, a study by Pastoureau et al. found increased fibrillation and reduced proteoglycan content in a guinea pig meniscectomized model at one month post-induction, similar to my findings at 4 weeks post-DMM [234].

This qualitative analysis of cartilage damage links in with the OARSI maximum and summed scores showing worsening cartilage degradation as the time course progressed in the DMM model. Glasson et al. evaluated the DMM model in 129/SvEv mice and found more cartilage damage in the DMM model compared to control at 4 and 8 weeks using the OARSI summed score method, which I have also found [192]. In addition, I also found severe cartilage damage at 12 and 16 weeks in the DMM model relative to sham. A similar study by Kim et al. using a murine DMM model also found a gradual increase in the OARSI cartilage score with time linking in with my results [229]. The progressive increase in cartilage damage with time that I have observed in the DMM model has also been found in a rat ACLT and ACLT + resection medial menisci OA models using the modified Mankin scoring system. This group found a significantly higher modified Mankin score in both ACLT rat models as early as two weeks post-surgery in the tibial plateau, which progressively got worse as the time course progressed, compared to sham [233]. Kuroki et al. also found in three different canine OA models significantly more cartilage damage in the MTP compared to sham using the Mankin scoring system [235]. Similarly, another study by Botter et al. observed significant cartilage damage in the MTP in a murine DMM model relative to control at 8 weeks post-induction using a modified

scoring system by Chambers et al. [239, 244]. Mohan et al. also found a significantly higher OARSI score of cartilage damage in the MTP at 10 weeks post MIA induced OA in a rat, compared to control where no cartilage damage was observed [65]. Sniekers et al. also observed a higher Mankin score of cartilage damage in the tibial plateau in a canine groove and ACLT OA model relative to control [66], and Lahm et al. found a higher Mankin score of cartilage damage in a canine trans-articular force induced OA model relative to sham [80]. In addition, Intema et al. found a higher modified Mankin score in both a canine ACLT and groove model, relative to sham [242]. My observations of significant cartilage damage using the OARSI scoring system are therefore similar to other relevant studies, which I have highlighted.

In addition (as mentioned) I and others have observed a correlation between cartilage damage and osteophyte size [238, 245]. Additionally, there is a correlation between worsening cartilage damage and worsening subchondral sclerosis/trabecular thickness as the time course progressed in the DMM model. This pattern has also been observed in a study by Pastoureau et al. using a guinea pig meniscectomized model [234]. This group found a significant negative correlation between cartilage thickness and subchondral plate thickening. So, the thinner the cartilage (indicating degradation) the thicker the subchondral plate is, ie. more sclerotic subchondral bone. I have noticed a similar observation in that the more severe the cartilage damage is, the worse the subchondral sclerosis is. (Positive correlation between cartilage damage and subchondral sclerosis) A similar correlation has been detected in a study by Kuroki et al. who found a positive correlation between subchondral plate thickness and Mankin scores in three different canine models [235]. I have also observed that more severe cartilage degradation positively correlates with thicker trabeculae, in a similar manner to sclerosis.

The increasing sclerotic bone with reduced trabeculae number in the murine DMM model represents bone stiffening effecting load transmission to the overlying cartilage (discussed in section 1.5.1), providing a link between the subchondral bone and cartilage changes that are observed in my study [79]. Therefore, these observations support the implication of subchondral bone remodelling in cartilage degeneration, but the next question is do the cartilage changes observed in OA drive the subchondral bone changes, or do the subchondral bone changes occur first causing cartilage degradation?

A recent study by Huesa et al. began to answer these questions using a murine DMM model. This group detected that subchondral sclerosis occurred at day 14 post-surgery, whereas significant cartilage damage did not occur until day 28 post-surgery. This is in support of the theory that subchondral bone changes precede cartilage damage in this model, and is in support of the work by Radin et al. who had the view that increased stiffness of the subchondral bone leads to overlying cartilage damage [232, 246]. It is likely that if I had started my time course of DMM and sham surgery from day 14, I also would have found similar results to Huesa et al. with early subchondral bone sclerosis preceding cartilage damage. In chapter 6, which analyses cartilage and subchondral bone changes in cartilage-specific and bone-specific PAR-2 ablated mice in a DMM model, my results begin to argue against the long standing view that subchondral bone changes drive cartilage damage as proposed by Radin et al. On the contrary, my results suggest that cartilage damage can indeed occur independently without any abnormal subchondral bone remodelling occurring, which corresponds with work carried out by Huesa et al., and will be discussed further in chapter 6.

4.3.7 Summary

- Baseline mouse weights and tibial bone measurements of wild type mice have been completed allowing any developmental deviances in the knock-out mice to be detected.
- Significant subchondral sclerosis (measured both by TbTh of the subchondral plate and BV/TV of the subchondral region) was observed in a murine DMM model increasing in severity from 4 to 16 weeks post-induction compared to sham.
- Trabecular morphology was altered in a murine DMM model, specifically increased trabecular thickness and reduced trabecular separation and number relative to sham.
- Osteophytes were present on the medial tibial contour at every time point in a murine DMM model, which increased in size and bone volume as the time course progressed. The osteophytes also decreased in number from 4 – 16 weeks post DMM surgery. There was a positive correlation between osteophyte size/bone volume and severity of cartilage damage/trabeculae thickness/subchondral sclerosis.

- Cartilage damage became progressively worse from 4 to 16 weeks post DMM surgery in a murine model as assessed using the OARSI scoring system, compared to sham where minimal cartilage damage was observed.
- There was a positive correlation between worsening cartilage damage and increased severity of subchondral sclerosis and increased trabecular thickness.

Chapter 5: Tissue-specific gene ablation of matriptase in a surgically-induced (DMM) murine OA model

5.1 Introduction

As detailed in chapter 4, the salient features of OA have been observed in a murine model. The next step was to identify whether there was any cartilage or subchondral bone protection in OA by ablating matriptase tissue-specifically. Matriptase is known to be involved in OA pathogenesis (as described in section 1.8) and represents a novel area of investigation in knock-out studies.

Matriptase is an activator of PAR-2 and is implicated in OA, as discussed in section 1.8. There have been no animal studies investigating the effects of matriptase ablation on OA pathology. Global matriptase ablation is lethal so in order to investigate its role in OA, cartilage-specific gene ablation has been utilised [188].

I have performed similar analyses on subchondral bone and cartilage using micro-CT and histological techniques to identify cartilage and subchondral bone remodelling events in the cartilage-specific matriptase ablated mice. All analyses in the tissue-specific gene ablated mice were carried out on mice 8 weeks post-surgery, as at this time point I have found significant OA pathology and so is a good time point to elicit any protection conferred by gene ablation.

The aims of this chapter were to:

1. Confirm gene ablation by using semi-quantitative PCR, (genotyping) qPCR and IHC techniques.
2. Obtain mouse weights and tibial measurements in the cartilage-specific matriptase ablated mice and compare these to the wild type mice measurements in order to detect any developmental deviances.
3. Analyse cartilage and subchondral bone remodelling events in the cartilage-specific matriptase ablated mice using a murine DMM model at eight weeks post-surgery, utilising histological and micro-CT techniques.
4. Compare the results I obtain from the ablated mice in terms of cartilage and subchondral bone remodelling to the wild type data to detect any differences, and any protection conferred by tissue-specific gene ablation.

5. Analyse osteophyte morphology and compare to wild type results.

5.2 Results

5.2.1 Confirmation of matriptase ablation

I used various different methods to confirm matriptase ablation including semi-quantitative PCR to detect excision of the gene for the cartilage-specific matriptase ablated mice, (genotyping section 2.2.6) qPCR analysis on RNA extracted from the xiphisternum (sections 2.2.4 and 2.2.7) and IHC. (Section 2.2.9) However, it was challenging to confirm gene ablation as matriptase is expressed at very low levels in normal physiological conditions, and is only up-regulated in disease states such as OA [122].

5.2.1.1 Semi-quantitative PCR analysis (genotyping)

Semi-quantitative PCR is a common technique used to confirm gene ablation in animal models therefore I used this method [239, 247-249]. All genotyping in this study was carried out by Valerie Affleck (Research Assistant, MRG). There were initial problems encountered optimising the PCR genotyping protocol for the cartilage-specific matriptase ablated mice. However, this has since been improved by Hua Lin (Research Assistant, MRG) and representative examples of the cartilage-specific matriptase ablated mice have been provided in Appendix D. Of note, all genotyping results shown in Appendix D were from the same line of mice used in my research. Represented in Appendix D, were the presence of col2:cre, the floxed ST14 allele and excised exon 2 for the cartilage-specific ST14 gene ablated strain.

5.2.1.2 qPCR - *matriptase*

To quantify gene expression qPCR was performed. The mice used were from the same line as for the genotyping. As shown in figure 5.1, quantification of gene expression in extracted RNA from cartilage confirmed that ST14 was successfully ablated in the knock-out mice, as there was ST14 expression in the control mice but no expression in the ST14 knock-out mice. However, this difference was not significant. There was collagen type II expression in all samples, confirming RNA had been successfully extracted from cartilage. However, there was also haemoglobin present in some samples (data not shown), which suggested that there was some degree of bone contamination.

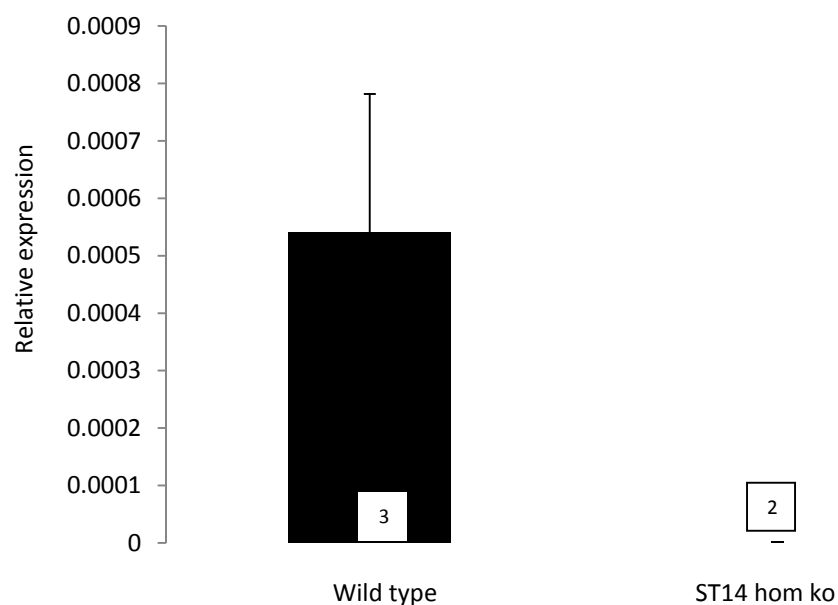


Figure 5.1: Quantitative PCR (ST14). Mouse xiphisternum was dissected from wild type mice and ST14 homozygous knock-out mice. RNA was subsequently extracted and reverse transcribed into cDNA, which was used for qPCR to quantify ST14 expression in cartilage. (Described in sections 2.2.4, 2.2.5 and 2.2.7) The primers used for qPCR were TaqMan gene expression assays as described in section 2.2.7. Data were normalised to 18S rRNA housekeeping gene. Error bars are +/- 1 SD of the mean. The number in the white box represents the number of mice in each group.

5.2.1.3 Immunohistochemistry - matriptase

As discussed in chapter 4, IHC analyses using a specific antibody (ST14 rabbit polyclonal antibody) failed to stain matriptase in the bone or cartilage, of any wild type DMM or sham mice. Similarly, there was a lack of matriptase staining in any of the cartilage-specific matriptase ablated mice. Due to this, IHC could not be used for confirmation of successful matriptase ablation.

5.2.2 Mouse weights and subchondral bone measurements

Represented over-page are mouse weights taken from wild type and cartilage-specific matriptase knock-out mice at the time of surgery. Ideally, mouse weights should have been taken throughout development as there may have been subtle deviances. However, no obvious visual differences in size between strains were observed. Subchondral tibial bone measurements were obtained from mice 8 weeks post-surgery using micro-CT SkyScanner software. This allowed comparison to the wild type mice to detect any gross abnormalities in development.

5.2.2.1 Mouse weights

No significant differences in mouse weights were recorded, with a mean mouse weight of 25.8g in the wild type mice and 27.3g in the cartilage-specific matriptase ablated mice. (Figure 5.2) These data suggest that ablation of ST14 in the cartilage did not cause any gross deviances in mouse development or growth.

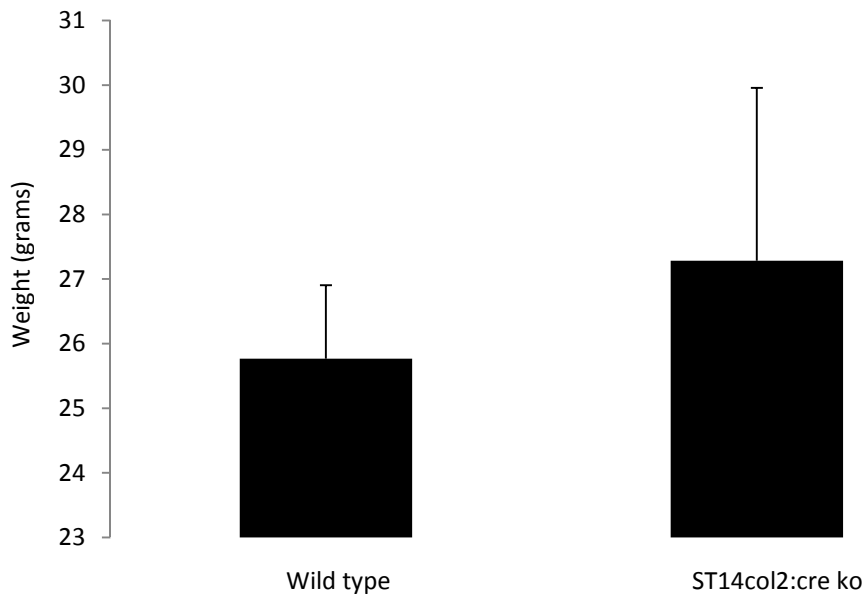


Figure 5.2: Weights of wild type and cartilage-specific matriptase ablated mice. Mouse weights were taken at the time of surgery at 10 weeks of age. Weights were measured using bench-top scales and recorded to one decimal point. This allowed mouse weights to be compared between the knock-out strains and wild type mice. There were six mice in each group, all naïve at the point of measurement. Error bars are +/- 1 SD of the mean.

5.2.2.2 Subchondral tibial bone measurements: wild type compared to cartilage-specific matriptase ablated mice

Figure 5.3A showed a general trend of increased tibial shaft width in the DMM relative to sham, reaching significance in the cartilage-specific matriptase ablated group. The tibial shaft width was similar between the DMM wild type and DMM matriptase ablated group. In the sham groups the tibial shaft width was significantly less in the matriptase ablated group relative to wild type.

The medial tibial epicondyle height (figure 5.3B) was significantly more in the wild type DMM group, relative to wild type sham. This pattern was not evident in the matriptase ablated group. There were no significant differences in the medial tibial epicondyle height in the DMM wild type mice relative to matriptase ablated DMM mice. The matriptase ablated sham group had a significantly increased medial tibial epicondyle height relative to the wild type sham group.

Figure 5.3C showed a pattern of increased lateral tibial epicondyle height in the DMM group relative to sham, in both wild type and matriptase ablated groups. There was a reduced lateral tibial epicondyle height in the matriptase ablated DMM group, relative to the wild type DMM group. This pattern was also observed in the sham groups, but did not reach significance.

The width of the subchondral region shown in figure 5.3D revealed a pattern of increased width of the tibial subchondral region in the DMM groups relative to sham, reaching significance in the wild type group. There were no significant differences in the width of the tibial subchondral region in the DMM groups. Similarly, there was not much variation in the width of the tibial subchondral region in the sham groups.

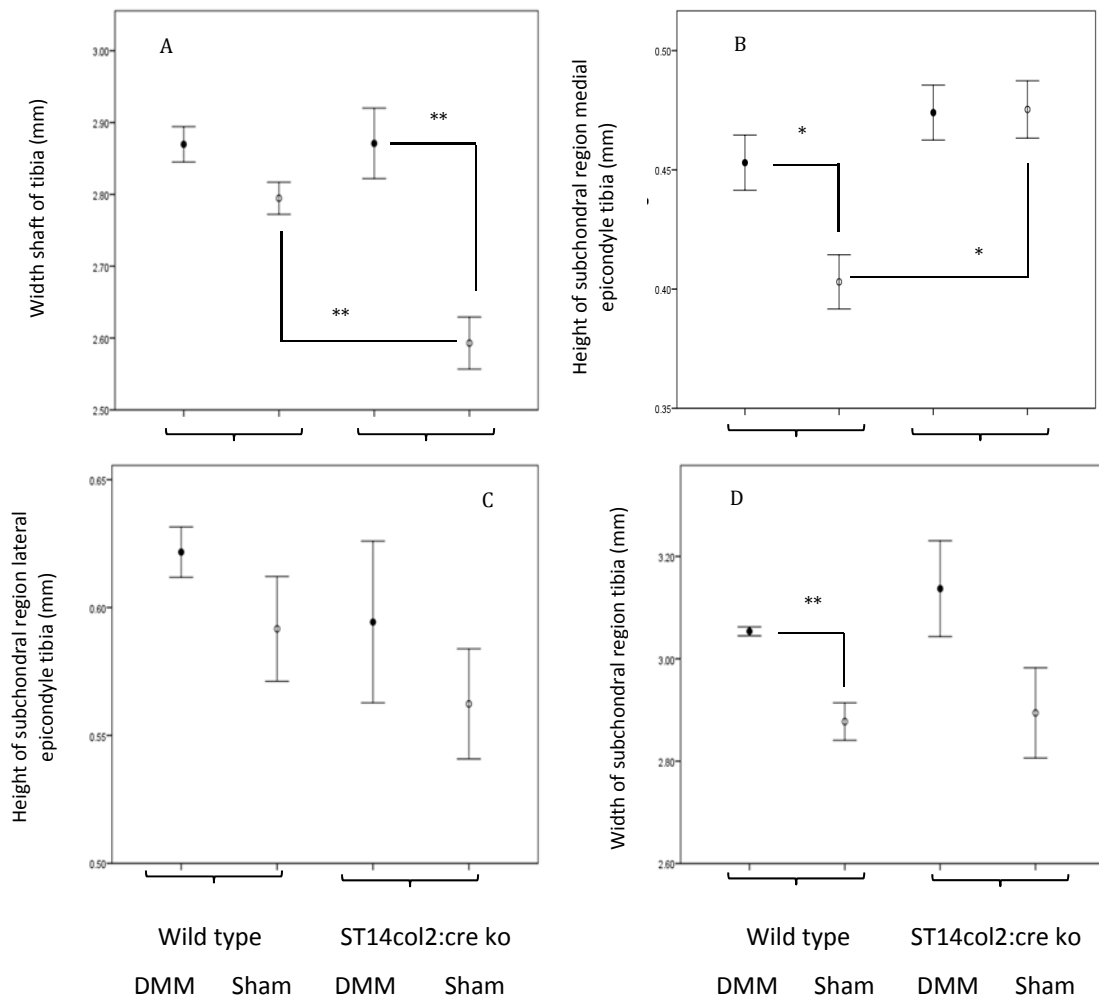


Figure 5.3: Subchondral tibial bone measurements. Mice were sacrificed at 8 week post-surgery and the left limb dissected and fixed in 10% paraformaldehyde. These limbs were subsequently scanned in a micro-CT SkyScanner. From the reconstructed scans, measurements of the subchondral bone were taken using CTan software (section 2.2.10.4). Tibial shaft width (A); medial tibial epicondyle height (B); lateral tibial epicondyle height (C); width tibial subchondral region (D). 3 DMM and 3 sham mice were used for measurements in each group. The mean width/height is given in mm (+/- 1 SE of the mean). * $p < 0.05$ ** $p < 0.01$. Independent samples T-test.

5.2.3 Micro-CT analysis of subchondral sclerosis and trabecular morphology

The results in chapter 4 showed significant subchondral sclerosis and altered trabecular morphology in the wild type DMM model relative to sham, which can now be compared to the cartilage-specific matriptase knock out mice to detect any bone protection in terms of reduced subchondral sclerosis and reduced trabecular remodelling.

5.2.3.1 Subchondral sclerosis

Shown in figure 5.4 there was no difference observed in terms of subchondral sclerosis between wild type DMM and cartilage-specific matriptase knock-out DMM groups. The wild type DMM group had significantly more sclerosis than the wild type sham group. Also, the cartilage-specific matriptase knock-out DMM group had significantly more sclerosis than the cartilage-specific matriptase knock-out naïve group. This difference was also observed in the cartilage-specific matriptase knock-out sham group, however was not significant. (Figure 5.4) A one-way ANOVA test was performed revealing significant differences between groups ($F(4,28) = 3.896$, $p < 0.05$), with the Tukey post hoc test revealing where these significant differences were found, as detailed in figure 5.4.

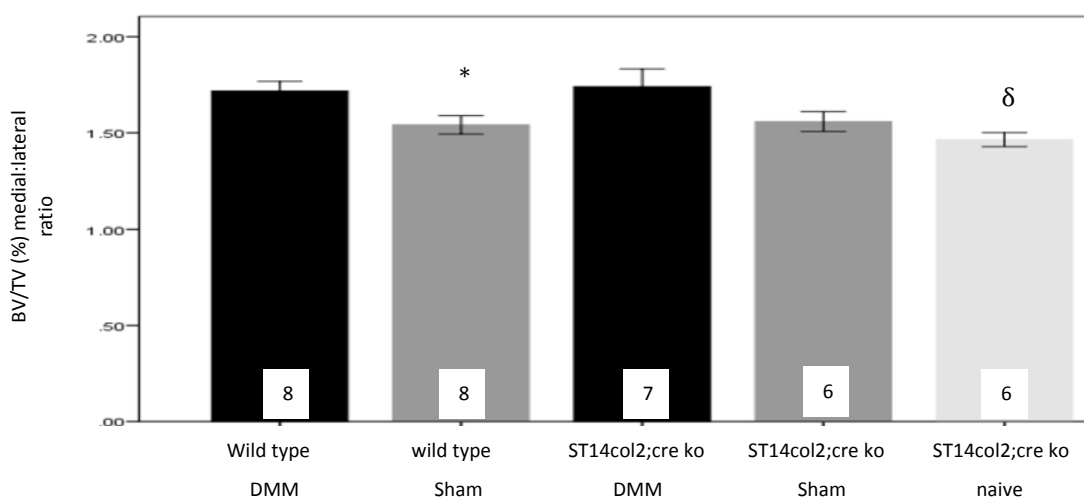


Figure 5.4: Measurement of subchondral sclerosis in wild type and cartilage-specific ST14 ablated mice. Mice underwent DMM or sham surgery at 10 weeks of age, or remained as naïve mice. At 8 weeks post-surgery mice were sacrificed and ipsilateral limbs harvested and fixed in 10% buffered paraformaldehyde for up to 72 hours. The limbs were then stored in 70% ethanol until use for micro-CT. Ipsilateral limbs were scanned in a micro-CT SkyScanner as described in section 2.2.10 and images analysed as described in section 2.2.10. * $p < 0.05$ compared to wild type DMM. δ $p < 0.05$ compared to ST14col2;cre ko DMM. The number in the white box represents the number of mice in each group. Error bars +/- SEM. A one-way ANOVA with post hoc Tukey test were performed.

5.2.3.2 Alterations in trabecular morphology

There was reduced trabecular thickness in the cartilage-specific matriptase knock-out DMM group relative to wild type DMM, however this did not reach significance. Also, significantly thicker trabeculae were observed in the cartilage-specific matriptase knock-out DMM group, relative to the corresponding sham and naïve groups. A similar pattern was also observed in the wild type DMM group relative to sham. The cartilage-specific matriptase knock-out sham group also had reduced trabecular thickness relative to the wild type sham group, but this did not reach significance. (Figure 5.5A) A one-way ANOVA was performed revealing significant differences between groups ($F(4,28) = 10.159, p < 0.001$) with the post hoc Tukey test showing where these significant differences were, shown in figure 5.5A.

The cartilage-specific matriptase knock-out DMM group had slightly increased separation between trabeculae compare to wild type DMM, however this difference was not significant. Trabecular separation was not significantly different between the cartilage-specific knock-out sham and naïve groups relative to the corresponding DMM group. However, the pattern was of reduced trabecular separation in the cartilage-specific matriptase knock-out DMM group relative to the corresponding sham and naïve groups, similar to the pattern observed in the wild type mice. (Figure 5.5B) These results correspond to figure 5.5A where the groups with thicker trabeculae have reduced trabecular separation. A one-way ANOVA revealed no significant differences between groups ($F(4,28) = 1.610, p = 0.200$).

The cartilage-specific matriptase knock-out DMM group had a slightly higher number of trabeculae compared to the wild type DMM group, (figure 5.5C) which fits in with the slightly thinner trabeculae and increased trabecular separation observed in this group shown in figures 5.5A and 5.5B, respectively. Additionally, the cartilage-specific matriptase knock-out DMM group had significantly fewer trabeculae relative to the corresponding sham and naïve groups, which is akin to the pattern observed in the wild type mice. (Figure 5.5C) Significant differences between groups were identified using a one-way ANOVA test ($F(4,28) = 12.088, p < 0.001$), with a post hoc Tukey test revealing where these differences were observed, as shown in figure 5.5C.

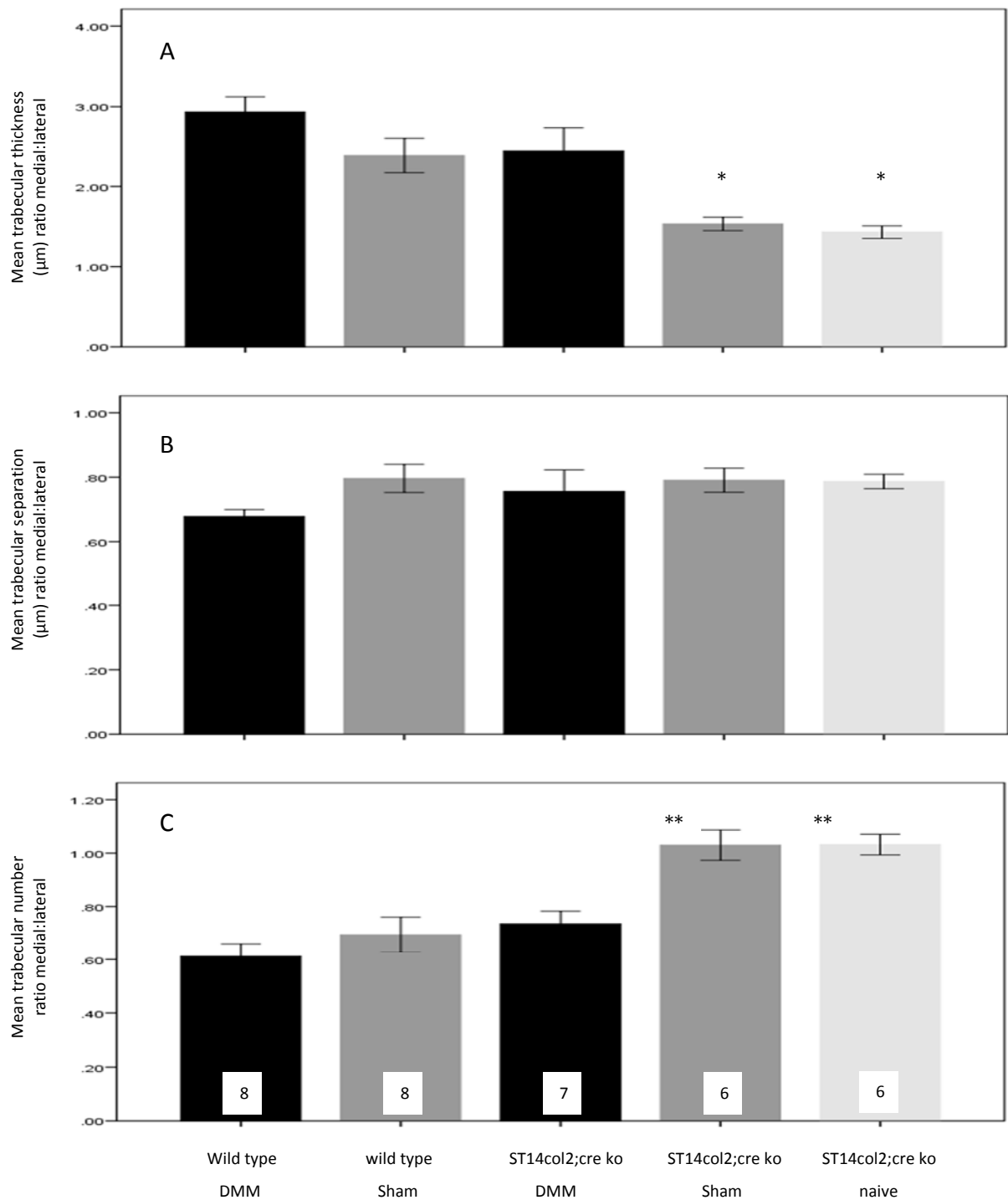


Figure 5.5: Measurement of trabecular morphology in wild type and cartilage-specific ST14 ablated mice. Images from murine joints as detailed in figure 5.4 were assessed for trabecular thickness (A), trabecular separation (B) and trabecular number (C). * $p < 0.05$ ** $p < 0.01$ compared to ST14 col2; cre ko DMM. ψ $p < 0.05$ compared to wild type sham. The number in the white box represents the number of mice in each group. Error bars +/- SEM. One-way ANOVA with post hoc Tukey test.

5.2.4 Micro-CT and histology images for osteophytes

Similar to the observations in the wild type mice, I observed osteophyte formation on the medial contour of the tibiae in the cartilage-specific matrix metalloproteinase knock-out DMM mice. (Figure 5.6, top panel) Similarly, I did not detect any osteophytes in the sham or naïve mice, (middle and lower panels, respectively) and no osteophytes were observed on the femora or lateral aspect of the tibiae. Again, similar to the wild type mice, the osteophytes seen in the DMM knock-out strain were marginal osteophytes rather than bulb-like osteophytes located at ligament insertion sites.

Micro-CT representation of the osteophytes in the cartilage-specific matrix metalloproteinase knock-out mice (DMM) are shown in figure 5.6, images A and B top panel. The osteophytes are also identified by histology staining (H&E and safranin-O) showing an area of increased cell proliferation and extension of the medial aspect of the tibia compared to sham and naïve. (Figure 5.6, images C and D top panel) The middle and lower panels in figure 5.6 show a smooth contour to the medial tibial plateau in the sham and naïve mice, respectively, with no evidence of osteophyte formation on micro-CT (images A and B) or histological analysis (images C and D).

From general observation of the osteophytes in figure 5.6, they appear to be larger in size compared to wild type osteophytes in mice eight weeks post-surgery. (Figure 4.10, chapter 4) Detailed analysis of osteophyte size, bone volume and number has been provided in section 5.2.5.

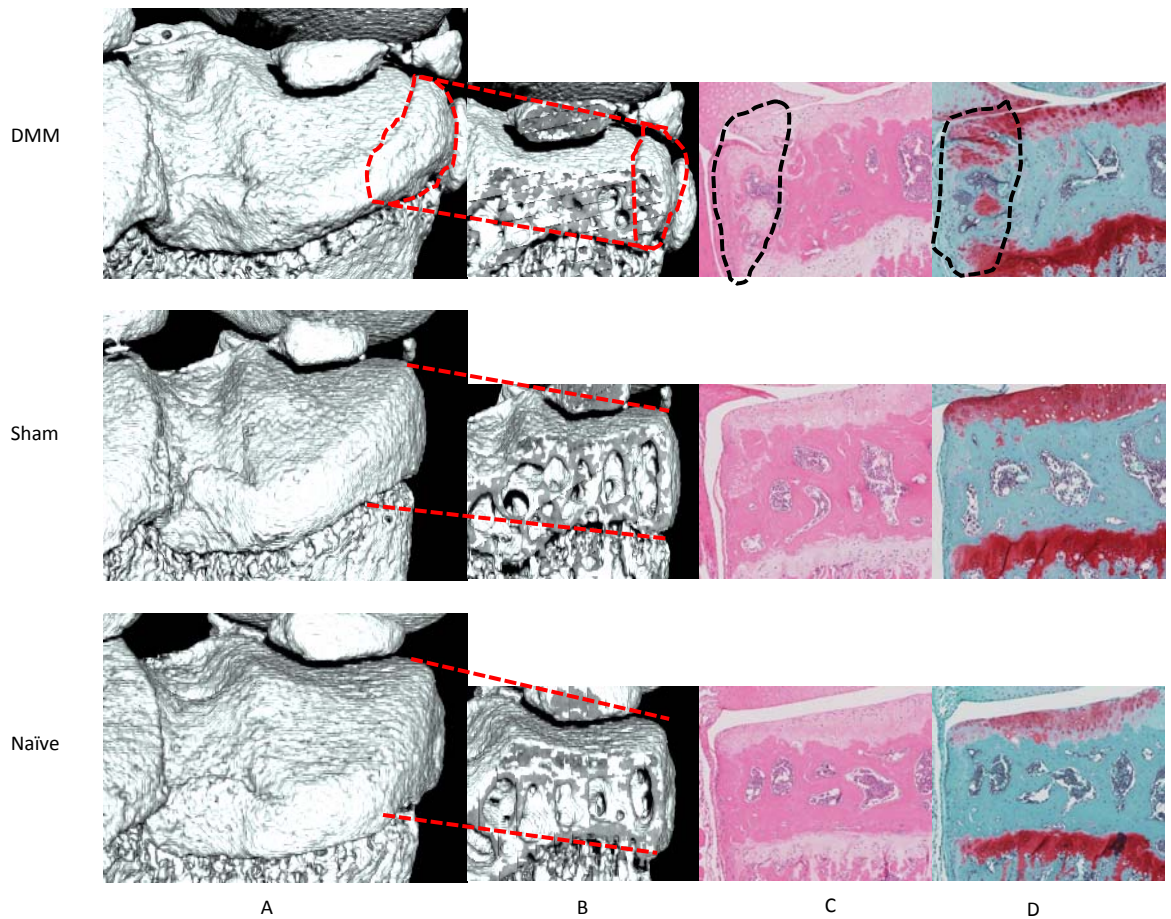


Figure 5.6: Osteophyte representation of cartilage-specific ST14 knock-out mice. ST14 col2:cre knock out mice underwent DMM or sham surgery at 10 weeks of age or remained naïve. These mice were then sacrificed at 8 weeks post-surgery. Limbs were processed for micro-CT as detailed in figure 5.4. 3D visualisation of the osteophytes then took place, using CTVox software as described in section 2.2.10.3. (Images A and B) Image B is a cross-sectional representation of image A, with the red slashed lines highlighting an osteophyte in the DMM model and smooth contour of the medial aspect of the tibia in the sham and naïve models. For images C and D, after the bones had been scanned, histological analysis then took place as described in sections 2.2.3 and 2.2.8 and visualisation of H&E (C) and Safranin-O (D) stained joints were performed using a microscope. The black slashed lines in images C and D in the DMM model highlight an osteophyte on the medial aspect of the tibia.

5.2.5 Micro-CT analysis of osteophyte morphology in cartilage-specific matriptase ablated mice relative to wild type

The results in chapter 4 showed a stepwise increase in tissue and bone volume of the osteophytes in a wild type DMM model as the time course progressed from 4 to 16 weeks post-surgery. Also observed was a reduction in the number of osteophytes with time. As shown in section 5.2.4, osteophytes were observed in the cartilage-specific matriptase knock-out DMM strain of mice, with none seen in the sham or naïve mice, which is similar to the observations in the wild type DMM mice relative to sham and naïve wild type mice detailed in chapter 4. Analysis has subsequently been performed to compare the characteristics of the osteophytes observed in the cartilage-specific matriptase knock-out strain of mice relative to wild type mice to detect any difference in the size, bone volume and number of osteophytes.

In the cartilage-specific ST14 knock-out mice the osteophytes were in fact larger (increased tissue volume) relative to wild type DMM mice osteophytes, however this did not reach significance. (Figure 5.7A) Observed in figure 5.7B, the cartilage-specific ST14 knock-out mice had an increased osteophyte bone volume relative to the osteophytes analysed in the wild type DMM model. Due to considerable variation between mice this did not reach significance. This corresponded with figure 5.7A where the cartilage-specific ST14 knock-out mice osteophytes were larger corresponding with an increased bone volume, relative to wild type DMM mice osteophytes. The cartilage-specific ST14 knock-out mice had significantly less osteophytes compared to wild type mice osteophytes. (Figure 5.7C)

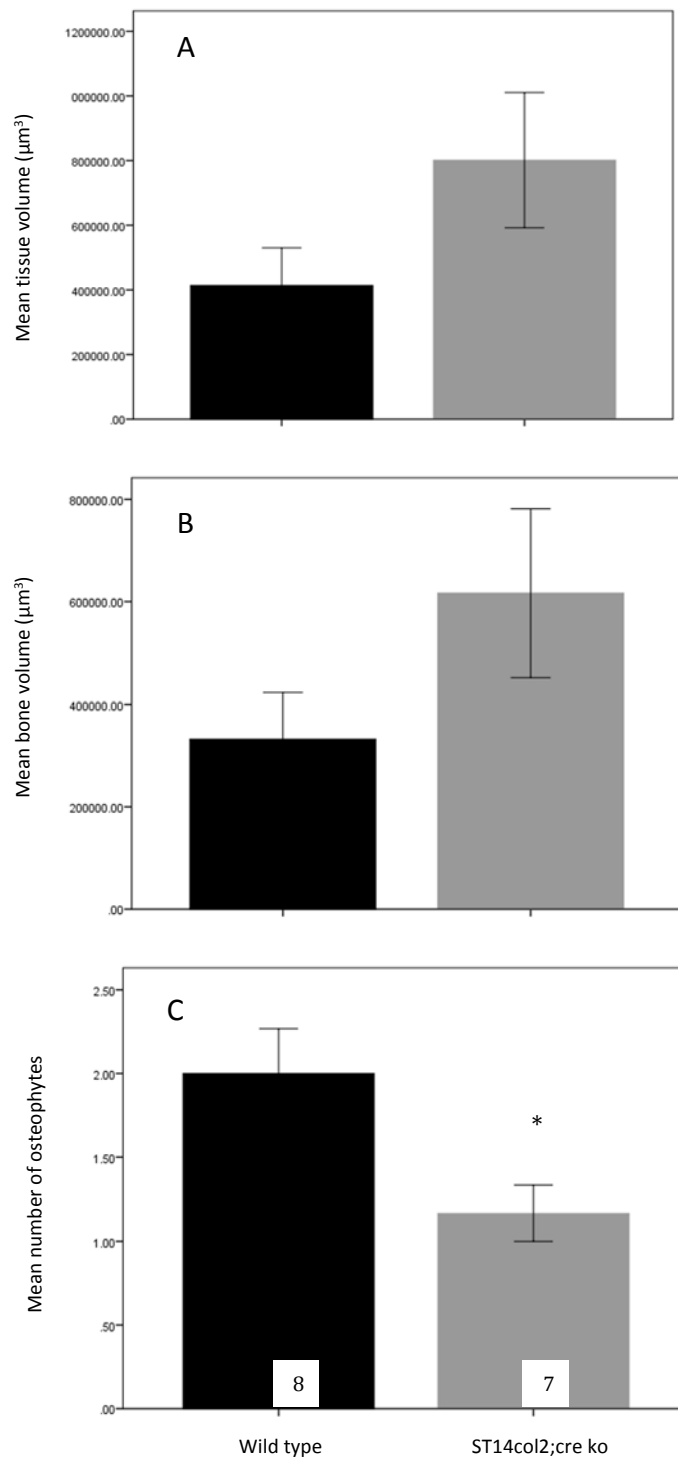


Figure 5.7: Analysis of osteophyte morphology, comparing cartilage-specific ST14 ablated mice to wild type mice. Mice underwent DMM surgery at 10 weeks of age and were sacrificed at 8 weeks post-surgery. The ipsilateral limbs were harvested and fixed in 10% buffered paraformaldehyde for up to 72 hours. Limbs were stored in 70% ethanol until micro-CT scanning using a SkyScanner micro-CT machine. Osteophytes were visualised using Ctvox and CTan software and analysis performed as described in section 2.2.10.3. The largest osteophyte in each mouse was analysed for tissue volume (A), bone volume (B) and number (C). The number in the white box represents the number of mice in each group. Error bars are +/- 1 SE of the mean. * p < 0.05 compared to wild type. Independent samples T-test.

5.2.6 Cartilage damage in cartilage-specific matriptase ablated mice relative to wild type

5.2.6.1 Qualitative assessment of cartilage damage

Qualitative assessment of cartilage damage in figure 5.8 shows more severe cartilage damage in the DMM group relative to sham and naïve wild type mice, with a similar pattern in the cartilage-specific ST14 knock-out mice. Shown in figure 5.8, the wild type DMM group had proteoglycan loss and fibrillations with a loss of viable chondrocytes and clustering, leaving exposed subchondral bone. This pattern was also observed in the cartilage-specific matriptase ablated DMM group. These features were best observed in the higher magnification (x10) images (DMM). The sham and naïve groups shown in figure 5.8 were very similar across mouse strains with no disruption of the proteoglycan layer. The cartilage damage has been formally assessed using the OARSI scoring system by two blinded colleagues within MRG, section 5.2.6.2.

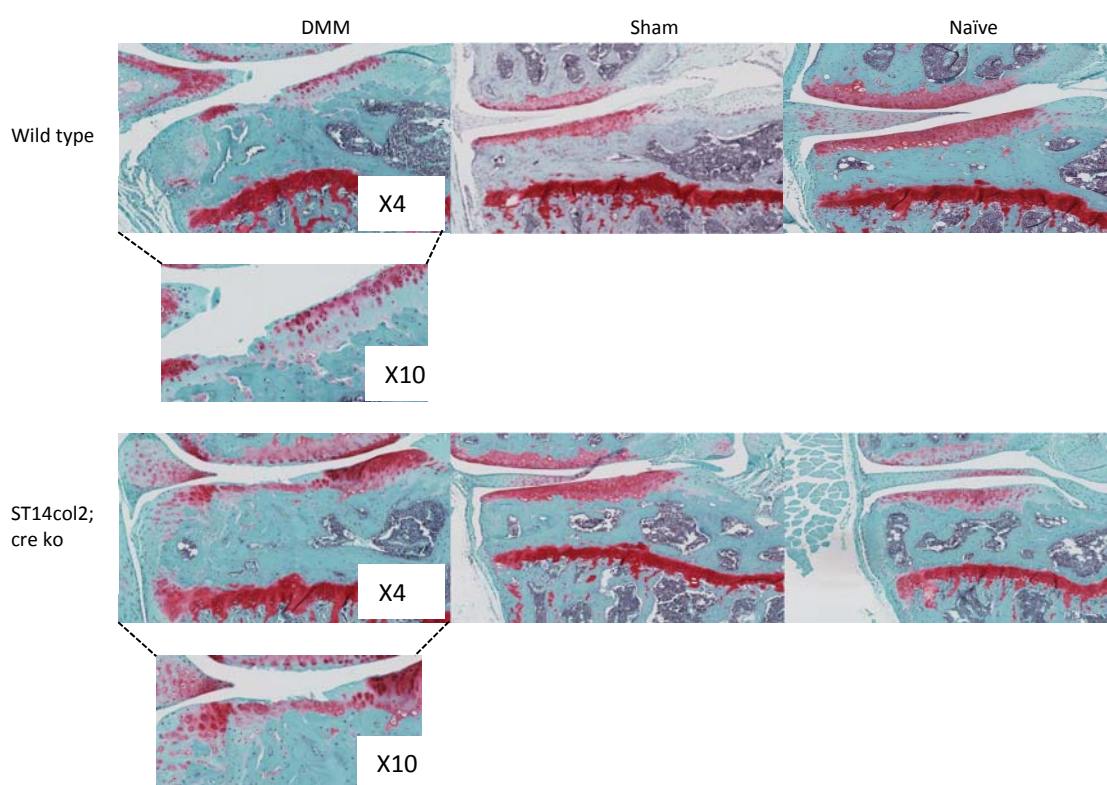


Figure 5.8: Qualitative assessment of cartilage damage. Wild type and gene ablation mice underwent DMM or sham surgery at 10 weeks of age or remained naïve. These mice were then sacrificed at 8 weeks post-surgery. The affected limb was then dissected and fixed in 10% buffered paraformaldehyde for up to 72 hours and then transferred into 70% ethanol. Histological analyses then took place using Safranin-O, as described in sections 2.2.3 and 2.2.8. The red staining is proteoglycan content on the medial aspect of the tibia. The black slashed lines highlight a higher magnification image (x10) in the DMM group, focussing on the medial aspect of the tibia.

5.2.6.2 Quantitative assessment of cartilage damage

The OARSI histological scoring system (mouse) was used, as detailed in chapter 4. Similarly, the medial tibial plateau was assessed as this is where most severe cartilage damage occurred in the DMM model. Best overall maximum score of cartilage damage (figure 5.9A) and best combined summed score of cartilage damage (figure 5.9B) were used to assess cartilage damage. The cartilage-specific matriptase knock-out DMM group had a similar degree of cartilage damage as the wild type DMM group. The sham and naïve groups had minimal cartilage damage compared to the corresponding DMM model.

5.2.7 Correlation analysis

No correlation was found between histologic score and subchondral sclerosis within the cartilage-specific matriptase group using Spearman's rank correlation analysis. Histologic cartilage damage score:subchondral sclerosis; cartilage-specific ST14 ablation $r = 0.194$.

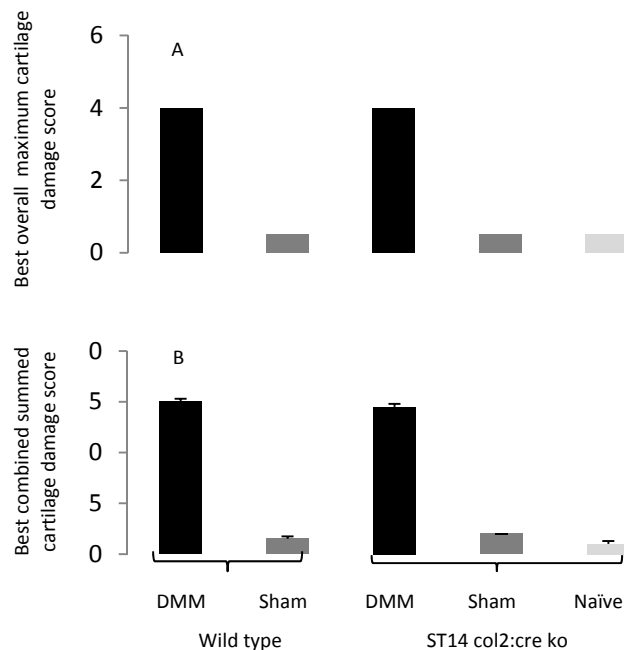


Figure 5.9: Quantitative assessment of cartilage damage. Wild type and gene ablated mice underwent DMM or sham surgery at 10 weeks of age or remained naïve, and were sacrificed at 8 weeks post-surgery. The affected limb was processed and histological analyses took place as detailed in figure 5.8. The Safranin-O stained sections were used to assess cartilage damage, as described by Glasson et al. [1] There were 4 mice in each group and 6 sections analysed per mouse (24 sections in total per group) giving a global representation of cartilage damage in each group. The scoring was carried out blinded. The best overall maximum score of cartilage damage at the medial tibial plateau per group is shown in bar chart A. Bar chart B represents the best combined summed score of cartilage damage at the MTP per group. (Section 2.2.16) Error bars +/- SD mean. A one-way ANOVA test and post hoc Tukey test were performed.

5.3 Discussion

5.3.1 Confirmation of gene ablation

For the cartilage-specific matriptase knock-out mice I was able to carry out genotyping (semi-quantitative PCR) and qPCR (section 5.2.1.2; cartilage dissected from xiphisternum) to confirm successful gene ablation. I also attempted cartilage micro-dissection from the tibiae of mice and extraction of RNA followed by reverse transcription qPCR in order to detect matriptase and confirm successful ablation in the cartilage. However, micro-dissection of cartilage from a mouse joint was very challenging to obtain pure cartilage. My initial experiments using qPCR measured collagen type II and haemoglobin (contained in blood), to give an indication of whether I had dissected pure cartilage. I persevered at this technique for many months however all my samples contained significant amount of haemoglobin, suggesting bone contamination. Due to this, I could not use this technique to determine successful gene ablation in the cartilage. The genotyping results for the cartilage-specific matriptase ablated mice (Appendix D) suggest that either exon 2 had not been excised completely, or there was contamination of the sample. However, using qPCR I did show that the cartilage-specific matriptase knock-out mice had no matriptase expression relative to control. IHC could not confirm successful matriptase ablation in the cartilage, due to the specific antibody used not detecting matriptase in the wild type DMM and sham models at the time point studied (discussed in chapter 4).

5.3.2 Mouse weights and subchondral tibial bone measurements

There were no significant differences in mouse weights between wild type and the cartilage-specific matriptase ablated group, suggesting no gross developmental deviances.

There were not any significant differences in any of the tibial subchondral bone measurements between the wild type DMM mice and cartilage-specific matriptase knock-out DMM mice. However, there were some significant differences when comparing the wild type sham mice to the cartilage-specific matriptase knock-out sham mice, specifically the width of the shaft of the tibia, and height of the subchondral region in the medial epicondyle.

As discussed in section 1.8, matriptase is involved in proteolytic cascades, via activation of MMPs, and therefore likely plays a role in bone remodelling. This may explain the differences observed in the cartilage-specific matriptase ablated sham group relative to wild type.

5.3.3 Does cartilage-specific ablation of matriptase confer any protection against cartilage degradation and subchondral bone remodelling?

As discussed in chapter 1, matriptase has a myriad of effects which can potentially be involved in OA pathology. These include activation of MMP-3 and MMP-1 causing collagen breakdown and signalling through PAR-2 causing up-regulation of MMP-1 and -3 and pro-inflammatory cytokines, causing cartilage degradation and subchondral bone remodelling. Therefore, it can be postulated that by ablating matriptase this could prevent OA changes occurring. The results shown in 5.2.3 and 5.2.6 show that cartilage-specific ablation of matriptase in a murine DMM model conferred no significant protection against subchondral bone remodelling or cartilage degradation.

It is important to bear in mind however that small numbers of mice were used in this study, (7 mice in the cartilage-specific matriptase ablated DMM group) therefore these are only preliminary data. Additionally, the genotyping data for the cartilage-specific matriptase ablated mice suggest that perhaps exon 2 was not successfully ablated. In contrast to my results, work carried out in the MRG laboratory has shown an inhibitor of matriptase used in a murine DMM model of OA, indeed protects against cartilage damage. (Personal communication with Professor Drew Rowan) Ideally, it will be important to increase the number of mice in this study and confirm successful matriptase ablation, to corroborate whether cartilage-specific matriptase ablation confers any cartilage or subchondral bone protection in a murine OA model.

Interestingly, research by Heffner et al. has highlighted significant problems with utilising cre-mediated gene excision. These include unexpected cre activity in off target tissues, maternal versus paternal inheritance of the cre transgene affecting cre excision patterns and inconsistent cre recombination between littermates. In order for accurate interpretation of experimental results, consistency in cre activity is critically important. Variability in cre activity is likely due to poor expression leading to inconsistent mosaicism in target tissues [250]. It was likely in this project that there was poor expression of cre in

the target tissue of the cartilage-specific matriptase ablated group. This resulted in inconsistent, or no excision of matriptase in the cartilage, explaining the results I have observed. Ongoing work in the MRG laboratory has begun to quantify expression of cre in the cartilage of the cartilage-specific PAR-2 and matriptase ablated groups. This will allow analysis of cre expression in the target tissue and guide future murine knock-out work.

Although my results suggest that cre-mediated matriptase excision in the cartilage was not effective in this study, there appeared to be some degree of bone protection. For example, in the cartilage-specific matriptase ablated DMM group the trabeculae were thinner, with increased separation and number relative to the corresponding wild type group. (Not significant) Additionally, the qPCR results suggest that matriptase was excised in the cartilage. These results suggest that some degree of matriptase excision had occurred. As explained above, this could be related to inconsistent cre-mediated excision of matriptase, due to mosaicism in target tissues. Additionally, there may be unexpected cre-mediated activity in off-target tissues, such as the bone.

Another aspect to consider for future work, is the effectiveness of using col2;cre to excise a floxed allele, specifically in cartilage. Work carried out by Chambers et al. has shown that actually aggrecan may be a more effective promoter of cre-mediated excision in the cartilage. This is because the aggrecan gene is expressed more robustly in articular cartilage than the gene for type II collagen. Therefore, it is worth considering the use of aggrecan as a promoter for cartilage-specific cre-mediated gene excision in the future [251].

5.3.4 Cartilage-specific matriptase ablation effects osteophyte morphology

Cartilage-specific ablation of matriptase caused the osteophytes to become larger with a higher bone volume. Also, in this genotype I found a reduced number of osteophytes compared to wild type. It may be that the osteophytes had coalesced, producing fewer and larger osteophytes, in the cartilage-specific matriptase ablated DMM group. These differences observed again suggest some degree of matriptase excision had occurred, as explained above. Larger numbers of mice with successful ablation of exon 2 (in the cartilage-specific matriptase ablated group) are required to confirm my observations.

5.3.5 Summary

- It is likely that exon 2 was not successfully ablated in this study, due to the reasons discussed above, and so further work is required in this area to fully elucidate the role of matriptase in OA pathology.

Chapter 6: Tissue-specific gene ablation of PAR-2 in a surgically-induced (DMM) murine OA model

6.1 Introduction

PAR-2 is thought to be involved in OA pathogenesis. (Section 1.6) By ablating PAR-2 in a tissue-specific manner this will enable one to understand more about whether cartilage or bone changes occur first in OA, initiating the OA pathology I have observed. Also, such studies will help to identify in which tissue (cartilage or bone) PAR-2 confers its protective effect and halt OA progression. This builds on work carried out investigating the effects of global PAR-2 gene ablation on the progression of OA, which found some degree of cartilage protection [137, 139, 232, 252, 253], and reduced subchondral sclerosis in PAR-2-deficient mice, relative to wild type [137, 232, 252]. Similar analyses were performed on cartilage and subchondral bone as described in chapter 5.

The aims of this chapter were to:

1. Confirm gene ablation by using semi-quantitative PCR, (genotyping) qPCR and IHC techniques.
2. Obtain mouse weights and tibial measurements in the tissue-specific PAR-2 ablated strains of knock-out mice and compare these to the wild type mice measurements in order to detect any developmental deviances.
3. Analyse cartilage and subchondral bone remodelling events in the tissue-specific PAR-2 ablated strains of knock-out mice using a murine OA model, with histological and micro-CT techniques.
4. Compare the results I obtain from the knock-out mice in terms of cartilage and subchondral bone remodelling to the wild type data to detect any differences, and any protection conferred by tissue-specific gene ablation.
5. Analyse osteophyte morphology and compare to wild type results.

6.2 Results

6.2.1 Confirmation of PAR-2 ablation in a murine OA model

Similar methods were used to confirm PAR-2 ablation, as discussed in chapter 5. Akin to matriptase, it was challenging to confirm ablation of PAR-2 as it is expressed at very low levels in normal physiological conditions, and is only up-regulated in joint tissues when diseased, such as OA [138].

6.2.1.1 Semi-quantitative PCR analysis (genotyping)

As discussed in chapter 5, there were initial problems encountered optimising the PCR genotyping protocol for all three strains of gene ablated mice, but this has since been improved by Hua Lin (Research Assistant, MRG) and representative examples of all three gene ablated mice have been provided in Appendix D. All genotyping results shown in Appendix D were from the same line of mice used in my research. Represented in Appendix D, were the presence of col2:cre, the floxed PAR-2 allele and excised exon 2 for the cartilage-specific PAR-2 gene ablated strains. For the bone-specific PAR-2 ablated strain (osteocalcin promoter) the effects of oc:cre will not be seen in the ear notch sample. Therefore, only oc:cre and the floxed PAR-2 allele were shown, which infers that exon 2 has been deleted in the bone.

6.2.1.2 qPCR (PAR-2)

As shown in figure 6.1, quantification of gene expression in extracted RNA from cartilage confirmed that PAR-2 was successfully ablated in the knock-out mice, with a stepwise reduction in PAR-2 expression. PAR-2 heterozygous knock-outs only had very modest PAR-2 expression compared to control, whilst PAR-2 homozygous knock-outs had no expression. All of the samples expressed collagen type II, which confirmed that the RNA extracted was from cartilage. No significant differences were found between groups. There was also haemoglobin expression in some samples, suggesting a degree of bone contamination. (Data not shown)

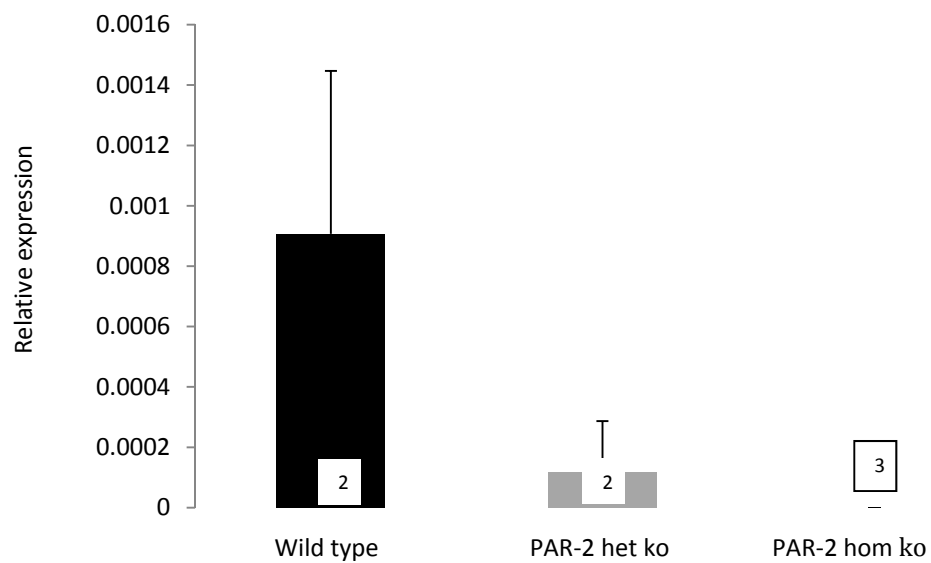


Figure 6.1: Quantitative PCR analysis of PAR-2. Mouse xiphisternum was dissected from mice of the indicated genotype. RNA was subsequently extracted and reverse transcribed into cDNA, which was used for qPCR to quantify PAR-2 expression in cartilage. (Described in sections 2.2.4, 2.2.5 and 2.2.7) Data were normalised to 18S rRNA housekeeping gene. Error bars +/- 1 SD of the mean. The number in the white box represents the number of mice in each group.

6.2.1.3 Immunohistochemistry (PAR-2)

It was apparent in figure 6.2 that there was absence of PAR-2 (brown) staining in the chondrocytes within the cartilage of cartilage-specific PAR-2 ablated DMM mice relative to wild type. This was best observed in figure 6.2 images F and H (higher magnification images of E and G), compared to wild type; figure 6.2 images B and D (higher magnification images of A and C). As mentioned in chapter 4, only a few osteoblasts stained positive for PAR-2 in wild type mice (also observed in figure 6.2 images A-D). Therefore, it was challenging to confirm the absence of PAR-2 staining in osteoblasts in the bone-specific PAR-2 ablated mice. However, referring to the bone-specific PAR-2 ablated DMM mice in figure 6.2 images J and L (higher magnification images of I and K), there were no osteoblasts staining positive for PAR-2, relative to wild type (figure 6.2; images A-D).

Figure 6.3 shows wild type sham mice and cartilage-specific and bone-specific PAR-2 ablated mice (sham). Again, there was a lack of PAR-2 staining in the chondrocytes in the cartilage-specific PAR-2 ablated mice (best observed in figure 6.3 images G and I; higher magnification images of F and H) relative to wild type sham (figure 6.3; images A-D). There were also no osteoblasts staining positive for PAR-2 in the bone-specific PAR-2 ablated sham mice (figure 6.3 images K and M; higher magnification images of J and L), relative to wild type sham (figure 6.3 images A-D). Image E, figure 6.3 represents a positive control for SAM-11 (murine heart), used as a control for all images in figures 6.2 and 6.3. As shown in chapter 4, there was no staining for PAR-2 in wild type naïve mice so the IHC (PAR-2) images for naïve PAR-2 ablated mice have not been presented. This confirmed that PAR-2 was not expressed in cartilage or bone under normal physiological conditions. All mice used for IHC were from the same line as for genotyping and qPCR.

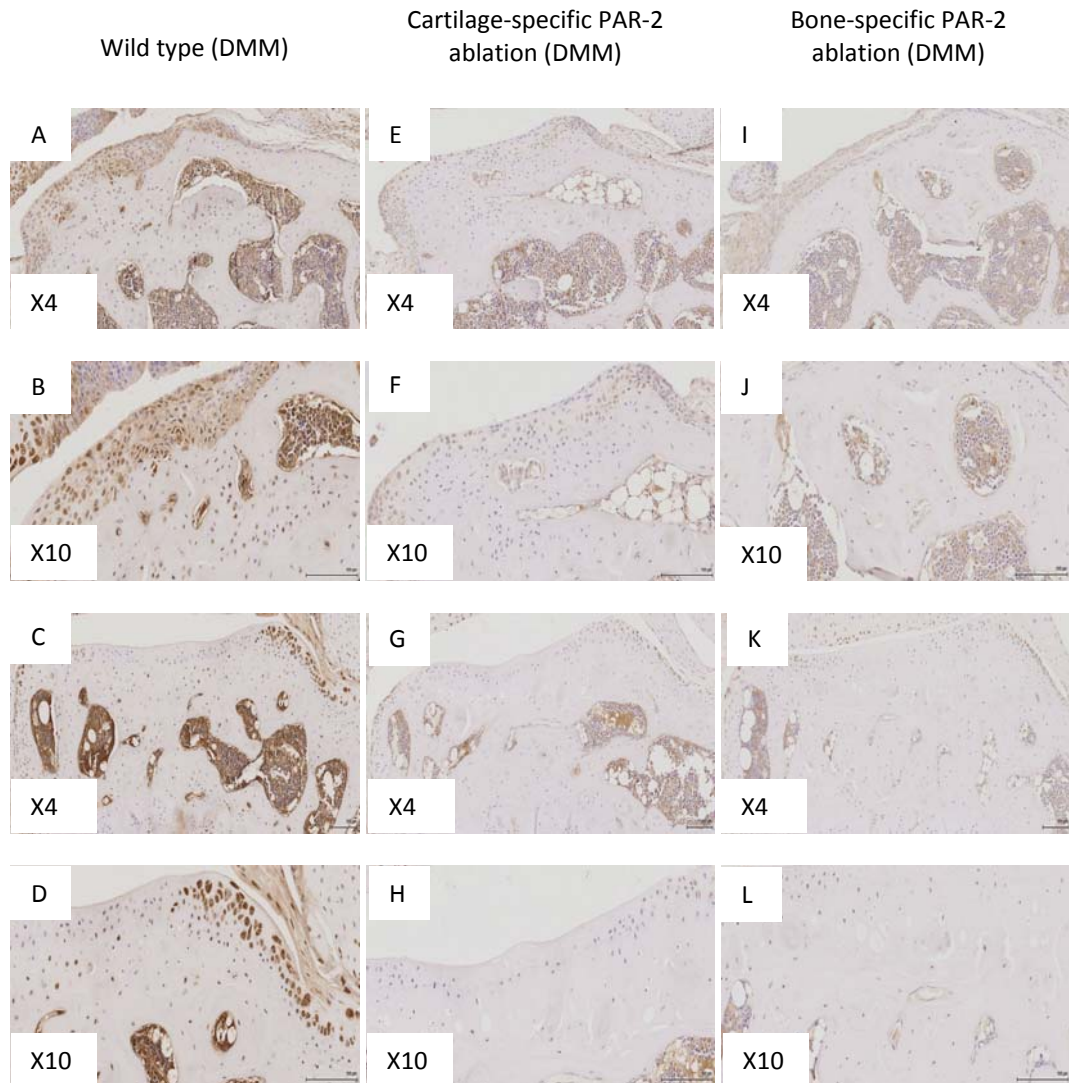


Figure 6.2: Immunohistochemistry (PAR-2) in wild type, cartilage-specific and bone-specific PAR-2 ablated DMM mice. Mice underwent DMM surgery at 10 weeks of age. The mice were sacrificed at 8 weeks post-surgery and the tibia and femur dissected. The joints were fixed in 10% paraformaldehyde for up to 72 hours and then transferred into 70% ethanol. The joints were then decalcified, processed and embedded and sectioned. Sections were cut longitudinally throughout the entire joint. PAR-2 (SAM-11) IHC was then performed as described in section 2.2.9. The stained sections were then analysed using a microscope to detect the presence of PAR-2. (Brown staining) The top two panels are representative of sections taken earlier on in sectioning the joint. The bottom two panels are representative of sections taken later on in sectioning the joint. Two separate magnifications were used, as detailed on image.

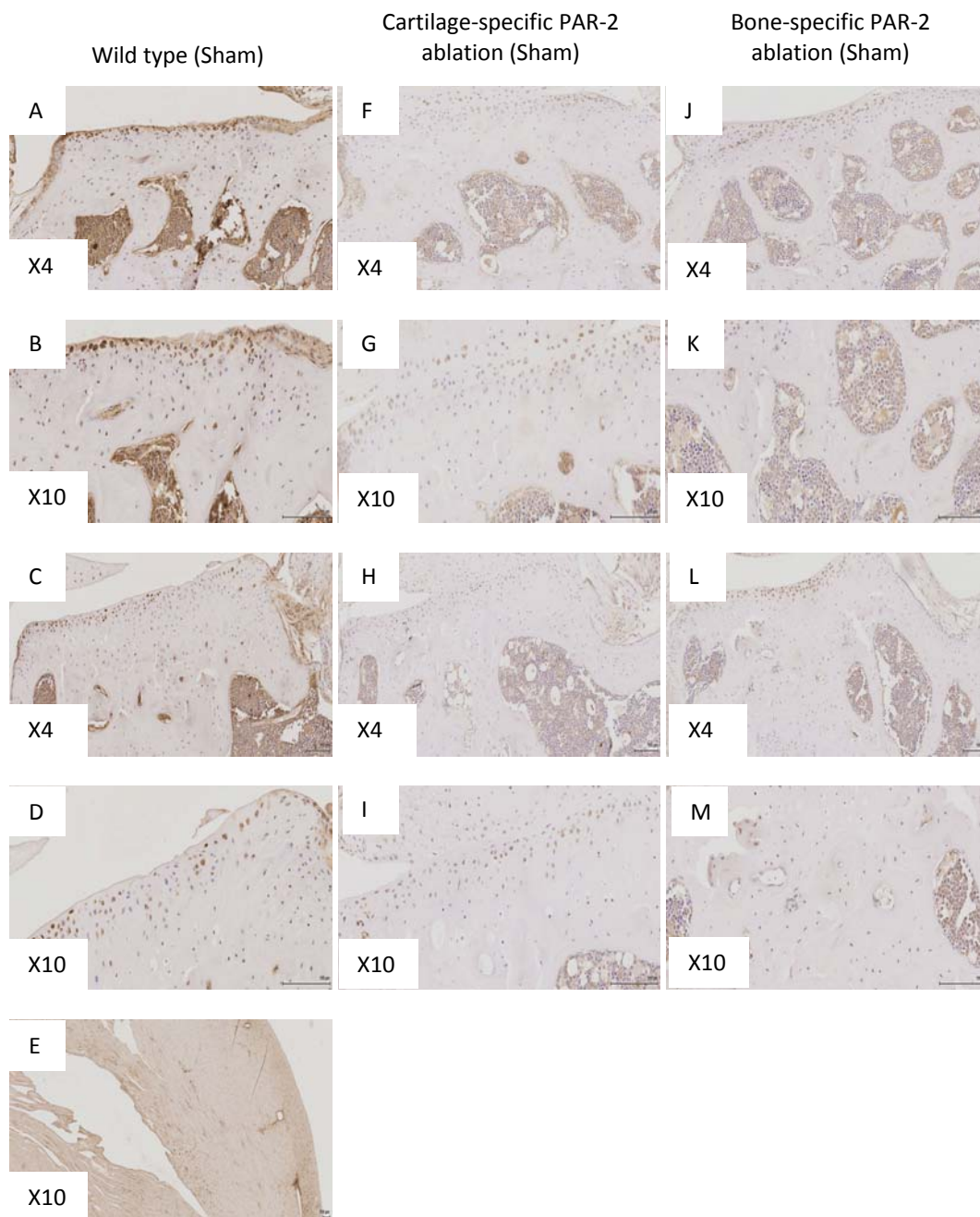


Figure 6.3: Immunohistochemistry (PAR-2) in wild type, cartilage-specific and bone-specific PAR-2 ablated sham mice. Mice underwent sham surgery at 10 weeks of age. The mice were sacrificed at 8 weeks post-surgery and the tibia and femur dissected. The joints were fixed in 10% paraformaldehyde for up to 72 hours and transferred into 70% ethanol. The joints were decalcified, processed and embedded and sectioned. Sections were cut longitudinally throughout the entire joint. PAR-2 (SAM-11) IHC was performed as described in section 2.2.9. The stained sections were then analysed using a microscope to detect the presence of PAR-2. (Brown staining) The top two panels are representative of sections taken earlier on in sectioning the joint. The bottom two panels are representative of sections taken later on in sectioning the joint. Two separate magnifications were used, as detailed on image. Image E is a positive control – murine heart. (Also used in figure 6.2)

6.2.2 Mouse weights and subchondral bone measurements

6.2.2.1 Mouse weights

The mean mouse weights between wild type and the tissue-specific PAR-2 ablated mice did not vary significantly. (Mean weights: wild type – 25.8g; cartilage-specific PAR-2 ablated mice – 25.9g and bone-specific PAR-2 ablated mice – 27.9g) These data suggest that ablation of PAR-2 specifically in the bone or cartilage did not cause any gross deviances in mouse development or growth. (Figure 6.4)



Figure 6.4: Mouse weights of wild type and tissue-specific PAR-2 ablated mice. Mouse weights were taken at the time of surgery at 10 weeks of age. Weights were measured using bench-top scales and recorded to one decimal point. This allowed mouse weights to be compared between the knock-out strains and wild type mice. There were six mice in each group, all naïve at the time of measurement. Error bars are +/- 1 SD of the mean.

6.2.2.2 Subchondral tibial bone measurements: tissue-specific PAR-2 ablated mice compared to wild type

Shown in figures 6.5A and 6.6A, the general trend was that the tibial shaft width was greater in all the DMM groups compared to their respective sham group. There were no significant differences in the tibial shaft width in the DMM groups in both knock-out strains, relative to wild type. In the sham groups, the tibial shaft width was generally less in both knock-out strains relative to wild type.

In figures 6.5B and 6.6B, the wild type medial tibial epicondyle height was significantly increased in the DMM relative to sham. This trend was not seen in any of the two knock-out strains, and in fact the medial tibial epicondyle height was very similar between DMM and sham in both knock-out strains with no significant differences. The heights of the medial epicondyle in the DMM groups were similar between wild type and both knock-out strains. The height of the medial epicondyle in the sham groups was higher in both knock-out strains relative to wild type.

The pattern shown in figures 6.5C and 6.6C was an increased lateral epicondyle height in the DMM groups compared to sham, but this was not significant in any group. The only outlier was the cartilage-specific PAR-2 knock-out strain, which had a similar height between DMM and sham. The general trend in figures 6.5C and 6.6C was a reduced height of the lateral epicondyle in the DMM group of both knock-out strains relative to wild type, which was significant in the cartilage-specific PAR-2 ablated group. This pattern was also seen in the sham groups but was not significant.

The width of the subchondral region shown in figures 6.5D and 6.6D revealed a pattern of increased width of the tibial subchondral region in the DMM groups relative to sham in the bone-specific PAR-2 knock-out strain of mice and wild type group. The cartilage-specific PAR-2 knock-out strain did not have this pattern and had a similar width between DMM and sham. There were no significant differences in the width of the tibial subchondral region in the DMM groups across strains. Similarly, there was little variation in the width of the tibial subchondral region in the sham groups across strains, apart from the cartilage-specific PAR-2 ablated strain which had a significantly greater tibial subchondral width compared to wild type.

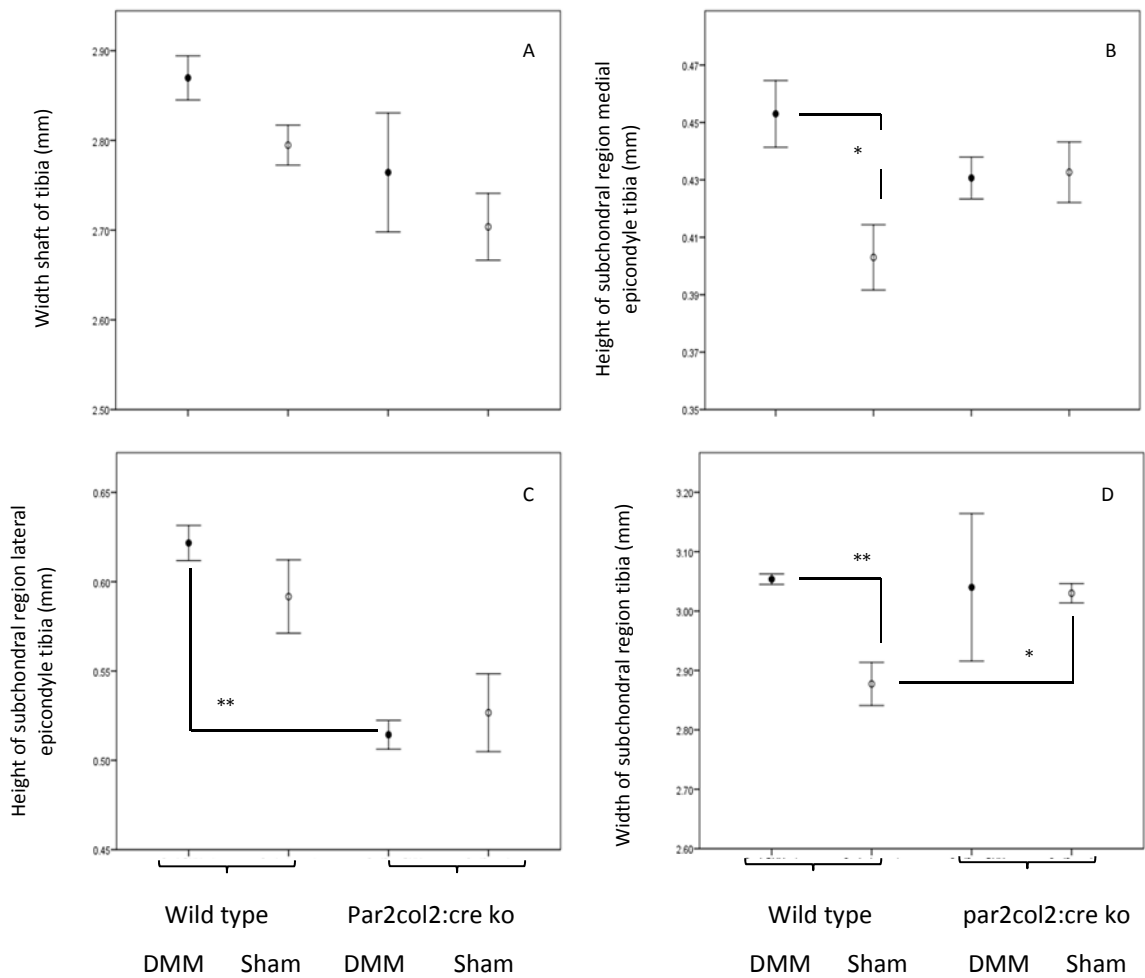


Figure 6.5: Subchondral tibial bone measurements; cartilage-specific PAR-2 ablated strain.

Mice were sacrificed at 8 week post-surgery and the left limb dissected and fixed in 10% paraformaldehyde. These limbs were subsequently scanned in a micro-CT SkyScanner. From the reconstructed scans, measurements of the subchondral bone were taken using CTan software (section 2.2.10.4). 3 DMM and 3 sham mice were used for measurement in each group. A – tibial shaft width; B – medial tibial epicondyle height; C – lateral tibial epicondyle height; D – width of tibial subchondral region. The mean width/height is given in mm (± 1 SE of the mean). Independent samples T-test.

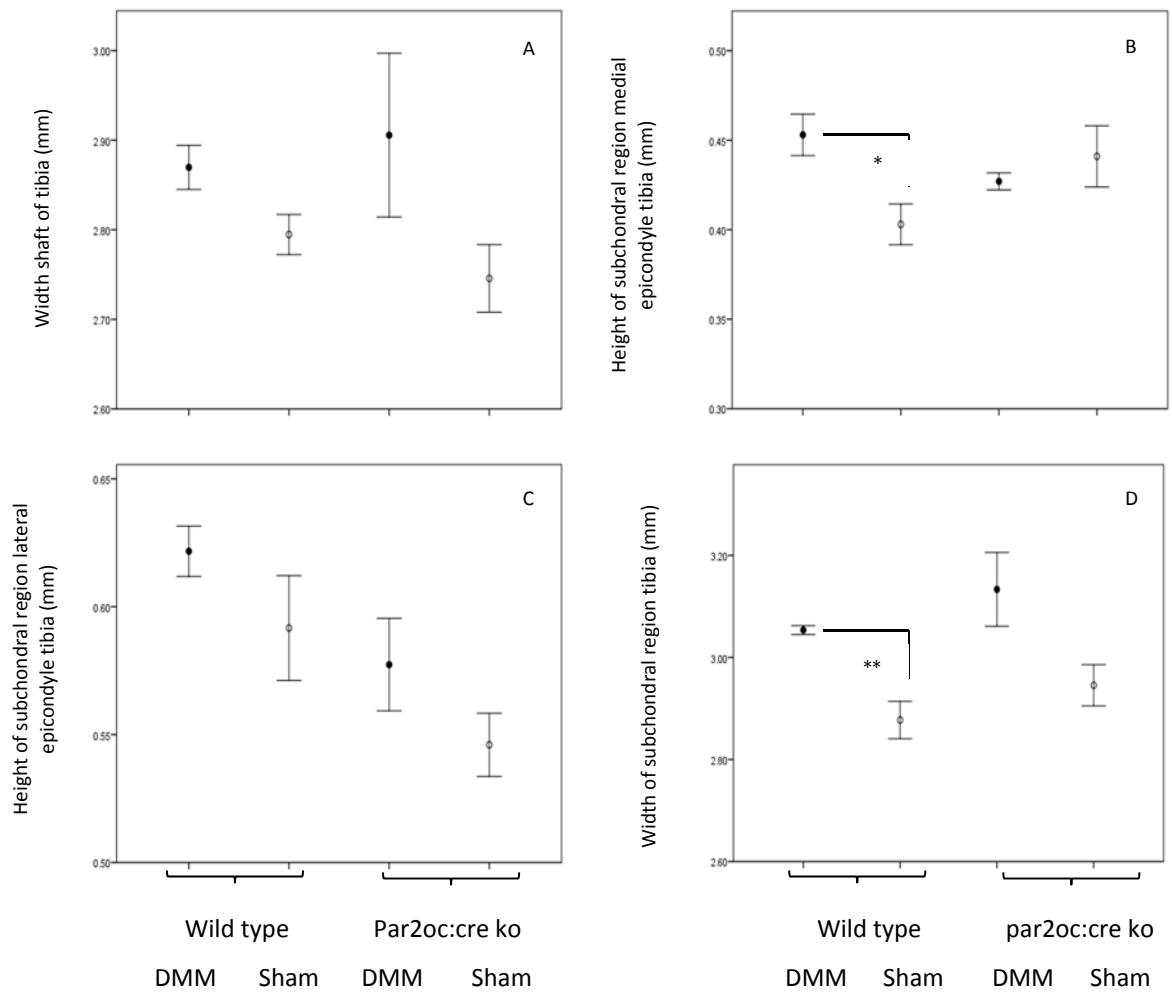


Figure 6.6: Subchondral tibial bone measurements; bone-specific PAR-2 ablated strain.

Mice were sacrificed at 8 week post-surgery and the left limb dissected and fixed in 10% paraformaldehyde. These limbs were subsequently scanned in a micro-CT SkyScanner. From the reconstructed scans, measurements of the subchondral bone were taken using CTan software (section 2.2.10.4). 3 DMM and 3 sham mice were used for measurement in each group. A – tibial shaft width; B – medial tibial epicondyle height; C – lateral tibial epicondyle height; D – width of tibial subchondral region. The mean width/height is given in mm (± 1 SE of the mean). Independent samples T-test.

6.2.3 Micro-CT analysis of subchondral sclerosis and trabecular morphology

The wild type bone remodelling results (chapter 4) can now be compared to the tissue-specific PAR-2 strains of knock out mice to detect any bone protection in terms of reduced subchondral sclerosis or reduced trabecular remodelling.

6.2.3.1 Cartilage-specific PAR-2 knock-out mice

6.2.3.1.1 Subchondral sclerosis

Shown in figure 6.7, the cartilage-specific PAR-2 ablated DMM mice exhibited subchondral sclerosis to similar levels as seen with the wild type sham mice, compared to the increased sclerosis observed in the wild type DMM mice. Furthermore, the DMM cartilage-specific PAR-2 ablated mice also had modestly more sclerosis compared to the corresponding sham and naïve groups, but not reaching significance. A one-way ANOVA test was performed revealing significant differences between groups ($F(4, 23) = 4.379$, $p < 0.01$), with the post hoc Tukey test showing where these differences were, as detailed in figure 6.7.

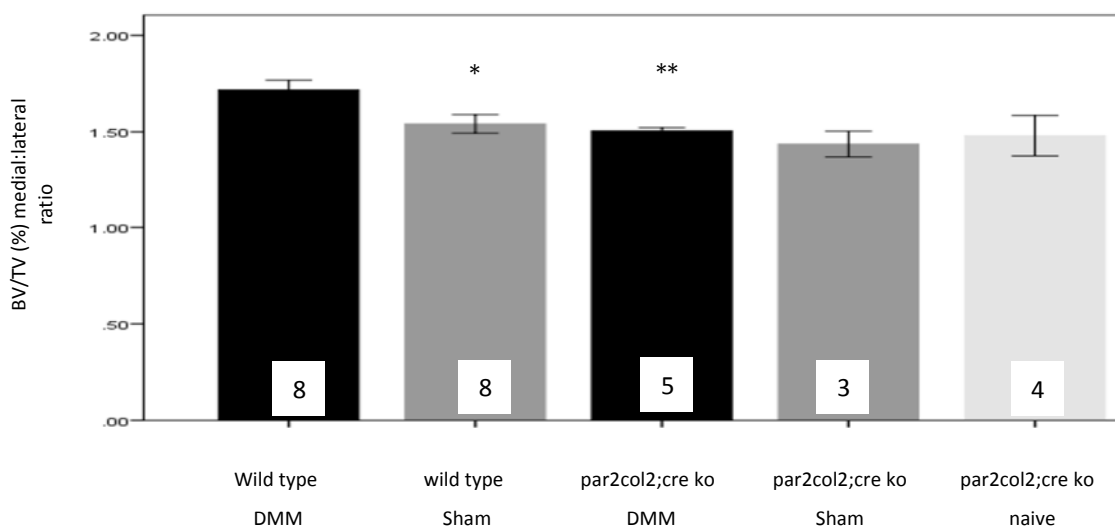


Figure 6.7: Measurement of subchondral sclerosis in wild type and cartilage-specific PAR-2 ablated mice. Mice underwent DMM or sham surgery at 10 weeks of age, or remained as naïve mice. At 8 weeks post-surgery mice were sacrificed and ipsilateral limbs harvested and fixed in 10% buffered paraformaldehyde for up to 72 hours. The limbs were then stored in 70% ethanol until use for micro-CT. Ipsilateral limbs were scanned in a micro-CT SkyScanner and images analysed as described in section 2.2.10. * $p < 0.05$ ** $p < 0.01$ compared to wild type DMM. The number in the white box represents the number of mice in each group. Error bars +/- SEM. One-way ANOVA test with post hoc Tukey test.

6.2.3.1.2 Alterations in trabecular morphology

Thicker trabeculae were observed in the wild type DMM group relative to wild type sham (figure 6.8A), and correlated with increased subchondral sclerosis in the wild type DMM group. Interestingly, the cartilage-specific PAR-2 knock-out DMM group had significantly thinner trabeculae compared to wild type DMM, and this corresponded with reduced subchondral sclerosis seen in this group. (Figures 6.7 and 6.8A) The cartilage-specific PAR-2 ablated DMM mice had modestly thicker trabeculae compared to the corresponding sham group (not reaching significance). Additionally, the cartilage-specific PAR-2 ablated sham group had reduced trabecular thickness compared to wild type sham (not significant). A one-way ANOVA revealed significant differences between groups ($F(4, 23) = 3.099, p < 0.05$), with the post hoc Tukey test detecting where these differences were, as detailed in figure 6.8A.

It would be expected that there would be increased trabecular separation in the groups with thinner trabeculae. Indeed, there was significantly increased trabecular separation in the cartilage-specific PAR-2 knock-out DMM group, relative to wild type DMM, with a similar pattern observed in the wild type sham group. (Figure 6.8B) The cartilage-specific PAR-2 ablated DMM group also had slightly reduced trabecular separation compared to the corresponding sham group, with trabecular separation almost equivalent between cartilage-specific PAR-2 ablated sham and wild type sham groups. There were significant differences between groups, as identified by a one-way ANOVA test ($F(4, 23) = 3.898, p < 0.05$), with the post hoc Tukey test identifying where these differences were, as shown in figure 6.8B.

The following observations described below relating to figure 6.8C were not significant, and increased numbers are required to corroborate these results. A higher number of trabeculae in the cartilage-specific PAR-2 knock-out DMM group relative to wild type DMM was observed, (with a similar pattern observed in the wild type sham group), however this did not reach significance. (Figure 6.8C) This was likely due to the observation that the wild type DMM group had thicker trabeculae compared to the other aforementioned groups, and these thickened trabeculae coalesce hence reducing the number of trabeculae. The cartilage-specific PAR-2 ablated DMM group also had a reduced number of trabeculae compared to the corresponding sham group, although this

was not significant. There were a greater number of trabeculae in the cartilage-specific PAR-2 ablated sham group relative to the wild type sham group. (Not significant) No significant differences between groups were identified using a one-way ANOVA test ($F(4, 23) = 1.618, p=0.204$).

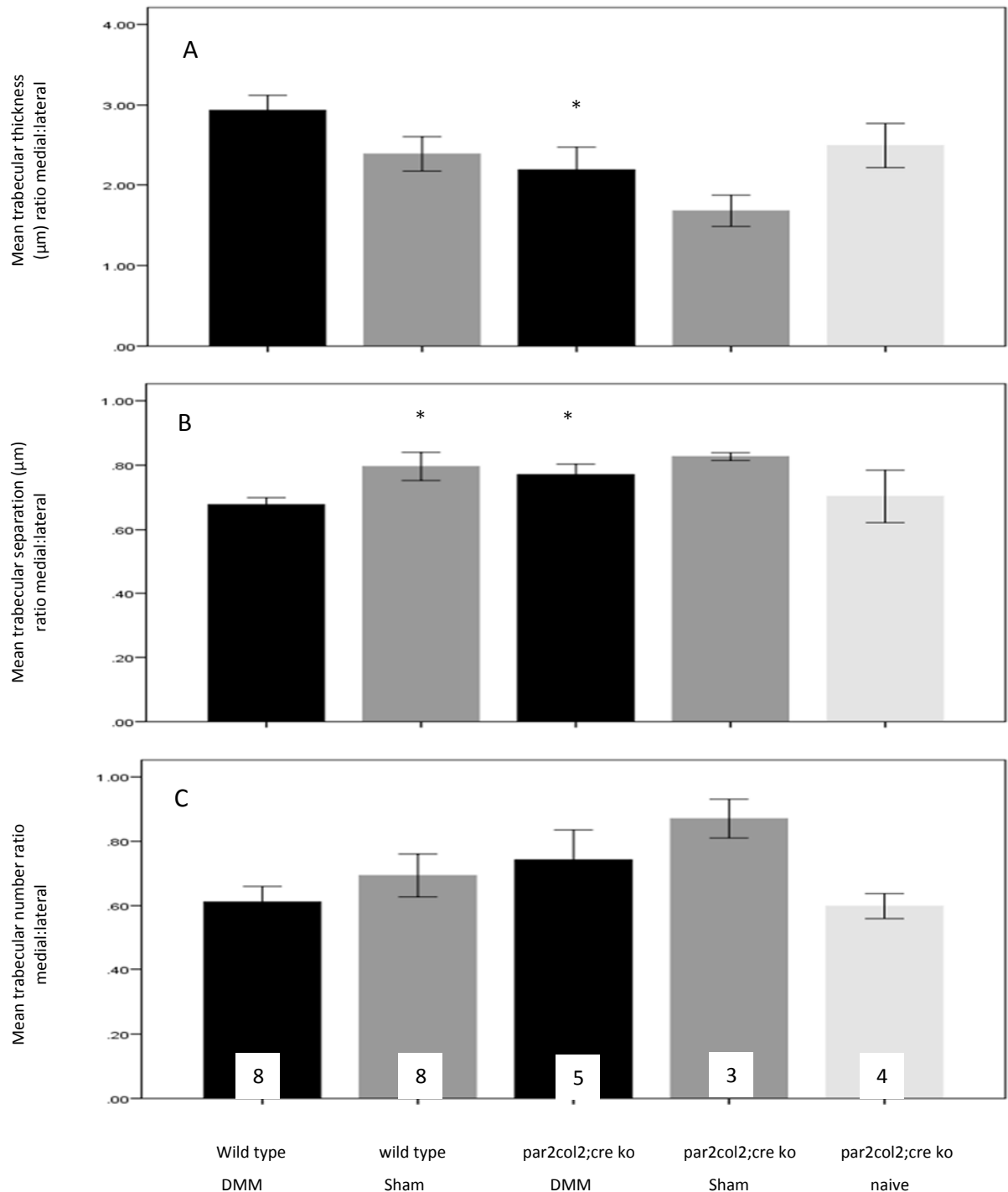


Figure 6.8: Measurement of trabecular morphology in wild type and cartilage-specific PAR-2 ablated mice. Images from murine joints (as detailed in figure 6.7) were assessed for trabecular thickness (A), trabecular separation (B) and trabecular number (C). * $p<0.05$ ** $p<0.01$ compared to wild type DMM. The number in the white box represents the number of mice in each group. Error bars are +/- 1 SE of the mean. One-way ANOVA test with post hoc Tukey test.

6.2.3.2 Bone-specific PAR-2 knock-out mice

6.2.3.2.1 Subchondral sclerosis

Shown in figure 6.9 there was significantly reduced subchondral sclerosis in the bone-specific PAR-2 knock-out DMM group relative to wild type DMM, similar to the wild type sham group. This pattern was also observed in the bone-specific PAR-2 sham and naïve groups, relative to the corresponding DMM group. A one-way ANOVA test revealed significant differences between groups ($F(4, 23) = 7.801, p < 0.001$), with the post hoc Tukey test revealing where these differences were, as shown in figure 6.9.

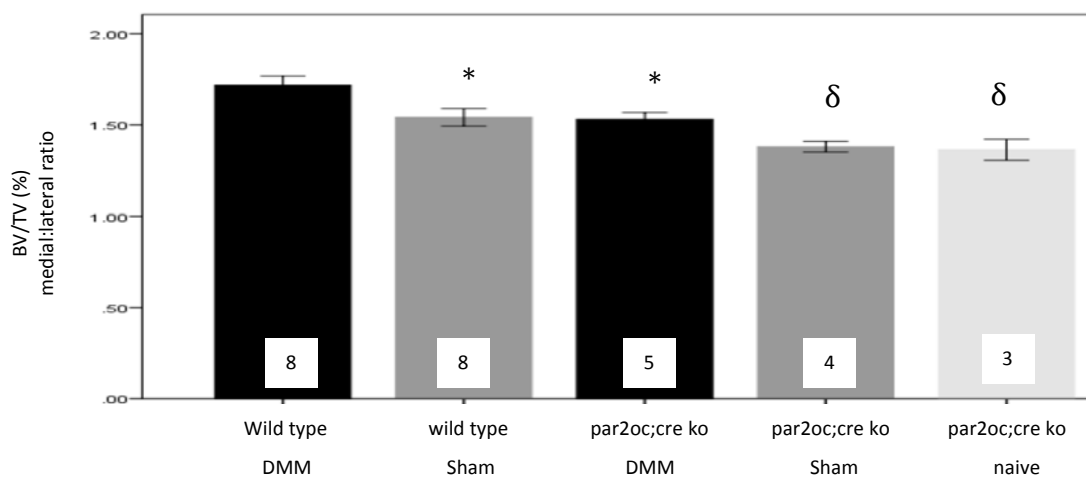


Figure 6.9: Measurement of subchondral sclerosis in wild type and bone-specific PAR-2 ablated mice.

Mice underwent DMM or sham surgery at 10 weeks of age, or remained as naïve mice. At 8 weeks post-surgery mice were sacrificed and ipsilateral limbs harvested and fixed in 10% buffered paraformaldehyde for up to 72 hours. The limbs were then stored in 70% ethanol until use for micro-CT. Ipsilateral limbs were scanned in a micro-CT SkyScanner and images analysed as described in section 2.2.10. * $p < 0.05$ compared to wild type DMM. δ $p < 0.05$ compared to par2oc;cre ko DMM. The number in the white box represents the number of mice in each group. Error bars +/- SEM. One-way ANOVA test with post hoc Tukey test.

6.2.3.2.2 Alterations in trabecular morphology

There were thicker trabeculae in the wild type DMM group relative to both the wild type sham and bone-specific PAR-2 knock-out DMM groups however, this difference was not significant. (Figure 6.10A) This corresponded with increased subchondral sclerosis observed in the wild type DMM group, shown in figure 6.9. Similarly, the bone-specific PAR-2 ablated DMM group had thicker trabeculae compared to both bone-specific PAR-2 knock-out sham and naïve groups (not significant), shown in figure 6.10A. There was also reduced trabecular thickness in the bone-specific sham group relative to the wild type sham group (not significant). A one-way ANOVA test revealed no significant differences between groups ($F(4, 23) = 2.404, p=0.079$).

As seen previously, the wild type DMM group had reduced separation between trabeculae compared to wild type sham, shown in figure 6.10B. However, although the bone-specific PAR-2 knock-out DMM group had reduced subchondral sclerosis and thinner trabeculae (figures 6.9 and 6.10A, respectively) this group did not have increased trabecular separation, compared to wild type DMM. (Figure 6.10B) This observation did not fit the pattern I had observed in the cartilage-specific PAR-2 knock-out strain, where reduced subchondral sclerosis and thinner trabeculae corresponded with increased trabecular separation. The bone-specific PAR-2 ablated DMM group had reduced trabecular separation compared to the corresponding sham and naïve groups, reaching significance compared to the naïve group. Trabecular separation was almost equivalent between wild type sham and bone-specific PAR-2 ablated sham groups. A one-way ANOVA test revealed significant differences between groups ($F(4, 23) = 3.574, p<0.05$), with the post hoc Tukey test revealing where these differences were, as detailed in figure 6.10B.

Shown in figure 6.10C, there was little difference between the bone-specific PAR-2 knock-out DMM group relative to wild type DMM in terms of the number of trabeculae. The bone-specific PAR-2 ablated DMM group had a reduced number of trabeculae compared to the corresponding sham and naïve groups, with a similar pattern observed in the wild type mice. (Not significant) Trabecular number was similar between wild type sham and bone-specific PAR-2 ablated sham groups. There were no significant differences between groups using a one-way ANOVA test ($F(4, 23) = 0.640, p=0.640$).

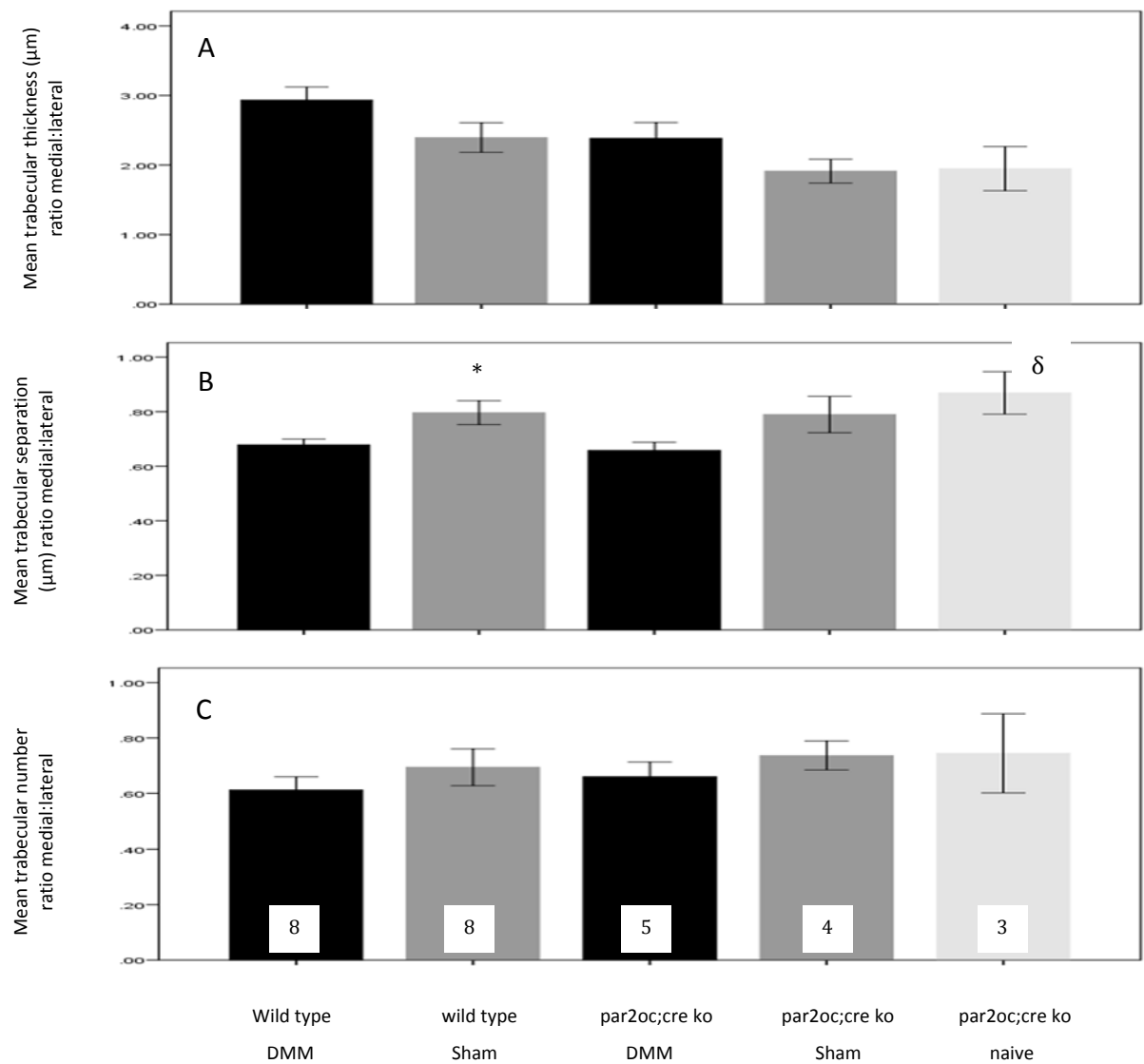


Figure 6.10: Measurement of trabecular morphology in wild type and bone-specific PAR-2 ablated mice. Images from murine joints (as detailed in figure 6.9) were assessed for trabecular thickness (A), trabecular separation (B) and trabecular number (C). * $p < 0.05$ compared to wild type DMM. δ $p < 0.05$ compared to par2oc;cre ko DMM. The number in the white box represents the number of mice in each group. Error bars +/- SEM. One-way ANOVA with post hoc Tukey test.

6.2.4 Micro-CT and histology images for osteophytes

Osteophytes were observed in both tissue-specific PAR-2 DMM ablated strains. Micro-CT representation of the osteophytes in both strains of knock-out mice (DMM) are shown in figures 6.11 and 6.12, images A and B top panel. The osteophytes are also identified by histology staining (H&E and safranin-O) showing an area of increased cell proliferation and extension of the medial aspect of the tibia compared to sham and naïve. (Figures 6.11 and 6.12, images C and D top panel) The middle and lower panels in figures 6.11 and 6.12 show a smooth contour to the medial tibial plateau in the sham and naïve mice, respectively, with no evidence of osteophyte formation on micro-CT (images A and B) or histological analysis. (Figures C and D)

From general observation of the osteophytes in figures 6.11 and 6.12, those in the cartilage-specific PAR-2 knock-out DMM strain (figure 6.11) appear to be smaller than in the wild type mice. (8 weeks post-surgery, figure 4.10 chapter 4) Also, the osteophytes in the bone-specific PAR-2 knock-out DMM group (figure 6.12) appear to be larger in size compared to wild type osteophytes in mice eight weeks post-surgery (figure 4.10, chapter 4) and cartilage-specific PAR-2 knock-out DMM strain. (Figure 6.11) Detailed analysis of osteophyte size, bone volume and number is provided in section 6.2.5.

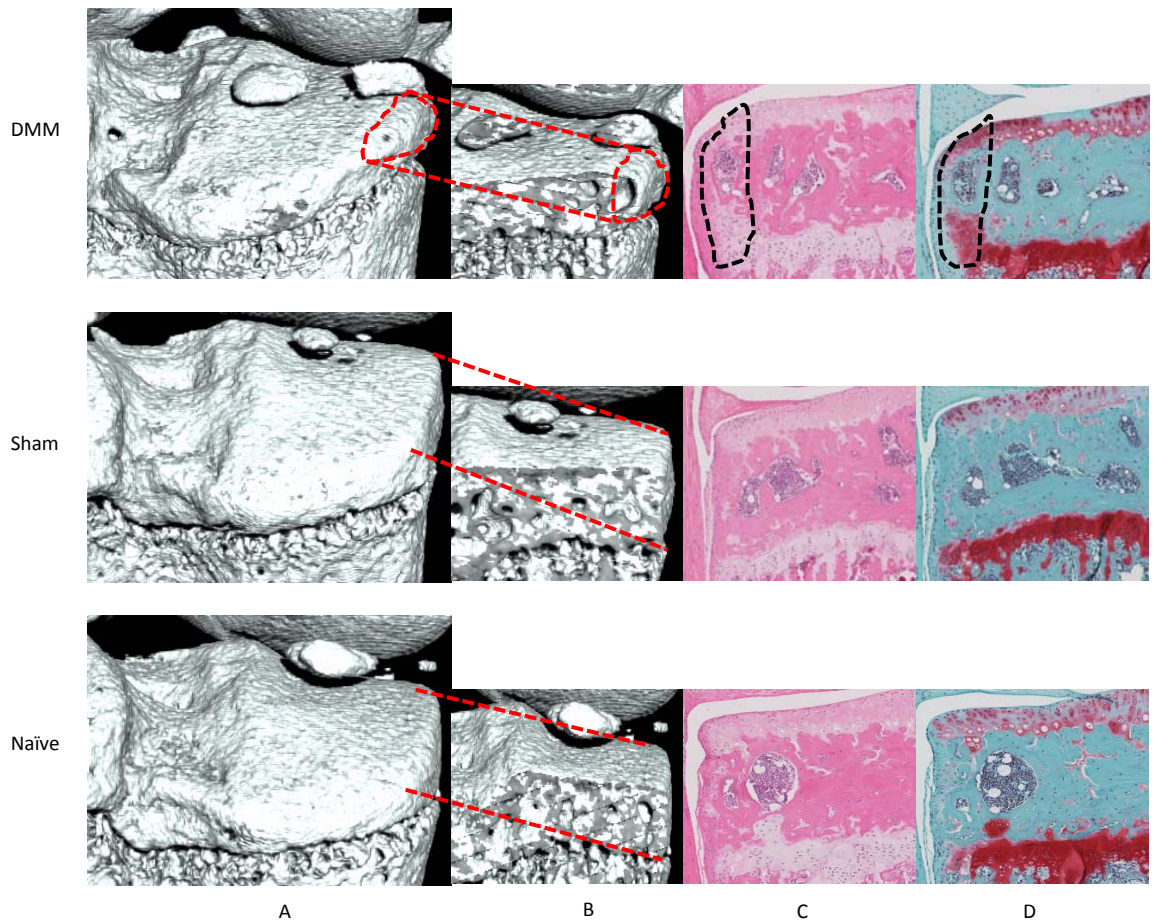


Figure 6.11: Osteophyte representation of cartilage-specific PAR-2 knock-out mice. PAR-2 col2;cre knock out mice underwent DMM or sham surgery at 10 weeks of age or remained naïve. These mice were then sacrificed at 8 weeks post-surgery. Limbs were processed for micro-CT as detailed in figure 6.9. 3D visualisation of the osteophytes then took place, using CTvox software as described in section 2.2.10.3. (Images A and B) Image B is a cross-sectional representation of image A, with the red slashed lines highlighting an osteophyte in the DMM model and smooth contour of the medial aspect of the tibia in the sham and naïve models. For images C and D after the bones had been scanned histological analysis then took place as described in sections 2.2.3 and 2.2.8 and visualisation of H&E (C) and Safranin-O (D) stained joints were carried out using a microscope. The black slashed lines in images C and D in the DMM model highlight an osteophyte on the medial aspect of the tibia.

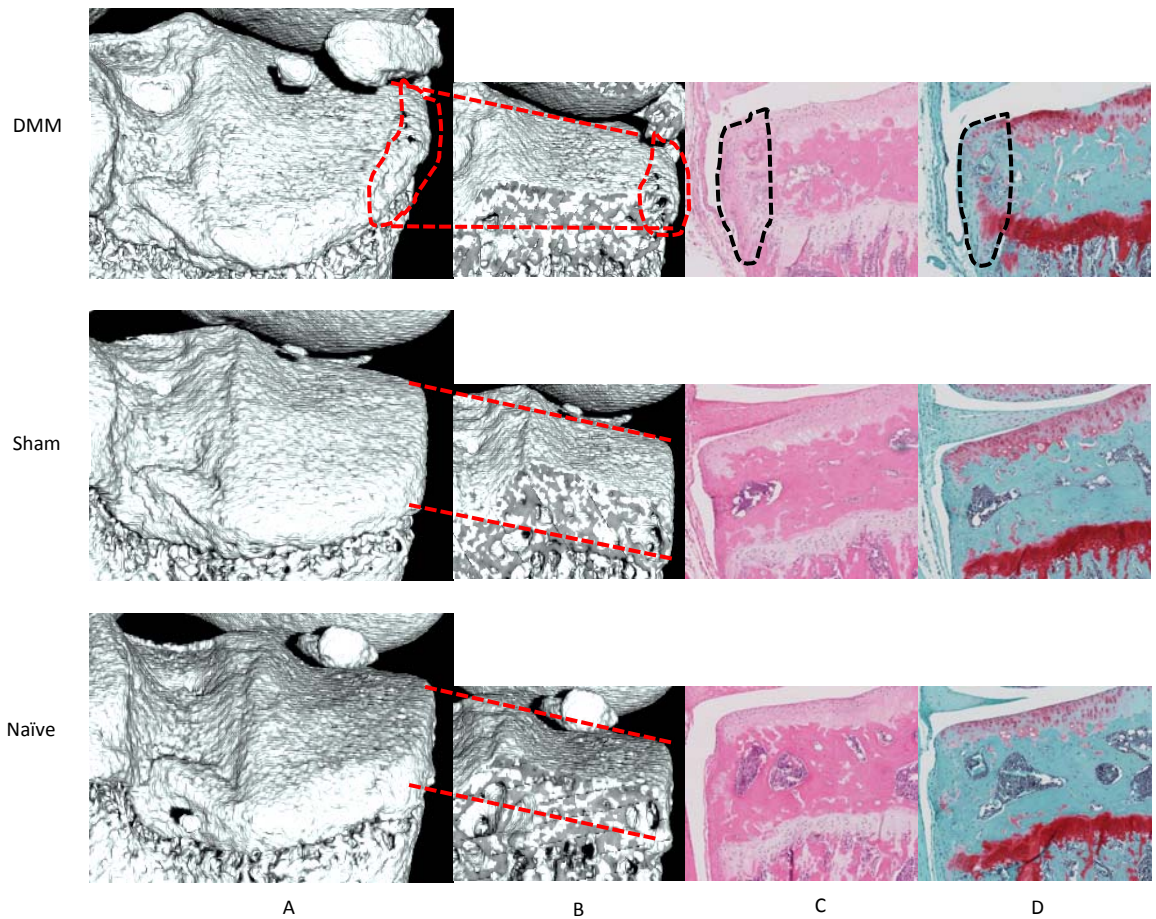


Figure 6.12: Osteophyte representation of bone-specific PAR-2 knock-out mice. PAR-2^{oc;cre} knock out mice underwent DMM or sham surgery at 10 weeks of age or remained naïve. These mice were then sacrificed at 8 weeks post-surgery. Limbs were processed for micro-CT as detailed in figure 6.9. 3D visualisation of the osteophytes then took place, using CTVox software as described in section 2.2.10.3. (Images A and B) Image B is a cross-sectional representation of image A, with the red slashed lines highlighting an osteophyte in the DMM model and smooth contour of the medial aspect of the tibia in the sham and naïve models. For images C and D after the bones had been scanned histological analysis then took place as described in sections 2.2.3 and 2.2.8 and visualisation of H&E (C) and Safranin-O (D) stained joints were carried out using a microscope. The black slashed lines in images C and D in the DMM model highlight an osteophyte on the medial aspect of the tibia.

6.2.5 Micro-CT analysis of osteophyte morphology in tissue-specific PAR-2 ablated mice relative to wild type

Analysis was performed to compare the characteristics of the osteophytes observed in the PAR-2 tissue-specific knock-out strains of mice relative to wild type mice, to detect any difference in the size, bone volume and number of osteophytes.

6.2.5.1 Cartilage-specific PAR-2 knock-out mice

Shown in figure 6.13A the size of the osteophytes measured (tissue volume) was less in the cartilage-specific PAR-2 knock-out DMM mice compared to the wild type DMM mice. However, this difference did not reach significance due to the variation between mice. The cartilage-specific PAR-2 knock-out mice had reduced osteophyte bone volume compared to wild type mice osteophytes, however this did not reach significance. (Figure 6.13B) This corresponded with the results in figure 6.13A, whereby the smaller osteophytes observed in the cartilage-specific PAR-2 knock-out mice had a reduced bone volume compared to wild type mice osteophytes. Also, the cartilage-specific PAR-2 knock-out mice had a reduced number of osteophytes than the wild type mice. Again this did not reach significance due to considerable variation between mice. (Figure 6.13C)

6.2.5.2 Bone-specific PAR-2 knock-out mice

The osteophytes in the bone-specific PAR-2 knock-out DMM mice were larger compared to the wild type DMM mice osteophytes, but this did not reach significance. (Figure 6.14A) Corresponding with the results in figure 6.14A, there was an increase in bone volume in the bone-specific PAR-2 knock-out mice relative to wild type DMM mice osteophytes (not reaching significance) shown in figure 6.14B. The bone-specific PAR-2 knock-out mice also had a reduced number of osteophytes detected compared to the wild type DMM mice, (figure 6.14C) but not reaching significance.

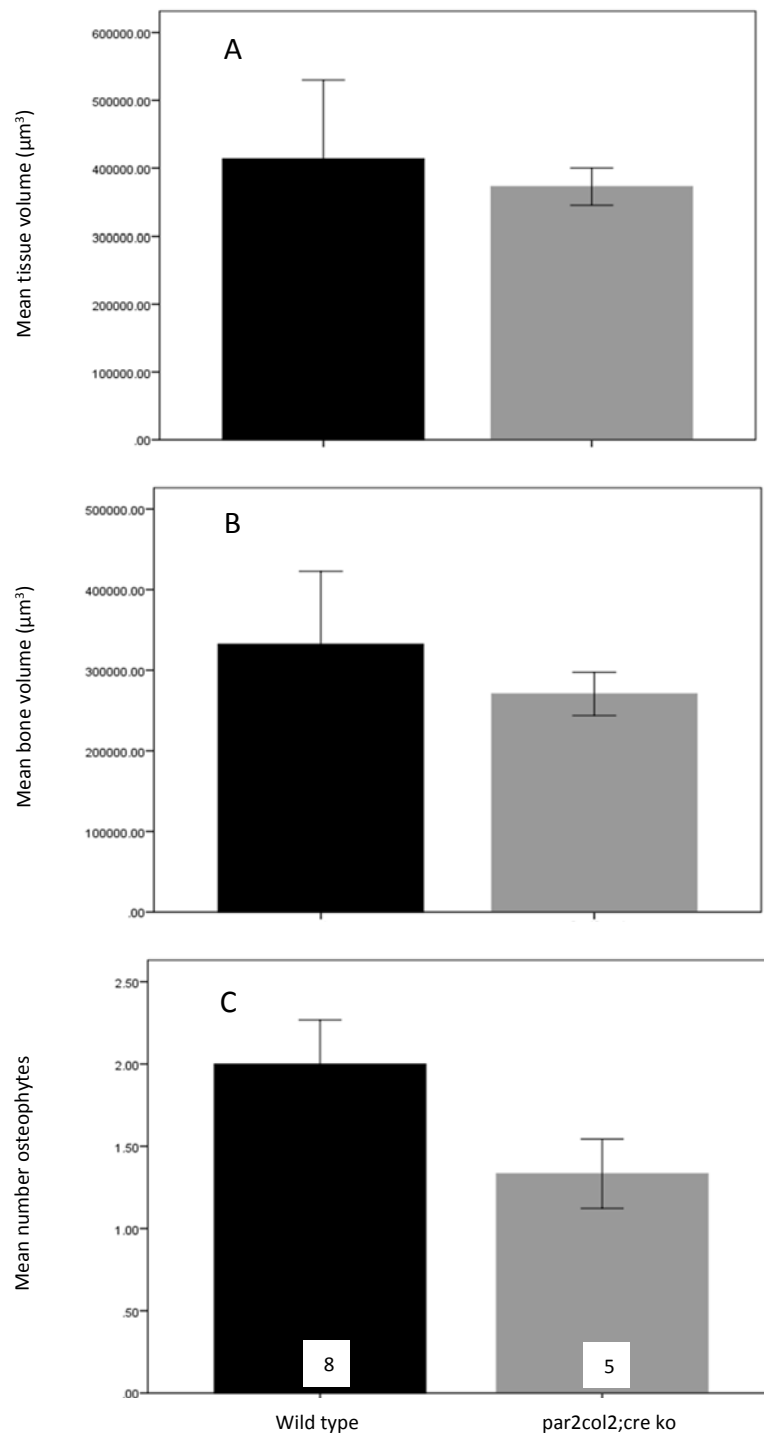


Figure 6.13: Analysis of osteophyte morphology; cartilage-specific PAR-2 ablated mice and wild type mice. Mice underwent DMM surgery at 10 weeks of age and were sacrificed at 8 weeks post-surgery. The ipsilateral limbs were harvested and fixed in 10% buffered paraformaldehyde for up to 72 hours. Limbs were then stored in 70% ethanol until micro-CT scanning using a SkyScanner micro-CT machine. Osteophytes were then visualised using Ctvox and CTan software and analysis performed as described in section 2.2.10.3. The largest osteophyte in each mouse was analysed for tissue volume (A), bone volume (B) and number (C). The number in the white box represents the number of mice in each group. Error bars are +/- SE of the mean. Independent samples T-test.

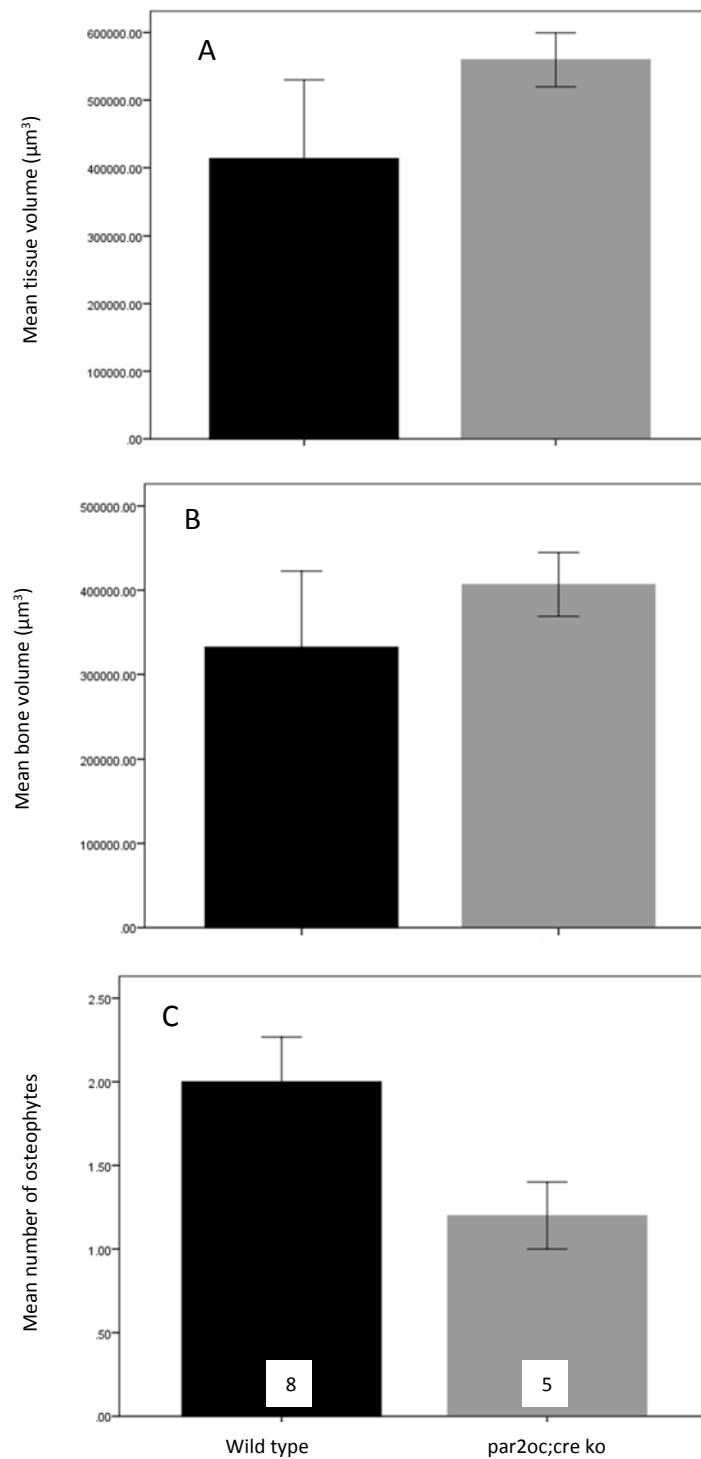


Figure 6.14: Analysis of osteophyte morphology; bone-specific PAR-2 ablated mice and wild type mice. Mice underwent DMM surgery at 10 weeks of age and were sacrificed at 8 weeks post- surgery. The ipsilateral limbs were harvested and fixed in 10% buffered paraformaldehyde for up to 72 hours. Limbs were stored in 70% ethanol until micro-CT scanning using a SkyScanner micro-CT machine. Osteophytes were visualised using Ctvox and CTan software and analysis performed as described in section 2.2.10.3. The largest osteophyte in each mouse was analysed for tissue volume (A), bone volume (B) and number (C). The number in the white box represents the number of mice in each group. Error bars are +/- 1 SE of the mean. Independent samples T-test.

6.2.6 Cartilage damage in tissue-specific PAR-2 ablated mice relative to wild type

6.2.6.1 Qualitative assessment of cartilage damage

Qualitative assessment of cartilage damage in figure 6.15 shows more severe cartilage damage in the DMM group relative to sham and naïve wild type mice, with a similar pattern in the cartilage-specific PAR-2 knock-out mice. Interestingly, referring to figure 6.15, the PAR2 oc;cre knock-out mice were an outlier to this trend, whereby the DMM group had less severe cartilage damage compared to wild type. Indeed, the PAR2 oc;cre DMM mice had very little cartilage damage compared to the sham and naïve mice in this group.

Shown in figure 6.15, the wild type DMM group had proteoglycan loss and fibrillations with a loss of viable chondrocytes and clustering, leaving exposed subchondral bone. This pattern was also observed in the cartilage-specific PAR-2 ablated group. However, this pattern was not seen in the PAR2 oc;cre DMM group whereby there was little proteoglycan loss and fibrillations, and there was no clustering of chondrocytes and no exposed subchondral bone. These features were best observed in the higher magnification (x10) images (DMM). The sham and naïve groups shown in figure 6.15 were very similar across all three genotypes with no disruption of the proteoglycan layer. This suggests some degree of cartilage protection in the bone-specific PAR2 knock-out group. This has been formally assessed using the OARSI scoring system by two blinded colleagues within MRG, section 6.2.6.2.

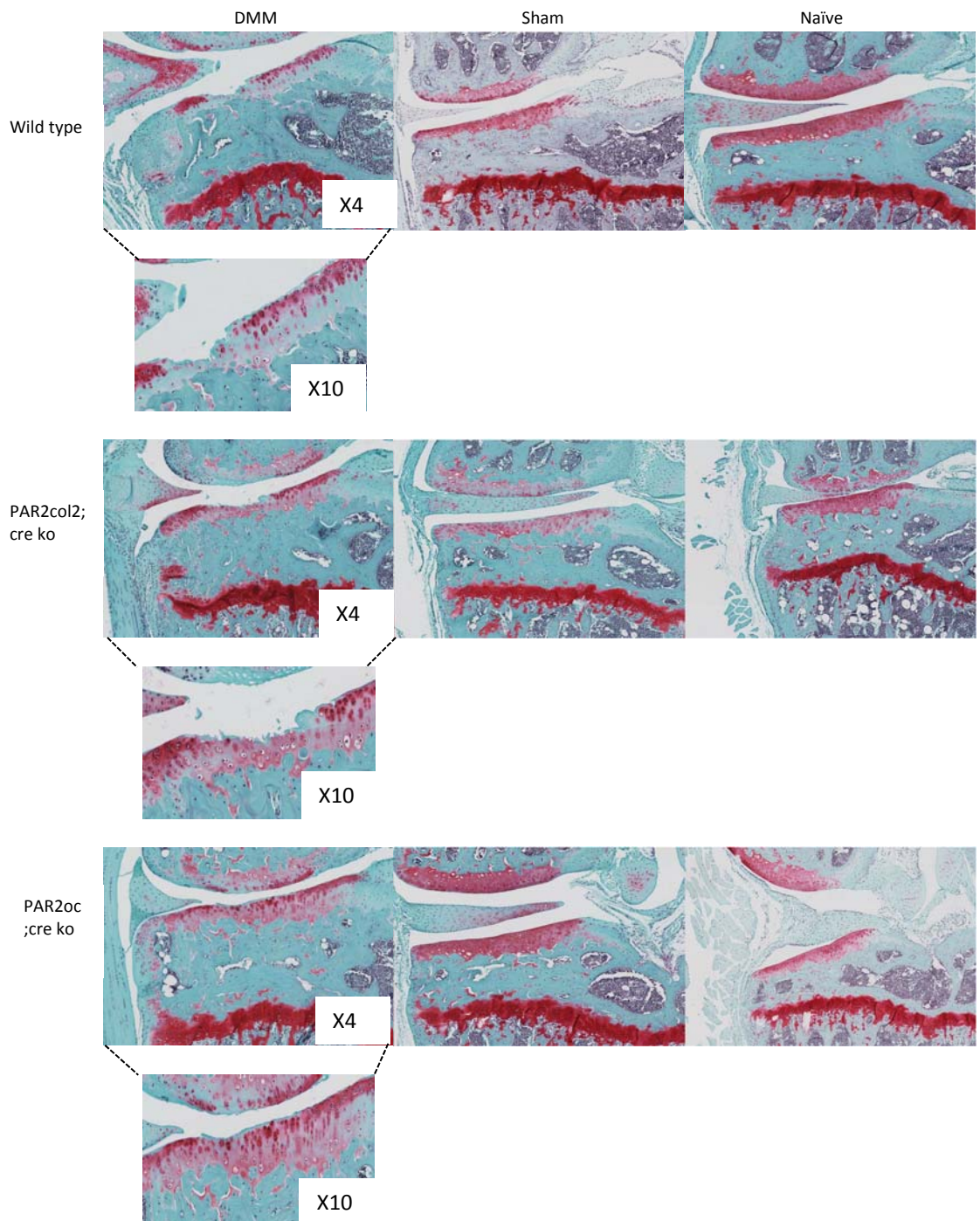


Figure 6.15: Qualitative assessment of cartilage damage. Wild type and PAR-2 ablated mice underwent DMM or sham surgery at 10 weeks of age or remained naive. These mice were then sacrificed at 8 weeks post-surgery. The affected limb was then dissected and fixed in 10% buffered paraformaldehyde for up to 72 hours and then transferred into 70% ethanol. Histological analyses then took place using Safranin-O, as described in sections 2.2.3 and 2.2.8. The red staining is proteoglycan content. The black slashed lines highlight a higher magnification image (x10) focusing on the medial aspect of the tibia.

6.2.6.2 Quantitative assessment of cartilage damage

Similar analyses using the OARSI histological scoring system for the mouse were used as described in section 2.2.16.

Referring to figure 6.16B, the cartilage-specific PAR2 knock-out DMM group had slightly less cartilage damage compared to the wild type DMM group (not significant, $p=0.315$) when using the summed scoring system. There was an outlier in the cartilage-specific PAR2 knock-out DMM group, which may explain why no significant differences were found between this group and the wild type DMM group. When using the best overall maximum score (figure 6.16A) there was no difference in cartilage damage between wild type and the cartilage-specific PAR-2 knock-out group. The bone-specific PAR2 knock-out DMM group had significantly less cartilage damage compared to the wild type DMM group. (Figure 6.16B) A similar pattern was seen in figure 6.16A where the bone-specific PAR-2 knock-out group had less cartilage damage compared to wild type DMM. The sham and naïve groups had very little cartilage damage in all three groups compared to the corresponding DMM model. A one-way ANOVA test was performed revealing significant differences between groups ($F(7, 24) = 42.209, p < 0.001$), with the post hoc Tukey test revealing where these differences were, as shown in figure 6.16 B.

These results corresponded with the qualitative assessment of cartilage damage (figure 6.15) where it was clear that the bone-specific PAR2 knock-out DMM group had significantly less cartilage damage than the wild type DMM group.

6.2.7 Correlation analysis

No correlation was found between histologic score and subchondral sclerosis within any of the two genotypes using Spearman's rank correlation analysis. Histologic cartilage damage score/subchondral sclerosis: cartilage-specific PAR-2 ablation $r=0.493$; bone-specific PAR-2 ablation $r=0.189$. (No significant results)

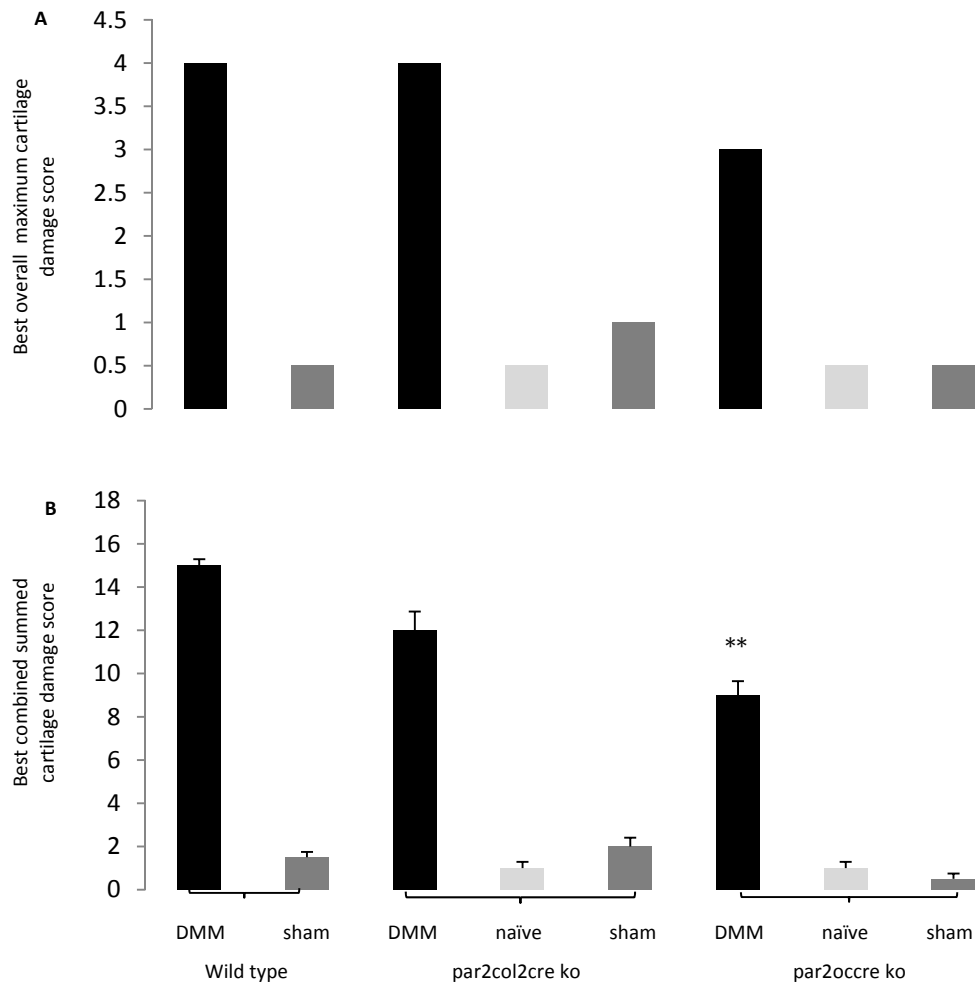


Figure 6.16: Quantitative assessment of cartilage damage. Wild type and gene ablated mice underwent DMM or sham surgery at 10 weeks of age or remained naïve. These mice were then sacrificed at 8 weeks post-surgery. The affected limb was then dissected and fixed in 10% buffered paraformaldehyde for up to 72 hours and then transferred into 70% ethanol. Histological analyses then took place as described in sections 2.2.3 and 2.2.8. The Safranin-O stained sections were then used to assess cartilage damage using the OARSI histological scoring system for the mouse, as described by Glasson et al. [1] There were 4 mice in each group and 6 sections analysed per mouse (24 sections total per group) giving a global representation of cartilage damage in each group. The scoring was carried out blinded by Prof Drew Rowan and Prof David Young. The best overall maximum score of cartilage damage at the medial tibial plateau (MTP) per group is shown in bar chart A. Bar chart B represents the best combined summed score of cartilage damage at the MTP per group. ** $p < 0.01$ compared to wild type DMM. Error bars +/- SD mean. One-way ANOVA test with post hoc Tukey test.

6.3 Discussion

6.3.1 Confirmation of gene ablation

As discussed in chapter 5, I carried out similar analyses including genotyping, qPCR (section 6.2.1.2; cartilage dissected from xiphisternum) and IHC to confirm successful gene ablation. Similarly, I attempted cartilage micro-dissection from the tibiae of mice and extraction of RNA followed by reverse transcription qPCR in order to detect PAR-2 and confirm successful ablation in the cartilage. However, as discussed in chapter 5, similar problems were encountered preventing use of this method to confirm gene ablation in the cartilage. Nevertheless, I was able to show successful PAR-2 ablation in the cartilage using genotyping, qPCR (cartilage dissected from xiphisternum; section 6.2.1.2) and IHC as shown in section 6.2.1 and Appendix D.

The bone-specific PAR-2 knock-out mice were more challenging to confirm successful ablation. Since the genotyping was performed using an ear notch the effects of *oc;cre* would not be observed, therefore I was able to show only the presence of *oc;cre* and the floxed PAR-2 allele, but not the excised product using semi-quantitative PCR. I was able to perform IHC on the bone-specific knock-out mice to show absent PAR-2 staining in osteoblasts. However, I was unable to perform qPCR on RNA to detect bone-specific ablation as there is no source of pure bone that I could dissect for RNA extraction, as the bone marrow contained in the bone would skew the results. I discussed the problem of confirming successful ablation of PAR-2 in the bone with various colleagues including Prof Rob van't Hof (University of Liverpool) and Dr Allie Gartland (University of Sheffield), but we could not come up with a solution.

Several ideas were suggested, such as isolating osteoblasts from the bone of wild type mice and bone specific knock-out mice and culture and expand these, extract the RNA and use for qPCR. However Prof Rob van't Hof was not too hopeful of the success of this method as there is very low expression of PAR-2 in osteoblasts, and there were time constraints to perform this. Another suggestion by Dr Gartland was perhaps to attempt in-situ hybridisation techniques on the bone. However, again this method would likely not be suitable to confirm gene ablation due to the heterogeneity of bone tissue. Also, IHC is a very similar technique, staining the protein rather than the RNA. Therefore, for the bone-specific knock-out I confirmed the presence of genomic *oc;cre* and the floxed allele

using semi-quantitative PCR (which alluded to successful ablation in the bone) and IHC showing absent staining for PAR-2 in the osteoblasts of the knock-out mice. Additionally, observation of a phenotype circumstantially implies excision.

6.3.2 Mouse weights and subchondral bone measurements of the transgenic mice compared to wild type

Similar to the cartilage-specific matriptase ablated mice, there were no significant differences in mouse weights between wild type and the two PAR-2 transgenic groups, suggesting no gross developmental deviances.

In the cartilage-specific PAR-2 ablated mice, there was little variation in the tibial measurements in the DMM or sham models, compared to wild type. The only significant findings were observed when measuring the lateral tibial epicondyle height, in the DMM model. Also, in the sham groups there was significant variation in the width of the subchondral region in the ablated group relative to the corresponding wild type group.

Additionally, in the bone-specific PAR-2 ablated group there were no significant differences in any of the tibial measurements in the DMM or sham groups, compared to wild type.

As discussed in chapter 1 (1.6), PAR-2 has multiple complex signalling pathways, which can induce the expression of pro-inflammatory cytokines and MMPs, with subsequent effects on bone remodelling. This may account for some of the differences I have observed in the tibial bone measurements in the tissue-specific PAR-2 ablated mice.

6.3.3 Does cartilage-specific gene ablation of PAR-2 confer any protection against cartilage degradation or subchondral bone remodelling?

Numerous animal studies have shown that global ablation of PAR-2 protects against cartilage degradation and abnormal subchondral bone remodelling in OA [117, 135, 137, 139, 232, 252]. However, the tissue in which primary protection is conferred upon ablation of PAR-2 remains unanswered. As discussed in chapter 4, a recent study by Huesa et al. showed that in a murine OA model subchondral bone sclerosis occurred first preceding cartilage damage [232]. This suggests that increased stiffness of the bone is a prerequisite for cartilage damage to occur, and that cartilage damage cannot occur

independently, as proposed by Radin et al. [246]. In contrast to this, I observed that by ablating PAR-2 specifically in the cartilage there was protection against subchondral sclerosis, whilst cartilage damage was still occurring to some degree. (Albeit less than wild type) This suggests that cartilage damage was occurring independently of subchondral sclerosis, corroborated by the fact that there was no correlation found between cartilage damage and subchondral sclerosis in the cartilage-specific PAR-2 ablated mice. Indeed, the study by Huesa et al. also found that in global PAR-2 ablated mice, transfection of hPAR-2 caused significant cartilage damage with no significant increase in subchondral sclerosis. This confirms my observations that cartilage damage can occur independently of subchondral sclerosis [232].

Therefore, it is apparent from my study that cartilage-specific PAR-2 ablation conferred its primary protective effect in the subchondral bone, and cartilage damage was occurring independently from subchondral sclerosis. My observations suggest that cartilage damage can occur first in OA pathology, which is in contrast to the long-standing view proposed by Radin et al. that subchondral sclerosis is a prerequisite for cartilage damage [246].

The debate about whether cartilage changes or subchondral bone changes occur first in OA remains controversial, with evidence to support both theories. In support of my work, a study by Botter et al. found in a murine global ADAMTS-5 knock out DMM model there was no correlation between cartilage damage and subchondral sclerosis, suggesting these changes occurred independently. The ADAMTS-5 knock-out mice had significant cartilage damage, but minimal worsening of subchondral sclerosis in a DMM model relative to control [239]. This suggests, similar to my results that cartilage damage can occur independently of subchondral sclerosis. Further confirming this observation is a study by Intema et al. who found in a canine Groove and ACLT model that there was a reduction in bone volume and trabecular thickness correlating with a significant increase in cartilage damage compared to sham. The decrease in bone volume likely results in more softened and fragile bone so the cartilage damage occurring in OA cannot be secondary to increased subchondral sclerosis with more stiffened bone, as the opposite was observed in this study [242].

In contrast to these findings and my results, a study by Wang et al. found that subchondral bone changes occurred first in a guinea pig spontaneous OA model. This group found no cartilage damage at 3 months, however found increased subchondral sclerosis and BV/TV and thicker trabeculae [81]. A similar study by Zamli et al. using the same model of OA, also observed that subchondral bone plate thickening occurred first subsequently followed by cartilage degradation [254]. Additionally, Huesa et al. found in a murine wild type DMM model that subchondral bone changes preceded cartilage damage [232]. This suggests that abnormal subchondral bone remodelling is occurring first at an early stage, predisposing to cartilage damage at a later stage, in support of the proposal by Radin et al. [246].

These contrasting results may be due to differences in the type of animal and model analysed. My study and research by Botter et al. were knock-out studies, and it may be that by ablating PAR-2 or ADAMTS-5 there was primary protection against subchondral sclerosis, however cartilage damage was still occurring independently [239]. Other research carried out by Wang et al., Zamli et al. and Huesa et al. were time course studies in a spontaneous or surgically-induced OA model, respectively, and found subchondral bone changes preceded cartilage damage [81, 232, 254]. These studies and my research suggest that in the progression of OA, subchondral sclerosis does indeed precede cartilage damage. However, cartilage damage is not necessarily dependent on subchondral sclerosis and can occur independently.

6.3.4 Does bone-specific gene ablation of PAR-2 confer any protection against cartilage degradation or subchondral bone remodelling?

The results in section 6.2.3.2 showed protection against abnormal subchondral bone remodelling and also significant cartilage protection in the bone-specific PAR-2 DMM ablated mice relative to wild type DMM mice. This suggests that ablating PAR-2 specifically in the bone had a primary beneficial effect in preventing abnormal subchondral bone remodelling, similar to the cartilage-specific PAR-2 ablated group. Looking closely at the results it would appear that the subchondral sclerosis and trabeculae thickness in the bone specific PAR-2 ablated mice (DMM) were equivalent to the wild type sham group. In contrast, the cartilage damage score in the bone specific PAR-2 ablated group (DMM) was significantly worse than the wild type sham group. This

would suggest, (similar to the discussion in 6.3.3) that cartilage damage was occurring independently from subchondral sclerosis and can indeed occur first in OA. The lack of correlation between histologic score and subchondral sclerosis within this group also suggested that cartilage damage was occurring independently. The argument that cartilage damage can occur independently of subchondral sclerosis has been discussed in section 6.3.3 and has been corroborated in several studies [232, 239, 242].

6.3.5 Cartilage specific PAR-2 ablation affects osteophyte morphology

Although the cartilage-specific ablation of PAR-2 reduced the size and bone volume of the osteophytes, this was only a slight reduction and not significant. The cartilage-specific PAR-2 ablated group also had a reduced number of osteophytes relative to control. In the study by Huesa et al. this group found that by globally ablating PAR-2 the osteophytes were smaller, did not increase in size with time and not all the mice displayed osteophytes relative to control. This suggests a role of PAR-2 in OA-related osteophyte maturation. My results suggest that PAR-2 expressed in the cartilage, may play a role in osteophyte maturation in regards to regulating osteophyte size, bone volume and formation, similar to the study by Huesa et al. [232]. This observation will be discussed further in chapter 7.

Bone-specific ablation of PAR-2 caused the osteophytes to become larger with a higher bone volume. Also, in this group, I found a reduced number of osteophytes compared to wild type. It may be that PAR-2 expressed in the bone is also involved in osteophyte size, bone volume and formation, but has differing effects on osteophyte maturation than PAR-2 expressed in the cartilage.

6.3.6 Summary

- PAR-2 ablation in cartilage or bone specifically, had its primary beneficial protective effect in the subchondral bone via modulation of subchondral bone remodelling, rather than through a direct chondroprotective role.
- My results support the argument that cartilage damage can occur independently of subchondral sclerosis, and indeed can occur first in OA. (Discussed further in chapter 7)

- Lack of PAR-2 expressed in the cartilage affects osteophyte morphology and number, whilst lack of PAR-2 expressed in the bone had opposing effects on osteophyte morphology, but reduced the number of osteophytes.

Chapter 7: General Discussion

The main aims of this study were:

1. To generate tissue-specific PAR-2 and matriptase ablated mice, and compare remodelling events in cartilage and subchondral bone to wild type mice in a surgical model of OA.
2. Produce a reliable and reproducible model of cartilage catabolism derived from a human source, in which I aimed to analyse the effects of matriptase and over-express PAR-2 allowing more detailed functional analysis.

7.1 Perspective

There are no current therapies to prevent or cure OA, with late stage OA resulting in surgical intervention. By using transgenic animal models, the role of specific genes in the pathogenesis of OA can be analysed, guiding future therapies. PAR-2 is a GPCR known to be involved in OA pathology, with an inhibitor of this receptor showing significant protection against OA in a murine DMM model [137]. Further extending this work, tissue specifically ablating PAR-2 has allowed observation of which tissue the primary protective effect was conferred and which tissue should be preferentially targeted with therapeutics.

There is a need for a model of cartilage catabolism derived from a human source, as this will allow detailed functional analysis of different genes involved in OA pathology. However, there has been significant difficulty in generating such a model, and so further work is needed in this area.

7.2 Tissue-specific ablation of PAR-2 confers some protection against abnormal subchondral bone remodelling and cartilage degradation, but should cartilage or bone be targeted with therapeutics?

As discussed in chapter 6, tissue-specific ablation of PAR-2 had its primary protective effect in the subchondral bone, whilst some degree of cartilage damage was still occurring. This shows cartilage damage can occur independently from subchondral sclerosis and can arise first in OA pathology. The most significant protection against cartilage damage and subchondral bone remodelling was observed in the bone-specific PAR-2 ablated mice. This suggests that targeting the bone may be most beneficial for OA

therapies. However, targeting the cartilage should still be considered, as my results show similar protection against cartilage damage (albeit to a lesser degree) and subchondral sclerosis. Larger numbers of mice are needed in each group to confirm my results. In favour of targeting the bone is the fact that it is vascularised, hence providing an easier target for therapies compared to the cartilage, which is avascular. There is evidence to show targeting either the subchondral bone or cartilage may be beneficial in preventing OA pathology progressing and this will now be discussed.

Cartilage-specific gene ablation and the effects on cartilage and subchondral bone remodelling have also been carried out by several other groups. A study by Kim et al. used a similar murine DMM model of OA with cartilage-specific ablation of Zip 8 (a zinc importer involved in zinc homeostasis and activation of matrix-degrading enzymes). This group observed that by ablating Zip 8 specifically in the cartilage there was significantly less cartilage damage and subchondral bone sclerosis [255]. Additionally, a study by Wang et al. ablated MMP-13 specifically in the cartilage using a murine meniscal-ligamentous injury (MLI) model of OA. (MMP-13 is a downstream product of PAR-2 signalling involved in collagen breakdown). Previous work by Little et al. globally ablated MMP-13 in a murine DMM model and found cartilage protection in the ablated group relative to control [256]. Wang et al. built on this body of work and showed that by ablating MMP-13 specifically in the cartilage there were significantly lower cartilage damage scores and reduced chondrocyte apoptosis, relative to control. This group did not analyse subchondral bone remodelling, so no data have been provided on this [257]. These studies are similar to my work using cartilage-specific PAR-2 ablation in a murine DMM model. The study I have carried out, and work by others discussed above, suggests that targeting the cartilage to prevent OA pathology may indeed be beneficial. However, this may be problematic for therapies due to the avascular nature of cartilage. Indeed, targeting the bone may be more advantageous and will now be discussed.

As discussed, abnormal subchondral bone remodelling has been implicated in the initiation and progression of OA [246]. This raises the possibility that early intervention which reduces bone sclerosis may retard the loss of articular cartilage. Alendronate (ALN) is a bisphosphonate, which inhibits osteoclastic bone resorption mainly used in the treatment of osteoporosis. It has been shown that patients with osteoporosis receiving ALN therapy have histologically normal bone [258]. Therefore, by using ALN to prevent

abnormal subchondral bone remodelling, the effects of this on cartilage remodelling can be observed.

Hayami et al. investigated the effects of ALN on abnormal cartilage and subchondral bone remodelling in a rat ACLT model. Interestingly, this group found ALN treatment reduced subchondral bone turnover (assessed measuring urinary CTX-I) and also completely inhibited the early bone loss and the subsequent late bone increase seen in the control group. Correspondingly, ALN treatment significantly reduced the severity of cartilage degradation relative to control [259]. This suggests that by preventing the abnormal subchondral remodelling events observed in OA, this can reduce cartilage damage.

Further supporting the argument of targeting bone to prevent OA pathology progressing, are studies by Mouritzen et al. and Christgua et al. Discussed in chapter 1 was the link between alterations in BMD and progression of OA. Indeed, the aforementioned studies found that by preventing a reduction in BMD there was reduced cartilage damage observed. Post-menopausal women are at higher risk of developing osteoporosis due to a reduction in oestrogen levels. Oestrogen has a protective effect on bone by decreasing osteoclast number and activity, and so slowing bone turnover. Indeed, Mouritzen et al. found that post-menopausal women taking hormone replacement therapy (HRT) had less cartilage turnover (measured by urinary CTX-II) compared to age- and BMI-matched women not receiving HRT [260]. On a similar note, an animal study by Christgau et al. found that by treating ovariectomized rats with a selective oestrogen-receptor modulator (SERM) there was a reduction in bone resorption (measured by the rCTX-I marker) and also a reduction in cartilage erosion observed and measured using the CTX-II marker, compared to control rats [261]. A further study by Behets et al. also targeted the bone using calcitonin in an ACLT dog model. This group found that in the operated group of dogs receiving calcitonin there was no reduction in BMD compared to the operated placebo group where the BMD was reduced. This corresponded with significantly reduced cartilage damage scores in the calcitonin treated group relative to control [262].

Thus, these studies suggest that by preventing alterations in BMD, there is less cartilage damage/turnover observed. It cannot be disregarded that HRT and SERMs have direct chondroprotective effects, however cartilage is not generally viewed as an oestrogen-responsive tissue, so it is likely that the cartilage protection observed in these studies is

via modulation of abnormal bone remodelling. The evidence discussed suggests that targeting either the bone or cartilage may be beneficial in preventing OA pathology but for ease of use, therapeutics targeted towards bone may be more useful.

The fact that I have observed protection against abnormal subchondral bone remodelling and some degree of cartilage protection in the cartilage- and bone-specific PAR-2 ablated mice explains why global PAR-2 ablation has such significant protection against subchondral sclerosis and cartilage damage, as observed by Ferrell et al. [137]. By showing that tissue-specific PAR-2 ablation also has similar protection this will allow more targeted therapeutics in the future. For example, it may be possible to design a bone-specific PAR-2 inhibitor in the future to prevent OA progression. This will be beneficial as PAR-2 is also involved in other important physiological processes, such as inflammation, immunological regulation and pain processing. Therefore, it can be postulated that there will be less side effects for the patient by using a tissue-specific PAR-2 inhibitor. However, designing such an inhibitor may be challenging, with associated expense.

7.3 Cross-talk between cartilage and subchondral bone in the progression of OA is not a prerequisite for cartilage damage to occur

As discussed in chapter 1, there is likely significant cross-talk between cartilage and subchondral bone in the progression of OA. This includes functional cross-talk and increased vascularization, allowing transfer of soluble factors (such as cytokines) between cartilage and bone. Recent research carried out by Huesa et al. supports the theory that subchondral bone changes do indeed precede cartilage damage in a murine OA model, and an element of cross-talk between these two tissues is involved in OA progression. This supports the hypothesis that subchondral sclerosis occurs first, altering load transmission to the overlying cartilage, resulting in cartilage damage as the time course progresses (functional cross-talk) [232]. Additionally, increased vascularization and transfer of soluble factors between sclerotic osteoblasts and the overlying cartilage, likely plays a role in cross-talk and progression of OA. As discussed in chapter 4, I would likely have found similar results if I had started the murine OA time course earlier.

However, as discussed in chapter 6, similar to the work carried out by Huesa et al. I found that cartilage damage can occur independently of subchondral sclerosis, and so functional cross-talk is not a prerequisite for cartilage damage to occur. Therefore, a preliminary

conclusion is that OA changes in bone are mediated by PAR-2, accelerating the pathogenic phenotype. So although bone changes do precede cartilage damage in the progression of OA, these changes are not necessarily required for cartilage damage to occur, which appeared to occur independently and did not involve cross-talk [232].

7.4 The effects of tissue-specific PAR-2 ablation on osteophyte development and maturation

Recent work carried out by Huesa et al. found that in PAR-2 deficient mice there were fewer osteophytes, which were smaller and did not increase in size with time compared to wild type mice. I have also observed a reduced number of osteophytes in the bone-specific and cartilage-specific PAR-2 ablated strains of mice, which were smaller in the cartilage-specific PAR-2 ablated group. In the paper by Huesa et al. histology also revealed these osteophytes expressed Sox-9 and Runx-2, which suggests hypertrophic chondrocytes. Additionally, PAR-2 was expressed in these osteophytes, but was absent in the growth plate, suggesting expression of PAR-2 in osteophytes is pathological. This implies that PAR-2 regulates early osteophyte formation via its presence in chondrocytes, or cells with a chondrocytic phenotype [232, 263].

Interestingly, a paper by Ono et al. found that cells expressing col2-cre contributed to perichondral pre-osteoblasts during embryonic development and also contributed to a great majority of osteoblasts during postnatal bone development. Therefore, most osteoblasts in endochondral bones are derived from mesenchymal progenitors that express col2-cre at some point in their development [264]. This finding is pertinent to osteophyte development, which form via endochondral ossification. This suggests that by ablating PAR-2 using the col2-cre promoter it is likely that PAR-2 is not only ablated in chondrocytes but also ablated in a vast number of osteoblasts too (or at least pre-osteoblasts). This may explain why ablating PAR-2 in the cartilage has more of an effect on osteophyte formation and maturation than the bone-specific PAR-2 ablated group.

7.5 PAR-2 and musculoskeletal ageing

Discussed in chapter 1 were the effects of ageing on the different components of the musculoskeletal system, with an increased incidence of OA as people age. In this study, the time course of a murine wild type surgically-induced OA model displays pertinent features of pathological musculoskeletal ageing, particularly cartilage catabolism. It can therefore be thought that this surgically-induced model of OA mirrors some aspects of pathological ageing in the musculoskeletal system, albeit at an accelerated rate.

Ideally, an aged mouse would be used as an OA model in this study. However, there would be significant variability in those mice developing OA and it would also be very expensive to perform such a study. It could be speculated from this study that by tissue-specifically ablating PAR-2, this can prevent the pathological ageing process of cartilage catabolism. Therefore, it may be useful to ablate PAR-2 tissue-specifically in wild type naïve mice, and analyse whether this protects against cartilage catabolism, compared to naïve wild type age-matched control mice. This would provide more information about the role of PAR-2 in ageing, specifically cartilage catabolism. Indeed, in personal communication with Professor Drew Rowan, research in Glasgow found in naïve aged mice with global ablation of PAR-2 there was less cartilage damage compared to naïve age-matched wild type mice. This confirms the important role of PAR-2 in musculoskeletal ageing, particularly cartilage catabolism.

7.6 Potential use of biomarkers to detect early stage OA

Although my results show that cartilage damage can occur independently from subchondral sclerosis, several studies analysing the time course of OA (surgically-induced or spontaneous) have found that subchondral bone changes precede cartilage damage [81, 232, 254]. As discussed, it is likely that in the progression of OA subchondral bone changes do indeed occur first, and I would also have found this in wild type mice if my time course study had begun earlier. Therefore, I suggest that biomarkers to detect early stage OA should be specific to bone. However, despite significant work, there is currently no biochemical test for early stage OA, so this is an area of interest [265, 266]. Many biomarkers are under investigation, including those linked to collagen, bone and aggrecan metabolism, inflammation and proteases, however none are currently in clinical use [266].

An avenue of interest for developing biomarkers to use in clinical practice is the use of antibodies as biomarker-based imaging probes. These probes represent a novel way of acquiring information on disease progression and onset that cannot be obtained using conventional metabolic tracers. For example, a study by LeBeau et al. developed an active-site-specific, recombinant human antibody for matriptase, which localizes to cancer cell lines and can be used as a tumorigenic biomarker, specifically in colon cancer. This allows the activity of the active form of matriptase to be imaged and quantified for potential clinical benefit [267]. The use of such biomarker-based imaging probes can be translated to other disease processes, such as OA.

A significant finding from my work, and others, is that PAR-2 is involved in OA pathology, and so represents a novel functional biomarker to identify those patients at risk of developing OA. Perhaps, preliminary work could set out to design a gamma-emitting radionuclide labelled antibody, which recognises PAR-2. This could then be used in a preclinical murine OA model, where single-photon emission computed tomography (SPECT) imaging could be used to quantify PAR-2 in OA, specifically in the bone. However, one disadvantage is that cartilage is avascular, and so PAR-2 could not be imaged in this tissue. This avenue of work has the potential to design a PAR-2 imaging probe, which could be used as a biomarker in clinical use for the onset and progression of OA.

7.7 Human-derived cartilage model of catabolism

None of the models I used provided a reliable or reproducible model of cartilage catabolism, with only the cartilage discs releasing collagen in response to a catabolic stimulus (albeit variable). This is a common problem, as there is no human-derived cartilaginous model which reproducibly and reliably proteolytically releases collagen in response to a cytokine stimulus. The reason for this is definitively unknown. In a study by Morgan et al. it was hypothesised that the lack of reproducible collagen release was due to the age of the tissue and the fact that the tissue was diseased resulting in increased collagen cross links and increased levels of advanced glycation end products, all contributing to the lack of collagen degradation [178]. Similarly, in my study using hMSCs to generate cartilage the age of the donor, gender, physiological status, clinical history and other lifestyle factors such as smoking likely all impact on the health of the donor hMSCs. This will cause differences in the growth kinetics and gene expression of the cells

and this may impact on the responsiveness of the cells to a cytokine stimulus and resultant collagen breakdown [223-225].

There was also significant donor variability in generating cartilage discs, preventing future work. As discussed in chapter 3, there is significant heterogeneity in hMSCs even within the same donor, and this will likely impact on chondrogenesis. Additionally, Kretlow et al. found that chondrogenic potential decreases with age and repeated passage number [268]. This donor variability may explain why many donors failed to form cartilaginous discs.

For clinical use, large variation among donors in composition of cells, growth, and response to chondrogenic signals may limit such use of hMSCs for cell and tissue engineering applications. Multiple samples of hMSCs may need to be harvested from an individual and carefully analysed in vitro before cells can be implemented in such therapies. Alternatively, for clinical production of hMSC markers that correlate to functional properties of hMSCs, preparations could be used for the development of assays to define characterization criteria for clinical applications [223-225].

7.8 Future work

- An initial improvement to the transgenic murine study would be to increase the numbers of transgenic mice in each group providing a more robust study, which would help corroborate the results I have obtained. Additionally, I would start analysis of cartilage and subchondral bone remodelling as early as 1 week post-surgery, similar to the study by Huesa et al., as this would allow a longer time course of OA (in a surgically-induced model) to be analysed and observe if subchondral bone changes precede cartilage changes as found by Huesa et al. [232].
- Ferrell et al. began to investigate the effectiveness of a PAR-2 inhibitor (SAM-11/p520) in a murine DMM model. Interestingly, this group found that when wild type DMM mice were treated with either of these inhibitors there was significantly less cartilage damage and reduced subchondral sclerosis compared to un-treated mice. Indeed, the effect of SAM-11 on cartilage and subchondral bone remodelling was equivalent to global PAR-2 ablation [137]. Adding to this work, research is currently taking place in the MRG laboratory to investigate the

effectiveness of a matriptase inhibitor in a murine DMM model. This will provide further information on whether future work should focus on a target up-stream of PAR-2 or focus on the receptor itself to prevent OA pathology occurring. This will help guide future therapies.

- Another avenue of work which has the potential to yield exciting results is using laser capture microscopy (as described by Curran et al. [269]) to micro-dissect cartilage from mouse tibiae. This technique allows exceptionally pure samples to be dissected. After dissecting the cartilage, RNA could be extracted, reverse transcribed and used for qPCR. This would help confirm successful cartilage-specific gene ablation. Additionally, this technique could be used in DMM and sham mice to observe any up-regulation of genes of interest, such as matriptase and PAR-2.
- As discussed, it may be useful to design a gamma-emitting radionuclide labelled antibody, which recognises PAR-2. This could be used as a probe based biomarker to assess the role of PAR-2 in OA onset and progression. Initially, preclinical animal models could be used and transferred to clinical trials, if appropriate.
- Producing a human derived cartilaginous model of catabolism has been challenging. However, it may be worthwhile to generate macro-pellets and over-express PAR-2 using a lenti-viral approach and assess its responsiveness to a cytokine stimulus +/- matriptase. This would allow analysis of the effects of PAR-2 on proteoglycan catabolism. Quantitative PCR could then be performed on these macro-pellets (with over-expression of PAR-2) to observe which proteinases are up-regulated.

7.9 Key findings of this study

Tissue-specific ablation of PAR-2 had its primary protective effect in the subchondral bone, by preventing subchondral sclerosis and abnormal trabecular remodelling. Cartilage damage was occurring independently of subchondral sclerosis, but there was some degree of protection, which was significant in the bone-specific PAR-2 ablated group. This was surprising, since a vast majority of osteoblasts are derived from cells expressing col2-cre. Indeed, the cartilage-specific PAR-2 ablated group had more of an effect on osteophyte maturation than the bone-specific PAR-2 ablated group. As mentioned, it is

necessary to increase the numbers of mice in each group to confirm the results I have obtained.

This study has shown that cartilage damage can occur independently from subchondral sclerosis, which is in contrast to work carried out by Radin et al. [246]. However, this does not confirm that cartilage changes precede subchondral bone remodelling in the time course of OA. Indeed, research has indicated that abnormal subchondral bone remodelling precedes cartilage damage in the progression of OA, using animal models [81, 232, 254]. There should be caution applied to extrapolating these results to the natural progression of OA in humans, as the mode of induction is significantly different for many OA sufferers.

In terms of which tissue should be targeted for therapeutics in OA, there is no conclusive answer. My results have shown protection against OA changes in both the cartilage- and bone-specific PAR-2 ablated groups, and as discussed there is evidence to support targeting either tissue. However, as mentioned, targeting the bone is less challenging than the cartilage due to the vascular nature of bone. However, this will likely increase systemic off-target effects.

Having attempted to generate a reliable and reproducible model of cartilage catabolism derived from a human source, none of the models used were suitable. Although the cartilage disc model was the most promising, future work using this model will be challenging due to significant donor variability in generating fully formed cartilaginous discs and responsiveness to a catabolic stimulus in terms of reliable and reproducible collagen breakdown. However, the macro-pellet model could be used to assess the role of PAR-2 in proteoglycan catabolism. Currently within the MRG laboratory, lentiviral transfection of SW cells (human chondrosarcoma cell line) with PAR-2 is producing promising results, so this could be used for some mechanistic studies.

LOCUS KO-first_condition_ready_78671_MGI:101910 23877
bp dna circular UNK
DEFINITION Mus musculus targeted KO-first, conditional ready,
lacZ-tagged
mutant vector F2r11 targeting project(s): 78671
ACCESSION unknown
SOURCE Mus musculus.
ORGANISM Mus musculus
Eukaryota; Metazoa; Chordata; Craniata; Vertebrata;
Euteleostomi;
Mammalia; Eutheria; Euarchontoglires; Glires; Rodentia;
Sciurognathi; Muroidea; Muridae; Murinae; Mus.
COMMENT cassette: L1L2_Bact_P
COMMENT design_id: 87373
COMMENT backbone: L3L4_pD223_DTA_T_spec
FEATURES Location/Qualifiers
misc_feature 29..49
/note="B4 Gateway"
misc_feature 74..111
/note="Transcription Terminator"
misc_feature complement(185..438)
/note="BGH pA"
CDS complement(563..1219)
/note="DTA"
promoter complement(1233..1745)
/note="PGK promoter"
promoter 1746..1896
/note="spectinomycin promoter"
CDS 1897..2907
/note="SpecR"
misc_feature 3055..3647
/note="pUC ori"
misc_feature 3918..3945
/note="rrnB T2"
misc_feature 4077..4120
/note="rrnB T1"
misc_feature 4216..4236
/note="B3 Gateway"
misc_feature 4242..4249
/note="AsiSI"
misc_feature 1..4274
/note="Synthetic Backbone"
misc_feature 4275..10181
/note="5 arm"
misc_feature 10209..10233
/note="B1 Gateway"
misc_feature 10246..10293
/note="Frt"
intron 10294..11168
/note="mouse En2 intron"
misc_feature 11166..11168
/note="Splice Acceptor"
exon 11169..11341
/note="mouse En2 exon"
misc_feature 11353..11946
/note="ECMV IRES"
gene 11947..15007
/gene="lacZ"
/note="lacZ"
misc_feature 15046..15289
/note="SV40 polyadenylation site"

```

misc_feature 15293..15326
              /note="loxP"
promoter     15353..15872
              /note="human beta actin promoter"
gene         15898..16692
              /gene="NeoR"
              /note="NeoR"
misc_feature 16892..17133
              /note="SV40 polyadenylation site"
misc_feature 17150..17197
              /note="Frt"
misc_feature 17204..17237
              /note="loxP"
misc_feature 11183..11260
              /note="FCHK std_gpr"
misc_feature 17253..17273
              /note="B2 Gateway"
misc_feature 10182..17303
              /note="Synthetic Cassette"
exon        17657..20206
              /db_xref="ENSEMBL:ENSMUSE00000300519"
              /type="targeted"
              /note="target exon 1 ENSMUSE00000300519"
misc_feature 17304..20387
              /note="Critical Region"
misc_feature 20411..20444
              /note="Downstream LoxP"
misc_feature 20388..20467
              /note="synthetic loxP region"
misc_feature 20468..23877
              /note="3 arm"

```

1 ctattgaggc tattgtaata atatatgcag aaggtagcca gcactagagc caggggtggga
61 tttgggatat gacatcaagt ggaattgctg acagatcaga tgtggaacat aagtagtcaag
121 gagcaaagca agtctttttt ttttccctta atctgaagaa ctggagggaa agaggtatgg
181 cctgaagtga tgaggagagt gtacaaagaa aggtgaggtg ctaggcgaat acatcaatac
241 tctagtgtga gacttaccce aaggaaatgc taggtgaata ttttatttta ttttaatttt
301 tttaatgtat gtgtgctctg tctgcatgta cacctgcatg cccgaagagg gcatcagctc
361 cttttataga tgatcatgag tcaccatgtg gttgctggca attgaactca ggatctgtgg
421 aagagcagtc agtgctctta gtcagagagc catctcccca gtctctggat gaatatgttc
481 tgtctgtcct ggagaaatct agggtagaaa aagttgtgga gttgctaata tatacagtac
541 ttcaaaccac aggagtggat caatcaacca atgaacaaat acacattttg gaaagaaact
601 caaaagatta acccagagtg tagagagggc agcagtgtgg taccaccatc agaggatcaa
661 ctgccaatga ggagactcaa gggcaggtgg gacctgggga ggtcaactgt atcatttcta
721 aagttgggta ttaggagcct ggaaagtgc taaaggattt atcatgtaaa agaagtttat
781 tgctagcctt atcgagcatg tctgctcaat ggatgggtga atgaatcgag cagcttttct
841 tccagctata gctggccagg gacttcaactg tccaggaag agtcacttgt ttttaacaaa
901 ataaatgaat aatgcagaat tctgtttctt ttttttaaaa gacttattta tttattatat
961 gtaagtacat tgtagctgtc ttcagacact ccagaagagg gagtcagatc tcggtatgga
1021 tggttgtgag ccactatgtg gttgctggga tttgaactct gaacctttgg aagagcagtc
1081 ggggtgctctt acccactgag ccatctccgc cagcccagaa ctctgtttct tttcttgctt
1141 cttctcccac agtctaaatg tctcttcaa attacagtga gtggaaaaac acaggaagcc
1201 ccctgtctct ggcaccagg cactcaggtg tcagctattc ctgagtgttt cacagattca
1261 tgcaatagat accccaaggc tgttcaggca aatgaatcat cagattaaaa agaaaaaaaa
1321 agctgcaaga tttgagaaaa acacctgcaa aactgtctgc tatgaatata cttcatttgt
1381 tcattttgac tgctcgggag acagtggcag gtggatctct gtgattcaa ggtcagctg
1441 gtctctagag tttcaggaca gctaacatta cacagagaac cttgtctcaa aactcccctc
1501 ccccctccaa tcacattaac taattaatta ctgtggtggt gctggggttg aaattcagag
1561 ctttgagtat gcctggcaag ctctttacc ctgaaataca tccccagacc aataaaccac
1621 catcttgaaa ttattaacgg atagcattgt tcaactagaac catttcttgg aaattttggt
1681 gattcaaaact cagttcctat gacgtgagtg tctgtggagc ttggaagcgt ctggaggctt
1741 acacatgggtt ctctgaagag aaggatttct cactgaaggc aatcaccaaa cagcggctct
1801 ctcttctgtg ccaggcgagg tctgtgctac ttcattgggca tctcaaatg cactctacia
1861 gaaaggagcc actatcatgg ccagataaca tgggtggtaat tacactgtat gaggtaggaa
1921 agactggagg atcatcagag atgaactggt gtctctcttc aggagtaggc tggccctttt
1981 cagaatggga ttctgttgag taggctcagc atcatccaaa ctgaggtgtt ttagggcagg
2041 aagggcgagag acagcagcat acaccagggc agttaacaga cgaccagggg cgtgggcctt
2101 cttgaacaaa gaggttagtt tccatgttct atcccaggat cagtgaatca accctccaga
2161 gaggaacttg gaccctacca tagaaaaaac accccagagg acctcactgc tgcacagtgg
2221 tcccttgagt catcactggc tactttagaa ttgtccagga tcatgtatgt aggtacacac
2281 aactacata aatacataaa cacatgtaaa aagaacacat taaaatacta acttatggcc
2341 ccactctctc ctagtcttct ctttctggtt aacagcattt cttttagatag atctggctgt
2401 cctggaactc tctccaaaga cctggctggt ctcaaactca gaattccaac agcctctgcc
2461 tcccaagttc tgggactaaa ggtgtgtgcc accaccgctt gccgctttc acctattgat
2521 tgacataagg aatgtttagg tttagattaca ctctgtgctt ttagaagtca attttctgaa
2581 gggaggggtcc tggagccaca ccctgaaagc tgtggtacag gcggtggggc aggtactcct
2641 gagagaaagg aaagattttt gttctacttc atatcagaac ctctgtttat ccctaggtgt
2701 ctttaaatag acaaaaatgct aatcccattt ccataagtga gaaatcaaaa catagtgtga
2761 atagtttatc caaggttata gaggcacaga aggagagaag ccagaccaca ccaaggcta
2821 cacaaaggaa aaagctaagt tccattcaca ttcccaaaga acttctttga gacacagcca
2881 cgggagacc ctccagagat gttccattaa agagaattgt ctcaaccctt gggctgcttt
2941 ttctgaccac tcttgagtgt gtgtccgtgt ccattacctg tccatttctg ttatctagaa
3001 aggaagcatt ctattttcat ggcctattca ggaccatttg cttctcttcc tttgatttct
3061 ggctgtgtgt gatcccgttg gggcagaatg aacaggcaga agactaacca tccatcaggg
3121 atgttgagggt gtgaccaga tcttgcatca gatggaagct gcattctaca cacttatggg
3181 acatggcggt gaccacttgg ctcaaggctg cgcagatatt aataactatc aacagtgact
3241 gcctgaccct tccctctgga gtggaacccc tctgcaacat gccaggtgga tgtcctcaa
3301 cctgagagaa atggctaact ccggtctctc ttctaactct gtcattcatt cagagctgtc
3361 caggactgca gccagccctt cctacattga aatcccctct ccgtggagac acctgctttg
3421 ggctcatccg agtctcttcc gtttatgaat cttccagta tcttctctgt aattcaaacc
3481 acagttttct tgaacaacag taaagtctga cttattgtcc tagttttaat ttttttaa
3541 gataggggtc tactatgtag cccaaatggt ctccaattct ttatgctcct gcctctgtct
3601 ctgtggggga gattcactct ggtccttggga catgctaagc atgtgctcta ctaccaagct
3661 acacacccca acccatgctt atatatttct ttggaacatg ggatcacgat gcagaagaga

3721 cccgagtggga atcaggtata gagcaacaag ttgtggacaa atttcagtca tagacttgag
3781 cttggacatt tacaaaactgt gccaaagaac tgtgtaaccc cagaggcagc aaacattcta
3841 agttccatct cctattctgt aaaatgggaa gacagatgga gcgggcacat acagtgtctga
3901 gggcattaga caagctaaca gtactgaacc attggcgggtt agtgcttccc acacatccag
3961 gtttgtttaa tgacactgga taacagatga gttaatccca gaactgggtgg aacaatcctg
4021 gcaccccagc acttagggag tgcaggctgg agaatcgtca caagtttgaa gtcagggtggg
4081 tagtagggaa agaaagcttt cgcaaaaagg caaaccaaga caacaatcaa caaaacaata
4141 accaacaaga acccctttca tatcgtccc gcaactgcca ttacaccaca aagccttcca
4201 caccaattac tgaagacaaa ggaactagc atagactttc taacattcac aggatgacct
4261 cactggttct ctgaagtaat taaaggttaa agatagtttt ggacatcgcc caggctctaa
4321 aaccctgggt cccaaccttc ctgtcatttg cattccaatg tagccacctc accggtccag
4381 cctcaccggc aggcgactcc agcagccaag tggacgctgg ccagcacacg ggagctacgg
4441 tcaggctgtg ctgggccagg tggcccgggg tgtggcctgc gtaggacgtt cgagggggcg
4501 tggctcctg ggggcgtggt cttccgcagg tgcgtctagg ggctccgggt tcaactgaaac
4561 aggtcccgcc ccaggaaggc tcagtgaagc tcgtgttaag ggaagggacc ctgtgctcag
4621 agtagggctc cgagtttcga accactggtg gcggattgcc cgcccggccc acgtccgggg
4681 atgcgaagtc tcagcctggc gtggctgctg ggaggtatca cccttctggc ggcctcggtc
4741 tcctgcagcc ggaccgagaa ccttgcaccg ggtgagctcg agcggcgaag gaacgctctg
4801 ggctgggtggg ggaatcgggg aaggcgggca caccctctg acaactctctg tagctttgat
4861 gggggtccct aaccaggacc aatcagccgg gacacctaag tgccaccaa gacgcgctag
4921 aaacaatcct ggtctgggca cttccaatct ctactcgtcg acgtggttcg gggagataag
4981 gaaggagcgc ccgcaggact cagcctcccc tccctgcgggt cgttccctta caaactga
5041 gtcagtaatt ggttttcgcg gaccctgcga actacgtcct atagggctct actagacccc
5101 cggattatag cagtttgatg gctcacgtat gggtaggtg agtgggagc cgtgcctgg
5161 gaagtccca cctcgagttt tacactcgca cccaccact cactgaacct tttcttgcg
5221 ggttgaacca cagtgttcaa gaccactcgc gggctacggt acctggcatc gcagtggatg
5281 cgctgggcac gggactcagg cggtttgaat gtcacgtggt ggtagaaggg gcccttctcg
5341 acccttacca ggtgaaatct ccagcctaga gatttcgaga ccttcccgcc gccgggagcg
5401 aacactggca gccacccagg tctctctctg aggtctgcat gcccaaggaa ccgaactgca
5461 ggaaagcggg tcggggcggt gctcctctgg cccgctgccg gcttgggctg tgcagctcct
5521 ggtgagctcg aactggccct tctagaagcc acggagacct ctgtaggctg taggggtggg
5581 tgggggggtg tttgctacca gtgatagcgc tattgcaaaa cccggcctgg cgtttccggt
5641 ctaaacttgc tgtagtctta aaggctatct ctcactttta ctttgcgtt aagttgtaga
5701 agagcgtcca acccctctcc gtttgcctgt catttaaagt tagaaattha aaaactcagg
5761 aacaaagtgt gtgcaaactt aaaaaaaaaag tggttggagg tgattacttt cgtgatttac
5821 ctagtatagg aagcataccc tgattagtcg gttcctctg ttttcagagt gaggagattg
5881 ggaggtagag gttcctagcg tacgtggtga acttgatttt aacaacaaca acaaaaaaat
5941 tgggttactt gttaaaccga gctacttaat atcccaactt ggcttttctc tctgcataat
6001 tatgctccat tgccggtaac tttcctaaag agttagtcta gtaacagaga ctttagatac
6061 cgggaggtat tgggtccgct ccccccccc cattgtaatt aaattaatt tggtaggac
6121 accgggcacc ttgcttgctc tctttgctca tgccgcttag gctcgctctt tctgcgtgct
6181 ccttggcctg ttaaacagca gattgagctt ggttttctcc acccccacaa aattgcttct
6241 cggaaagggg cccagctggg gggaggggca ctgaattgcy aatgtgacgt ttaagtcagt
6301 tccccacaga cacaatcact actactgtct ccctctcctg ctccccctcc cctcttccat
6361 ctccatattt tgtttcttga tttcttgcca tgctgggcat ccaacctagg gctttgcaca
6421 ggctgggcaa gtgctggacc gttgctatct tccctagtcac acagtcagtc catttcagtt
6481 ttaagactgg atcttcttgg gtgtgtgttt gtttttttgt tgtagtcttc cttttcttcc
6541 tttgaattag tctcattgtg tatccctggg tgctctgaaa ttgtctatgt tgaccacact
6601 ggccttgaac ttgcaacact tttgtctgct ctctctgaat atgggattac agaatgcac
6661 taccatacct agacaacatt ttaaaatgta attttagaaa aattatgtgc actgggtggtt
6721 ttgcctgcat tcatatctgg gtgaggggtg tggatcccct tgaactagag ttacagacag
6781 ttgtgagtc acgaggggtac aatgctgagg catctttcca gctcccgata acattttctt
6841 tttttaaatt ataacattaa tatgtggtca ctgagaagag aaaacagggg aaggagaaat
6901 ttaacggaat catcctaaac attggtactt aaaataacca cttgctaaca ttttgattta
6961 tatctttccc atgcttttgt acatgaggaa tacataaaat acacatttct aaattagaaa
7021 gccttgtaca agtatgggat ttaacatgta aaggctcagta acacaattht aacagcttta
7081 aaagatggca tatacacact aacatgcaca cacacacaca cacacaccag gtgtggccca
7141 ggtacttagc actaaacctt gggcctctgt gtattaacca gtcactttgc cactgaccta
7201 gagcctcagc cctaatttta cattttatth tgaggcaaaag tctccttaaa ttcgcaaac
7261 tttcctcgag tccactagg aacctcaggt ggccttgaac ctggggttct acttctcat
7321 cccgagtagc tatggttata gaccagacc ggcaaacctg gcttctgctt gttaaattaa
7381 tgttttgtga acaggcacac aggatctttc cgaggtctcg tagtataaaa gaactctagt
7441 gaacgtggag atgggacttg aggttgatgc ttgggtgctc tgcttctctc ctgttactga

7501 ttaaccgtga tccctcaggc ctcatgaagt ctgtatttga ctttcttatg gttttactat
7561 ctggacaaat gttgaggaaa acagttcccc ttgggaaaaa gaaaaagagt ttgcaaagtt
7621 cgctaaaagt gtacctagga aaggatggat aggttgaata ttaatagttg ttaatagcaa
7681 ctgaaacctt tttttctctc catctgggtgc tcccaagagt tggtagcgaa gaactctggg
7741 aaagggccaa aacactgaga ccaagcctac caccaactgg tgcacctaa accacagaag
7801 gaccatcctg ctgtcctagg acttacttgc atttcaacaa taaatctata tacagtcagg
7861 agacaggctt ctgtgcatgt tttgtagggg tgttatagct cttgtaagtt actgaaatag
7921 ttttgatatg gagatgatta tttgtacca tggtaaaca gtgattcaac ttttaaaaag
7981 attgtgtcag cttgcattat gagtggccga aaacctaaga cagagagagc aaggtttgct
8041 cttctcccga tgttctgctt caaggaaaca cactttttat agcttggaga gaggaaagcc
8101 ttgtacaagt atgggattta acatgtaaag gtcagtaaca caattttaac agctttaaaa
8161 gatggcatat acacactaac atgcacacac acacacacac acacacacac acacacacac
8221 acacacacac acacaccagg tgtggcccag gtattaggca ctaaacctag ggctctgtg
8281 tattaaccag tcactttgcc actgagctag agcctcagcc ctaattttac attttatttt
8341 gaggcagccc taattttaca ttttatattg agaggacct agatttcagg tttttgaaat
8401 aatgtacatt agagtcttat gaagcagatg acagcgtatt attttattgg tttcttgttt
8461 acagttggct gtatatattcc tgtaggaagg tgagtgtcta atcttaggac taggggtata
8521 gtaacttaga agcaggctga tacacaggcc cgtttcctgt ttggcagtcg tgggggctgg
8581 gtgtggccac gaacatgagt ggggtgatgt tttgtatgc ctgacaggaa ctgttgattg
8641 tagccctaca aataagatgc actcagagcc aggtactctg gtgtgtcccc agttcgtagt
8701 caccatagat ctccgctcag ttttgaaaca ctgagcctgg tttacaacta gcacagggga
8761 taccagcagt ttggatgca atacagaaaag gacagagcct caaggacct tgaactggga
8821 cacagagtgg tttaatgtga atggctgcta ccgtttgctg gttgtttggt ttctgtattc
8881 aagatcttgc tgaatagccc agacttgcct ggaactcatg atctctgtc ccagactctt
8941 cagtgttgag tttaaagctg gatttcccaa ctctattttg tgaggggctt ggggagccag
9001 cctggaaatc aagccttgtc catccatgct gggcaagcac tttaccactg aggtgcagcc
9061 ccaaccttta cagtggata tctgcacagg gcttggggaa tcgaagaatg acgcctcctc
9121 ctccctctag tctttcttcc tcttctttt ttaaagtttt aaccgagcc atacttcttt
9181 agttggaatg ttgttcttag ttacttcttt ctctttatca ttcttataca ttagttttgg
9241 taccaccac aacagcagtg atcagtaatt cttgggtaga tgtgtttcat ctctaccctc
9301 agcctgtctt tctgtgttac ttttaatagc tttattaggg tctcagtgcc aaataatttt
9361 catacacac agttagccca tttaaagaga gtccagtgcc tttcggata cttacagaat
9421 tgtgaccatc ccagtggta atttgaacgc attttgatga cccacaggaa tcccctttgt
9481 tgttgcataa cagccttccc ataaccagcc ctggccactg atagtcaact ttctacctat
9541 ggacttgccct gttctagata tttgattaga ttcacataat gtatgggctg ctgtgactgg
9601 cttcttattt aatggtttgt ttgtttgttt tcaagactta cccatgttgc agcatgcatc
9661 aacaacctat ttcttctctt ccttactttt tttttttttt ttttgaacac caatcatgga
9721 ctatcacgcc cagcatgttt ggttgcatgt tttgttgctt tgggtgcatg tttgggtgag
9781 tctctgagtc tcatatggct catgatggcc ttgaactcac actcaagtta gccatgttgt
9841 gaacggaggg gttgaagctc ccgtcctcat ggagtgtgtg gattagtgtg ggcttaccat
9901 acccagtttt ataggtgtct agtgcataa cttccggctt ctggtagaag cctccagggc
9961 atgtagaagc tgagctatat cccagctgtt ttagttttga gatgggttct agttctgctg
10021 gggcagacta tcaaattcct aggccttaagc aattcccata cctcagccaa ggtctgcgcc
10081 aagcataggg taccatgtct ggcctcagta cttgatcttt cttgtcattg ctaggtgcca
10141 tctcattgtg gacacttctc gttttgttta tttgttcttc tgttgatgga cttttgagtt
10201 gtttccattt agggctatta ggaataacgc tgccttgagt gctaaggtaac aagttgtttc
10261 atgaatata ttaccttttt cttggggatc gtgggtgatc ttcgctgtcg acttgactgg
10321 attggaatca tcacaaaaac attcctgtgg gcatatccat gaagcgtttt cagaacagtt
10381 ttttctaata ttctgtttgt ttgtttgggt ggttgggtgg ttgggtgggt ggtttttttc
10441 cccagacagg gtttttctgt atagccctgg ctgtcctgga gctcactctg tagaccaggc
10501 tgatctcgat ctcagagact cactccctcg gcctcccatg tgctaggatt cgtgccctgc
10561 cagaacagtt ctaattgagg agggaattcc tattctgagt gtggctgggc acccaccctt
10621 tccataggct ggtcccagcc tgcgtacaag gagagggcaa actgagcatc agcatgcatg
10681 tctaccacce ctctccttca gagtgtgact gtctgtgtgg cattcgtgct ttgagcctaa
10741 ggaaacactt cctcccttag ttatgtgctg aatcctagca acaagaaacc taaggcttgt
10801 gaggatgcag gcgaagctgg cagtttggga gagagagagg gcgctcacac cagatcctag
10861 ccgtgctgtg gctccccctc cccccatttt tgtccaccac aactgtgaag aatgtgtatg
10921 ttgtgtctaa accacttttt tttttgagac agggctctct tghttagccc tggctgtcct
10981 ggaactcact ttgtagacca ggtggcctc gaactcagaa atccacctgc ctctgcctcc
11041 cgagtgtctg gattaaaggc gtgcaccatc acgcctaacc cactttttaa attacagccc
11101 ccccccttc cccgattttt gtccaccaca actgtgagga atatgtatgt tgtgtctaaa
11161 ccacttttta aattgcagcc cccctcccc atctgtgtgt gtgtatgtgt gtgtgtgtgt
11221 gtttgaacat accattgtgt acatggggag ataagcttgt ggtgtggggac ttgtttctct

11281 caaccacgtg cgttctgggg ttcagagtca ggtatgccag cttggaacca agcaccttta
11341 ctcgatgagc catcttgcca cccctggctg ctcaactttt atctctgtta catctgcgca
11401 gatgtactgt gatcacaatg aggtcagagt ctgttccagc aagatttctt cagagtgtct
11461 aatcatctct tattttgtgt ggccttagta gttacagaac attatgtaac tttctttggg
11521 aacagaagaa aatggatttt ccttgcgaga actctcaagc ctcaaggccac tgaccacaga
11581 agttcagggg gctttgaatg agagcgcacc cccaatccc caataggctc gaatatttga
11641 atacctgctc tctagtgagt ggcctgtctt ggaagggtg gttgtgctgg ggcaggcttt
11701 gaggttaagt gtctccacca cttttgattt tcctctgct ttgtacttgc gtttgaagg
11761 gtgagttccg atcttctagt tcctgctgcc atgcctgcag cttgtggcct ggtctcccca
11821 ccatgacaca ccctgagcgc tccggaactg taggcccaca taacattttc cttctgaaaa
11881 ttgccttgct cataatattg tgtcatagga acagaaaact aaccaccaat acatgcagcg
11941 ggctgtttca ggcctggatg cctttgcaga tgagtggggg cccagagca ctggcccact
12001 gctcacgggt cctctgggca gctgtggagg atttacaaag cctttttatt ttaaaccct
12061 ctaaagggtt ggcaggacat gttgacattg atacagggtg ctgtgttaat ttttgaagga
12121 ggggctaatt gaagaaagta acttttagtg tgttaaattt acaattttag atattttgct
12181 tgaggaaatg tatgtgtaga atccatgcag gttgggcaga tctctgtgcg gtctaactg
12241 tagtaccagt taggtgtgat gagggatagc gagcaaaacc atggcttctg gtaatgaact
12301 aatttttccc acataacaac tgtttaacct taggaccac acttagttac tgatttgtgc
12361 cttagcttct tcatctataa aatgaggcaa aatagcatga gctgccttct ccgctttgtg
12421 gtgattgtgg tacaggtgcc ttgctatag tgcagaccgt agtttcagac ccacagtgag
12481 tcagtgtctaa tctctatgat ggcacccatg gtctctgta tttgtgtgg tctatgtgcg
12541 gcctctggca ttcgggtgtt cagtccaacg tcctgtagaa atgcgtagt gaggcgtggc
12601 tttgatccc ccctcacttc ttcagggat gtgggtagct gagcattgta atccagaggt
12661 atgctcaggg tgggccaggg gctgggttaa agacacctt aatcctatat aggtttcctt
12721 cgagctggtt agtctgcaaa cacatcatta ctgttctctt gatgcttctc aatgttagtc
12781 agtctggtt ctggcttaaa aaaacactcc agagaaccaa catgcattct gtatagaagg
12841 gtattttgtg caatattcca ttatggatct atgtactaag tactgggtta ccgtgcagaa
12901 catattcttc atggagttac ctaattcagt atctgaagaa cattgtaata ttcaggaata
12961 atctttcttg agacatgtat cccaggctgg cctcaaacct actatgtagc tgcaggcacc
13021 cttggattta caattatcct gcctctacct cctgagtctt ggggttacag tgtctggtac
13081 acaataggca aacactctac caattgagct acattcccca tctccttagg aatatttgtt
13141 ttaatttttt aattaattaa ctagagatgg gagctctata tagcctggc tggcctggaa
13201 ttctataatt ctatcaagct ggcctcaaaa tcatagaggt ctatttgcct ctgcctccaa
13261 agtcccatac taaaggcata tgccgctaca cctggctttg ttttaaaatt gtaagtgat
13321 ttatgtatth tatgaatgag tagtctatct gcatggcacc tgtatgccag aagaggacat
13381 cagaacttat tatagatggc tgtgagccac catgtttgtt ctgagaattg aattcaggac
13441 ctctggaaga gcagctagtc ctcttaaccg atgagccctc tctccagccc ttgttttaat
13501 tttttctttt aatcttattt aatataatgag tgctctgttg catatacatc tgcagaccag
13561 aaagagcatc agatcccatt acagatggtc acgagccacc atgagggtgt tgggaattga
13621 actaaggacc tctgaaagaa ccagtgtctt taaccgctga accatctctc cagctctctg
13681 cccccatttt aatttttaaa aagtgtcttt tttttggac agttatagaa gaaatgaaa
13741 caatatatat gtttacgtca aatgctttta ttttcctaag gccactgtga gagcagagc
13801 tataaaacaa cagatgtcac tctctgggtt ctgaggtgag gggcaggaa tgaaagtgg
13861 ggggaaagag aatctgccc tctccagcat ccggttgggt gctgccatct ttgggtcccc
13921 ttggcacagt gccagccttt gttcccattg tccatcatgt tgtttactct gctgtttct
13981 ccttttctgt cccagcttc cctatgtctt gttaaaagac cattgtcatt ggaccgagg
14041 cctgactgga taacctggat agtgttggtt agatcgtacc ttagggttgc aaagaccctt
14101 gtctactggg gattaggact tgaacacctt ctttttggg tagggagcat ctttattttt
14161 ctacagtggg tggaaagggg actgctgatc tctgtaacct ccagtgtctc tcccattacc
14221 cctgtgtcag cgcaacgtgg tgaagcctac agaagcgaac ggtcctgtag aacctgagtc
14281 tggaaaccaga agcggatcag ataactgagc acacaatata ttagagaaag tcaggagagg
14341 tatactgtct tccttgtcaa cgtgaacaat gttcaggtgt ttccagacgg tggaggcctc
14401 agtctcatca ttaaagttaa attccttagc gttcaccctt cctccttcag gtcagtgagg
14461 gaatacagga tggggcagga tgaagactgg gcttgcccgt cactgcttgg tagggttgtt
14521 ctgtttctgct ttgctttgga tggaaatctca ctatgtcacc caggctggtc tcagattcct
14581 taagtgaaaa cagtccattc acctcagctt tccaaatagc tgagactata ggcacaacct
14641 accacgccc gggttatttg tggtttagaa tgttcaattc atggatgaa ggaagcatcc
14701 taagttaaag cttgctgtta cacgctcaaa agtcagagca catttggctc tgatgctaaa
14761 aggcttgccct gccaaactgag ctcagtgagg ggatgtttat gaagccagca gagaggtggg
14821 gaatgcctac ccattatagt atttctgtg ggcggacaag ggaatgcctc ctggttctgg
14881 aatctcccta ggctggcccc tggggcaggg tgtgggtgac ggctaggttg aatcttggct
14941 taaggccaga gtaggataga aaatgagaac caagacagct gatggcaaga caaggctgcc
15001 ttactcacca aagactcggg aagagttacc acacaatcct agactgatct aaggcgcata

15061 acgataccac gatatcaaca agtttgtaca aaaaagcagg ctggcgccgg aaccgaagtt
15121 cctattccga agttcctatt ctctagaaag tataggaact tcgaaccctt tcccacacca
15181 ccctccacac ttgccccaaa cactgccaac tatgtaggag gaaggggttg ggactaacag
15241 aagaaccggt tgtggggaag ctggtgggag ggtcacttta tgttcttgcc caaggtcagt
15301 tgggtggcct gcttctgatg aggtgggtccc aaggtctggg gtagaaggtg agagggacag
15361 gccaccaagg tcagccccc cccctatcc cataggagcc aggtccctct cctggacagg
15421 aagactgaag gggagatgcc agagactcag tgaagcctgg ggtaccctat tggagtccct
15481 caagaaaca aacttggcct caccaggcct cagccttggc tcctcctggg aactctactg
15541 cccttgggat cccctttagg ttgtgggtta cataggaagg gggacgggat tccccttgac
15601 tggctagcct actcttttct tcagtcttct ccatctcctc tcacctgtct ctcgaccctt
15661 tccctaggat agacttggaa aaagataagg ggagaaaaca aatgcaaacy aggccagaaa
15721 gattttggct gggcattcct tccgctagct tttattggga tcccctagtt tgtgataggc
15781 ctttttagcta catctgcaa tccatctcat tttcacacac acacacacca ctttcttct
15841 ggtcagtggg cacatgtcca gcctcaagtt tatatcacca ccccaatgc ccaacacttg
15901 tatggccttg ggcgggtcat ccccccccc acccccagta tctgcaacct caagctagct
15961 tgggtgctgt ggttgtggat aagtagctag actccagcaa ccagtaacct ctgcccttc
16021 tcctccatga caaccaggtc ccaggtcccg aaaaccaaag aagaagaacc ctaacaaaga
16081 ggacaagcgg cctcgcacag ccttactgct tgagcagctc cagaggctca aggctgagtt
16141 tcagaccaac aggtacctga cagagcagcg gcgccagagt ctggcacagg agctcggtac
16201 ccggaagatc tggactctag agaattccgc cctctccct ccccccccc taacgttact
16261 ggccgaagcc gcttgggaata aggcgggtgt gcggttgtct atatgttatt ttccaccata
16321 ttgccgtctt ttggcaatgt gagggcccg aaacctggcc ctgtcttctt gacgagcatt
16381 cctaggggtc tttcccctct cgccaaagga atgcaaggtc tgttgaatgt cgtgaaggaa
16441 gcagttcctc tggagcttc ttgaagcaa acaacgtctg tgcgacctg tagcagcct
16501 cggaacccc cactggcga caggtgcctc tgcggccaaa agccacgtgt ataagataca
16561 cctgcaaagg cggcacaacc ccagtgccac gttgtgagtt ggatagttgt ggaagagtc
16621 aatggctct cctcaagcgt attcaacaag gggctgaagg atgccagaa ggtacccat
16681 tgtatgggat ctgatctggg gcctcgggtc acatgcttta catgtgttta gtcgaggta
16741 aaaaacgtct agggcccccg aaccagggg acgtggtttt cctttgaaaa acacgatgat
16801 aagcttgcca caaccatgga agatcccgtc gttttacaac gtctgactg ggaaaacct
16861 ggcgttacct aacttaatcg ccttgcagca catccccctt tcgccagctg gcgtaatagc
16921 gaagaggccc gcaccgatcg ccttcccaa cagttgcgca gctgaatgg cgaatggcgc
16981 tttgcctggg ttccggcacc agaagcgggtg ccggaaagct ggtggagtg cgatcttct
17041 gaggccgata ctgtcgtcgt cccctcaaac tggcagatgc acggttacga tgcgccatc
17101 tacaccaacg tgacctatcc cattacggtc aatccgccgt ttgttcccac ggagaatccg
17161 acgggttgtt actcgctcac atttaatgtt gatgaaagct ggctacagga aggccagacg
17221 cgaattattt ttgatggcgt taactcggcg tttcatctgt ggtgcaacgg gcgctgggtc
17281 ggttacggcc aggacagtcg tttgcgctct gaatttgacc tgagcgcatt tttacgcgcc
17341 ggagaaaacc gcctcgcggt gatggtgctg cgctggagtg acggcagtta tctggaagat
17401 caggatatgt ggcggatgag cggcattttc cgtgacgtct cgttctgca taaccgact
17461 acacaaatca gcgatttcca tgttcccact cgctttaatg atgatttcag ccgctgtga
17521 ctggaggctg aagttcagat gtgcggcgag ttgcgtgact acctacgggt aacagtttct
17581 ttatggcagg gtgaaacgca ggtcggcagc ggcaccgcgc ctttcggcgg tgaattatc
17641 gatgagcgtg gtggttatgc cgatcgcgtc acactacgtc tgaacgtcga aaaccgaaa
17701 ctgtggagcg ccgaaatccc gaatctctat cgtgcgggtg ttgaaactgca caccgcgcgac
17761 ggcacgctga ttgaagcaga agcctgcgat gtcggtttcc gcgaggtgcg gattgaaaat
17821 ggtctgctgc tgctgaacgg caagccgttg ctgattcgag gcgtaaacg tcacgagcat
17881 catcctctgc atggtcaggt catggatgag cagacgatgg tgcaggatat cctgctgatg
17941 aagcagaaca actttaacgc cgtgcgctgt tcgcattatc cgaaccatcc gctgtggtac
18001 acgctgtgcg accgctacgg cctgtatgtg gtggatgaag ccaatattga aaccacggc
18061 atggtgcaa tgaatcgtct gaccgatgat ccgcgctggc tacggcgat gagcgaacgc
18121 gtaacgcgaa tgggtgcagcg cgatcgtaat caccgagtg tgatcatctg gtcgctgggg
18181 aatgaatcag gccacggcgc taatcacgac gcgctgtatc gctggatcaa atctgtcgat
18241 cttcccgc ccggtgcagta tgaagcggc ggagccgaca ccacggccac cgatattatt
18301 tgcccgatgt acgcgcgcgt ggatgaagac cagcccttcc cggctgtgcc gaaatggtcc
18361 atcaaaaaat ggctttcgtc acctggagag acgcgcccgc tgatcctttg cgaatacgc
18421 cacgcgatgg gtaacagtct tggcggtttc gctaaatact ggcaggcgtt tcgctcagtat
18481 ccccgctttac agggcggctc cgtctgggac tgggtggatc agtcgctgat taatatgat
18541 gaaaacggca acccgtggtc ggcctacggc ggtgattttg gcgatcgc gaacgatcgc
18601 cagttctgta tgaacggtct ggtctttgcc gaccgcacgc cgcatacagc gctgacggaa
18661 gcaaacacc agcagcagtt tttccagttc cgtttatccg ggcaaacat cgaagtgacc
18721 agcgaatacc tgttccgtca tagcgataac gagctcctgc actggatggg ggcgctggat
18781 ggtaagccgc tggcaagcgg tgaagtgcct ctggatgtcg ctccacaagg taaacagttg

lacZ

18841 attgaactgc ctgaactacc gcagccggag agcgcggggc aactctggct cacagtacgc
18901 gtagtgaac cgaacgcgac cgcattggtc gaagccggggc acatcagcgc ctggcagcag
18961 tggcgtctgg cggaaaacct cagtgtgacg ctccccgcgc cgtcccacgc catcccgcac
19021 ctgaccacca gcgaaatgga tttttgcata gagctgggta ataagcgttg gcaatttaac
19081 cgccagtcag gctttctttc acagatgtgg attggcgata aaaaacaact gctgacgcgc
19141 ctgcgcgata agttcaccgc tgcaccgctg gataacgaca ttggcgtaag tgaagcgacc
19201 cgcattgacc ctaacgcctg ggtcgaacgc tggaaagcgc cgggcccatta ccagcccgaa
19261 gcagcgttgt tgcagtgcac ggcagataca cttgctgatg cgggtctgat tacgaccgct
19321 cacgcgtggc agcatcaggg gaaaacctta tttatcagcc ggaaaaccta ccggattgat
19381 ggtagtggtc aaatggcgat taccgttgat gttgaagtgg cgagcgatac accgcatccg
19441 gcgcggattg gcctgaactg ccagctggcg caggtagcag agcgggtaaa ctggctcgga
19501 ttagggccgc aagaaaacta tcccgaccgc cttactgccc cctgttttga ccgctgggat
19561 ctgccattgt cagacatgta taccocgtac gtcttccoga gogaaaaagg tctgcgctgc
19621 gggacgcgcg aattgaatta tggcccacac cagtggcgcg gogacttcca gttcaacatc
19681 agccgctaca gtcaacagca actgatggaa accagccatc gccatctgct gcacgcggaa
19741 gaaggcacat ggctgaatat cgacggtttc catatgggga ttggtggcga cgaactcctg
19801 agcccgtcag tatcggcgga attccagctg agcgcgggct gctaccatta ccagttggct
19861 tgggtgcaaa aataataata accgggcagg ggggatctaa gctctagata agtaatgatc
19921 ataatcagcc atatcacatc tgtagagggt ttacttgctt taaaaacct cccacacctc
19981 cccctgaacc tgaaacataa aatgaatgca attggtgttg ttaacttggt tattgcagct
20041 tataatgggt acaataaag caatagcatc acaaatttca caaataaagc atttttttca
20101 ctgcattcta gttgtgggtt gtccaaactc atcaatgtat cttatcatgt ctggatccgg
20161 aataacttcg tatagcatac attatacga gttatgttta aacggcgcgc cccggaattc
20221 gccttctgca ggagcgtaca gaaccaggg ccctggcacc cgtgcagacc ctggcccacc
20281 ccacctgggc gctcagtgcc caagagatgt ccacacctag gatgtcccgc ggtgggtggg
20341 gggcccgaga gacgggcagg ccgggggcag gcctggccat gcggggccga accgggcact
20401 gccagcgtg ggcgcggggg ccacggcgcg cccccccagc ccccgggccc agcaccacca
20461 ggcggccaac gccaaaactc tccctcctcc tcttctcaa tctcgtctc gctctttttt
20521 tttttcga aaggagggga gagggggtaa aaaaatgctg cactgtgcgg cgaagccggt
20581 gagtgagcgg cgcggggcca atcagcgtgc gccgttccga aagttgcctt ttatggctcg
20641 agcggccgcg gcgggcctct ataaaacca gcggcgcgac gcgccaccac cgcgagacc
20701 gcgtccgccc cgcgagcaca gaggcctcgc tttgcccgat ccttagagtc gagatccgcc
20761 gccaccatga ttgaacaaga tggattgcac gcaggttctc cggccgcttg ggtggagagg
20821 ctattcggct atgactgggc acaacagaca atcggctgct ctgatgccgc cgtgttccgg
20881 ctgtcagcgc aggggcgccc ggttcttttt gtcaagaccg acctgtccgg tgccctgaat
20941 gaactgcagg acgaggcagc gcggctatcg tggctggcca cgacgggctg tccctgcgca
21001 gctgtgctcg acgttgtcac tgaagcggga agggactggc tgcattggg cgaagtgccg
21061 gggcaggatc tctgtcatc tcacctgtct cctgbcgaga aagtatccat catggctgat
21121 gcaatgcggc ggctgcatac gcttgatccg gctacctgcc cattedgacca ccaagcga
21181 catcgcacgc agcagacagc tactcggatg gaagccggctc ttgtcgatca ggatgatctg
21241 gcaagagc atcaggggct cgcgccagcc gaactgttcg ccaggctcaa ggcgcgatg
21301 cccgacggcg aggatctcgt cgtgacctac ggcgatgctt gcttgcgaa tatcatggtg
21361 gaaaatggcc gcttttctgg attcatcgac tgtggccggc tgggtgtggc ggaccgctat
21421 caggacatag cgttggctac ccgtgatatt gctgaagagc ttggcggcga atgggctgac
21481 cgcttctcgc tgccttacgg tategcgct cccgattcgc agcgcategc cttctatcgc
21541 cttcttgacg agttcttctg agcgggactc taaaattcaa aatga gc
21601 ccaacctgcc atcagagat ttcgattcca atgaatgcg tatg Forward Primer P1
21661 gaatcgttt ccgggacgcc gatgatga gggg For to detect deleted
21721 tcttcgcca cccccggat ctcta atca exon before loxP
21781 catctgtaga ggttttactt gtttataaaa cccccctg aacctgaaac
21841 ataaaatgaa tgcaattggt gttgttaact tgtttattgc agcttataat ggttacaat
21901 aaagcaatag catcacaat ttcacaata aagcattttt ttcactgcat tctagtgtg
21961 gttgtccaa actcatcaat gatctttatc atgtctggat ccgggggtac cgcgctcaga
22021 agttcctatt ccgaagttcc tattctctag aaagtatagg aacttcgctg agataacttc
22081 gtatagcata cattatacga agttatgtcg agtatctag acccagcttt cttgtacaaa
22141 gtggttgata tctctatagt cgcagtaggc ggaagaacta atgagtatag ctacttaaac
22201 aaaataaaat gaaaccctgt cagtcttaag atttctagaa gtcgctgtcc tatacggaac
22261 ccaaaactct cactgttaat gaaataccat tgcggggcg aagatgtagc tcagtggtaa
22321 aatacttgcc agcacacaca agaattagac ttcaaccgct accaactgct ctgtgtagga
22381 cggtcggctc ctgaaagaga atattgtctg caatactcta atgacatctg tctgtgtta
22441 tctgaaatgt tccatttaaa acacagcagc cttactgttg gaccatttat ctcagtaatg
22501 attctgctcc gctttctttg tacaggaagc aacaacagta aaggaagaag tcttattggc
22561 agattagaaa cccagcctcc aatcactggg aaaggggttc cggtagaac aggcttttcc

22621 atcgatgagt tctctgcgct catcctcacc ggggaagctga ccacgggtctt tcttccggctc
 22681 gtctacatta ttgtgtttgt gattggtttg cccagtaatg gcatggccct ctggatcttc
 22741 cttttccgaa cgaagaagaa acaccccgcc gtgatttaca tggccaacct ggcccttggcc
 22801 gacctcctct ctgtcatctg gttccccctg aagatctcct accacctaca tggcaacaac
 22861 tgggtctacg gggaggccct gtgcaagggt ctcatctggct ttttctatgg taacatgtat
 22921 tgtccatcc tcttcatgac ctgctcagc gtgcagaggt actgggtgat cgtgaacccc
 22981 atgggacacc ccaggaagaa ggcaaacatc gccgttggcg tctccttggc aatctggctc
 23041 ctgatttttc tggtcacat ccctttgtat gtcatgaagc agaccatcta cattccagca
 23101 ttgaacatca ccacctgtca cgatgtgctg cctgaggagg tattggtggg ggacatgttc
 23161 aattacttcc tctcactggc cattggagtc ttctgttcc cggccctcct tactgcatct
 23221 gcctacgtgc tcatgatcaa gacgctccgc tcttctgcta tggatgaaca ctcagagaag
 23281 aaaaggcaga gggctatccg actcatcacc accgtgctgg ccatgtactt catctgcttt
 23341 gctcctagca accttctgct cgtagtgcac tatttctaa tcaaaaacca gaggcagagc
 23401 cacgtctacg ccctctacct tgtgcacctc tgctgtcga cctcaacag ctgcatagac
 23461 ccctttgtct attactttgt ctcaaaagat ttcagggatc acgccagaaa cgcgctcctc
 23521 tgccgaagtg tccgcactgt gaatcgcacg caaatctcgc tcagctccaa caagtctcc
 23581 aggaagtccg gctcctactc ttcaagctca accagtgta aaacctocta ctgagctgta
 23641 cctgaggatg tcaagcctgc ttgatgatga tgatgatgat ggtgtgtgtg tgtgtgtgtg
 23701 tgtgtgtgtg tgtgtgtgtg tgcaccctg tgtgagtgcg tggtagggat gcaccaacat
 23761 gcatggggct gtcatttctt atccaagctg cctgtctctg caccaatcac aagcatgcag
 23821 ctctcccag gattgccaga agcctcctcc tttgcatgag aacagtcttc cactctgatg
 23881 aaaagcatca gtatcagaaa ctgaaacgaa ctgagaggag cttgttttgt gaaagtgaag
 23941 agaagatgga gggtcagtga cttgcaaaaa aaaccaacca acaaaaaact acacctggca
 24001 agaaggctaa gactctctga aatgcttctt ttccatctg gagtctctc cggccttgtt
 24061 caggacctga ggcctggta gagcttcagt ccagttgatt gactttacag acttgagaga
 24121 ggagtgaatg aggagtgaat gaggctcctg gcggcatcct aaccggctaa cagtggcctt
 24181 gctggacaat aggattcaga tggctggagt tacatttca caccatttca tcagaactat
 24241 tggggatctt gatcaatgtg caggctcctt agcgtcagta accctgggag ctcagacacg
 24301 atgggggtga ggggtgggggt ggggggtggg gtgaggctct acaaacctta gtgatgactg
 24361 cagacacaga accatggagc tgagcctgct tctgcttggc agggcaccac tgtaatgttg
 24421 gcaaagaaaa accaacagca gtgttttgag cctctttttt tggtcagttt atgatgaatt
 24481 tgcctattgg tttattggga ttttcagttc ctttattact ttgttgaat tttgtgtgtt
 24541 tattagtcaa gaaaaagaag atgaggctct taaaaatgta aataaaattt ttggtttttt
 24601 ggttttttaa cttgggcca ctacaaatac tgcttaggtt ttttctaac ttaattgta
 24661 actacatcat gtgaacttaa gacattttca tgataaagca ttactgtagt gtcagttttc
 24721 cctcaccctc gatcatagtc cttcccgtga agcagggcc ttcccctccc ccccctttgc
 24781 cgtttccctc cccaccagat agtcccctgt ctgctttaac ctaccagtta gtattttata
 24841 aaaacagatc attggaatat ttattatcag ttttgttcac tgttatcagt tttgttact
 24901 aatttgtcca ataattggaat taacgtcttc tcatctgttt gaggaagatc tgaacaagg
 24961 ggccattgca ggagtacatg gctccaggct tactttatat actgctgta tttgtggctt
 25021 taaaaaaatg accttgttat atgaaatgct taaaaataaa taatgataga actttaaaaa
 25081 aaaaaaaaaac aagttctttc aggtctgtgt tttgtatgaa ggggggaggg gaggaagaga
 25141 ggggaatcct gctgttctag acattgtgat ctgacgcccc ccccacctg tctgttcttt
 25201 tctttctttc tttcaatttt aaacagtggt atgctcactc cacccttcc ttcttgaga
 25261 tggcgcacag caattaatga taacttcgta tagcatacat tatacgaagt tatggctcga
 25321 gctcgccatc agttcaacac acaacactag gaatctacac ctggccttgt gaatttacac
 25381 tttttctcac actagttttt caaataaagt gtagtctctg ttgttctgcc acaactacct
 25441 ttcgttaatt gttatgtcta aaattgtttt ctgtgtattt ctacaacgtg gtcattccatt
 25501 tttaaagggt atagaccctt taatagtctg gatataattac aatgaatata ttcccctctg
 25561 gatggcacct tgacttaggc taactcacgt gatttttttt tctttttgac tatttcagca
 25621 ttattgcttt gtacatctgt gtgtaggcat cattggcatt tactttactt ttatttagac
 25681 gggtttctact atattgcctt gaaactctct atgtacacca ggctgaccoc tcaactcct
 25741 agagatctgc ttgcctctgc ctcccagtg ctgggattaa ctgtatgtat gcaccatcac
 25801 agctggatct ttgagaatgt ttgtgaaggc tgtatttctg gaatagaacg gtcagctgaa
 25861 aagggtgtgtg tctagggggc ctggagagat ggctccctag ttaagagcat ttgtttcttt
 25921 tccagaggac cttggttcag ttctgctgtt ctgacagca gttctaagca ccatggtagt
 25981 aatggcttac aaaccatcct taactccggg tccagggcc ttgatggctc ctctgaccac
 26041 tggaggcatt cagcgtgcat gtggctggct ctctctctct ctctctctct ctctctctct
 26101 ctctctctct ctccctcaca cacacacaca gacacacaca cacacataca cgaaggacaa
 26161 acacacacac attaaataaa aacaactaaa tctttttttt ttaatttttt ttttttaaag
 26221 atttttattt attattatat gtaagtacac tgtagctgtc ttcagacact ccagaagagg
 26281 gcatcagatc ctgttacaga tgggtgtgag ccaccatgtg gttgctggga tttgaactct
 26341 ggacctttgg aaaagcagtc ggggtgctctt acccactgag ccatctcacc agcccaaac

Par-2
exon 2

P2 For

loxp

P3 rev

26401 aactaaatct taaaagaaga agttgcatat ctattgtggg gtgtgctaga tgcttattct
26461 aaatthttgat aatctthttgc caaatgtgct cagtatctaa atgcctgtat ctgthttccca
26521 aagcacttga ccacatttcc tgccaccagc cthttgaaat thttgctggtc agatthtgata
26581 cctctctgta ctcaagcatc actgtgtagc agthtgaagta caggcctgat ctatgtctgaa
26641 gctthggctct gccccttagc tctccgagag cgtthgcttg gaggataatt acgtctthtca
26701 cataaggctc agggatgagc tactgggcac atthctgtat tcccaagtht catgtagcag
26761 aataacacca gtctcctcat tcccaaggct tggctctgtg tagatcagth acccaaagtc
26821 aaactgctct gaaaatgcta aatgggaatt tghtcattth aaaacgtgca tghtctgagt
26881 aaggattgag gcaggactgg tgtgtgggtga gtctthtgccc agaattthcca ggcggthttgc
26941 cactatccag ctgtgtthttg gttatcagag tgggtgtctc agcccttgta thcaggtagc
27001 atattcttga aaggagagag tgtctgaaaa gggagataag aagacactac acgaagtgtc
27061 gagaccacat tcatgtaaact cctthttgggg actthtgtgat tghtctgtat taagthtgtca
27121 ctctctthtct gtgtthttata agthtgaattth tatcactggt atthtgtthtt gggagcatgc
27181 acatgcaggg gtccgtgggc ccacagthtgt thgtctgggga thcttggaatg catcccctaa
27241 gggtaagggt thctctgagat tggatctatg thtactagtaa gaaatgaaga gaaagatgag
27301 ataaaaaggt ccagagagcc thccacatgtc atctataaat thgtccagta gtaaaaaagct
27361 thtctgggtat thtgccattth thggcaattth thtaataat atatgtctgat tatgtthttta
27421 aaaaatcaaa cagctgagct ggagagatgg thcagthggt aagagcaggg gctggtcttc
27481 cagaagthct gagthttaat thccagcacc catggtgatt cacaaccatc tataaaggga
27541 thtagtgtcc thctctggta tgtgggtgta catgcagcat agaactcata tataagataa
27601 ataaatgaca taaacaacta taagthaaat gaactggtgg ccaagthtgg thgtgcacac
27661 thctaatccc agcactgagg aggcagaggc aggcagatcg ctgagthgcaa ggcagthctg
27721 gtctgcagag ctaathttcag gccagccagg gctacatagt gagaacctth thcaaaaata
27781 aaggatggag agatggthttc gtggthtggga actthtgtctc tathtgcagag aactggatt
27841 cagthcccgg cacacacatg gcagctcaca agaaactcca gthcccagg thctgcact
27901 gtctgttgt thccatgggt thccaagcaag cactthtgtg cacacgcaga cacagaatct
27961 atgtaaaaaat aaaaatgaca thccaacaaac gtaacagthta thtctthcac thttgcagag
28021 thctthggaga thctatthaaa thgthaaacgat ggtccaggat gthtgtact agthtagthac
28081 aggggtgtgg gctgaccctt agthactatth aaacgthaaa gthtagataca athagthatt
28141 tgagaaagaa thcaaaagaat atthtttagat acaaaagct thctggthaa thttacctth
28201 thttthttth thttctgtt thggagctca thgttagacca ggtggctc aaactcacia
28261 aggtcatct gtctctgtca cccgagthgt gggatcaaa ccatgtatca thcactacca
28321 ctgctgggca gthccatgag gthtagctthg aagctctgth thcttaagthta gacctggt
28381 tggagacaga aggaacctg cccagacaa gcagagacac thtgggtgca gthcatctgth
28441 thttthtgggt caactactgca thgcctgatt cgtctgaagg acctgagthct aacctgagaa
28501 tgagcattth gtactcccct gggccattth ctaggaaggc cctthaatth gaaagcagth
28561 tagactthgt thctctgtgca ggcctaaagth caaagctgac thcactgaaa thgaattctct
28621 gagcattthca thgtggtagg agththcaaag thgtaatthaa thtctggt atcaggattth
28681 cataaacct gtggtthtag thctcatctgt atgcacact cattgattac aactthattg
28741 ctgaaactth aatgctthtga gaggctctgth gaaggactag aatathttag aatcaagth
28801 agthcgtthgt tggagthttta ctggagact tghtctthtag aagthgaagth ctgagthcat
28861 atatgtatat gthtgtgctg thtatgtcat gaatathatg atacatacaa gthgtgtgtg
28921 tghtgtgtat gthtgtgtgt aagacagctg thcagthctc cctthgaatc cagthctaaa
28981 gggaaacacc thcctthgag thtaggaatca agacctcca cattaccaa gctthgagth
29041 aaagagthtgg thgtctagata thctatata aagcggggtc acggggtgca cacgctctta
29101 thgagggaaag tgtggaggcc thctgtgctt gggthtaggc tactctgtc thctactatt
29161 gthtaaatctc tghtctcatct gthtctgtct thctctgtag gggagagggth gcagctctgt
29221 gcagagthtgt gggacatcgt caacacaaac cacagacgth gctgacagga thctctgca
29281 gcagagcatc atcacccggc aggcagcagc ctgactggct catacatcac cacacattaa
29341 ctgcagacga cthagthcagg actctactc gggcatcagc cthagccatgg aggtgagth
29401 thccagthgaa thgcgggggth cthagaacgg cthagagaaat agctcatggg thaaaagthgc
29461 aaagthgctth thgtctthtag agaggatcaa gthttggtht ccaaaacctg ggtgactcaa
29521 aacctgthg aaggccagth cctggaaatc thaatgctgc cctctctthg actthgcacac
29581 acacacacac ccacaccccc cccacacacac acacacacac acacacacac acacacacac
29641 acacacatac acacacacac acacacacac acacacacac acatacacac acacacacac
29701 acacacacac acacacacac acacacccac acacacacac accacacacac ccacacatac
29761 acacacacac acacacacac acacacacac acatacacac acacacacac acatacacac
29821 acacacacac acacacacac acacacacac acatacacac acacacacac acatacacac
29881 acacacacac ccacacacac acacacacac acatacacac acacacacac acacacacac
29941 actcacacac acatacacac acacacacac acacacatac acacacacac acacacacac
30001 acacacacac acacacacac acggcacata aagctcatga agagacaagc atgcacatag
30061 thgaaaagaa aaatthcggct thctagagth taggtgctc aaaagcacth aaaacatcgt
30121 gthccaaagg gthtagagaac caagacaaac acaaaagagc thgtgtcatg gcgctgctc

30181 ttaatcccag cacttaggac gcagaggcag ggggatctgt atgagtgtgg ggccagcctg
30241 ggctacatag actctatctt acaacaacaa caacaacaag aaaacaagaa gacaagtggg
30301 gtggggggtt ggagagctag caagaacact tctgctatta tagaggacct gggtaggct
30361 cccagcacct atatcagggt gctcacaact acatataact ccagcctcag gtgatctagt
30421 gttctcttct gaccaccgtg ggcactggac aaatatggta cacactcaga caagcaggca
30481 tacacatcat atataaaaca aaacaacaaa acaaaaacca acccaaaaca aaacaacaaa
30541 aaaacaggga gagataccat gtaattacaa atttcttatg gattgcatgt tttgttcagt
30601 ttaggttttg gttttataat attttctttt tgaacagtc tccagtagt tctgacttgc
30661 ctagaattct ccatataggc ccgactgggc tcagagtcac ggggatctgc ctgcttctgc
30721 ctccaaagtg ctgggattac accgcactgt ttacttttat tttgttttat tttgagataa
30781 ggtttcacac tgtagctcag gctggcctga aagttactac gtagcccaag ttggctctga
30841 agtcatagca gccctcctat ttcagtctcc taaattctga gaaccacagg agagagccac
30901 catgcctggg tcaccctgtc ttagttactg ttcaactgct gtgatgacca cagcaactct
30961 tataaaagaa agcatttaac ggggggctgg cttacagttg agaggctcag tccattatca
31021 tcacggcaga gcacagcggg gcacacgtgg ctggaacgga agctgagagt tgtatcctgt
31081 tcctcaggca gagtgaggag cgagagactg ggcctggcat gagcttttga aacctcaaaa
31141 cccactccca gtgacacttt ccagtgcacat gactacatgt atcccaataa cccatacctc
31201 ctattccttt tcaaatagtt ccacaacctg gtgactattc aatgaatga gcctataaga
31261 ccattcttgt tcaactatc tatcacacac tttttaacaa tagcttaaaa tttacaaatc
31321 aaatacacat caaatgcctt gtagatctaa agatgttaac aagaagggaag gcccaagtta
31381 agaggcttga ataccactta gaagggggaa caaaatagtc atgggaggaa ggaagcatct
31441 ggggtgggaga gaggaggggt agaggaacag gggccaggat caggcatggg gagaaacgag
31501 agagtccag agaacaggag aatgagtga aatatgcagc tgtgtgtgta gggggttggg
31561 gatagctatg tgtgggggga ggaattcttt aggaagtccc agagacctgg gatgaaggag
31621 gctcccagga gtcaatagag gtggccttag ccaaaatgcc cagtggggat atggaatccg
31681 aagaaaacac ctgcagtagc cagataggac ccagtgagg ggatagggac accaaccac
31741 ctacaaaact ttttaccbaa aatttatcct gcgtaaaaga attgcagaga caaagatgga
31801 gcagtgacta atggaatggc agaccagtga ccagaccatt ttaggatcta tcacataggc
31861 aggaaccaat ccctcacact ataatgatg ctatgctgtg cttgcagaca ggagcctagg
31921 ttagcagccc tctgagaggc tttaccagc agctgactga ggctgatgca gagactcaca
31981 gacacacatt cgggtggagg tgaggacccc tgaggaagag ttaggggaag gattgaagac
32041 ccttaaggag atggcaaccc cacaggaaga ccaatagtgt caactaacca ggaccctgg
32101 gaactcccat aaactgagcc accaaccaaa gagcatacat gggctggctc gaggctccca
32161 acacatatgt agcagaggac tgccttgtct ggtctcgggt ggagaggatg tgcctaattc
32221 tgcaagactt gatgccttag agttggggga catgaagggg caccctctca gaggcaaaagg
32281 ggagggggga ggagggagga agtctgtgag gggggactag gaggggacag cgtttgggat
32341 gtaaagaaag aaaaggaagg agggaggagg gaggggaggga agggaggatg aaggacaaat
32401 caagtggtag aaaaacgtga tagtataaaa gcttatagag aagaataaag agccgggagg
32461 tgggtggcaca cgcttttaat cccagaactt gggaggcaga agcaggttga tttctgagtt
32521 tgaggccagc ctggcttaca aagtgagttc caggacagcc aggactatac agagaaaccc
32581 tgtctcaaaa aaaaaaaaaa caaaaaacaa aaaaaacaa aaaaaaaccc accaaaaaaa
32641 caaaacaaaa caaaacaaaa aaaaaaaaaa aataaagaac ccttctcaac caccacatc
32701 agaacacagt agctctcttt gtgaataact tgatgtgttc tatgctgga caagcatatg
32761 ttttgtatcc atgtttatat cttaattgca ttacctacta gtaatatatta cacataaatt
32821 gcctcagagt ttagtggctt acccaaccat ttgttaacat attctaggat catgaattca
32881 agagcaattg atcttcacca gtctaccttg gggctctgtt tgggtggccac caagatcttg
32941 gatgggtgctg atgtcaactg caggcctggg acacagtgcc aatgcagctc actcacaggg
33001 cagcctggga cacagtgcc ctgtggcact cacagggctg gtgagagctg ctctggcag
33061 caagcttcca ttccacctca cgaggatctc tccacagggc tgcttgagtg acctcacagc
33121 ataaaagcag gcttccttcc aaacaagcga cccaggaaaa caagagggaa gctgtaaaat
33181 cttgcttcag aggtcacacg ctgtcgtttc gttccacca tgctgacct gacacacaga
33241 ctagctacaa cccagctcgg gcagagactt ccaaggagag cgggcaagca ggtgagggcc
33301 attgagcaat ttggagtctg gcttgtatac tgtgcaggaa catacctcag gcagtatcat
33361 cgcacttaca catgcagact tgccccactg ttttaaatga ctgtgtctat tgtacacaca
33421 cacacacaca cacacacaca cacacacaca cacagaaaca cacacagaaa cacacacaat
33481 gcaatctgca gaatactata taacaatac ctgcatacct ttatcttgag tgcttgtctca
33541 cttaatatct tcctattcct ttttttttta aatctgtgtg ttatttcaag acagaatttt
33601 tttgtatagc cctggctgtc ctggaactca ctctgcagac cagactggcc tcaactcag
33661 aaactgtcct gcctctgctt ctgagtgct gggatcaaa ggtgtgtgcca cggctccac
33721 agccaccaac cggcttcttc tgttctttt atgtgccagg cttgtctag ttctaaatg
33781 gtattattgc agagaataaa ctagagcaag aatcttgttc ttgtggaatt tactttctga
33841 ttgggggaag aaagaaaact atgcataat ccaagtcag tcaacgggag agtaagtgcc
33901 atgggtgttc tatattgggg aatggtctta tctgaagggtg aaacttgagc accacatatt

33961 gtggtttctc attgctgtga ctaaataccc aaccagaagc accataaggg aggaaggggt
34021 tttttgact ttcagtttaa gaagagataa agtccctcac cgtaggaggg catgggtggg
34081 taagccggag acatctggtc acattgtatc tgcagtcaga aagtaggggac aggacagtaa
34141 atgggtccag gctacaaacc ctgaaggcct gcccacccaa ccacttcttc agttaaggat
34201 ccaccctta aatgttttta caacctacca aagaagcagg ttcacctaga gaccaatggt
34261 caaacacctc agctagtggg ggacatttca gatcagaacc acagcatgaa ggaccatggg
34321 tagacaaaaa gccaaaggctt catggagcaa ttaaggaaca gagagtgtgg gccagcaggt
34381 tacagagcta tcaaccctt ggtgtctgaa gggtaagaag cttgactctc attcttggtg
34441 agacaacgta ttcactggcc atttagaagg ccacaggtta ccatatgggt tgtggattga
34501 caagagcaag agcaagaaca gttcagggtg acccaagcga gagccaatgc tggtaggaat
34561 atgggtagta acaaagatgg agaggaagg gaccaactac actccattct ggagacaata
34621 ccaactgata ttaggaaagg aagattagag agtgtactga ctttttttct tgcctgaaga
34681 tgatggtgaa gtacctttcc atatctacct gttagcacac cgcaccaggc tggactggag
34741 ggagagaagc ttagccaggt cctgggtggg tggaggcagg atcttgggtg gtggtgagtg
34801 tgtgggcaaa gaacacatac acccatgaac acccagaacc tgactcagct tcatcgaggg
34861 tgagggtgag ggaggtggga ggaaggagta tttgtgccc tgggggtgg tcaagggtctc
34921 tggggaagtg tttgtgtggc catgaacaat tggccaggac aagggtgggtg gtggaaaagg
34981 ctccatctac atactaaagg cacctaataa ggtctaaca ggagtgaagc ctgatgactt
35041 tcagggtaat aaattcttac tagggtggat ggtggggcag ctggctttat ggtgccaggt
35101 tgggaggggg aggagggagc caactcctgc catcctgatc tgaggtttaa gatctccttg
35161 aaccttcttc tgaccagtcc tccataacc tgggccattg tggcccatg gagaagtact
35221 tgggtgtgag ctagtttgga atttgaaaag taaaggttct gttttgacca tggcatagcc
35281 ttaaatgtct tgatcagttt tctgttacca taaaaaata cttgaggtgc tgtgtctat
35341 aaagaaaaga agtttactta acccaacttt tgtttgtgtg tgctttctt tttctctaat
35401 ttatttcttt taattcactt tatgtgccga ttgtagcccc ccttctctc tctctccag
35461 tctctccctt acaaatccct cctcccatta cctcctcccc ttcttagtga aggaaagccc
35521 accctgggta ccaccccacc ctgggacatc tagccactgc aggactaggc atatcctctc
35581 ccgctgaggc ccaagaaggc agtccaggta gagaaagggg atccaatggc aggcaacaga
35641 gtcagagaca gccctgctc caattgttag gtgaccaca tgaagacca gccgcacatc
35701 tgctacaaat ttaaccaca gttttggagg tcagatatct aagaccagcc agctcaattg
35761 attcagcctc tggtaagggc cttatgggtg atgggtgcat aatgcagagg gtatacaaaa
35821 gagatggtaa gacaaaaaga cagagattca aagagcagac tctctctctc tctctttttt
35881 ataacaactt attcttggg gcactaacca ggggccatg aggactgtat tgatcctttc
35941 tgaagatggg gccctcaata gcctaaccac cttccacttg gataacgtgc tctctctctc
36001 tctctctctc tctctctctc tctgtgtgtc tgtgtgtgtg tctgtgtgtc tgtgtgtgtg
36061 tgtctgtgtg tgaatgtttg agacagggtt tctctgtgtg gtccctgggtg tccctgggtct
36121 cactctgtac tgctcctgaa ctcacagaga tctgttgett ctgtctctca ggttctggga
36181 ttaaggggtg gcgccaccac tgccctggctt ctttattggg ggtttgggga gactcccatc
36241 tcttaaagg tccactactt ttcagcacat tgccacacta aggggcaccc tcccccaac
36301 cctctaagg gacaaactca accatgtcct aaccatagca ctgagttga gatgtctaca
36361 gagacaagta aggcatttgg aaccagtcca gattttttct ttcttaattt aagaagagat
36421 ttataatatt aatttctatg tgtatgagtg ttttgcccac atgtctcacc atgcaccaca
36481 tgtgttcagt gactgcagag gccagaagag agctgaggtc acatgggggt gtgagtggt
36541 atgcctgtgc caggaacaac agcagcagtg gttaaatgct ttaaacgct gagacatctc
36601 cccagccctt agaatatctc ctaagcagca gttgggaatg gagcagtggc tttgccattg
36661 tgctagcatt taaatgaagc ttctttaagg gagagcacac aggtggagag gaggaagttt
36721 agggaggagg cttttaacag ttacaccatt gtggacaaaa gaagggccaa taaatagac
36781 caaaaatgag tgatgctggc cccggaggaa ctccatggaa gtcacaggca taaatcagag
36841 cttgcccata ttttctggat gcttctaagg ggtcaggtaa gataagagca aagaaggcaa
36901 tgagggtcat gctggcacac acacagaggt ggagacgatc agctgaggga gcaggaaagg
36961 gctttggatg ttctgcattc tagatatggc atctctaggt caaatgacat gtgtgacttt
37021 ctgatcataa taagttgctt ttctgaaccg ttgtgtggat atatacatct gccaatatta
37081 tgtgactatt ataaattttt gcattttatt ttatgtgtgt gcatgttttg cctgcatgca
37141 tgtctgcta tcacgtgtga gcctcgtatc tgtggaggcc agggagaggag ctacagcctg
37201 gagttacgga tacgatgatc gtgagcagcc atgttcatgc tagagattga accggatcga
37261 tctccagga gcatagccag tgccttggc tctcagagcc atcttttccag tcccaaatat
37321 gagtgtatct ttatacacgc catagaaaaa accaagcttc cactgctctt ggtacgtaaa
37381 agggagaaat taaagcctga gtcgacaatt attcggagtg tgggcaactg ggaagcagc
37441 aattgtttgc tttgtatttt acatcggggt ttatctgtca ctctctcca ctaagggagc
37501 agggatgggt tcacagtggc agaggagaca gtaaacaga tccatgggaa atctgatcct
37561 atctttcttt ctttctttct ttctttcttt ctttctttct ttctttcttt ctttctttct
37621 ttctttcttc cctccctccc tccctccctc cctccctccc tccctctctc tccctctctc
37681 cttccttctc tcttctcttc cttccttctc tcttctcttc ctttctttct tcttctttct

```

37741 tttcttttctt tcttttcttct tttcttttctt tctctttaaag atttatttat ttatttcatg
37801 tatgtgggta cactgtcact gtcttcagac acaccagaag agggcatcag atcccattac
37861 agaaggttgt gagctatcac gtggttgctg ggaaatgaac tcaggacctc tggagagca
37921 gtcagggctc ttaatcactg agccatctct ccagctcctg atcccacttt tctatgtgtt
37981 attgaaacaa aacctgagtt cttctgggta ggctcttcag ggagggatca tttgacattt
38041 gtgctttaga aggatccgtg ccattcttct gaggaggatg tgggggcatg gctcatacaa
38101 ttggcctgag agccttagcc ctgcaccctg gccagcttac cttaaagatca gggcttaatc
38161 ttcagcattt ggccaagtct ctactccag ctttacgggg agcctgcggc gagtactta
38221 cgtctggaga aagctcaaca gtgcttctgt gtagcattag gccaaactaat tagctaatac
38281 tgggagtgca ttttggccta gtcttctgct gggagctctt tcagatgcc a cctgggaacc
38341 tggaggggac tttgttcctt ctgcttctgct gtatccacca gaagggtctg tggacatggg
38401 gttaagacag tagaaagtcc cagcctagca cctagccttt cttagagtga gcttttaagc
38461 acaaaaatct atgtccatac atagagattg acatactttg gttgacaaga acactttgcc
38521 agaactagag aagtcaaaaa gcaaggctcag tacattttaga gactttccca gagctagact
38581 ttgatggatt aggtcttagt tttcattttt ggcagggtct tgctgtctaa gtgctgagtt
38641 tcacagcatg aatggactt ccagcatgga gacagctgcg ctaagatctg ggggcttact
38701 aaagtctggg gccctgctac aatccccact ggtcttagtg agtgagtcaa atcatggact
38761 catcctgttt tagtttgaga tgcagggcct cactgttaat cctaacagaa tgagcattta
38821 aggctcaggc aatgaggata gcagagctat tagccagagg gaccaggaga agagaaacca
38881 gtactaatta tttccccaac catggcaagg ctttctctaa ttactcctga tcagttagta
38941 cagaaacaac acttttctcc ccaaaccaca ccatttcctt tatttcatga gaagtctaag
39001 cgtctccaat tttgttggga ctatttcttc aagggaaatct aacttgctat aattctgaaa
39061 tggaaacttt taatacctct agggcctgat caacctgtct gcttagtttg gaaagcatca
39121 gaagaggttc atttagtcac tgatacatac tcaccagtgc tctcagagac ccagtaatat
39181 tgccgctatt caaatgaatt aactaaccga ctaggcagaa tagcaaacat ccgaataaac
39241 agaagtacct cggttaaagg ttttggatat taatcaagtt tgagccctt ataagtcctc
39301 tgacattegt ttgggctgtc cccagtcaca atgagttttg tcagttaacg ggctggccat
39361 ctggtttgtt cctgcctgtg tgtagtacag gggctgggtg tctgagcata accagcagtc
39421 ctggctgatt tcacctggga atgactaatc tctatcccca gggacataga atctgcttcc
39481 ccaggatfff tctgttttcc caaaggccag aatcttttaa aggatfffft caggaagcct
39541 cagttttaca acccccattt tcacagtgtg aactcccttg tttctggcaa ctagggggcc
39601 cagcctcagg acatgtatag aattgtaaat tctgtattcc tgtctcaaaa gataaattcc
39661 cacatctttc ctttctcca tacaagcaaa cacttaaagt gtgcatcagc aggtaaaggc
39721 ccacgtggaa tataggttgc tggctatag tcacactagc taattaatgc cttccctgta
39781 tctgtcttcc tcatgttca gcaggcctga gggctgtgag gcttagacca taaccctgtc
39841 ttcacatcca taatgtaaaa cataactcca ggggaggtgg agaggcaggc agaggaggaa
39901 cctcaggccc caggaaacct tactttcaat ggggttcgag tccagagaca gtccatttgg
39961 catcagtgtc tgtggcttct gctttctcta tctgggtgtg gtgggtctgt ggtgtaagtc
40021 agctaccttc acagctataa ggagtcgcaa gaatcacctt gtaggggtcac tttcagatta
40081 gttccagtgc ccctttgact ccttgcttga cccagatggt atcactggac tacgacaagg
40141 ttcagaaact ggtggtaaac tcagggttgg gtgggtctct cagatagttt aatgatcgcc
40201 tgtatggaag actggagcac cgacaatggc ctgagaaagg aatgattaca gatttttgcc
40261 aattgctggg ttctgagcag ggggaagcag gggggaaaca taatctcata tgagggcgaa
40321 taccttcata agtggggtgc agtgggctga agccaagcag aggagggaga cccaccatt
40381 ctttgt

```

Figure 8.2: Floxed PAR-2 allele. Primers, lox-p sites and exon 2 have been highlighted as detailed.

Appendix B – Wild type PAR-2 allele

The forward primers (p1/p2) were not specific to the wild type genomic sequence, so again no product was shown if the wild type sequence was present. Exon 2 has been highlighted in blue, and the reverse primer (p3) highlighted in purple.

W/T Mouse F2rl1 DNA sequence UCSC database

```
>mm10_dna range=chr13:95507912-95521422 5'pad=0 3'pad=0 strand=-
repeatMasking=none
TCAGGTTTTTTGAATAATGTACATTAGAGTCTTATGAAGCAGATGACAGC
GTATTATTTTATTTGGTTTCTTGTTTACAGTTGGCTGTATATTTCCGTAG
GAAGGTGAGTGTCTAATCTTAGGACTAGGGGTATAGTAACCTTAGAAGCAG
GCTGATACACAGGCCCGTTTCCCTGTTTGGCAGTCGTGGGGGCTGGGTGTG
GCCACGAACATGAGTGGGTGTATGTTTTTGTATGCCGTGACAGGAACGTGT
GATTGTAGCCCTACAAATAAGATGCACTCAGAGCCAGGTACTCTGGTGTG
TCCCCAGTTCGTAGTCACCCATAGTCTCCGCTCAGTTTTTGAAACACTGAG
CCTGGTTTACAAC TAGCATCAGGGATACCAGCAGTTTTGGTATGCAATACA
GAAAGGACAGAGCCTCAAGGACCTTTGAACTGGGACACAGATGGTTTTAA
TGTGAATGGCTGCTACCGTTTGCCTGTTGTTTGTGTTCTGTATTCAAGAT
CTTGCTGAATAGCCAGACTTGCCCTGGAACCTCATGATCTCCTGTCCCAGA
CTCTTCAGTGTGAGTTTAAAGCTGGGATTCCCAACTCTATTTTGTGAGG
GGCTTGGGGAGGCAGCCTGGAAATCAAGCCTTGTCATCCATGCTGGGCA
AGCACTTTACCACTGAGGTGCAGCCCCAACCTTTACAGTGGTATATCTGC
ACAGGGCTTGGGGAATCGAAGAATGACGCCCTCCTCCTCCTAGTCTTT
CTTCTCTTCTTTTTTAAAGTTTTTAACCCGAGCCATACTTCTTTAGTTG
GAATGTTGTTCTTAGTTACTTCTTTCTTTTATCATTCTTATACATTAGT
TTTGGTACCCACCACAACAGCAGTGATCAGTAATCTTGGGTAGATGTGT
TTCATCTCTACCCCTCAGCCTGTCTTTCTGTGTTACTTTTTAATAGCTTTAT
TAGGGTCTCGATGCCAAATAATTTTCATAACACACAGTTAGCCCATTTAA
AGAGAGTCCAGTGCCTTTTCGGTATACTTACAGAAATGTGACCATCCCAGT
GGTCAATTTGAACGCATTTTGATGACCCACAGGAATCCCCTTTGTGTGTTG
CATAACAGCCTTCCATAACAGCCCTGGCCACTGATAGTCAACTTTCTA
CCTATGGACTTGCCCTGTTCTAGATAATTTGATTAGATTCACATAAATGTATG
GGCTGCTGTGACTGGCTTCTTATTTAATGGTTTTGTTTTGTTTTTCAAG
ACTTACCCATGTTGCAGCATGCATCAACAACCTATTTCCCTTCCCTTCA
CTTTTTTTTTTTTTTTTTTTGAAACACCAATCATGGACTATCACGCCAGCA
TGTTTTGGTTGCATGTTTTGTTGCTTTGGTTGCATGTTTTGGTTGAGTCTCT
GAGTCTCATATGGCTCATGATGGCCTTGAACCTCACACTCAAGTTAGCCAT
GTTGTGAACGGAGGCGTTGAAGCTCCCCTCCTCATGGAGTGCCTGTGATTA
GTGTGGGCTTACCATAACCAGTTTTTATAGGGTGCTAGTGATCAGACTTCC
GGCTTCTGGTAGAAGCCCTCAGGCATGTAGAAGCTGAGCTATATCCCAG
CCTGTTTAGTTTTGAGATGGGTCTAGTTCTGCTGGGGCAGACTATCAA
TTCTTAGGCTTAAGCAATTTCCATACCTCAGCCAAGGTCTGCGGCAAGCA
TAGGCTACCATGTCTGGCTTCAGTACTTGATCTTTCTTGTGCTATGCTAGG
TGCCATCTCATGTGGACACTTCTCGTTTTTGTGTTTTGTTCTTCTGTTG
ATGGACTTTTTGAGTTGTTTCCATTTAGGGCTATTAGGAATAACGCTGCTT
TGAGTGCTAAGGTACAAGTTGTTTTCATGAATATATTTACCTTTTTCTTGG
GGATCGTGGTTGATCTTCGCTGTCGACTTGACTGGATTGGAATCATCACA
AAAACATTCCTGTGGGCATATCCATGAAGCGTTTTTCAGAACAGTTTTTTT
TAATGTTCTGTTTGTGTTTGGTTGGTTGGTTGGTTGGTTGGTTGGTTGGTT
TTTTCCCAGACAGGGTTTTTCTGTATAGCCCTGGCTGTCCCTGGAGCTCA
CTCTGTAGACCAGGCTGATCTCGATCTCAGAGACTCACTCCCTCGGCCCTC
CCATGTGCTAGGATTCGTGCCCTGCCAGAACAGTTCTAATTGAGGAGGGGA
ATTCTTATTCTGAGTGTGGCTGGGCACCCACCCTTTCCATAGGCTGGTCC
CAGCCTGCGTACAAGGAGAGGGCAAACCTGAGCATCAGCATGCATGTCTAC
CACCCCTCTCCTTCAGAGTGTGACTGTCTGTGTGGCATTCGTGCTTTGAG
CCTAAGGAAAACACTTCCCTCCCTTAGTTATGTGCTGAATCCTAGCAACAAG
AAACCTAAGGCTTGTGAGGATGCAGGCGAAGCTGGCAGTTTTGGGAGAGAG
AGAGGGCGCTCACACCAGATCCTAGCCGTGCTGTGGCTCCCCCTCCCCC
```

ATTTTTGTCCACCACAACTGTGAAGAATGTGTATGTTGTGTCTAAACCAC
TTTTTTTTTTGAGACAGGGTCTCTCTGTTTAGCCCTGGCTGTCTGGAAC
TCACTTTGTAGACCAGGCTGGCCTCGAACTCAGAAAATCCACCTGCCTCTG
CCTCCCAGTGTCTGGGATTAAAGGCGTGCACCATCACGCCATAACCACGTT
TTTAAATTACAGCCCCCCCCCTTCCCCGATTTTTTGTCCACCACAACTGT
GAGGAATATGTATGTTGTGTCTAAACCACTTTTTAAATTGCAGACCCCCCT
CCCCATCTGTGTGTGTATGTGTGTGTGTGTGTGTGTGTGTGTGTGTGTGT
TGTGTACATGGGGAGATAAGCTTGTGGTGTGGGACTTGTTCCTCTCAACC
ACGTGCGTTCTGGGGTTCAGAGTCAGGTATGCCAGCTTGGAAACCAAGCAC
CTTTACTCGATGAGCCATCTTGCCACCCCTGGCTGCTCACTTTTTATCTC
TGTTACATCTGCGCAGATGTACTGTGATCACAATGAGGTGAGAGTCTGTT
CCAGCAAGATTTCTTCAGAGTGTCTAATCATCTCTTATTTTTGTGTGGCCT
TAGTAGTTACAGAACATTATGTAACTTTTCTTTGGGAACAGAAGAAAATGG
ATTTTCCTTGCGAGAACTCTCAAGCCTCAGGCCACTGACCACAGAAGTTC
AGGGTGCTTTGAATGAGAGCGCACCCCCAATCCCAATAGGCTCGAATA
TTTGAATACCTGCTCTCTAGTGAGTGGCCCTGTCTGGAAGGTGTGGTGT
GCTGGGGCAGGCTTTGAGGTTAAGTGTCTCCACCACTTTTTGATTTTCCCT
CTGCTTTGTACTTGCCTTTGAAGGTGTGAGTTCCGATCTTCTAGTTCCCTG
CTGCCATGCCTGCAGCTTGTGGCCTGGTCTCCCCACCATGACACACCCTG
AGCGCTCCGAACTGTAGGCCCAAATAACATTTTTCTTCTGAAAATGGC
TTGCTCATAATATTGTGTATAGGAACAGAAAACTAACCACCAATACATG
CAGCGGGCTGTTTCAGGCCTGGATGCCTTTGCAGATGAGTGGGGTCCCCA
GACACTGGCCCACTGCTCACGGGTCTCTGGGCAGCTGTGGAGGATTTA
CAAAGCCTTTTTATTTTAAATCCCTCTAAAGGGCTGGCAGGACATGTTGA
CATTGATACAGGTGACTGTGTTAATTTTTGAAGGAGGGGCTAATTGAAGA
AAGTAACTTTTAGTGTGTTAAATTTACAATTTTAGATATTTTTGCTTGAGG
AAATGTATGTGTAGAAATCCATGCAGGTTGGGCAGATCTCTGTGCGGTCTA
ACATGTAGTACCAGTTAGGTGTGATGAGGGATAGCGAGCAAAACCATGGC
TTCTGGTAATGAACTAATTTTTCCACATAACAACGTTTTAACCTTAGGA
CCCACACTTAGTTACTGATTTGTGCCTTAGCTTCTTCATCTATAAAATGA
GGCAAAATAGCATGAGCTGCCTTCTCCGCTTTGTGGTGTATGTGGTACAG
GTGCCTTGCGTATAGTGCAGACCCTAGTTTCAGACCCACAGTGTGAGTGT
GCTAATCTCTATGATGGCACCCATGGTCTGTAAATTTGTTGTGGTCTAT
GTGCGGCCCTTGGCATTCCGTTTCCAGTCCAACGTCCTGTAGAAATGGC
TAGTGGAGCGGTGGCTTTGGATCCCCCTCACTTCTTCCAGGGATGTGGG
TAGCTGAGCATTGTAATCCAGAGGTATGTGAGGGCTGGGCCAGGGGCTGG
GTTAAAAGACACCTTTAATCCTATATAGGTTTCTTGCAGCTGTTGAGTCT
GCAAAACACATCATTACTGTTTCTTGGAGCTGCTTCAATGTTAGTGTGAGTCC
TGGTCTGCTTAAAAAAACACTCCAGAGAACCAACATGCATTTCTGTATA
GAAGGGTATTTTGTGCAATATTCATTATGGATCTATGTACTAAGTACTG
GGTTACCGTGCAGAACATATTTCTCATGGAGTTACCTAATTCAGTATCTG
AAGAACATTGTAATATTCAGGAATAATCTTTCTTGGAGACATGTATCCAG
GCTGGCCTCAAACTCACTATGTAGCTGCAGGCACCCCTTGGATTTACAATT
ATCCTGCCTCTACCTCCTGAGTCTTGGGGTTACAGTGTCTGGTACACAAT
AGGCAAAACACTCTACCAATTTGAGCTACATTTCCCCTCTCCTTAGGAATAT
TTGTTTTAATTTTTTAATTAATTAACCTAGAGATGGGAGCTCTATATAGCC
CTGGCTGGCCTGGAATTTCTATAATTTCTATCAAGCTGGCCTCAAAATCATA
GAGGTCTATTTGCCTCTGCCTCCAAAGTCCCATACTAAAGGCATATGCCG
CTACACCTGGCTTTGTTTTAAAATTGTTAAGTGATTTATGTATTTTATGA
ATGAGTAGTCTATCTGCATGGCACCTGTATGCCAGAAGAGGACATCAGAA
CTTATTATAGATGGCTGTGAGCCACCATGTTGTTGCTGAGAATTGAATTC
AGGACCTCTGGAAGAGCAGCTAGTCCCTTTAACCAGATGAGCCCTCTCTCC
AGCCCTTGTTTTTAATTTTTTCTTTTAAATCTTATTTAATATATGAGTGTCT
TGTTGCATATACATCTGCAGACCAGAAAAGAGCATCAGATCCCATACAGA
TGGTCACGAGCCACCATGCGGTTGTTGGGAATTTGAACCTAAGGACCTCTGA
AAGAACCAGTGTCTTAAACCCTGAACCATCTCTCCAGCTCTCTGCCCCC
ATTTTTAATTTTTTAAAAAGTGCTTTTTTTTTTTGGACAGTTATAGAAGAAAT
AGAAACAATATATATGTTTACGTCAAATGCTTTTTATTTTTCTTAAAGCCAC
TGTGATGAGCAGAGCTATAAAAACAACAGATGCTACTCTCTGGGTTCTGAG
GTGAGGGGTGAGGAATGAAAAGTGGTGGGGAAAAGAGAATCTGCCCATCTCC
AGCATCCGGTTGGGTGCTGCCATCTTTGGTGGCCCTTGGCACAGTGGCAG
CCTTTGTTCCCATTTGTCCATCATGTTGTTTACTCTGCTGTTTTCTCCTTT
TCTGTCCCCAGCTTCCCTATGTCTTGTAAAAGACCATTGTCTATTGGACC

GAGGGCCTGACTGGATAACCTGGATAGTGTGTTAAGATCGTACCTTAGG
GTTGCAAAAGACCCTTGTCTACTGGGGATTAGGACTTGAACACCTTCTTTT
TTGGGTAGGGAGCATCTTTATTTTTCTACAGTGGGTGGAAAGGGAAGTGC
TGATCTCTGTAACCTCCAGTGCCTCCCATTACCCCTGTGTGACGCGAA
CGTGGTGAAGCCTACAGAAGCGAACGGTCCCTGTAGAACCAGTGTGGAA
CCAGAAGCGGATCAGATAACTGAGCACACAATATATTAGAGAAAGTCAGG
AGAGGTATACTGTCTTCCCTTGTCAACGTGAACAATGTTTCAGGTGTTTCCA
GACGGTGGAGGCCTCAGTCTCATCAATTAAGTTAAATTCCTTAGCGTTCA
CCCTTCCCTCCTTTCAGGTGAGTGGGGAATACAGGATGGGGCAGGATGAAG
ACTGGGCTTGCCCGTCACTGCTTGGTAGGGTGTCTGTTTCGCTTTGCT
TTGGATGGAATCTCACTATGTCACCCAGGCTGGTCTCAGATTCCCTAAGT
GAAAACAGTCCATTACCTCAGCTTTCCAAATAGCTGAGACTATAGGCAC
AACCTACCACGCCAGGGTTATTTGTGGTTTAGAATGTTCAATTCATGGT
ATGAAGGAAGCATCCTAAGTTAAAGCTTGTCTGTTACACGCTCAAAGTCA
GAGCACATTTGGTCTGATGCTAAAAGGCTTGCCTGCCAAGTGTGAGCTCAG
TGGGAGGATGTTTATGAAGCCAGCAGAGAGGTGGGGAATGCCTACCCATT
ATAGTATTTCTTGTGGGCGGACAAGGGAATGCCTCCTGGTTCTGGAATCT
CCCTAGGCTGGCCCTGGGGCAGGGTGTGGTTGACGGCTAGGTTGAATCT
TGGCTTAAGGCCAGAGTAGGATAGAAAATGAGAACCAAGACAGCTGATGG
CAAGACAAGGCTGCCTTACTCACCAAAGACTCGGGAAGAGTTACCACACA
ATCCTAGACTGATCTATCTATCTATCTATCTATCTATCTATCTATCTATCT
TATCTATCTATCTATCTATCTATCTATCTATCTATCTATCTATCTATCTATCT
ACCAATCAAAGACTGCTGGTGGTGTGTGATCAAATAAAGAAGAAATGA
GTATAGCTACTTAAAGAAAATAAAAATGAAAACCTGTGAGTCTTAAAGATTT
CTAGAAGTCGCTGTCTTATACGGAACCCAAAACCTCTCACTGTTAATGAAA
TACCATTGTCGGGGCGAAGATGTAGCTCAGTGGTAAAATACTTGCCAGCA
CACACAAGAATTAGACTTCAACCGTCAACCACTGCCCTGTGTAGGACGGT
CGGTCACTGAAAAGAGAATATTGCTGCAATACTCTAATGACATCTGTCTG
TGTTCACTGAAATGTTCCATTTAAAACACAGCAGCCTTACTGTTGGACC
ATTTATCTCAGTAATGATTCTGCTCCGCTTTCTTTGTACAGGACGCAACA
ACAGTAAAGGAAGAAGTCTTATTGGCAGATTAGAAAACCCAGCCTCCAATC
ACTGGGAAAGGGTTCCGGTAGAACAGGCTTTTCCATCGATGAGTTCTC
TGCGTCCATCCTCACCGGAAGCTGACCACGGTCTTTCTTCCGGTCGTCT
ACATTATTGTGTTTGTGATTGGTTTGGCCAGTAATGGCATGGCCCTCTGG
ATCTTCCCTTTTCCGAACGAAGAAGAAAACCCCGCCGTGATTTACATGGC
CAACCTGGCCTTGCCGACCTCCTCTCTGTCTATCTGGTTCCCCCTGAAGA
TCTCCTACCACCTACATGGCAACCACTGGGTCACGGGGAGGCCCTGTGC
AAGGTGCTCATTGGCTTTTTCTATGGTAACATGTATTGCTCCATCCTCTT
CATGACCTGCCTCAGCGTGCAGAGGTACTGGGTGATCGTGAACCCCATGG
GACACCCAGGAAGAAGGCAACATCGCCGTTGGCGTCTCCTTTGGCAATC
TGGTCTCTGATTTTTCTGGTCAACCATCCCTTTGTATGTCATGAAGCAGAC
CATCTACATTCCAGCATTGAACATCACACCTGTACGATGTGCTGCCCTG
AGGAGGTATTGGTGGGGGACATGTTCAATTACTTCCCTCTCACTGGCCATT
GGAGTCTTCCGTGTTCCCGGCCCTCCTTACTGCATCTGCCCTACGTGCTCAT
GATCAAGACGCTCCGCTCTTCTGCTATGGATGAACACTCAGAGAAGAAAA
GGCAGAGGGCTATCCGACTCATCATCACCGTGTGGCCATGTACTTTCATC
TGCTTTGCTCCTAGCAACCTTCTGCTCGTAGTGCATTTATTTCCTAATCAA
AACCCAGAGGCAGAGCCACGTCTACGCCCTTACCTTGTGCGCCCTCTGCC
TGTCGACCCCTCAACAGCTGCATAGACCCCTTTGTCTATTACTTTGTCTCA
AAAGATTTAGGGATCACGCCAGAAACGCGCTCCTCTGCCGAAGTGTCCG
CACTGTGAATCGCATGCAAATCTCGCTCAGCTCCAACAAGTTCTCCAGGA
AGTCCGGCTCCTACTCTTCAAGCTCAACCAGTGTAAAACCTCCTACTGA
GCTGTACCTGAGGATGTCAAGCCTGCTTGTGATGATGATGATGATGATGGTG
TGT
AGTGCCTGGTAGGGATGCACCAACATGCATGGGGCTGTCAATTTCCATACC
AAGCTGCCTGTCTCTGCACCAATCACAAGCATGCAGCTCTCCCCAGGATT
GCCAGAAGCCTCCTCTTTGCATGAGAACAGTCTTCCACTCTTGTATGAAAA
GCATCAGTATCAGAACTGAAACGAACTGAGAGGAGCTTGTTTTGTGAAA
GTGAAGAGAAGATGGAGGGTCACTGACTTGCAAAAAAAACCAACCAAAACA
AAAACCTACACCTGGCAAGGAGGCTAAGACTCTCTGAAATGCTTCCTTTTTC
CATCTGGAGTTTCGTCTCGGCCCTTGTTCAGGACCTGAGGCCCTGGTAGAGC
TTCAGTCCAGTTGATTGACTTTACAGACTTGAGAGAGGAGTGAATGAGGA
GTGAATGAGGCTCCTGGCGGCATCCTAACCGGCTAACAGTGGCCTTGCTG

Seq starts to align 6789

start of exon - 7144

Exon 2 -1107 bp

End of exon - 8251

GACAATAGGATTCAGATGGCTGGAGTTACATTCTCACACCATTTTCATCAG
AACTATTGGGGATCTTGATCAATGTGCAGGTCCTTTAGCGTCAGTAACCC
TGGGAGCTCAGACACGATGGGGGTGAGGGTGGGGGTGGGGGTGGGGGTGA
GGCTCTACAAACCTTAGTGATGACTGCAGACACAGAACCATGGAGCTGAG
CCTGCTTCTGCTTGCCAGGGCACCCTGTAATGTTGGCAAAGAAAAACCA
ACAGCAGTGTTTTGAGCCTCTTTTTTTGGTCAGTTTTATGATGAATTTGCC
TATTGGTTTATTGGGATTTTCAGTTCCTTTATTACTTTTGTGTAATTTTGT
TGTGTTTATTAGTCAAGAAAAAGAAGATGAGGCTCTTAAAAATGTAAATA
AAATTTTTTGGTTTTTTTTGGTTTTTTAACTTGGGCCAACTACAAATACTGCT
TAGGTTTTTTTTCTAACTTAATTTGTTAACTACATCATGTGAACCTAAGACA
TTTTTCATGATAAAGCATTACTGTAGTGTGAGTTTTTCCCTCATCCTCGATC
ATAGTCCTTCCCGTGAAGCAGGGCCCTTCCCCCCCCCCCCCTTTGCCGTT
TCCCTCCCCACCAGATAGTCCCCTGTCTGCTTTAACCTACCAGTTAGTAT
TTTTATAAAACAGATCATTTGGAATATTTATTATCAGTTTTTGTTCAGTGT
ATCAGTTTTGTTCACTAATTTGTCCAATAATGGAATTAACGTCTTCTCAT
CTGTTTGAGGAAGATCTGAAACAAGGGGCCATTGCAGGAGTACATGGCTC
CAGGCTTACTTTATATACTGCCGTGATTTTGTGGCTTTAAAAAAATGACCT
TGTTATATGAATGCTTTATAAAATAAATAATGCATGAACCTTAAAAA
AAAAACAAGTTCTTTTCCAGGCTGTGTGTTTGTATGAAGGGGGGAGGGGAGG
AAGAGAGGGGAATCCTGCTGTTCTAGACATTGTGATCTGACGCCACCC
ACCCTGTCTGTTCTTTCTTTCTTTCTTTCAATTTTAAACAGTGTGATGC
TCACTCCACCCCTTCCCTCCCTTCCCTCCCTTCCCTTCCCTTCCCTTCCCT
CCTTCCCTCCCTCAGCCCCCTCCACCCCCCACTCACACACACACACAC
ACTAGGAATCTACAC
CTGGCCTTGTGAATTTACACTTTTTCTCACACTAGTTTTTCAAATAAAGT
GTAGTTCCCTGTTGTTCTGCCACAACCTACCTTTTCGTTAATTGTTATGTCTA
AAATTGTTTTCTGTGTATTTCTACAACGTGGTCATCCATTTTTAAAGGTT
ATAGACCCCTTAAATAGTCTGGATATATTACAATGAATATATCCCTCCTG
GATGGCACCTTGACTTAGGCTAACTCACGTGATTTTTTTTTTCTTTTTGAC
TATTTACAGCATTATTGCTTTGTACATCTGTGTGTAGGCATCATTGGCATT
TACTTTACTTTTATTTAGACGGGTTTCACTATATTGCCCTGAAACTCTCT
ATGTACACCAGGCTGACCCGTTCAACTCCTAGAGATCTGCTTGCCTCTGC
CTCCCGAGTGCTGGGATTAACGTATGTATGCACCATCACAGCTGGATCT
TTGAGAATGTTTGTGAAGGCTGTATTTCTGGAATAGAACGGTCAGCTGAA
AAGGTGTGTGCTAGGGGGCCTGGAGAGATGGCTCCCTAGTTAAGAGCAT
TTGTTTTCTTTCCAGAGGACCTTGGTTTCACTTCTGCTGTTCTAGACAGCA
GTTCTAAGCACCATGGTAGTAATGGCTTACAAACCATCCTTAACTCCGGT
TCCAGGGCCCTTGATGGTCTCTCTGACCACTGGAGGCATTCAGCGTGCAT
GTGGCTGGCT
CTCCCTCACACACACACACAGACACACACACACACACATACACGAAGGACAA
ACACACACACATTAATAAAAAACAATAAATTTTTTTTTTTTTAATTTTTTT
TTTTTTAAAGATTTTTATTTATTTATTTATATGTAAGTACACTGTAGCTGTC
TTCAGACACTCCAGAAGAGGGCATCAGATCCTGTTACAGATGGTTGTGAG
CCACCATGTGGTTGCTGGGATTTGAACTCTGGACCTTTGGAAAAGCAGTC
GGGTGCTCTTACCCACTGAGCCATCTCACCAGCCAAAACAATAAATCT
TAAAAGAAGAAGTTGCATATCTATTGTGGGGTGTGCTAGATGCTTATTCT
AAATTTTGATAATCTTTTGCCAAATGCTTTCAGTATCTAAATGCCCTGTAT
CTGTTTCCCAAAGCACTTGACCACATTTCCCTGCCACCAGCCTTTTGAAT
TTTGCTGGTCAGATTTGATACCTCTCTGTACTCAAGCATCACTGTGTAGC
AGTTGAAGTACAGGCTGATCTATGCTGAAGCTTGGCTCTGCCCTTAGC
TCTCCGAGAGCGTTGCTTGTGAGGATAATTACGTCTTTCACATAGCGCTC
AGGGATGAGCTACTGGGCACATTTCTGTATTCCCAAGTTGCATGTAGCAG
AATAACACCAGTCTCCTCATTTCCCAAGGCTTGGTCTTGTGTAGATCAGTT
ACCCAAAGTCAAACCTGCTCTGAAAATGCTAAATGGGAATTTGTTTCAATTT
AAAACGTGCATGTTCTGAGTAAGGATTTGAGGCAGGACTGGTGTGTGGTGA
GTCTTTGCCCAGAATTTCCAGGCGGTTTGGCACTATCCAGCTGTGTTTTG
GTTATCAGAGTGGGTGTCTCAGCCCTTGTATTTCAGGTAGCATATCTTGA
AAGGAGAGAGTGTCTGAAAAGGGAGATAAGAAGACACTACACGAAGTGC
GAGACCACATTCATGTAACCTTTTGGGGACTTTGTGATTGTCTTGTAT
TAAGTTGTCACTCTCTTCTGTGTTTTATAAGTTGAATTTTTATCACTGGT
ATTTGTTTTTGGGAGCATGCACATGCAGGGTCCGTGGGCCACAGTTGT
TTGCTGGGATCTTGGAAATGCATCCCTAAGGGTAAGGGTCTTCTGAGAT
TGGATCTATGTTACTAGTAAGAAATGAAGAGAAAGATGAGATAAAAAGGT

P2forward

P3 rev

CCAGAGAGCCTCCACATGTCATCTATAAAATTTGTCCAGTAGTAAAAAGCT
TTTCTGGTATTTGCCATTTATTTGGCAATTTTTTAAATAATATATGCTGAT
TATGTTTTTAAAAAATCAAACAGCTGAGCTGGAGAGATGGTTCAGTGGTT
AAGAGCAGGGGCTGGTCTTCCAGAAGTCTGAGTTTTAATTTCCAGCACCC
CATGGTGATTACAACCATCTATAAAGGGATCTAGTGTCCCTTCTGGTA
TGTGGGTGTACATGCAGCATAGAACTCATATATAAGATAAAATAAATGACA
TAAACAACCTATAAGTAAATGAACTGGTGGCCAAGTGTGGTGGTGCACAC
TTCTAATCCCAGCACTGAGGAGGCAGAGGCAGGCAGATCGCTGAGTGCAA
GGCCAGTCTGGTCTGCAGAGCTAATTTTCAGGCCAGCCAGGGCTACATAGT
GAGAACCCTTTCTCAAAAAATAAAGGATGGAGAGATGGTTTTCTGGTTGGGA
ACTTTGCTCCTATTGCAGAGAACTTGGATTTCAGTTCCCGGCACACACATG
GCAGCTACAAGAACTCCAGTTCCAGGGATCTGACACTGTCTTGTGTGT
CTCCATGGGTACCAAGCAAGCACTTGTGTGCACACGCAGACACAGAATCT
ATGTAAAAATAAAAAATGACATCCAACAAACGTAACAGTTACTTTCTTCAC
TTTTGCAGAGTCTTTGGAGATCTATTAATAATGTAAACGATGGTCCAGGAT
GTTGCTTACTAGTAGAGTACAGGGGTGTGGGCTGACCCTTAGTACTATTG
AAACGTAAAAGGTAGATACAATAAGTATTTTTGAGAAAAGAAATCAAAGAAT
ATTTTTAGATACAAAAGCTTTCTTGGTAAGTTTTTACCTTTTTTTTTTTTTT
TTTTCTGTCTGGAGCTCATTGTAGACCAGGCTGGCCCTCAAACCTCACAA
AGGTCATCCTGTCTCTGTCAACCGAGTGTGGGATCAAAGCCATGTATCA
TTCATACCCTGTCTGGGCAGTTCCATGAGGGTAGCTTGGAAAGCCTCTGG
TCTTAAGTTAGACCCTTGGTTGGAGACAGAAGGAACCATGCCCCAGACAA
GCAGAGACACCTTGGGTGCAGTCATCTTGGCTTTTTGTGGTCAATACTGCA
TCGCCTGATTCTGTCTGAAGGACCTGAGTCTAACCCGAGAATGAGCATTTTT
GTACTCCCCTGGGCCATTTACTAGGAAGGCCCTTAATTTGAAAGCAGTG
TAGACTTGTCTTTCTGTGCAGGCCAAAGTTCAAAGCTGACTTCACTGAAA
TGAATTTCTGAGCATTTCAATTGTGGTAGGAGTTTCAAAGTTGTAATTA
TTTCTGGTTATCAGGATTTTATAAACCCTGTGGTTATAGTCTCATCTGT
ATGCACACTTCATTGATTACAACCTTTATTGCTGAAACCTTTAATGCTTTGA
GAGGCTCTGGGAAGGACTAGAATAATTTAGAAATCAAGGTTAGTCGCTTGT
TGGAGTTTTACTGGAGAGCTTGTCTCTTAGAAGTGAAGTTCTCGAGTCAT
ATATGTATATG

Figure 8.3: Wild type PAR-2 allele. Primer and exon 2 have been highlighted.

Appendix C – Measurement of subchondral sclerosis separating the subchondral plate from the underlying trabecular bone

Analysis was performed only in the medial epicondyle of the tibiae in this method, as this was where most significant subchondral bone changes were observed in animal OA models [65, 229, 233]. Shown below was the initial method of separating the sclerotic subchondral plate from the underlying trabecular bone and analyzing trabecular thickness (μm) in the sclerotic plate region as a measurement of sclerosis. Significant sclerosis was observed at 4, 12 and 16 weeks post-surgery in the DMM group relative to sham, with a similar pattern observed at 8 weeks post-surgery (not significant). (Figure 8.4)

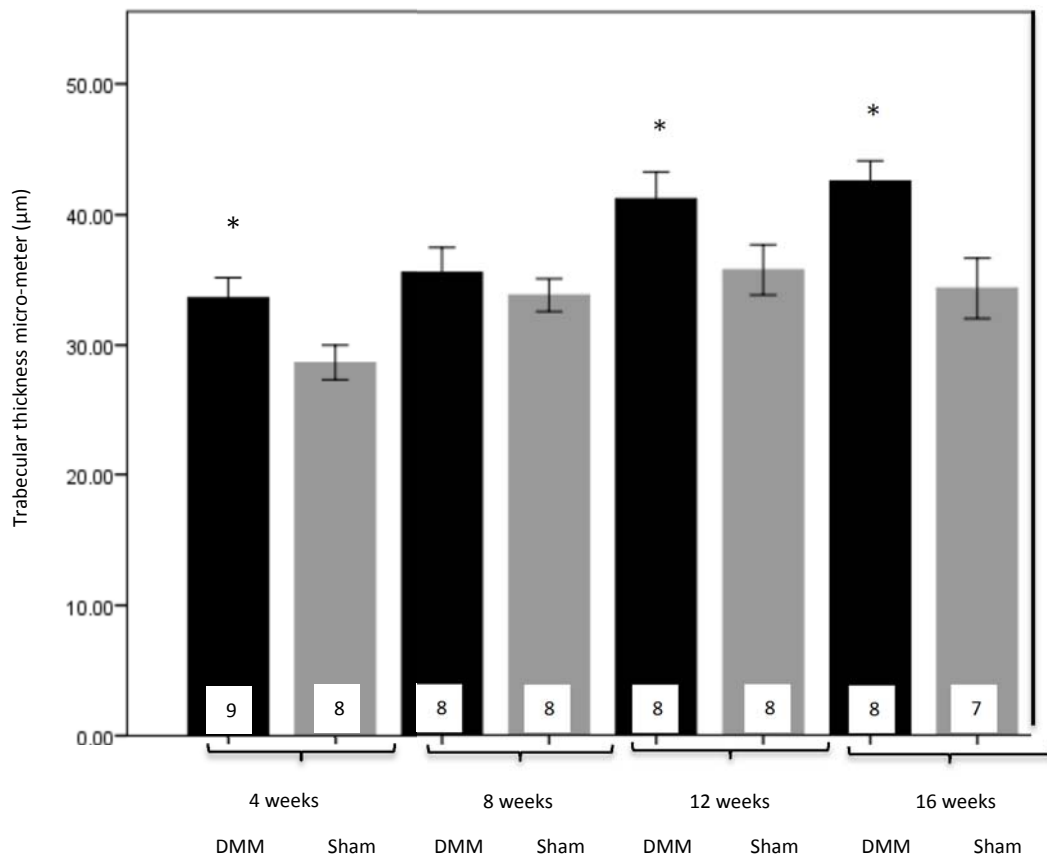


Figure 8.4: Measurement of subchondral sclerosis in a wild type murine OA model. Wild type mice underwent DMM or sham surgery at 10 weeks of age. These mice were then sacrificed at 4, 8, 12 or 16 weeks post-surgery. The affected limb was then dissected and fixed in 10% buffered paraformaldehyde for up to 72 hours and then transferred into 70% ethanol. The limb was then scanned using a micro-CT SkyScanner and the images reconstructed as described in section 2.2.10. Analysis then took place using CTan software as described in section 2.2.10 to measure subchondral sclerosis (trabecular thickness μm). * represents DMM compared to sham. * $p < 0.05$. The number in the white box represents the number of mice in each group. Error bars +/- SEM. Independent samples T-test.

Appendix D – Genotyping

All mice represented below were from the same lineage used in this research, and genotyping was performed by Hua Lin. (Research Associate, MRG)

Matriptase (ST14) floxed allele

In order to detect the floxed matriptase allele, primers p4/p5 (table 2.1, section 2.2.6) were used with a product of 450bp for the floxed allele and 425bp for the non-floxed allele (figure 8.5), with the reference ladder as shown in figure 8.6. There were some initial problems with the PCR protocol producing false positive results for the homozygous floxed allele however, this has since been improved.

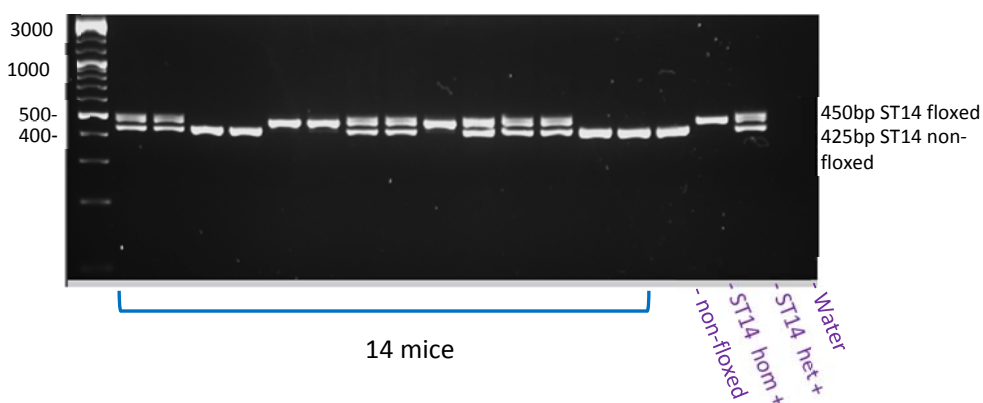


Figure 8.5: Semi-quantitative PCR for floxed ST14 allele. An ear notch was taken and genomic DNA extracted as described in section 2.2.6. Subsequently the DNA was amplified by PCR using specific primers as detailed in section 2.2.6. The resultant product was then visualised by intercalation of ethidium bromide and UV light generated by a GelDoc machine. A reference ladder was used (O'Gene Ruler DNA ladder mix, below) to identify the size of the product. The primers used for floxed ST14 were p4/p5. A positive control (+) for non-floxed, homozygous floxed and heterozygous floxed were used as a reference. Water was used as a negative control.

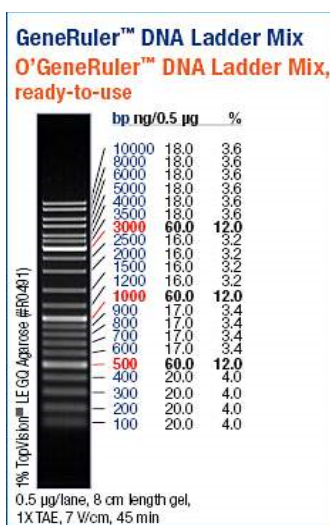


Figure 8.6: DNA reference ladder

Matriptase exon 2 ablation

To detect excision of exon 2, primers p5/p3 were used (table 2.1, section 2.2.6), with a product of 900bp for non-excision (with neomycin cassette) and 450bp for successful excision (figure 8.7), with the reference ladder shown in figure 8.6. As observed below, many of the samples have a band at 900bp and 450bp suggesting that exon 2 had not been successfully ablated. As discussed in chapter 5, this was likely due to poor expression of cre in the target tissue, resulting in inconsistent or no excision of exon 2 in the target tissue.

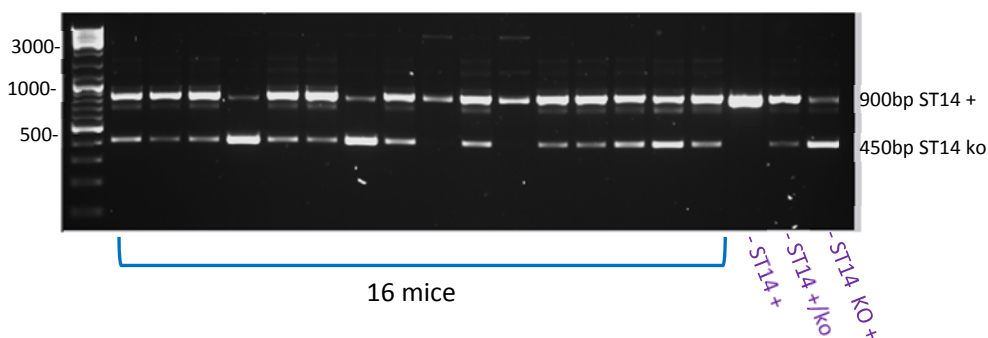


Figure 8.7: Semi-quantitative PCR (genotyping) cartilage-specific matriptase exon 2 ablated mice. An ear notch was taken and genomic DNA extracted as described in section 2.2.6. Subsequently the DNA was amplified by PCR using specific primers as detailed in section 2.2.6. The resultant product was then visualised by intercalation of ethidium bromide and UV light generated by a GelDoc machine. A reference ladder was used (O'Gene Ruler DNA ladder mix) to identify the size of the product and confirm successful ablation of exon 2. The primers used for excision were p3/p5. A positive control (+) for ST14 + with no excision (neomycin cassette present), ST14 +/-knock-out and ST14 knock-out were used as a reference.

PAR-2 floxed allele (PAR-2 col2;cre)

Primers p2/p3 (table 2.1, section 2.2.6) were used to detect the floxed allele, giving a product of 173bp (non-floxed allele) and 149bp, (floxed allele) observed in figure 8.8, with the reference ladder shown in figure 8.6. For confirmation of base pair product size, refer to appendix A and B.

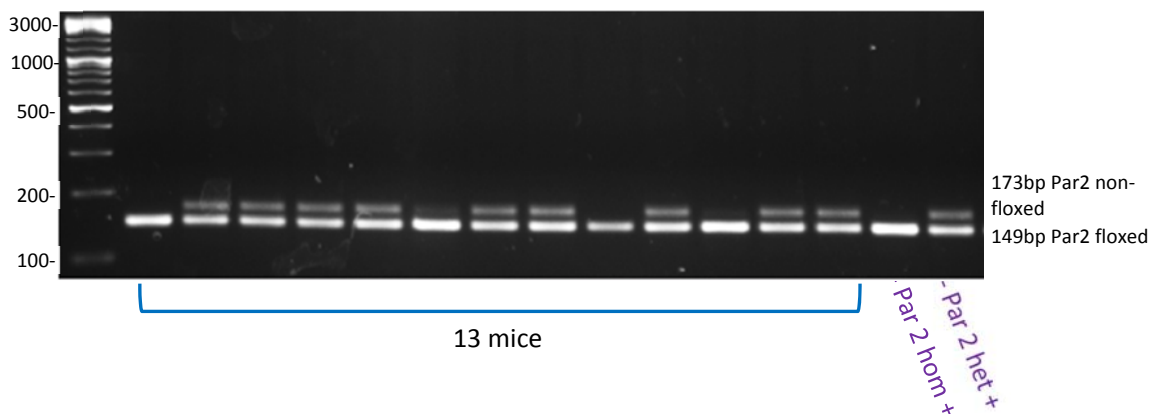


Figure 8.8: Semi-quantitative PCR (genotyping) floxed PAR-2 allele. An ear notch was taken and genomic DNA extracted as described in section 2.2.6. Subsequently the DNA was amplified by PCR using specific primers as detailed in section 2.2.6. The resultant product was then visualised by intercalation of ethidium bromide and UV light generated by a GelDoc machine. A reference ladder was used (O'Gene Ruler DNA ladder mix) to identify the size of the product. The primers used for floxed PAR-2 were p2/p3. A positive control (+) for PAR-2 homozygous floxed and PAR-2 heterozygous floxed were used as a reference.

PAR-2 exon 2 ablated allele (PAR-2 col2;cre)

To detect ablation of exon 2 primers p1/p3 (table 2.1, section 2.2.6) were used, giving a product of 116bp for successful ablation, and no product for non-excision (product too large to detect on PCR). (Figure 8.9)

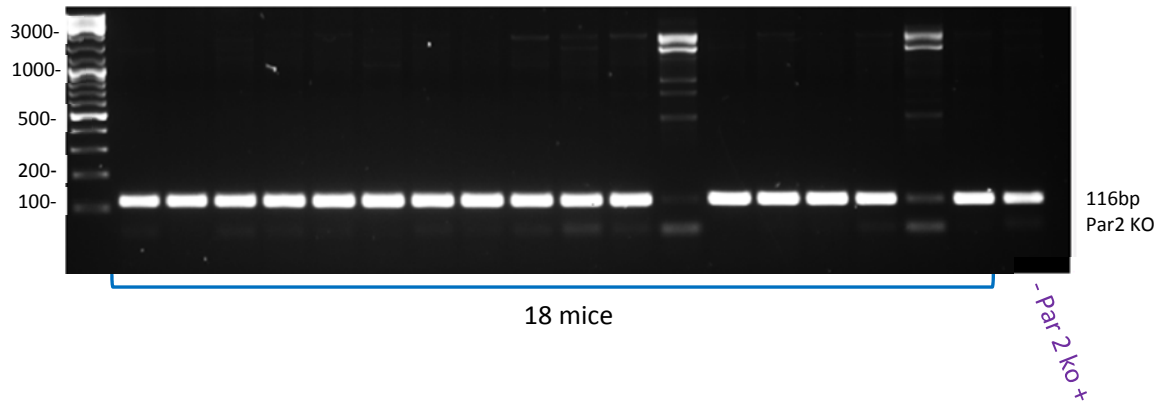


Figure 8.9: Semi-quantitative PCR (genotyping) cartilage-specific PAR-2 exon 2 ablated mice. An ear notch was taken and genomic DNA extracted as described in section 2.2.6. Subsequently the DNA was amplified by PCR using specific primers as detailed in section 2.2.6. The resultant product was then visualised by intercalation of ethidium bromide and UV light generated by a GelDoc machine. A reference ladder was used (O'Gene Ruler DNA ladder mix) to identify the size of the product and confirm successful ablation of exon 2. The primers used for excision of exon 2 were p1/p3. A positive control (+) for PAR-2 exon 2 knock-out was used as a reference.

PAR-2 floxed allele (PAR-2 oc;cre)

Similar to the PAR2 col2;cre mice, primers p2/p3 (table 2.1, section 2.2.6) were used to detect the floxed allele, (figure 8.10) with the reference ladder shown in figure 8.6. The effects of oc;cre will not be observed in the cartilage, so ablation of exon 2 cannot be shown in an ear notch sample.

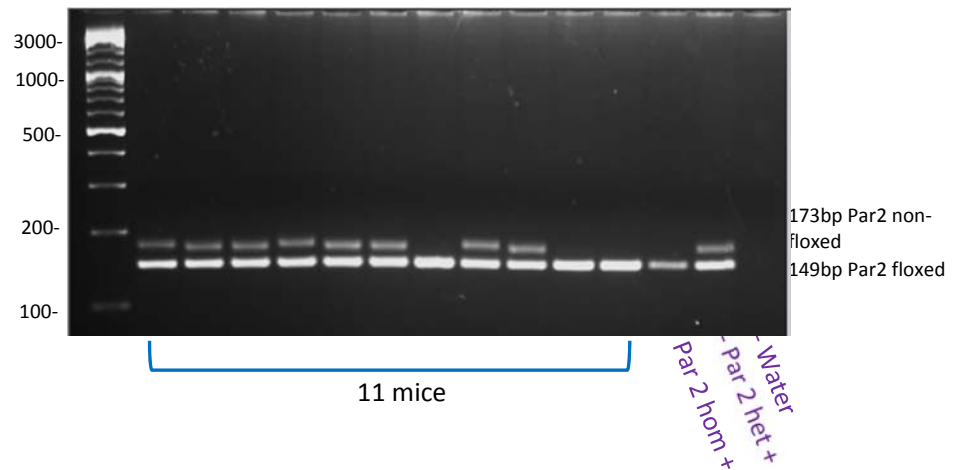


Figure 8.10: Semi-quantitative PCR (genotyping) floxed PAR-2 allele. An ear notch was taken and genomic DNA extracted as described in section 2.2.6. Subsequently the DNA was amplified by PCR using specific primers as detailed in section 2.2.6. The resultant product was then visualised by intercalation of ethidium bromide and UV light generated by a GelDoc machine. A reference ladder was used (O'Gene Ruler DNA ladder mix) to identify the size of the product. The primers used for floxed PAR-2 were p2/p3. A positive control (+) for PAR-2 homozygous floxed and PAR-2 heterozygous floxed were used as a reference, and water as a negative control.

Col2;cre

Shown in figure 8.11, forward and reverse primers were used to detect the presence of col2;cre (table 2.1, section 2.2.6), with the reference ladder shown in figure 8.12.

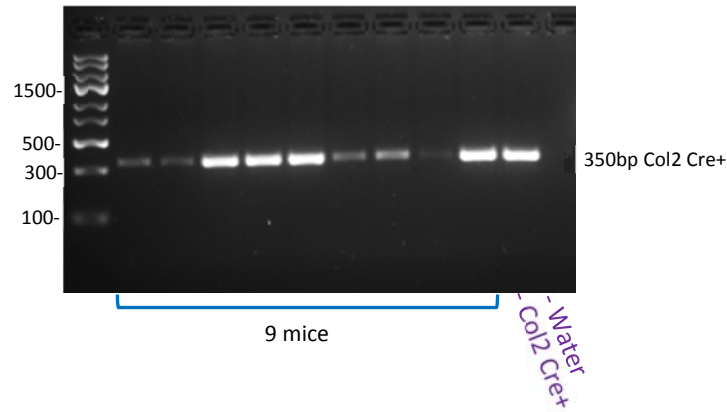


Figure 8.11: Semi-quantitative PCR (genotyping) col2;cre. An ear notch was taken and genomic DNA extracted as described in section 2.2.6. Subsequently the DNA was amplified by PCR using specific primers as detailed in section 2.2.6. The resultant product was then visualised by intercalation of ethidium bromide and UV light generated by a GelDoc machine. A reference ladder was used (O'GeneRuler Express DNA Ladder, below) to identify the size of the product. Primers used for col2;cre were forward and reverse as detailed in section 2.2.6. A positive control (+) for col2;cre was used as a reference, and water as a negative control.

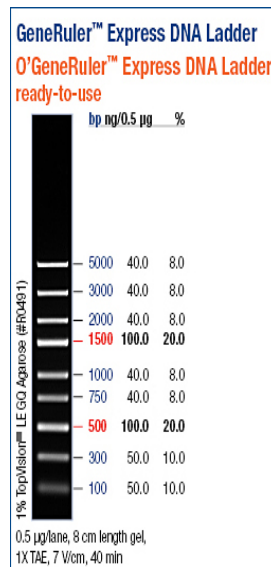


Figure 8.12: DNA reference ladder

Oc;cre

Observed in figure 8.13, forward and reverse primers were used to detect the presence of oc;cre (table 2.1, section 2.2.6), with the reference ladder shown in figure 8.14.

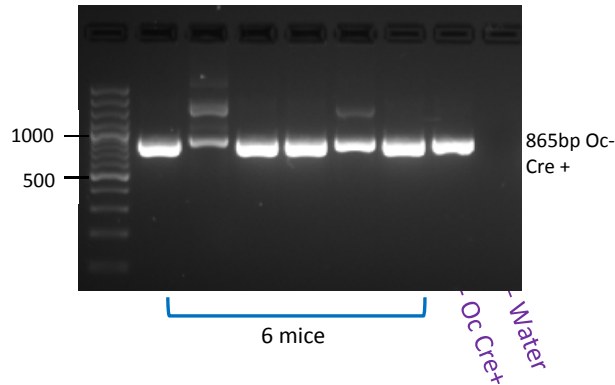


Figure 8.13: Semi-quantitative PCR (genotyping) oc;cre. An ear notch was taken and genomic DNA extracted as described in section 2.2.6. Subsequently the DNA was amplified by PCR using specific primers as detailed in section 2.2.6. The resultant product was then visualised by intercalation of ethidium bromide and UV light generated by a GelDoc machine. A reference ladder was used (O'GeneRuler 100bp Plus DNA Ladder, below) to identify the size of the product. Primers used for oc;cre were forward and reverse as detailed in section 2.2.6. A positive control (+) for oc;cre was used as a reference, and water as a negative control.

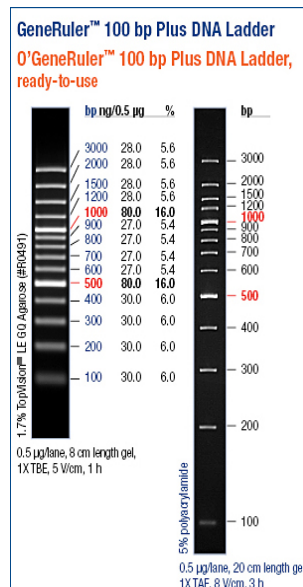


Figure 8.14: DNA reference ladder

References

1. Glasson, S.S., et al., *The OARSI histopathology initiative - recommendations for histological assessments of osteoarthritis in the mouse*. *Osteoarthritis Cartilage*, 2010. **18 Suppl 3**: p. S17-23.
2. Williams, G.N., M.J. Higgins, and M.D. Lewek, *Aging Skeletal Muscle: Physiologic Changes and the Effects of Training*. *Physical Therapy*, 2002. **82(1)**: p. 62-68.
3. Collins, J., *Letter from the Editor: Effects of Aging on the Musculoskeletal System*. *Seminars in Roentgenology*, 2013. **48(2)**: p. 105-106.
4. Hamerman, D., *Clinical implications of osteoarthritis and ageing*. *Annals of the Rheumatic Diseases*, 1995. **54(2)**: p. 82-85.
5. Hamerman, D., *Aging and the musculoskeletal system*. *Annals of the Rheumatic Diseases*, 1997. **56(10)**: p. 578-585.
6. Karasik, D. and M. Cohen-Zinder, *The genetic pleiotropy of musculoskeletal aging*. *Frontiers in Physiology*, 2012. **3 AUG**.
7. Sulzbacher, I., *Osteoarthritis: histology and pathogenesis*. *Wiener Medizinische Wochenschrift*, 2012: p. 1-8.
8. Sacco, A., et al., *Short telomeres and stem cell exhaustion model Duchenne muscular dystrophy in mdx/mTR mice*. *Cell*, 2010. **143(7)**: p. 1059-71.
9. Rogers, M.A. and W.J. Evans, *Changes in skeletal muscle with aging: effects of exercise training*. *Exerc Sport Sci Rev*, 1993. **21**: p. 65-102.
10. Nair, K.S., *Aging muscle*. *Am J Clin Nutr*, 2005. **81(5)**: p. 953-63.
11. Hügle, T., et al., *Aging and osteoarthritis: An inevitable encounter?* *Journal of Aging Research*, 2012. **2012**.
12. Syed, F.A. and A.C. Ng, *The pathophysiology of the aging skeleton*. *Current Osteoporosis Reports*, 2010. **8(4)**: p. 235-240.
13. Rahmani, P. and S. Morin, *Prevention of osteoporosis-related fractures among postmenopausal women and older men*. *Cmaj*, 2009. **181(11)**: p. 815-20.
14. Khosla, S., et al., *Effects of age and estrogen status on serum parathyroid hormone levels and biochemical markers of bone turnover in women: a population-based study*. *J Clin Endocrinol Metab*, 1997. **82(5)**: p. 1522-7.
15. Rosen, C.J., L.R. Donahue, and S.J. Hunter, *Insulin-like growth factors and bone: the osteoporosis connection*. *Proc Soc Exp Biol Med*, 1994. **206(2)**: p. 83-102.

16. Boonen, S., et al., *Down-regulation of the serum stimulatory components of the insulin-like growth factor (IGF) system (IGF-I, IGF-II, IGF binding protein [BP]-3, and IGFBP-5) in age-related (type II) femoral neck osteoporosis.* J Bone Miner Res, 1999. **14**(12): p. 2150-8.
17. Zhu, S., et al., *Alendronate protects against articular cartilage erosion by inhibiting subchondral bone loss in ovariectomized rats.* Bone, 2013. **53**(2): p. 340-349.
18. Lotz, M. and R.F. Loeser, *Effects of aging on articular cartilage homeostasis.* Bone, 2012. **51**(2): p. 241-248.
19. Loeser, R.F., *Aging and Osteoarthritis: The Role of Chondrocyte Senescence and Aging Changes in the Cartilage Matrix.* Osteoarthritis and cartilage / OARS, Osteoarthritis Research Society, 2009. **17**(8): p. 971-979.
20. Loeser, R.F., et al., *Reduction in the chondrocyte response to insulin-like growth factor 1 in aging and osteoarthritis: studies in a non-human primate model of naturally occurring disease.* Arthritis Rheum, 2000. **43**(9): p. 2110-20.
21. Blaney Davidson, E.N., et al., *Reduced transforming growth factor-beta signaling in cartilage of old mice: role in impaired repair capacity.* Arthritis Res Ther, 2005. **7**(6): p. R1338-47.
22. Verzijl, N., et al., *AGEing and osteoarthritis: a different perspective.* Curr Opin Rheumatol, 2003. **15**(5): p. 616-22.
23. Loeser, R.F., et al., *Articular chondrocytes express the receptor for advanced glycation end products: Potential role in osteoarthritis.* Arthritis Rheum, 2005. **52**(8): p. 2376-85.
24. Nah, S.S., et al., *Advanced glycation end products increases matrix metalloproteinase-1, -3, and -13, and TNF-alpha in human osteoarthritic chondrocytes.* FEBS Lett, 2007. **581**(9): p. 1928-32.
25. Nah, S.S., et al., *Effects of advanced glycation end products on the expression of COX-2, PGE2 and NO in human osteoarthritic chondrocytes.* Rheumatology (Oxford), 2008. **47**(4): p. 425-31.
26. Mitsuyama, H., et al., *Calcification of human articular knee cartilage is primarily an effect of aging rather than osteoarthritis.* Osteoarthritis Cartilage, 2007. **15**(5): p. 559-65.
27. Fuerst, M., et al., *Calcification of articular cartilage in human osteoarthritis.* Arthritis Rheum, 2009. **60**(9): p. 2694-703.

28. Taaffe, D.R. and R. Marcus, *Musculoskeletal health and the older adult*. Journal of Rehabilitation Research and Development, 2000. **37**(2): p. 245-254.
29. Frontera, W.R., et al., *Strength conditioning in older men: skeletal muscle hypertrophy and improved function*. J Appl Physiol (1985), 1988. **64**(3): p. 1038-44.
30. Charette, S.L., et al., *Muscle hypertrophy response to resistance training in older women*. J Appl Physiol (1985), 1991. **70**(5): p. 1912-6.
31. Pyka, G., et al., *Muscle strength and fiber adaptations to a year-long resistance training program in elderly men and women*. J Gerontol, 1994. **49**(1): p. M22-7.
32. Kelley, G.A., *Exercise and regional bone mineral density in postmenopausal women: a meta-analytic review of randomized trials*. Am J Phys Med Rehabil, 1998. **77**(1): p. 76-87.
33. Walker, J.A., *Osteoarthritis: pathogenesis, clinical features and management*. Nursing standard (Royal College of Nursing (Great Britain) : 1987), 2009. **24**(1): p. 35-40.
34. Pulsatelli, L., et al., *New findings in osteoarthritis pathogenesis: Therapeutic implications*. Therapeutic Advances in Chronic Disease, 2013. **4**(1): p. 23-43.
35. Kellgren, J.H., J.S. Lawrence, and F. Bier, *GENETIC FACTORS IN GENERALIZED OSTEO-ARTHROSIS*. Ann Rheum Dis, 1963. **22**: p. 237-55.
36. Griffin, T.M. and F. Guilak, *Why is obesity associated with osteoarthritis? Insights from mouse models of obesity*. Biorheology, 2008. **45**(3-4): p. 387-98.
37. Wluka, A.E., C.B. Lombard, and F.M. Cicuttini, *Tackling obesity in knee osteoarthritis*. Nat Rev Rheumatol, 2013. **9**(4): p. 225-235.
38. Zhang, Y. and J.M. Jordan, *Epidemiology of Osteoarthritis*. Clinics in geriatric medicine, 2010. **26**(3): p. 355-369.
39. Buckwalter, J.A., et al., *The Roles of Mechanical Stresses in the Pathogenesis of Osteoarthritis: Implications for Treatment of Joint Injuries()*. Cartilage, 2013. **4**(4): p. 286-294.
40. Griffin, T.M. and F. Guilak, *The role of mechanical loading in the onset and progression of osteoarthritis*. Exerc Sport Sci Rev, 2005. **33**(4): p. 195-200.
41. Goldring, M.B. and S.R. Goldring, *Articular cartilage and subchondral bone in the pathogenesis of osteoarthritis*, in *Skeletal Biology and Medicine*, M. Zaidi, Editor. 2010. p. 230-237.

42. Castañeda, S., et al., *Subchondral bone as a key target for osteoarthritis treatment*. *Biochemical Pharmacology*, 2012. **83**(3): p. 315-323.
43. Goldring, M.B. and S.R. Goldring, *Osteoarthritis*. *Journal of Cellular Physiology*, 2007. **213**(3): p. 626-634.
44. Buckwalter, J.A. and H.J. Mankin, *Articular cartilage: tissue design and chondrocyte-matrix interactions*. *Instr Course Lect*, 1998. **47**: p. 477-86.
45. Buckwalter, J.A., H.J. Mankin, and A.J. Grodzinsky, *Articular cartilage and osteoarthritis*. *Instr Course Lect*, 2005. **54**: p. 465-80.
46. Ateshian, G.A., *The Role of Interstitial Fluid Pressurization in Articular Cartilage Lubrication*. *Journal of biomechanics*, 2009. **42**(9): p. 1163-1176.
47. Buckwalter, J.A., *Articular cartilage: injuries and potential for healing*. *J Orthop Sports Phys Ther*, 1998. **28**(4): p. 192-202.
48. Buckwalter, J.A., V.C. Mow, and A. Ratcliffe, *Restoration of Injured or Degenerated Articular Cartilage*. *J Am Acad Orthop Surg*, 1994. **2**(4): p. 192-201.
49. Ulrich-Vinther, M., et al., *Articular cartilage biology*. *J Am Acad Orthop Surg*, 2003. **11**(6): p. 421-30.
50. Alford, J.W. and B.J. Cole, *Cartilage Restoration, Part 1: Basic Science, Historical Perspective, Patient Evaluation, and Treatment Options*. *The American Journal of Sports Medicine*, 2005. **33**(2): p. 295-306.
51. Franchimont, P. and C. Bassleer, *Effects of hormones and local growth factors on articular chondrocyte metabolism*. *J Rheumatol Suppl*, 1991. **27**: p. 68-70.
52. Guilak, F. and V.C. Mow, *The mechanical environment of the chondrocyte: a biphasic finite element model of cell-matrix interactions in articular cartilage*. *Journal of Biomechanics*, 2000. **33**(12): p. 1663-1673.
53. Buckwalter, J.A., *Mechanical Injuries of Articular Cartilage*. *The Iowa Orthopaedic Journal*, 1992. **12**: p. 50-57.
54. Gao, Y., et al., *The ECM-Cell Interaction of Cartilage Extracellular Matrix on Chondrocytes*. *BioMed Research International*, 2014. **2014**: p. 8.
55. Martel-Pelletier, J., et al., *Cartilage in normal and osteoarthritis conditions*. *Best Practice and Research: Clinical Rheumatology*, 2008. **22**(2): p. 351-384.
56. Hardingham, T.E. and A.J. Fosang, *Proteoglycans: many forms and many functions*. *Faseb j*, 1992. **6**(3): p. 861-70.
57. Kiani, C., et al., *Structure and function of aggrecan*. *Cell Res*, 2002. **12**(1): p. 19-32.

58. Li, Y., et al., *The age-related changes in cartilage and osteoarthritis*. BioMed Research International, 2013. **2013**.
59. Kawcak, C.E., et al., *The role of subchondral bone in joint disease: a review*. Equine Vet J, 2001. **33**(2): p. 120-6.
60. Saarakkala, S., et al., *Depth-wise progression of osteoarthritis in human articular cartilage: investigation of composition, structure and biomechanics*. Osteoarthritis and Cartilage, 2010. **18**(1): p. 73-81.
61. Mahjoub, M., F. Berenbaum, and X. Houard, *Why subchondral bone in osteoarthritis? The importance of the cartilage bone interface in osteoarthritis*. Osteoporosis International, 2012: p. 1-6.
62. Neogi, T., *Clinical significance of bone changes in osteoarthritis*. Therapeutic Advances in Musculoskeletal Disease, 2012. **4**(4): p. 259-267.
63. Suri, S. and D.A. Walsh, *Osteochondral alterations in osteoarthritis*. Bone, 2012. **51**(2): p. 204-211.
64. Thambyah, A. and N. Broom, *On how degeneration influences load-bearing in the cartilage-bone system: a microstructural and micromechanical study*. Osteoarthritis and Cartilage, 2007. **15**(12): p. 1410-1423.
65. Mohan, G., et al., *Application of in vivo micro-computed tomography in the temporal characterisation of subchondral bone architecture in a rat model of low-dose monosodium iodoacetate-induced osteoarthritis*. Arthritis Research and Therapy, 2011. **13**(6).
66. Sniekers, Y.H., et al., *A role for subchondral bone changes in the process of osteoarthritis; A micro-CT study of two canine models*. BMC Musculoskeletal Disorders, 2008. **9**.
67. Botter, S.M., et al., *Osteoarthritis induction leads to early and temporal subchondral plate porosity in the tibial plateau of mice: An in vivo microfocal computed tomography study*. Arthritis and Rheumatism, 2011. **63**(9): p. 2690-2699.
68. Sanchez, C., et al., *Regulation of subchondral bone osteoblast metabolism by cyclic compression*. Arthritis and rheumatism, 2012. **64**(4): p. 1193-1203.
69. Sanchez, C., et al., *Osteoblasts from the sclerotic subchondral bone downregulate aggrecan but upregulate metalloproteinases expression by chondrocytes. This*

- effect is mimicked by interleukin-6, -16 and oncostatin M pre-treated non-sclerotic osteoblasts. Osteoarthritis and Cartilage, 2005. 13(11): p. 979-987.*
70. Sanchez, C., et al., *Subchondral bone osteoblasts induce phenotypic changes in human osteoarthritic chondrocytes. Osteoarthritis and Cartilage, 2005. 13(11): p. 988-997.*
71. Lavigne, P., et al., *Subchondral and trabecular bone metabolism regulation in canine experimental knee osteoarthritis. Osteoarthritis and Cartilage, 2005. 13(4): p. 310-317.*
72. Hilal, G., et al., *Osteoblast-like cells from human subchondral osteoarthritic bone demonstrate an altered phenotype in vitro: Possible role in subchondral bone sclerosis. Arthritis and Rheumatism, 1998. 41(5): p. 891-899.*
73. Boyce, B.F. and L. Xing, *Biology of RANK, RANKL, and osteoprotegerin. Arthritis Res Ther, 2007. 9 Suppl 1: p. S1.*
74. Troen, B.R., *The role of cathepsin K in normal bone resorption. Drug News Perspect, 2004. 17(1): p. 19-28.*
75. Rengel, Y., C. Ospelt, and S. Gay, *Proteinases in the joint: Clinical relevance of proteinases in joint destruction. Arthritis Research and Therapy, 2007. 9(5).*
76. Poole, K.E. and J. Reeve, *Parathyroid hormone - a bone anabolic and catabolic agent. Curr Opin Pharmacol, 2005. 5(6): p. 612-7.*
77. Chen, G., C. Deng, and Y.-P. Li, *TGF- β and BMP Signaling in Osteoblast Differentiation and Bone Formation. International Journal of Biological Sciences, 2012. 8(2): p. 272-288.*
78. Chappard, C., et al., *Subchondral bone micro-architectural alterations in osteoarthritis: a synchrotron micro-computed tomography study. Osteoarthritis and Cartilage, 2006. 14(3): p. 215-223.*
79. Boyd, S.K., et al., *Early morphometric and anisotropic change in periarticular cancellous bone in a model of experimental knee osteoarthritis quantified using microcomputed tomography. Clin Biomech (Bristol, Avon), 2000. 15(8): p. 624-31.*
80. Lahm, A., et al., *Subchondral and trabecular bone remodeling in canine experimental osteoarthritis. Archives of Orthopaedic and Trauma Surgery, 2006. 126(9): p. 582-587.*

81. Wang, T., et al., *Spatial and temporal changes of subchondral bone proceed to microscopic articular cartilage degeneration in guinea pigs with spontaneous osteoarthritis*. *Osteoarthritis and Cartilage*, 2013. **21**(4): p. 574-581.
82. Boyd, S.K., R. Muller, and R.F. Zernicke, *Mechanical and architectural bone adaptation in early stage experimental osteoarthritis*. *J Bone Miner Res*, 2002. **17**(4): p. 687-94.
83. Duncan, R.L. and C.H. Turner, *Mechanotransduction and the functional response of bone to mechanical strain*. *Calcif Tissue Int*, 1995. **57**(5): p. 344-58.
84. Ehrlich, P.J. and L.E. Lanyon, *Mechanical strain and bone cell function: a review*. *Osteoporos Int*, 2002. **13**(9): p. 688-700.
85. Cox, L.G., et al., *Analysis of bone architecture sensitivity for changes in mechanical loading, cellular activity, mechanotransduction, and tissue properties*. *Biomech Model Mechanobiol*, 2011. **10**(5): p. 701-12.
86. Hardcastle, S.A., et al., *Osteoarthritis and bone mineral density: are strong bones bad for joints[quest]*. *BoneKEy Rep*, 2015. **4**.
87. Lee, J.Y., et al., *Relationship of bone mineral density to progression of knee osteoarthritis*. *Arthritis Rheum*, 2013. **65**(6): p. 1541-6.
88. Cox, L.G.E., et al., *Decreased bone tissue mineralization can partly explain subchondral sclerosis observed in osteoarthritis*. *Bone*, 2012. **50**(5): p. 1152-1161.
89. Spector, T.D., L.A. Perry, and R.W. Jubb, *Endogenous sex steroid levels in women with generalised osteoarthritis*. *Clinical Rheumatology*, 1991. **10**(3): p. 316-319.
90. Sowers, M., et al., *Association of bone mineral density and sex hormone levels with osteoarthritis of the hand and knee in premenopausal women*. *American Journal of Epidemiology*, 1996. **143**(1): p. 38-47.
91. Ham, K.D. and C.S. Carlson, *Effects of estrogen replacement therapy on bone turnover in subchondral bone and epiphyseal metaphyseal cancellous bone of ovariectomized cynomolgus monkeys*. *Journal of Bone and Mineral Research*, 2004. **19**(5): p. 823-829.
92. Ham, K.D., et al., *Effects of long-term estrogen replacement therapy on osteoarthritis severity in cynomolgus monkeys*. *Arthritis and Rheumatism*, 2002. **46**(7): p. 1956-1964.
93. Funck-Brentano, T., et al., *Targeting bone alleviates osteoarthritis in osteopenic mice and modulates cartilage catabolism*. *PLoS ONE*, 2012. **7**(3).

94. Bailey, A.J., T.J. Sims, and L. Knott, *Phenotypic expression of osteoblast collagen in osteoarthritic bone: production of type I homotrimer*. *Int J Biochem Cell Biol*, 2002. **34**(2): p. 176-82.
95. Mansell, J.P. and A.J. Bailey, *Abnormal cancellous bone collagen metabolism in osteoarthritis*. *J Clin Invest*, 1998. **101**(8): p. 1596-603.
96. Nevitt, M.C., et al., *Radiographic osteoarthritis of the hip and bone mineral density*. *Arthritis & Rheumatism*, 1995. **38**(7): p. 907-916.
97. Sowers, M., et al., *The associations of bone mineral density and bone turnover markers with osteoarthritis of the hand and knee in pre- and perimenopausal women*. *Arthritis Rheum*, 1999. **42**(3): p. 483-9.
98. Hart, D.J., et al., *The relationship of bone density and fracture to incident and progressive radiographic osteoarthritis of the knee: the Chingford Study*. *Arthritis Rheum*, 2002. **46**(1): p. 92-9.
99. Nevitt, M.C., et al., *High systemic bone mineral density increases the risk of incident knee OA and joint space narrowing, but not radiographic progression of existing knee OA: the MOST study*. *Ann Rheum Dis*, 2010. **69**(1): p. 163-8.
100. Li, B. and R.M. Aspden, *Composition and mechanical properties of cancellous bone from the femoral head of patients with osteoporosis or osteoarthritis*. *J Bone Miner Res*, 1997. **12**(4): p. 641-51.
101. Li, B. and R.M. Aspden, *Mechanical and material properties of the subchondral bone plate from the femoral head of patients with osteoarthritis or osteoporosis*. *Annals of the Rheumatic Diseases*, 1997. **56**(4): p. 247-254.
102. Day, J.S., et al., *A decreased subchondral trabecular bone tissue elastic modulus is associated with pre-arthritis cartilage damage*. *J Orthop Res*, 2001. **19**(5): p. 914-8.
103. Pan, J., et al., *Elevated cross-talk between subchondral bone and cartilage in osteoarthritic joints*. *Bone*, 2012. **51**(2): p. 212-217.
104. Funck-Brentano, T. and M. Cohen-Solal, *Crosstalk between cartilage and bone: When bone cytokines matter*. *Cytokine and Growth Factor Reviews*, 2011. **22**(2): p. 91-97.
105. Thambyah, A. and N. Broom, *Micro-anatomical response of cartilage-on-bone to compression: Mechanisms of deformation within and beyond the directly loaded matrix*. *Journal of Anatomy*, 2006. **209**(5): p. 611-622.

106. Ding, M., *Microarchitectural adaptations in aging and osteoarthrotic subchondral bone issues*. Acta Orthopaedica, 2010. **81**(SUPPL. 340): p. 1-53.
107. Day, J.S., et al., *A decreased subchondral trabecular bone tissue elastic modulus is associated with pre-arthritic cartilage damage*. Journal of Orthopaedic Research, 2001. **19**(5): p. 914-918.
108. Ko, F.C., et al., *In vivo cyclic compression causes cartilage degeneration and subchondral bone changes in mouse tibiae*. Arthritis and Rheumatism, 2013. **65**(6): p. 1569-1578.
109. Henrotin, Y., L. Pesesse, and C. Sanchez, *Subchondral bone and osteoarthritis: biological and cellular aspects*. Osteoporosis International, 2012: p. 1-5.
110. Kobayashi, M., et al., *Role of interleukin-1 and tumor necrosis factor alpha in matrix degradation of human osteoarthritic cartilage*. Arthritis Rheum, 2005. **52**(1): p. 128-35.
111. Roach, H.I., *Association of matrix acid and alkaline phosphatases with mineralization of cartilage and endochondral bone*. Histochem J, 1999. **31**(1): p. 53-61.
112. Shen, G., *The role of type X collagen in facilitating and regulating endochondral ossification of articular cartilage*. Orthod Craniofac Res, 2005. **8**(1): p. 11-7.
113. Tat, S.K., et al., *Modulation of OPG, RANK and RANKL by human chondrocytes and their implication during osteoarthritis*. Rheumatology, 2009. **48**(12): p. 1482-1490.
114. Byron, C.R., et al., *In vitro expression of receptor activator of nuclear factor- κ B ligand and osteoprotegerin in cultured equine articular cells*. American Journal of Veterinary Research, 2010. **71**(6): p. 615-622.
115. Lajeunesse, D., *The role of bone in the treatment of osteoarthritis*. Osteoarthritis and Cartilage, 2004. **12**(SUPPL.): p. S34-S38.
116. Shen, J., S. Li, and D. Chen, *TGF- β signaling and the development of osteoarthritis*. Bone Research, 2014. **2**.
117. Ferrell, W.R., et al., *Essential role for proteinase-activated receptor-2 in arthritis*. Journal of Clinical Investigation, 2003. **111**(1): p. 35-41.
118. Loeser, R.F., E.A. Erickson, and D.L. Long, *Mitogen-Activated Protein Kinases as Therapeutic Targets in Osteoarthritis*. Current opinion in rheumatology, 2008. **20**(5): p. 581-586.

119. Thalhamer, T., M.A. McGrath, and M.M. Harnett, *MAPKs and their relevance to arthritis and inflammation*. Rheumatology (Oxford), 2008. **47**(4): p. 409-14.
120. Mengshol, J.A., et al., *Interleukin-1 induction of collagenase 3 (matrix metalloproteinase 13) gene expression in chondrocytes requires p38, c-Jun N-terminal kinase, and nuclear factor kappaB: differential regulation of collagenase 1 and collagenase 3*. Arthritis Rheum, 2000. **43**(4): p. 801-11.
121. Mengshol, J.A., M.P. Vincenti, and C.E. Brinckerhoff, *IL-1 induces collagenase-3 (MMP-13) promoter activity in stably transfected chondrocytic cells: requirement for Runx-2 and activation by p38 MAPK and JNK pathways*. Nucleic Acids Research, 2001. **29**(21): p. 4361-4372.
122. Milner, J.M., et al., *Matriptase is a novel initiator of cartilage matrix degradation in osteoarthritis*. Arthritis and Rheumatism, 2010. **62**(7): p. 1955-1966.
123. Kobilka, B., *The Structural Basis of G-Protein-Coupled Receptor Signaling (Nobel Lecture)*. Angewandte Chemie International Edition, 2013. **52**(25): p. 6380-6388.
124. Kroeze, W.K., D.J. Sheffler, and B.L. Roth, *G-protein-coupled receptors at a glance*. J Cell Sci, 2003. **116**(Pt 24): p. 4867-9.
125. Tuteja, N., *Signaling through G protein coupled receptors*. Plant Signaling & Behavior, 2009. **4**(10): p. 942-947.
126. Hamm, H.E., *The many faces of G protein signaling*. J Biol Chem, 1998. **273**(2): p. 669-72.
127. Oldham, W.M. and H.E. Hamm, *Heterotrimeric G protein activation by G-protein-coupled receptors*. Nat Rev Mol Cell Biol, 2008. **9**(1): p. 60-71.
128. Steinhoff, M., et al., *Proteinase-activated receptors: Transducers of proteinase-mediated signaling in inflammation and immune response*. Endocrine Reviews, 2005. **26**(1): p. 1-43.
129. Macfarlane, S.R., et al., *Proteinase-activated receptors*. Pharmacol Rev, 2001. **53**(2): p. 245-82.
130. Kelso, E.B., et al., *Therapeutic promise of proteinase-activated receptor-2 antagonism in joint inflammation*. Journal of Pharmacology and Experimental Therapeutics, 2006. **316**(3): p. 1017-1024.
131. Boileau, C., et al., *Activation of proteinase-activated receptor 2 in human osteoarthritic cartilage upregulates catabolic and proinflammatory pathways*

- capable of inducing cartilage degradation: A basic science study.* Arthritis Research and Therapy, 2007. **9**(6).
132. Kelso, E.B., et al., *Expression and proinflammatory role of proteinase-activated receptor 2 in rheumatoid synovium: Ex vivo studies using a novel proteinase-activated receptor 2 antagonist.* Arthritis and Rheumatism, 2007. **56**(3): p. 765-771.
133. McIntosh, K.A., et al., *The therapeutic potential of proteinase-activated receptors in arthritis.* Current Opinion in Pharmacology, 2007. **7**(3): p. 334-338.
134. Lam, F.F.Y., *Role of protease-activated receptor 2 in joint inflammation.* Arthritis and Rheumatism, 2007. **56**(11): p. 3514-3517.
135. Palmer, H.S., et al., *Protease-activated receptor 2 mediates the proinflammatory effects of synovial mast cells.* Arthritis and Rheumatism, 2007. **56**(11): p. 3532-3540.
136. Milner, J.M., A. Patel, and A.D. Rowan, *Emerging roles of serine proteinases in tissue turnover in arthritis.* Arthritis and Rheumatism, 2008. **58**(12): p. 3644-3656.
137. Ferrell, W.R., et al., *Protease-activated receptor 2: A novel pathogenic pathway in a murine model of osteoarthritis.* Annals of the Rheumatic Diseases, 2010. **69**(11): p. 2051-2054.
138. Amiable, N., et al., *Proteinase-activated receptor (PAR)-2 activation impacts bone resorptive properties of human osteoarthritic subchondral bone osteoblasts.* Bone, 2009. **44**(6): p. 1143-1150.
139. Amiable, N., et al., *Proteinase-activated receptor-2 gene disruption limits the effect of osteoarthritis on cartilage in mice: A novel target in joint degradation.* Journal of Rheumatology, 2011. **38**(5): p. 911-920.
140. Sandy, J.D., et al., *The structure of aggrecan fragments in human synovial fluid. Evidence for the involvement in osteoarthritis of a novel proteinase which cleaves the Glu 373-Ala 374 bond of the interglobular domain.* J Clin Invest, 1992. **89**(5): p. 1512-6.
141. Tetlow, L.C., D.J. Adlam, and D.E. Woolley, *Matrix metalloproteinase and proinflammatory cytokine production by chondrocytes of human osteoarthritic cartilage: associations with degenerative changes.* Arthritis Rheum, 2001. **44**(3): p. 585-94.

142. Sandy, J.D., et al., *Catabolism of aggrecan in cartilage explants. Identification of a major cleavage site within the interglobular domain*. J Biol Chem, 1991. **266**(14): p. 8683-5.
143. Tortorella, M.D., et al., *Purification and cloning of aggrecanase-1: a member of the ADAMTS family of proteins*. Science, 1999. **284**(5420): p. 1664-6.
144. Tortorella, M.D., et al., *Sites of aggrecan cleavage by recombinant human aggrecanase-1 (ADAMTS-4)*. J Biol Chem, 2000. **275**(24): p. 18566-73.
145. Tortorella, M.D., et al., *The role of ADAM-TS4 (aggrecanase-1) and ADAM-TS5 (aggrecanase-2) in a model of cartilage degradation*. Osteoarthritis Cartilage, 2001. **9**(6): p. 539-52.
146. Cawston, T.E. and D.A. Young, *Proteinases involved in matrix turnover during cartilage and bone breakdown*. Cell and Tissue Research, 2010. **339**(1): p. 221-235.
147. Chakraborti, S., et al., *Regulation of matrix metalloproteinases: an overview*. Mol Cell Biochem, 2003. **253**(1-2): p. 269-85.
148. Fosang, A.J., et al., *Development of a cleavage-site-specific monoclonal antibody for detecting metalloproteinase-derived aggrecan fragments: detection of fragments in human synovial fluids*. Biochemical Journal, 1995. **310**(Pt 1): p. 337-343.
149. Fosang, A.J., K. Last, and R.A. Maciewicz, *Aggrecan is degraded by matrix metalloproteinases in human arthritis. Evidence that matrix metalloproteinase and aggrecanase activities can be independent*. J Clin Invest, 1996. **98**(10): p. 2292-9.
150. Struglics, A., et al., *Human osteoarthritis synovial fluid and joint cartilage contain both aggrecanase- and matrix metalloproteinase-generated aggrecan fragments*. Osteoarthritis Cartilage, 2006. **14**(2): p. 101-13.
151. Sandy, J.D. and C. Verscharen, *Analysis of aggrecan in human knee cartilage and synovial fluid indicates that aggrecanase (ADAMTS) activity is responsible for the catabolic turnover and loss of whole aggrecan whereas other protease activity is required for C-terminal processing in vivo*. Biochem J, 2001. **358**(Pt 3): p. 615-26.
152. Sandy, J.D., *A contentious issue finds some clarity: on the independent and complementary roles of aggrecanase activity and MMP activity in human joint aggrecanolysis*. Osteoarthritis Cartilage, 2006. **14**(2): p. 95-100.

153. van Meurs, J.B., et al., *Kinetics of aggrecanase- and metalloproteinase-induced neoepitopes in various stages of cartilage destruction in murine arthritis*. *Arthritis Rheum*, 1999. **42**(6): p. 1128-39.
154. Little, C.B., et al., *Aggrecanase versus matrix metalloproteinases in the catabolism of the interglobular domain of aggrecan in vitro*. *Biochemical Journal*, 1999. **344**(Pt 1): p. 61-68.
155. Little, C.B., et al., *Matrix metalloproteinases are involved in C-terminal and interglobular domain processing of cartilage aggrecan in late stage cartilage degradation*. *Matrix Biol*, 2002. **21**(3): p. 271-88.
156. Cawston, T.E. and A.J. Wilson, *Understanding the role of tissue degrading enzymes and their inhibitors in development and disease*. *Best Practice and Research: Clinical Rheumatology*, 2006. **20**(5): p. 983-1002.
157. Billingham, R.C., et al., *Enhanced cleavage of type II collagen by collagenases in osteoarthritic articular cartilage*. *J Clin Invest*, 1997. **99**(7): p. 1534-45.
158. Reboul, P., et al., *The new collagenase, collagenase-3, is expressed and synthesized by human chondrocytes but not by synoviocytes. A role in osteoarthritis*. *Journal of Clinical Investigation*, 1996. **97**(9): p. 2011-2019.
159. Nagase, H., *Activation mechanisms of matrix metalloproteinases*. *Biol Chem*, 1997. **378**(3-4): p. 151-60.
160. Visse, R. and H. Nagase, *Matrix metalloproteinases and tissue inhibitors of metalloproteinases: structure, function, and biochemistry*. *Circ Res*, 2003. **92**(8): p. 827-39.
161. Milner, J.M., S.F. Elliott, and T.E. Cawston, *Activation of Procollagenases Is a Key Control Point in Cartilage Collagen Degradation: Interaction of Serine and Metalloproteinase Pathways*. *Arthritis and Rheumatism*, 2001. **44**(9): p. 2084-2096.
162. Milner, J.M., et al., *Inhibition of furin-like enzymes blocks interleukin-1alpha/oncostatin M-stimulated cartilage degradation*. *Arthritis Rheum*, 2003. **48**(4): p. 1057-66.
163. Hooper, J.D., et al., *Type II transmembrane serine proteases-insights into an emerging class of cell surface proteolytic enzymes*. *Journal of Biological Chemistry*, 2000.

164. Szabo, R. and T.H. Bugge, *Type II transmembrane serine proteases in development and disease*. International Journal of Biochemistry and Cell Biology, 2008. **40**(6-7): p. 1297-1316.
165. Lin, C.Y., et al., *Molecular cloning of cDNA for matriptase, a matrix-degrading serine protease with trypsin-like activity*. J Biol Chem, 1999. **274**(26): p. 18231-6.
166. Oberst, M.D., et al., *The activation of matriptase requires its noncatalytic domains, serine protease domain, and its cognate inhibitor*. Journal of Biological Chemistry, 2003. **278**(29): p. 26773-26779.
167. Jin, X., et al., *Matriptase activates stromelysin (MMP-3) and promotes tumor growth and angiogenesis*. Cancer Science, 2006. **97**(12): p. 1327-1334.
168. Rowan, A., et al., *Adenoviral gene transfer of interleukin-1 in combination with oncostatin M induces significant joint damage in a murine model*. American Journal of Pathology, 2003. **162**(6): p. 1975-1984.
169. Jubb, R.W. and H.B. Fell, *The effect of synovial tissue on the synthesis of proteoglycan by the articular cartilage of young pigs*. Arthritis & Rheumatism, 1980. **23**(5): p. 545-555.
170. Dingle, J.T., et al., *A cartilage catabolic factor from synovium*. Biochemical Journal, 1979. **184**(1): p. 177-180.
171. Arner, E.C., et al., *Cytokine-induced cartilage proteoglycan degradation is mediated by aggrecanase*. Osteoarthritis and Cartilage, 1998. **6**(3): p. 214-228.
172. Dingle, J.T., *The effect of synovial catabolin on cartilage synthetic activity*. Connect Tissue Res, 1984. **12**(3-4): p. 277-86.
173. Tyler, J.A., *Articular cartilage cultured with catabolin (pig interleukin 1) synthesizes a decreased number of normal proteoglycan molecules*. Biochemical Journal, 1985. **227**(3): p. 869-878.
174. Dingle, J.T., et al., *In vivo studies of articular tissue damage mediated by catabolin/interleukin 1*. Annals of the Rheumatic Diseases, 1987. **46**(7): p. 527-533.
175. Pelletier, J.P., et al., *In vivo suppression of early experimental osteoarthritis by interleukin-1 receptor antagonist using gene therapy*. Arthritis Rheum, 1997. **40**(6): p. 1012-9.
176. Fernandes, J., et al., *In Vivo Transfer of Interleukin-1 Receptor Antagonist Gene in Osteoarthritic Rabbit Knee Joints : Prevention of Osteoarthritis Progression*. The American Journal of Pathology, 1999. **154**(4): p. 1159-1169.

177. Sandy, J.D., R.E. Boynton, and C.R. Flannery, *Analysis of the catabolism of aggrecan in cartilage explants by quantitation of peptides from the three globular domains*. J Biol Chem, 1991. **266**(13): p. 8198-205.
178. Morgan, T.G., et al., *Human nasal cartilage responds to oncostatin M in combination with interleukin 1 or tumour necrosis factor α by the release of collagen fragments via collagenases*. Annals of the Rheumatic Diseases, 2006. **65**(2): p. 184-190.
179. Carroll, G.J. and M.C. Bell, *Leukaemia inhibitory factor stimulates proteoglycan resorption in porcine articular cartilage*. Rheumatol Int, 1993. **13**(1): p. 5-8.
180. Bell, M.C. and G.J. Carroll, *Leukaemia inhibitory factor (LIF) suppresses proteoglycan synthesis in porcine and caprine cartilage explants*. Cytokine, 1995. **7**(2): p. 137-41.
181. Hui, W., M. Bell, and G. Carroll, *Oncostatin M (OSM) stimulates resorption and inhibits synthesis of proteoglycan in porcine articular cartilage explants*. Cytokine, 1996. **8**(6): p. 495-500.
182. Durigova, M., P.J. Roughley, and J.S. Mort, *Mechanism of proteoglycan aggregate degradation in cartilage stimulated with oncostatin M*. Osteoarthritis and Cartilage, 2008. **16**(1): p. 98-104.
183. Cawston, T.E., et al., *Interleukin-1 and oncostatin M in combination promote the release of collagen fragments from bovine nasal cartilage in culture*. Biochemical and Biophysical Research Communications, 1995. **215**(1): p. 377-385.
184. Cawston, T.E., et al., *The role of oncostatin M in animal and human connective tissue collagen turnover and its localization within the rheumatoid joint*. Arthritis & Rheumatism, 1998. **41**(10): p. 1760-1771.
185. Li, W.Q., F. Dehnade, and M. Zafarullah, *Oncostatin M-induced matrix metalloproteinase and tissue inhibitor of metalloproteinase-3 genes expression in chondrocytes requires Janus kinase/STAT signaling pathway*. J Immunol, 2001. **166**(5): p. 3491-8.
186. El Mabrouk, M., J. Sylvester, and M. Zafarullah, *Signaling pathways implicated in oncostatin M-induced aggrecanase-1 and matrix metalloproteinase-13 expression in human articular chondrocytes*. Biochim Biophys Acta, 2007. **1773**(3): p. 309-20.
187. Desilets, A., et al., *Inhibition of human matriptase by eglin c variants*. FEBS Lett, 2006. **580**(9): p. 2227-32.

188. List, K., et al., *Epithelial integrity is maintained by a matriptase-dependent proteolytic pathway*. American Journal of Pathology, 2009. **175**(4): p. 1453-1463.
189. Staunton, D., K.R. Hudson, and J.K. Heath, *The interactions of the cytokine-binding homology region and immunoglobulin-like domains of gp130 with oncostatin M: implications for receptor complex formation*. Protein Eng, 1998. **11**(11): p. 1093-102.
190. Lander, E.S., et al., *Initial sequencing and analysis of the human genome*. Nature, 2001. **409**(6822): p. 860-921.
191. van der Weyden, L., D.J. Adams, and A. Bradley, *Tools for targeted manipulation of the mouse genome*. Vol. 11. 2002. 133-164.
192. Glasson, S.S., T.J. Blanchet, and E.A. Morris, *The surgical destabilization of the medial meniscus (DMM) model of osteoarthritis in the 129/SvEv mouse*. Osteoarthritis Cartilage, 2007. **15**(9): p. 1061-9.
193. Majumdar, M.K., et al., *Immortalized cell lines from mouse xiphisternum preserve chondrocyte phenotype*. J Cell Physiol, 2006. **209**(2): p. 551-9.
194. Chomczynski, P. and N. Sacchi, *Single-step method of RNA isolation by acid guanidinium thiocyanate-phenol-chloroform extraction*. Anal Biochem, 1987. **162**(1): p. 156-9.
195. Garibyan, L. and N. Avashia, *Polymerase Chain Reaction*. J Invest Dermatol, 2013. **133**(3): p. e6.
196. Joshi, M. and J.D. Deshpande, *POLYMERASE CHAIN REACTION: METHODS, PRINCIPLES AND APPLICATION*. 2011, 2011. **2**(1): p. 17.
197. VanGuilder, H.D., K.E. Vrana, and W.M. Freeman, *Twenty-five years of quantitative PCR for gene expression analysis*. Biotechniques, 2008. **44**(5): p. 619-26.
198. Schmitz, N., et al., *Basic methods in histopathology of joint tissues*. Osteoarthritis Cartilage, 2010. **18 Suppl 3**: p. S113-6.
199. Burghardt, A.J., T.M. Link, and S. Majumdar, *High-resolution computed tomography for clinical imaging of bone microarchitecture*. Clinical Orthopaedics and Related Research, 2011. **469**(8): p. 2179-2193.
200. Holdsworth, D.W. and M.M. Thornton, *Micro-CT in small animal and specimen imaging*. Trends in Biotechnology, 2002. **20**(8): p. S34-S39.
201. Schambach, S.J., et al., *Application of micro-CT in small animal imaging*. Methods, 2010. **50**(1): p. 2-13.

202. Pittenger, M.F., et al., *Multilineage potential of adult human mesenchymal stem cells*. Science, 1999. **284**(5411): p. 143-7.
203. Murdoch, A.D., et al., *Chondrogenic differentiation of human bone marrow stem cells in transwell cultures: generation of scaffold-free cartilage*. Stem Cells, 2007. **25**(11): p. 2786-96.
204. Johnstone, B., et al., *In vitro chondrogenesis of bone marrow-derived mesenchymal progenitor cells*. Exp Cell Res, 1998. **238**(1): p. 265-72.
205. Tyler, J.A., *Insulin-like growth factor 1 can decrease degradation and promote synthesis of proteoglycan in cartilage exposed to cytokines*. Biochemical Journal, 1989. **260**(2): p. 543-548.
206. Hascall, V.C., et al., *Biosynthesis and turnover of proteoglycans in organ culture of bovine articular cartilage*. J Rheumatol Suppl, 1983. **11**: p. 45-52.
207. Schneider, M. and G. Goldstein, *Digestion of articular cartilage by papain in vitro*. Proc Soc Exp Biol Med, 1967. **124**(3): p. 991-4.
208. Taylor, K.B. and G.M. Jeffree, *A new basic metachromatic dye, 1:9-Dimethyl Methylene Blue*. The Histochemical Journal, 1969. **1**(3): p. 199-204.
209. Farndale, R.W., D.J. Buttle, and A.J. Barrett, *Improved quantitation and discrimination of sulphated glycosaminoglycans by use of dimethylmethylene blue*. Biochimica et Biophysica Acta (BBA)-General Subjects, 1986. **883**(2): p. 173-177.
210. Garnjanagoonchorn, W., L. Wongekalak, and A. Engkagul, *Determination of chondroitin sulfate from different sources of cartilage*. Chemical Engineering and Processing: Process Intensification, 2007. **46**(5): p. 465-471.
211. Bergman, I. and R. Loxley, *Two Improved and Simplified Methods for the Spectrophotometric Determination of Hydroxyproline*. Analytical Chemistry, 1963. **35**(12): p. 1961-1965.
212. Neumann, U., et al., *Characterization of Mca-Lys-Pro-Leu-Gly-Leu-Dpa-Ala-Arg-NH₂, a fluorogenic substrate with increased specificity constants for collagenases and tumor necrosis factor converting enzyme*. Anal Biochem, 2004. **328**(2): p. 166-73.
213. Moos, V., et al., *Immunohistological analysis of cytokine expression in human osteoarthritic and healthy cartilage*. J Rheumatol, 1999. **26**(4): p. 870-9.

214. Durigova, M., P.J. Roughley, and J.S. Mort, *Mechanism of proteoglycan aggregate degradation in cartilage stimulated with oncostatin M*. Osteoarthritis Cartilage, 2008. **16**(1): p. 98-104.
215. Cawston, T.E., et al., *The role of oncostatin M in animal and human connective tissue collagen turnover and its localization within the rheumatoid joint*. Arthritis and Rheumatism, 1998. **41**(10): p. 1760-1771.
216. McNulty, A.L., et al., *Synovial fluid concentrations and relative potency of interleukin-1 alpha and beta in cartilage and meniscus degradation*. J Orthop Res, 2013. **31**(7): p. 1039-45.
217. Tsuchida, A.I., et al., *Cytokine profiles in the joint depend on pathology, but are different between synovial fluid, cartilage tissue and cultured chondrocytes*. Arthritis Research & Therapy, 2014. **16**(5): p. 441.
218. Ni, J., et al., *OSM is overexpressed in knee osteoarthritis and Notch signaling is involved in the effects of OSM on MC3T3-E1 cell proliferation and differentiation*. Int J Mol Med, 2015. **35**(6): p. 1755-60.
219. Pelttari, K., E. Steck, and W. Richter, *The use of mesenchymal stem cells for chondrogenesis*. Injury, 2008. **39**(1 SUPPL.): p. 58-65.
220. Koshy, P.J.T., et al., *The modulation of matrix metalloproteinase and ADAM gene expression in human chondrocytes by interleukin-1 and oncostatin M: A time-course study using real-time quantitative reverse transcription-polymerase chain reaction*. Arthritis and Rheumatism, 2002. **46**(4): p. 961-967.
221. Milner, J.M., et al., *Metalloproteinase and inhibitor expression profiling of resorbing cartilage reveals pro-collagenase activation as a critical step for collagenolysis*. Arthritis Res Ther, 2006. **8**(5): p. R142.
222. Wilkinson, D.J., D. Rowan, and J. Milner, *Identifying the key enzymes involved in matrix metalloproteinase-induced cartilage aggrecan and collagen resorption*. Osteoarthritis and Cartilage. **20**: p. S119-S120.
223. Phinney, D.G., et al., *Donor variation in the growth properties and osteogenic potential of human marrow stromal cells*. J Cell Biochem, 1999. **75**(3): p. 424-36.
224. Siegel, G., et al., *Phenotype, donor age and gender affect function of human bone marrow-derived mesenchymal stromal cells*. BMC Med, 2013. **11**: p. 146.

225. Siddappa, R., et al., *Donor variation and loss of multipotency during in vitro expansion of human mesenchymal stem cells for bone tissue engineering*. J Orthop Res, 2007. **25**(8): p. 1029-41.
226. Russell, K.C., et al., *In vitro high-capacity assay to quantify the clonal heterogeneity in trilineage potential of mesenchymal stem cells reveals a complex hierarchy of lineage commitment*. Stem Cells, 2010. **28**(4): p. 788-98.
227. Barksby, H.E., et al., *Interleukin-1 in combination with oncostatin M up-regulates multiple genes in chondrocytes: Implications for cartilage destruction and repair*. Arthritis and Rheumatism, 2006. **54**(2): p. 540-550.
228. Koshy, P.J., et al., *The modulation of matrix metalloproteinase and ADAM gene expression in human chondrocytes by interleukin-1 and oncostatin M: a time-course study using real-time quantitative reverse transcription-polymerase chain reaction*. Arthritis Rheum, 2002. **46**(4): p. 961-7.
229. Kim, B., et al., *Comparison between subchondral bone change and cartilage degeneration in collagenase- and DMM- induced osteoarthritis (OA) models in mice*. Tissue Engineering and Regenerative Medicine, 2013. **10**(4): p. 211-217.
230. Ma, H.L., et al., *Osteoarthritis severity is sex dependent in a surgical mouse model*. Osteoarthritis and Cartilage, 2007. **15**(6): p. 695-700.
231. Botter, S.M., et al., *Cartilage damage pattern in relation to subchondral plate thickness in a collagenase-induced model of osteoarthritis*. Osteoarthritis and Cartilage, 2008. **16**(4): p. 506-514.
232. Huesa, C., et al., *Proteinase-activated receptor 2 modulates OA-related pain, cartilage and bone pathology*. Ann Rheum Dis, 2015.
233. Hayami, T., et al., *Characterization of articular cartilage and subchondral bone changes in the rat anterior cruciate ligament transection and meniscectomized models of osteoarthritis*. Bone, 2006. **38**(2): p. 234-243.
234. Pastoureau, P., et al., *Quantitative assessment of articular cartilage and subchondral bone histology in the meniscectomized guinea pig model of osteoarthritis*. Osteoarthritis Cartilage, 2003. **11**(6): p. 412-23.
235. Kuroki, K., C.R. Cook, and J.L. Cook, *Subchondral bone changes in three different canine models of osteoarthritis*. Osteoarthritis and Cartilage, 2011. **19**(9): p. 1142-1149.

236. Chiba, K., et al., *In vivo structural analysis of subchondral trabecular bone in osteoarthritis of the hip using multi-detector row CT*. Osteoarthritis and Cartilage, 2011. **19**(2): p. 180-185.
237. Ding, M., A. Odgaard, and I. Hvid, *Changes in the three-dimensional microstructure of human tibial cancellous bone in early osteoarthritis*. J Bone Joint Surg Br, 2003. **85**(6): p. 906-12.
238. Van Osch, G.J.V.M., et al., *The relation between cartilage damage and osteophyte size in a murine model for osteoarthritis in the knee*. Rheumatology International, 1996. **16**(3): p. 115-119.
239. Botter, S.M., et al., *ADAMTS5^{-/-} mice have less subchondral bone changes after induction of osteoarthritis through surgical instability: implications for a link between cartilage and subchondral bone changes*. Osteoarthritis and Cartilage, 2009. **17**(5): p. 636-645.
240. Hashimoto, S., et al., *Development and regulation of osteophyte formation during experimental osteoarthritis*. Osteoarthritis Cartilage, 2002. **10**(3): p. 180-7.
241. McNulty, M.A., et al., *Histopathology of naturally occurring and surgically induced osteoarthritis in mice*. Osteoarthritis and Cartilage, 2012. **20**(8): p. 949-956.
242. Intema, F., et al., *Similarities and discrepancies in subchondral bone structure in two differently induced canine models of osteoarthritis*. J Bone Miner Res, 2010. **25**(7): p. 1650-7.
243. Van Valburg, A.A., et al., *Quantification of morphometric changes in murine experimental osteoarthritis using image analysis*. Rheumatology International, 1996. **15**(5): p. 181-187.
244. Chambers, M.G., et al., *Matrix metalloproteinases and aggrecanases cleave aggrecan in different zones of normal cartilage but colocalize in the development of osteoarthritic lesions in STR/ort mice*. Arthritis Rheum, 2001. **44**(6): p. 1455-65.
245. van Valburg, A.A., et al., *Quantification of morphometric changes in murine experimental osteoarthritis using image analysis*. Rheumatol Int, 1996. **15**(5): p. 181-7.
246. Radin, E.L. and R.M. Rose, *Role of subchondral bone in the initiation and progression of cartilage damage*. Clin Orthop Relat Res, 1986(213): p. 34-40.

247. Pest, M.A., et al., *Disturbed cartilage and joint homeostasis resulting from a loss of mitogen-inducible gene 6 in a mouse model of joint dysfunction*. *Arthritis Rheumatol*, 2014. **66**(10): p. 2816-27.
248. Glasson, S.S., et al., *Characterization of and osteoarthritis susceptibility in ADAMTS-4-knockout mice*. *Arthritis Rheum*, 2004. **50**(8): p. 2547-58.
249. Glasson, S.S., et al., *Deletion of active ADAMTS5 prevents cartilage degradation in a murine model of osteoarthritis*. *Nature*, 2005. **434**(7033): p. 644-8.
250. Heffner, C.S., et al., *Supporting conditional mouse mutagenesis with a comprehensive cre characterization resource*. *Nature Communications*, 2012. **3**: p. 1218.
251. Chambers, M.G., et al., *Expression of collagen and aggrecan genes in normal and osteoarthritic murine knee joints*. *Osteoarthritis and Cartilage*. **10**(1): p. 51-61.
252. Jackson, M.T., et al., *Depletion of protease-activated receptor 2 but not protease-activated receptor 1 may confer protection against osteoarthritis in mice through extracartilaginous mechanisms*. *Arthritis Rheumatol*, 2014. **66**(12): p. 3337-48.
253. Busso, N., et al., *Evaluation of protease-activated receptor 2 in murine models of arthritis*. *Arthritis Rheum*, 2007. **56**(1): p. 101-7.
254. Zamli, Z., et al., *Subchondral Bone Plate Thickening Precedes Chondrocyte Apoptosis and Cartilage Degradation in Spontaneous Animal Models of Osteoarthritis*. *BioMed Research International*, 2014. **2014**: p. 10.
255. Kim, J.H., et al., *Regulation of the catabolic cascade in osteoarthritis by the zinc-ZIP8-MTF1 axis*. *Cell*, 2014. **156**(4): p. 730-43.
256. Little, C.B., et al., *Matrix metalloproteinase 13-deficient mice are resistant to osteoarthritic cartilage erosion but not chondrocyte hypertrophy or osteophyte development*. *Arthritis Rheum*, 2009. **60**(12): p. 3723-33.
257. Wang, M., et al., *MMP13 is a critical target gene during the progression of osteoarthritis*. *Arthritis Res Ther*, 2013. **15**(1): p. R5.
258. Chavassieux, P.M., et al., *Histomorphometric assessment of the long-term effects of alendronate on bone quality and remodeling in patients with osteoporosis*. *J Clin Invest*, 1997. **100**(6): p. 1475-80.
259. Hayami, T., et al., *The Role of Subchondral Bone Remodeling in Osteoarthritis: Reduction of Cartilage Degeneration and Prevention of Osteophyte Formation by*

- Alendronate in the Rat Anterior Cruciate Ligament Transection Model*. Arthritis and Rheumatism, 2004. **50**(4): p. 1193-1206.
260. Mouritzen, U., et al., *Cartilage turnover assessed with a newly developed assay measuring collagen type II degradation products: influence of age, sex, menopause, hormone replacement therapy, and body mass index*. Ann Rheum Dis, 2003. **62**(4): p. 332-6.
261. Christgau, S., et al., *Suppression of elevated cartilage turnover in postmenopausal women and in ovariectomized rats by estrogen and a selective estrogen-receptor modulator (SERM)*. Menopause, 2004. **11**(5): p. 508-18.
262. Behets, C., et al., *Effects of calcitonin on subchondral trabecular bone changes and on osteoarthritic cartilage lesions after acute anterior cruciate ligament deficiency*. J Bone Miner Res, 2004. **19**(11): p. 1821-6.
263. Lieben, L., *Osteoarthritis: Osteophyte formation involves PAR2*. Nat Rev Rheumatol, 2016. **advance online publication**.
264. Ono, N., et al., *A Subset of Chondrogenic Cells Provides Early Mesenchymal Progenitors in Growing Bones*. Nature cell biology, 2014. **16**(12): p. 1157-1167.
265. Ahmed, U., et al., *Biomarkers of early stage osteoarthritis, rheumatoid arthritis and musculoskeletal health*. Scientific Reports, 2015. **5**: p. 9259.
266. Lotz, M., et al., *Value of biomarkers in osteoarthritis: current status and perspectives*. Ann Rheum Dis, 2013. **72**(11): p. 1756-63.
267. LeBeau, A.M., et al., *Imaging a functional tumorigenic biomarker in the transformed epithelium*. Proc Natl Acad Sci U S A, 2013. **110**(1): p. 93-8.
268. Kretlow, J.D., et al., *Donor age and cell passage affects differentiation potential of murine bone marrow-derived stem cells*. BMC Cell Biol, 2008. **9**: p. 60.
269. Curran, S., et al., *Laser capture microscopy*. Molecular Pathology, 2000. **53**(2): p. 64-68.